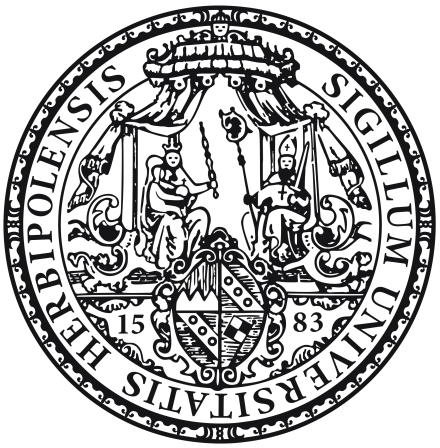

Genome-wide reporter screens identify transcriptional regulators of ribosome biogenesis

Genomweite Reporterscreens identifizieren transkriptionelle Regulatoren ribosomaler Biogenese

Doctoral thesis for a doctoral degree

at the Graduate School of Life Sciences,

Julius-Maximilians-Universität Würzburg,

Section Biomedicine

submitted by

Jessica Denise Schwarz

from

Nürnberg

Würzburg 2021

Submitted on: .....

Office stamp

Members of the Thesis Committee

Chairperson: Prof. Dr. Christoph Sotriffer

Primary Supervisor: Prof. Dr. Elmar Wolf

Supervisor (Second): Prof. Dr. Martin Eilers

Supervisor (Third): Dr. Björn von Eyß

Supervisor (Fourth): Prof. Dr. Andreas Winterpacht

Date of Public Defence: 24.06.2022

Date of Receipt of Certificates: .....

Contents

1 Abstract

Cellular growth and proliferation are among the most important processes for cells and organisms. One of the major determinants of these processes is the amount of proteins and consequently also the amount of ribosomes. Their synthesis involves several hundred proteins and four different ribosomal RNA species, is highly coordinated and very energy-demanding. However, the molecular mechanims of transcriptional regulation of the protein-coding genes involved, is only poorly understood in mammals.

In this thesis, unbiased genome-wide knockout reporter screens were performed, aiming to identify previously unknown transcriptional regulators of ribosome biogenesis factors (RiBis), which are important for the assembly and maturation of ribosomes, and ribosomal proteins (RPs), which are ribosomal components themself. With that approach and follow-up (validation) experiments, ALDOA and RBM8A among others, could be identified as regulators of ribosome biogenesis.

Depletion of the glycolytic enzyme ALDOA led to a downregulation of RiBi- and RP-promoter driven reporters on protein and transcript level, as well as to a downregulation of ribosome biogenesis gene transcripts and of mRNAs of other genes important for proliferation.

Reducing the amount of the exon junction complex protein RBM8A, led to a more prominent downregulation of one of the fluorescent reporters, but this regulation was independent of the promoter driving the expression of the reporter. However, acute protein depletion experiments in combination with nascent RNA sequencing (4sU-Seq) revealed, that mainly cytosolic ribosomal proteins (CRPs) were downregulated upon acute RBM8A withdrawal. ChIP experiments showed RBM8A binding to promoters of RP genes, but also to other chromatin regions. Total POL II or elongating and initiating POL II levels were not altered upon acute RBM8A depletion.

These data provide a starting point for further research on the mechanisms of transcriptional regulation of RP and RiBi genes in mammals.

2 Zusammenfassung

Zelluläres Wachstum und Proliferation zählen zu den wichtigsten Prozessen für Zellen und Organismen. Eine der größten Determinanten dieser Prozesse ist die Menge an Proteinen und in der Konsequenz auch die Menge an Ribosomen. Deren Synthese erfordert mehrere hundert Proteine und vier verschiedene ribosomale RNA-Spezies, ist stark koordiniert und sehr energiefordernd. Dennoch sind die molekularen Mechanismen der transkriptionellen Regulation der beteiligten protein-kodierenden Gene in Säugetieren nur schlecht verstanden.

In dieser Arbeit wurden hypothesenfreie genomweite Knockout-Reporterscreens mit dem Ziel durchgeführt, bisher unbekannte transkriptionelle Regulatoren von ribosomalen Biogenesefaktoren (RiBis), welche wichtig für den Zusammenbau und die Reifung der Ribosomen sind, und ribosomalen Proteinen (RPs), welche selbst ribosomale Bestandteile sind, zu identifizieren. Durch diesen Ansatz und nachfolgende (Validierungs-)Experimente, konnten unter anderem ALDOA und RBM8A als Regulatoren ribosomaler Biogenese identifiziert werden.

Eine Depletion des glykolytischen Enzyms ALDOA führte sowohl zu einer Herunterregulation von RiBi- und RP-Promotor-gesteuerten Reportern auf Protein- und Transkriptebene, als auch zu einer Herunterregulation von ribosomalen Biogenesegentranskripten und von mRNAs anderer für die Proliferation wichtiger Gene.

Eine Reduktion der Menge des Exon-Junction-Komplexproteins RBM8A führte zu einer deutlicheren Herunterregulation eines der beiden fluoreszierenden Reporter, aber diese Regulation war unabhängig vom Promotor, der die Expression des Reporters steuert. Akute Proteinabbauexperimente in Verbindung mit einer Sequenzierung naszenter RNA (4sU-Seq) zeigten allerdings, dass hauptsächlich zytosolische ribosomale Proteine (CRPs) nach akuter RBM8A-Depletion herunterreguliert waren. ChIP-Experimente zeigten RBM8A-Bindung an Promotoren von RP-Genen, aber auch an andere Chromatinregionen. Gesamt-POL II- oder elongierende und initiierende POL II-Mengen waren nach akuter RBM8A-Depletion nicht verändert.

Diese Daten stellen einen Ausgangspunkt für weitere Forschung zu den Mechanismen transkriptioneller Regulation von RP- und RiBi-Genen in Säugetieren dar.

3 Introduction

3.1 Cellular growth and proliferation are coupled to energy-demanding ribosome biogenesis

For multicellular organisms, growth and proliferation of cells are essential throughout the whole lifespan of an organism. In order to grow, cells need to synthesize huge amounts of proteins, which in turn are produced by ribosomes. Hence, a large proportion of a cell's energy is spent on ribosome biogenesis, the process needed to build ribosomes [Mayer and Grummt, 2006]. In fact, about 7500 ribosomes are synthesized every minute in a proliferating HeLa cell [Mayer and Grummt, 2006]; with the existence of 80 ribosomal proteins (RPs) [Gilles et al., 2020], this would correspond to about 600.000 RP molecules. Moreover, during the same amount of time, about 2×10^6 functional proteins are produced in total [Yewdell, 2001], illustrating that RP production accounts for up to 30% of all protein biosynthesis events.

Moreover, RPs alone are not sufficient to produce functional ribosomes. More than 200 ribosome biogenesis factors (RiBis) are needed for the maturation and assembly of ribosomes and their expression needs to be coordinated with RP and rRNA production. In line with the energy-demanding expression of sufficient amounts of RiBis and RPs, rRNA synthesis also poses a huge energetic effort to cells: rRNA constitutes the dominant RNA species, accounting for about 80% of total RNA amount in mammalian cells [Lodish et al., 2000]. These numbers strongly indicate, that proliferating cells depend heavily on ribosome biogenesis.

3.2 Components of ribosomes

Two distinct ribosomes exist in mammals: the (cyto)ribosome and the mitoribosome, which are located in the cytoplasm and in the mitochondrial matrix, respectively [Pecoraro et al., 2021]. The human 55S mitoribosome is needed for the translation of the thirteen mitochondrially-encoded genes required for ATP synthesis [Li et al., 2021]. This thesis, however, mainly focuses on the cytoribosome, hereafter called ribosome. The human 80S ribosome comprises of a large 60S subunit and a small 40S subunit with

a total of about 80 ribosomal proteins (RPs) and four different species of ribosomal ribonucleic acid (rRNA) [Natchiar et al., 2017]. The large subunit contains the 5S, 5.8S and 28S rRNAs, as well as numbered ribosomal proteins specific to the large subunit (named RPLs), whereas the small subunit contains 18S rRNA and numbered ribosomal proteins specific to the small subunit (named RPS') [Natchiar et al., 2017]. The catalytic reaction of the amino acid linkage is performed by the peptidyl transferase, a ribozyme placed in the large subunit [Moore and Steitz, 2011].

3.3 Ribosome biogenesis

Ribosome biogenesis involves the action of all three RNA polymerases. RNA Polymerase II transcribes RiBis, RPs and small nucleolar RNAs (snoRNAs) [Kufel and Grzechnik, 2019], the latter being involved in the modification and maturation of rRNAs within the context of small nucleolar ribonucleoprotein particles (snoRNPs) [Ellis et al., 2010]. In mammals, RNA polymerase I (POL I) transcribes the long 47S pre-rRNA precursor molecules from several hundred tandemly repeated ribosomal DNA (rDNA) clusters in the nucleolus [Henras et al., 2015]. The 27S pre-rRNA precursor is further processed into 18S, 5.8S and 28S rRNA [Cory and Adams, 1977, Kominami et al., 1981, Gonzalez and Sylvester, 1995, Mullineux and Lafontaine, 2012]. RNA polymerase III (POL III) is needed for the transcription of 5S rRNA [Sakonju et al., 1980, Bogenhagen et al., 1980, Turowski and Tollervey, 2016], as well as tRNAs and other RNAs needed for ribosome biogenesis [Canella et al., 2010]. The 5S rRNA precursor is transcribed from multiple gene copies close to the nucleolus [Fedoriw et al., 2012].

rRNA precursors are cleaved and further modified by snoRNPs, as already mentioned above. 136 sites of rRNA modification were found [Natchiar et al., 2017], comprising of 2'-O-methylation at riboses, pseudouridylation [Sloan et al., 2017] and other base modifications [Natchiar et al., 2017]. They are catalyzed by two different classes of snoRNPs, box H/ACA and box C/D snoRNPs [Sloan et al., 2017]. The snoRNAs within these complexes base-pair with rRNA, while the proteins catalyze the modification reaction on the rRNA molecules [Sloan et al., 2017]. One example of an important ribosomal biogenesis factor that associates with C/D box snoRNAs is the class I methyltransferase fibrillarin (FBL) [Yu et al., 2018], which catalyzes the site-specific transfer of a methyl group from S-Adenosyl methionine to a ribose 2'-hydroxyl group in its target rRNA [Smith and Steitz, 1997, Bratkovič et al., 2020].

The mRNAs encoding cytosolic and mitochondrial ribosomal proteins (CRPs and MRPs, respectively) are translated in the cytoplasm and the produced proteins are then imported into the nucleus or the mitochondrion, where they assemble with the (pre-)rRNAs [Pecoraro et al., 2021]. The final maturation and assembly of cytosolic ribosomes, however, takes place in the cytoplasm [Pecoraro et al., 2021].

In figure 3.1 the important steps of ribosome biogenesis are highlighted.

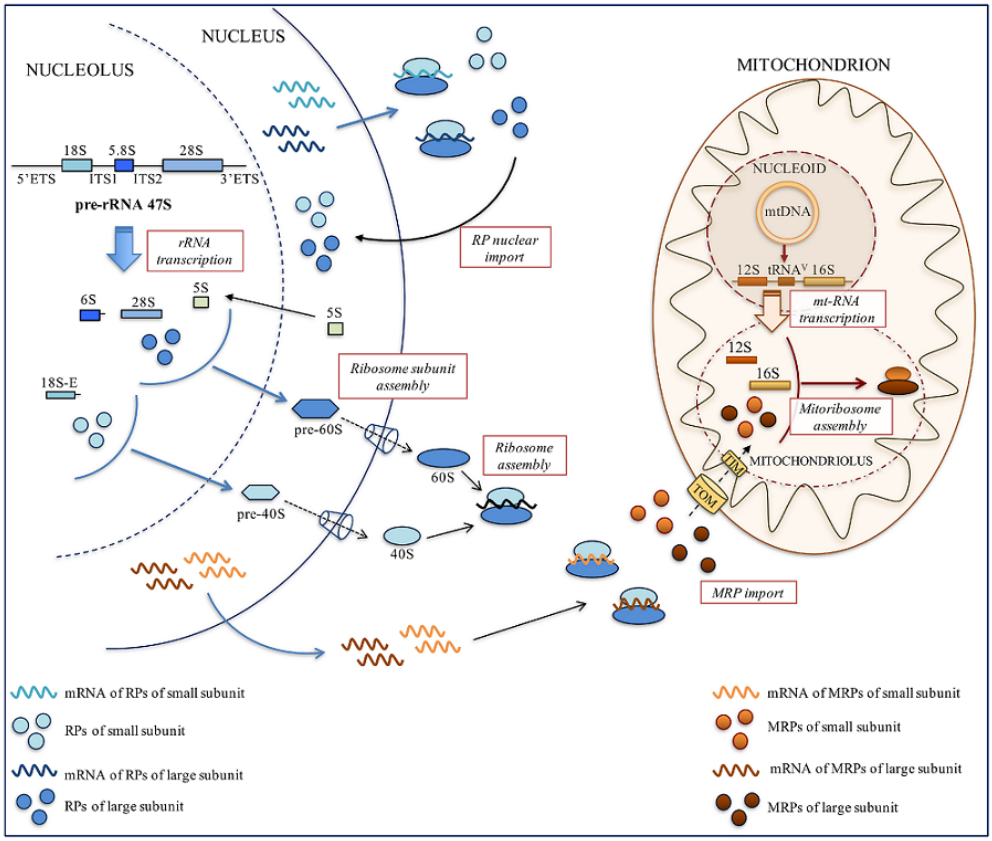

Figure 3.1: Scheme of eukaryotic cytoribosome and mitoribosome biogenesis. POL I transcribes a long precursor RNA (47S rRNA) containing the 18S, 5.8S, 28S rRNA, the 5' and 3' external transcribed spacers (ETS) and the internal transcribed spacers (ITS1 and ITS2) in the nucleolus. RiBis modify and cleave the precursor transcript. POL III transcribes 5S rRNA in the nucleus. POL II transcribes RiBi and RP genes. CRPs and RiBis are translated in the cytoplasm and transported back into the nucleus. CRPs assemble with pre-rRNAs in the nucleus to form the small and the large pre-ribosomal subunits (pre-40S and pre-60S, respectively), which are then exported and finally assembled to mature ribosomes in the cytoplasm with the help of RiBis. Similarly, MRPs are transcribed by POL II in the nucleus, translated in the cytoplasm and imported into the mitochondrion, where they assemble with mitochondrially encoded mitochondrial rRNA (mt-rRNA). From [Pecoraro et al., 2021], CC-BY 4.0.

Taken together, ribosome biogenesis is a highly energy-demanding process involving many proteins and RNAs, that are transcribed by all three RNA polymerases in a strongly regulated and coordinated manner.

3.4 Regulation of ribosome biogenesis

Since protein production and ribosome biogenesis are particularly important for growth and proliferation, cells need to be able to rapidly adjust the synthesis of ribosomes to environmental changes that favor or disfavor growth. Important pathways, that can become activated or repressed upon such stimuli, are for example the Hippo pathway [Judson et al., 2012] or the phosphatidylinositol-3-kinase (PI3K)/AKT/mammalian target of rapamycin (mTOR) pathway [Yang et al., 2019, Iadevaia et al., 2014]. The mTORC1 complex consists of mTOR, the catalytic kinase subunit, RAPTOR and mLST8 [Zhou and Huang, 2010], with mTOR being considered a master regulator of growth and proliferation [Iadevaia et al., 2014].

3.4.1 mTORC1 regulates ribosome biogenesis on a translational and on a transcriptional level

Mechanistically, mTORC1 activation leads to increased translation of mRNAs containing a 5' terminal oligopyrimidine tract (5' TOP) sequence [Thoreen et al., 2012, Meyuhas, 2000], which is a common feature of mRNAs encoding proteins of the translational apparatus [Meyuhas, 2000]. The 5' TOP sequence is defined more precisely by a "C" at the +1 position and pyrimidines at the positions from -1 to +4 [Yamashita et al., 2008]. A large fraction of mRNAs containing the 5' TOP motif are RP genes [Philippe et al., 2020].

However, mTORC1 does not only promote the translation of RPs, but also their transcription [Rosario et al., 2020], as well as the transcription of RiBis [Chauvin et al., 2014] and rRNAs [Hannan et al., 2003], highlighting the important function of mTORC1 in the regulation of ribosome biogenesis.

In more detail, rRNA transcription in mammals is regulated by mTORC1 via activation of its downstream target ribosomal protein S6 kinase 1 (S6K1) and subsequent regulation of upstream binding factor (UBF) phosphorylation, which influences the interaction with selective factor 1 (SL1), a basic rRNA transcription factor [Hannan et al., 2003]. Moreover, mTOR binds to POL III-dependent gene promoters and influences transcription of the respective genes, presumably via TFIIIC and MAF1 binding [Kantidakis et al., 2010].

Transcriptional regulation of RiBis by mTORC1 occurs via activation of S6K1 and S6K2 [Chauvin et al., 2014], whereas mechanistic details for the transcriptional regulation of RP genes by mTORC1 [Rosario et al., 2020] are still missing.

3.4.2 MYC is a regulator of all three RNA polymerases

In addition to mTORC1 as a key regulator of ribosome biogenesis, one of the transcription factors majorly influencing ribosome biogenesis by regulating transcription from all three RNA polymerases in mammals is MYC [Campbell and White, 2014, Lorenzin et al., 2016] (see scheme in figure 3.2A). MYC binds to POL I/III promoters and regulates rRNA transcription [Arabi et al., 2005, Grandori et al., 2005, Gomez-Roman et al., 2003], presumably due to its interaction with the SL1 complex at POL I-dependent gene promoters [Grandori et al., 2005] and TFIIIB at POL III-dependent promoters [Gomez-Roman et al., 2003]. Potentially, TFIIIB may also play a role in recruitment or stabilization of MYC at POL III-dependent promoters, since MYC's canonical E-box recognition motif "CACGTG" [Blackwell et al., 1990, Nair and Burley, 2003] is mostly missing at these sites [Gomez-Roman et al., 2003, Gallant and Steiger, 2009]. In addition to POL I/III-target genes, MYC indirectly regulates rRNA transcription by inducing the expression of POL I/III subunits and of POL I/III-specific transcriptional co-activators [Campbell and White, 2014, Grewal et al., 2005].

MYC also regulates the expression of RPs and RiBis [Lorenzin et al., 2016]. In fact, they are among the most strongly downregulated genes upon depletion of MYC [Lorenzin et al., 2016]. However, although both are high-affinity (meaning that low concentrations of MYC are still able to occupy these promoters efficiently), core MYC target gene sets [Lorenzin et al., 2016, Ji et al., 2011], the mechanism how MYC regulates RiBis and RPs is expected to be different, since MYC's canonical E-box recognition motif is very common in RiBi genes [Brown et al., 2008], but absent in the promoters of many RP genes, as revealed by an analysis performed by Elmar Wolf. In this analysis, the high-affinity MYC target genes with or without canonical E-box sequence in their respective promoters were analyzed for gene ontology (GO) terms. Genes without canonical E-box were enriched in ribosomal protein genes, but not RiBi genes (see figure 3.2B). This observation suggests, that similar to POL III-target genes, MYC might interact with a yet unknown factor at RP promoters, which may recruit or stabilize MYC at the respective sites (see purple box and question mark in figure 3.2A).

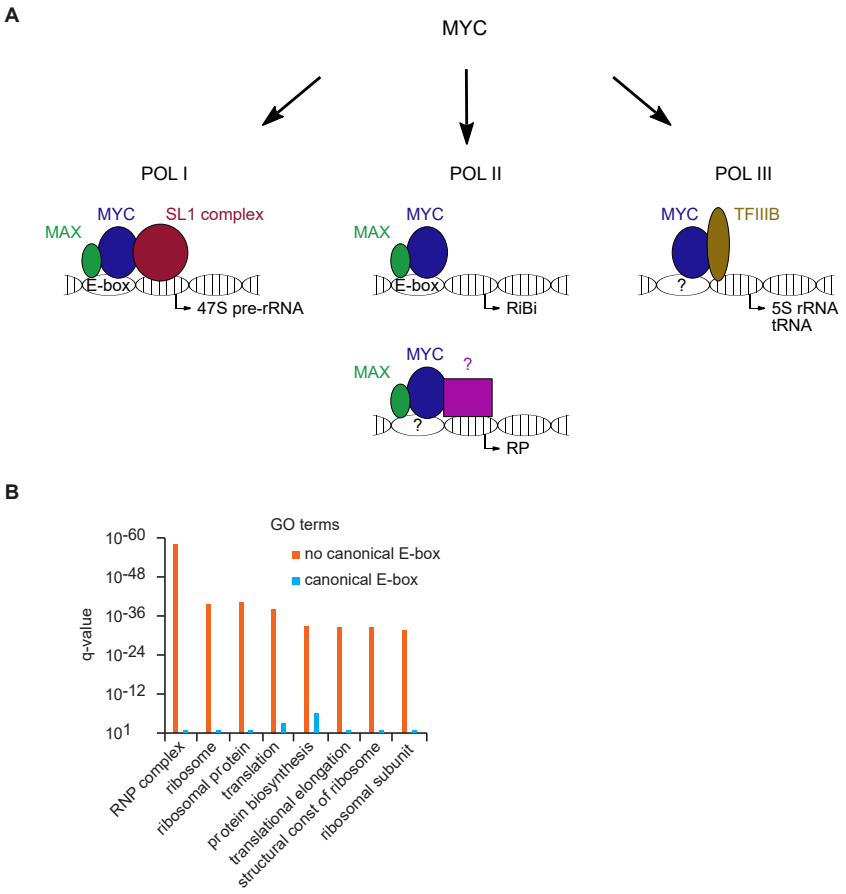

Figure 3.2: MYC regulates transcription from all three RNA polymerases through interaction with various proteins and binding activity does not strictly depend on the occurrence of its canonical E-box recognition motif. (A) Models of MYC binding to POL I/II/III-target gene promoters. Interacting proteins are depicted. ? = unknown interacting partner or binding motif. (B) Gene ontology (GO) term analysis of the high-affinity MYC target gene promoters without E-boxes. The indicated GO terms are enriched in ribosomal protein (RP) genes. This subpanel was modified from Elmar Wolf with permission.

3.5 Transcription factors regulating ribosome biogenesis are not well conserved from yeast to mammals

As described above, mTORC1 and MYC play major roles in the regulation of ribosome biogenesis. But which other proteins are involved in this complex process? Of special interest to us was our observation, that RiBi and RP genes appear to be regulated via different mechanisms (see subsection 3.4.2), although both gene sets are required at the same time, in large amounts and in a very tightly coordinated manner. It is conceivable, that the occurrence or absence of an E-box for instance, may contribute to the binding of different transcription factors and co-activators that may fine-tune transcrip-

tion from RiBi and RP promoters to balance production of ribosomal components. To my knowledge, however, no specific regulators of RiBi or RP genes have been found in mammals so far, in contrast to the model organism *Saccharomyces cerevisiae* (yeast). Studies in yeast discovered, that some transcription factors, that are regulated downstream of Torc1[1] for instance, appear to be specific regulators of RiBi or RP genes (see figure 3.3). Examples for RP-specific regulators are Fhl1 and Ifh1 among others [Jorgensen et al., 2002, 2004, Shore et al., 2021], whereas Dot6 and Tod6 are involved in RiBi-specific regulation downstream of Torc1 activity [Lippman and Broach, 2009]. Nevertheless, there are also transcription factors, that are involved in the regulation of both, RiBis and RPs, such as the zinc-finger protein Sfp1 [Lempiäinen and Shore, 2009]. Notably, MYC is considered to be the functional homologue of Sfp1 in mammals [Lempiäinen et al., 2009].

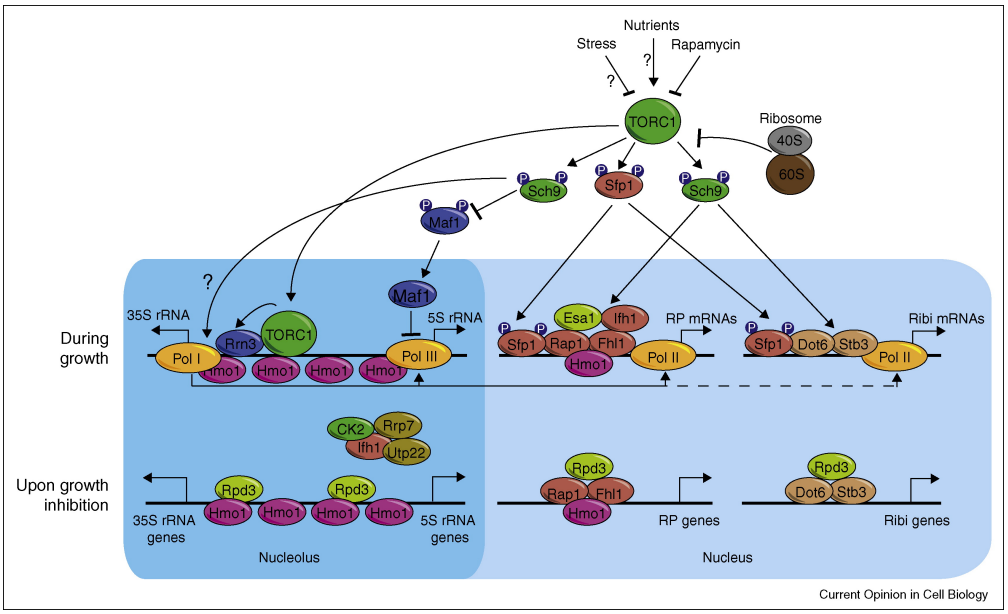

Figure 3.3: TORC1-mediated transcriptional regulation of RiBis and RPs in *Saccharomyces cerevisiae*. Different external stimuli can modulate TORC1 activity. Positive signals, such as mitogens or nutrients can activate TORC1 signaling (upper panel), resulting in promoter-specific transcription factor binding. Additionally, POL I influences POL II and POL III transcription, as indicated by arrows. The lower panel indicates promoter occupancies upon conditions that disfavor growth. A feedback mechanism exists between ribosome function and TORC1 activity. The scheme does not reflect the full regulatory network. From [Lempiäinen and Shore, 2009] with permission.

However, transferring knowledge about (differential) transcriptional regulators of ribosome biogenesis from yeast to mammals is difficult for several reasons:

(i) There is generally little RP promoter sequence and transcription factor motif conser-

[1] Yeast gene and protein names start with a capital letter followed by lower case letters with gene names being italicized.

vation in RP promoters across distant species [Hu and Li, 2007, Perina et al., 2011].
(ii) Some yeast proteins implicated in ribosome biogenesis have no obvious mammalian homologue, such as Ifh1 (as determined by a Blast search[2]).
(iii) About one third of human ribosome biogenesis factors have different or extra functions in ribosome biogenesis than their yeast counterparts [Tafforeau et al., 2013].

Taken together, there is a need for more research on the transcriptional mechanisms driving coordinated RP and RiBi production.

3.6 Sequence motifs in ribosomal protein gene promoters

First insights towards possible transcriptional regulators of RiBis or RPs were gained by bioinformatic analyses of the respective promoter sequences [Brown et al., 2008, Perry, 2005]. As described above, RiBi gene promoters often contain E-box sequences. However, this motif is not enriched in RP gene promoters. One of the sequence motifs, that is found in mammalian RP gene promoters, is located approximately 62 base pairs (bp) downstream of the TSS in the first intron and is called localized tandem sequence motif (LTSM) [Roepcke et al., 2011]. Several other motifs are enriched in the promoters of human RP genes, such as SP1, GABP or YY1 binding sites [Perry, 2005]. One additional important sequence motif shared by basically all human ribosomal protein gene promoters is the polypyrimidine tract initiator motif placed around the transcription start site (TSS) [Perry, 2005], which encloses the 5' TOP sequence, that was already introduced above. Besides translation, the presence of this motif may also lead to increased levels of transcription of the respective gene itself, as shown for the elongation factor 1A-1 (eEF1A-1) [Shibui-Nihei et al., 2003]. All the data presented so far suggest and indicate, that different mechanisms of regulation of ribosome biogenesis evolved in mammals, which are still not fully understood [Zencir et al., 2020].

[2]https://blast.ncbi.nlm.nih.gov/Blast.cgi?PAGE=Proteins (October 18, 2021)

3.7 Deregulated ribosome biogenesis and associated diseases

With hundreds of proteins involved, ribosome biogenesis generally is a tightly regulated and coordinated process. However, imbalances in this process may occur, leading to cell cycle arrest and apoptosis [Turi et al., 2019] and to diseases such as ribosomopathies [Narla and Ebert, 2010] or cancer [Turi et al., 2019]. Ribosomal imbalance, e.g. due to defects in rRNA processing or transcription, may lead to reduced mature rRNA production and subsequently an accumulation of free ribosomal proteins, which cannot be assembled into functional ribosomes. Free RPL5 or RPL11 can then bind to MDM2, an E3 ligase required for efficient degradation of the tumor suppressor p53. Binding of these RPs to MDM2 blocks MDM2's ability to induce p53 degradation, with stabilized p53 promoting cell cycle arrest and apoptosis. The aforementioned process is described in detail in [Bursac et al., 2014] and is often referred to as the impaired ribosome biogenesis checkpoint (IRBC) [Turi et al., 2019].

Mutations in ribosome biogenesis or ribosomal protein genes lead to reduced ribosome biogenesis, which may lead to diseases such as ribosomopathies [Turi et al., 2019]. Patients show tissue-specific defects and abnormalities, which are caused by p53-dependent and -independent processes [Danilova and Gazda, 2015]. Examples for ribosomopathies are Diamond-Blackfan anemia (DBA) or Treacher-Collins syndrome (TCS) [Nakhoul et al., 2014]. DBA for example is caused in the majority of cases by mutations in ribosomal protein genes [Nakhoul et al., 2014] and TCS is mostly caused by mutations in the *TCOF1* gene, which is involved in rRNA transcription and processing [Nakhoul et al., 2014]. Clinical features of ribosomopathies involve craniofacial abnormalities, anemia or elevated risks of cancer, among others [Narla and Ebert, 2010]. However, there is a broad range of clinical manifestations within each ribosomopathy, even among patients with mutations in the same genes [Willig et al., 1999, Teber et al., 2004]. Possible explanations for the varying degrees of manifestation of the diseases and the tissue-specific clinical defects may be additional functions of RPs outside their role in ribosomes (as described above for RPL5 and RPL11, for instance) or altered translation of selective mRNAs [Armistead and Triggs-Raine, 2014]. Indeed, translation of specific mRNAs can be differentially regulated by varying ribosome compositions [Genuth and Barna, 2018].

On the other hand, deregulated ribosome biogenesis may also lead to diseases such as cancer, with evidence for ribosomomal proteins appearing to act as proto-oncogenes

[Zhang et al., 1997, Kitahara et al., 2001] or as tumor suppressors with compromised activity when their levels are reduced[Amsterdam et al., 2004]. An example for a ribosomal protein gene that may serve as a proto-oncogene is *RPL24*. Mice overexpressing MYC in B cells showed an increased risk of lymphomagenesis due to increased protein synthesis, which could be reduced upon heterozygous knockout of *RPL24* [Barna et al., 2008]. In contrast, overexpression of *RPL11*, a target gene of MYC, represses MYC function and controls MYC protein levels through a negative feedback loop [Dai et al., 2007].

All in all, these data imply, that imbalanced ribosome production in either direction may promote cancer formation as well as other diseases. Thus, a detailed understanding of the basic mechanisms regulating ribosome biogenesis in mammals is needed, with this thesis identifying transcriptional regulators of RiBi and RP genes.

3.8 Scalable gene editing as a tool for targeted knockouts and knock-ins

In order to identify genes involved in certain processes, techniques modulating the expression of a large number of genes and measuring their impact on a phenotype, have been successfully applied. These genetic screens have helped elucidate processes such as ribosome biogenesis [Wild et al., 2010] or oxidative phosphorylation [Arroyo et al., 2016]. During the last years, the clustered regularly interspaced short palindromic repeat-associated 9 nuclease (CRISPR/Cas9) genetic tool was developed, allowing unbiased, genome-wide knockout screens [Sanjana et al., 2014]. With the help of complementary guide RNAs, the endonuclease Cas9 can localize to specific DNA sequences of interest and induce double-strand breaks (DSBs), which need to be repaired by the cellular DNA repair pathways [Li et al., 2020]. During this repair, errors may be introduced, that potentially destroy gene function due to deletions, missense or nonsense mutations for example. However, gene editing also enables the insertion of a sequence of interest into a specific locus via the homology-directed repair (HDR) mechanism, when a corresponding HDR DNA template is offered to the cells by the investigator.

As depicted in figure 3.4, a designable 20 bp sequence of a single guide RNA (sgRNA) binds to the target locus and recruits Cas9 [Ran et al., 2013]. The target sequence must be directly adjacent to the 5'-NGG protospacer adjacent motif (PAM) sequence,

which is recognized by the CRISPR/Cas9 system, and the DSB occurs about three bp upstream of this PAM motif [Ran et al., 2013].

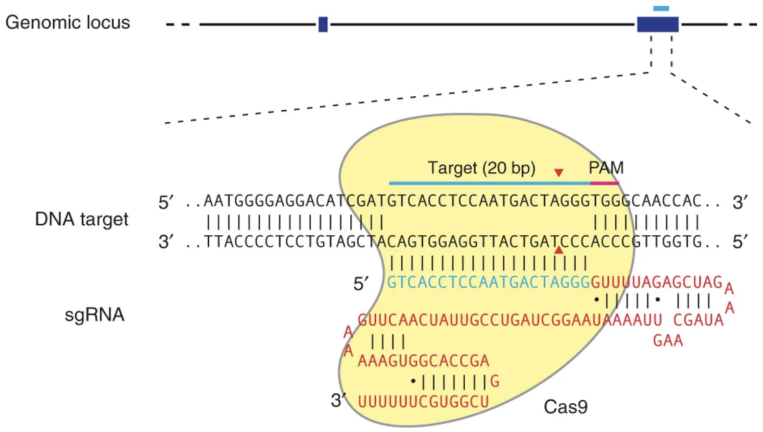

Figure 3.4: Cas9 is targeted to a specific genomic loci via an sgRNA. The sgRNA consists of 20 nucleotides (blue), which base pair with the genomic DNA (the human *EMX1* gene is shown as an example), and a scaffold (red). The base pairing part of the sgRNA binds directly adjacent to an obligate PAM site ("NGG" motif) in the genome (pink) and the double-strand break is then performed by the Cas9 protein approx. three bp upstream of this PAM site (red arrow heads). From [Ran et al., 2013] with permission.

In this thesis, CRISPR/Cas9 was used to knockout individual genes within a genome-wide screen and for validation experiments, but also to generate cell lines, in which one allele of a gene was replaced by a reporter or to homozygously introduce tags N-terminally of a gene of interest.

3.9 Objectives

Ribosomes biogenesis is a process, that involves several hundred proteins and the coordinated expression of all three RNA polymerases. A tight and balanced regulation of the involved genes is required in order to enable growth and proliferation and to prevent cell cycle arrest, apoptosis and cancer development. Detailed knowledge of the mechanisms regulating ribosome biogenesis is thus needed to enable the development of novel therapeutics for cancer and ribosomopathies. However, substantial knowledge is missing with regard to the transcriptional regulation of RP and RiBi genes in mammals, partially because the mechanisms cannot easily be transferred from yeast to mammals due to the lack of similar TF binding motifs in the promoters, different or additional functions of homologous proteins, and sometimes even the lack of identifiable homologous proteins, among other reasons. However, the occurrence of specific motifs in RP and RiBi promoters of mammals suggests, that these two gene sets, which are both transcribed by POL II, may also be transcriptionally regulated in mammals, potentially even by different proteins. To gain deeper insights into the regulation of RP and RiBi genes in mammals, we thus performed a genome-wide CRISPR/Cas9 knockout reporter screen on cells expressing a green fluorescent reporter under the control of a RiBi gene promoter and a red fluorescent reporter under the control of an RP gene promoter. Changes in the intensity of the fluorescent reporters upon knockout were expected to reflect a role of the knocked out gene in controlling expression of the respective set of genes. To this end, several things needed to be considered prior to the screen:

1.) The promoters needed to fulfill certain criteria in order to be considered suitable for the screen, e.g. they needed to be functional.
2.) The used fluorescent reporters had to be stable enough to cross a certain threshold of fluorescence intensity, while at the same time being just as stable as necessary to still be able to rapidly adjust to transcriptional changes.
3.) In order to increase chances of identifying hits with our screening strategy, a preliminary screen was performed to establish the protocol and to test, whether positive control sgRNAs (sgRNAs targeting the fluorescent reporters) could become enriched in the conditions they were expected to appear.

In a second step, after the screen was performed, resulting hits needed to be validated and characterized further. Potential problems, that occurred during the first screen,

could then be addressed in a second screen to increase the likelihood of finding new transcriptional regulators of RiBi and RP genes in mammals.

4 Materials

4.1 Consumables

Consumable	Manufacturer	Order number
Blotting paper (Whatman paper)	Hartenstein	GB40
Cell scraper	Sarstedt	83.3951/83.3952
Falcon 5 mL Round Bottom Polystyrene Tubes	Corning	352235
Falcon 14 mL Round Bottom High Clarity PP Tubes	Corning	352059
Immobilon-P PVDF Membrane	Merck	IPVH00010
MicroAmp EnduraPlate Optical 96-Well Fast Multicolor Reaction Plates with Barcode	Thermo Fisher Scientific	4483496
MicroAmp Fast Optical 96-Well Reaction Plate, 0.1 mL	Thermo Fisher Scientific	4346907
MilliTUBE 1ml AFA Fiber Case (1000)	Covaris	520131
Needles Sterican long bevel facet, 25 mm, 0.60 mm, blue	Carl Roth	C719.1
Neubauer improved counting chamber	Hartenstein	ZK06
Nitrile gloves	Starlab	SG-C-S
Paper filter	Carl Roth	CA20.1
Parafilm	Hartenstein	PF10
Pasteur pipettes	Carl Roth	4518.1
PCR tubes	Starlab	I1402-3700
5 ml glass pipettes	Avantor	612-1153
10 ml glass pipettes	Avantor	612-1154
25 ml glass pipettes	Avantor	612-1156
0.2 µm filter	Sarstedt	831.826.001

0.45 µm filter	Sarstedt	83.1826
1000 µl filter tips	Biozym	VT0260
200 µl filter tips	Starlab	S1120-8810-C
1.5 ml Low binding tubes	Biozym	710176
1000 µl pipette tips	Starlab	S1111-6001-C
200 µl pipette tips	Starlab	S1111-1006-C
10 µl pipette tips	Sarstedt	701116100
5 ml plastic pipettes	Greiner Bio-One	606180
10 ml plastic pipettes	Greiner Bio-One	607180
25 ml plastic pipettes	Greiner Bio-One	760180
96-well plates	VWR/Thermo Fisher Scientific	734-2097
24-well plates	Greiner Bio-One	662160
12-well plates	Greiner Bio-One	665180
6-well plates	Greiner Bio-One	657160
6 cm plates	VWR/Thermo Fisher Scientific	734-2040
10 cm plates	Greiner Bio-One	664160
10 cm plates (for HEKs and MEFs)	VWR/Thermo Fisher Scientific	734-2043
15 cm plates	Greiner Bio-One	639160
1.5 ml reaction tube	Sarstedt	72706
2 ml reaction tube	Sarstedt	72695500
15 ml reaction tube	Greiner Bio-One	188271-N
50 ml reaction tube	Greiner Bio-One	227261

Table 4.1: List of used consumables.

4.2 Equipment

Equipment	Manufacturer
AxioVert A1 Microscope	Zeiss
Axiovert 40 CFL Microscope	Zeiss
BBD 6220 incubator	Heraeus
BD FACS Aria III	BD Biosciences
BD FACSCanto II	BD Biosciences
Casy cell counter	Innovatis
Centrifuge Avanti J-26 XP	Beckman Coulter
Centrifuge Galaxy MiniStar	VWR
Centrifuge Megafuge 40R	Heraeus
Centrifuge Multifuge 1S-R	Heraeus
Centrifuges 5417R / 5424 / 5430	Eppendorf
Consort EV231/EV243	Carl Roth
C1000 Thermal Cycler	Bio-Rad
Digital Sonifier S-250D	Branson Ultrasonics
Dry Bath Heating System (dual block)	Starlab
Dry Block Thermostat Bio TDB-100	Biosan
DynaMag-2 Magnet	Thermo Fisher Scientific
ED-5M water bath	Julabo
Experion	Bio-Rad
Fragment Analyzer	Advanced Analytical
Hamilton pipette (#7637-01)	Hamilton
HeraSafe sterile bench	Heraeus
Infinite 200 PRO Microplate Reader	Tecan
Laminair HB2448S	Heraeus
LAS-4000 mini	Fujifilm

MAGNUM EX Universal Magnet Plate (96-well)	Alpaqua
Mastercycler pro S	Eppendorf
Maxi UV fluorescent table	Peqlab
Memmert water bath	Memmert
Millipore Milli-Q Integral 15	Millipore
Mini-PROTEAN Tetra Cell	Bio-Rad
Mixer HC	Starlab
Multiskan Ascent plate reader	Thermo Labsystems
M220 Focused-ultrasonicator	Covaris
NanoDrop 1000	Thermo Fisher Scientific
NextSeq 500	Illumina
PerfectBlue Tank Electro Blotter Web S	Peqlab
Power Pac	Bio-Rad
StepOnePlus Real-time PCR System	Applied Biosystems
Thermomixer comfort	Eppendorf
Vortex-Genie 2	Scientific Industries

Table 4.2: List of used equipment.

4.3 Software and bioinformatic tools

Software	Developer (or source for online tools)
Affinity Designer	Serif Europe
ApE plasmid editor	M. Wayne Davis
BD FACSDiva v6.1.2	BD Biosciences
ExPASy	https://web.expasy.org/translate/
FlowJo v10	FlowJo, LLC
Fragment Analyzer Systems Software	Agilent Technologies

ImageJ	[Abràmoff]
ImageStudio Lite	LI-COR Biosciences
Integrated Genome Browser	[Freese et al., 2016]
LAS-4000 mini 2.1	Fujifilm
Mendeley Reference Manager	Elsevier
Microsoft Office	Microsoft
Model-based Analysis of Genome-wide CRISPR-Cas9 Knockout (MAGeCK) v0.5.7	[Li et al., 2014]
Multi Gauge	Fujifilm
NanoDrop 1000 3.8.1	Thermo Fisher Scientific
NCBI	https://www.ncbi.nlm.nih.gov/
R v4.1.0	R Core Team
RStudio v1.4.1717	RStudio
SnapGene Viewer	GSL Biotech LLC
StepOne Software	Applied Biosystems
Tecan i-control	Tecan
T_m calculator	`https://www.thermofisher.com/de/de/home/brands/thermo-scientific/molecular-biology/molecular-biology-learning-center/molecular-biology-resource-library/thermo-scientific-web-tools/tm-calculator.html`
UCSC Genome Browser	https://genome.ucsc.edu/

Table 4.3: List of used softwares used.

4.4 Chemicals

Chemical	Manufacturer	Order number
Agarose	Carl Roth	2267.4
Bicinchoninic acid solution	Sigma-Aldrich	B9643-1L
CutSmart Buffer	NEB	B7204S
Chloroform – isoamyl alcohol mixture (24:1)	Sigma	25666-500ML
Dimethylformamide (DMF)	Thermo Fisher Scientific	20673
Dimethyl sulfoxide (DMSO)	Sigma-Aldrich	41640-1L-M
Ethanol (EtOH)	Sigma-Aldrich	32205-2.5L-M
Ethidium bromide (1%)	Carl Roth	2218.1
GlycoBlue	Thermo Fisher Scientific	AM9516
Immobilon Western HRP Substrate	Merck	WBKLS0500
Isopropanol	Carl Roth	6752.4
Lipofectamine RNAiMAX Transfection Reagent	Thermo Fisher Scientific	13778-150
Phenol/Chloroform/Isoamyl alcohol	Carl Roth	A156.3
Pierce Dithiothreitol (DTT) No-Weigh-Format	Thermo Fisher Scientific	A39255
QIAzol Lysis Reagent	Qiagen	79306
Rotiphorese Gel 30	Carl Roth	3029.1
Sodium chloride (NaCl)	Carl Roth	9265.3
SYBR Green (10.000x concentrated) in DMSO	Thermo Fisher Scientific	S7563
Trichloromethane (Chloroform)	Carl Roth	6340.2
Vaseline	Carl Roth	5775.2

Table 4.4: List of chemicals used.

4.5 Solutions and buffers

Unless otherwise stated in table 4.5, all solutions and buffers were prepared in water and stored at RT.

Solution or buffer	Ingredients
10% Ammonium persulfate (APS)	0.1 g/ml APS aliquoted and stored at -20℃; storage at 4℃ after first usage
Annexin V binding buffer	2.5 mM $CaCl_2$ 10 mM HEPES (pH 7.4) 140 mM NaCl stored at 4℃
BCA Solution A	1% (w/v) BCA-N_2 2% (w/v) Na_2CO_3
BCA Solution B	4% (w/v) $CuSO_4$
Biotin-HPDP-DMF	1 mg/ml EZ-Link HPDP-Biotin in DMF (heated up to 37℃ for approx. 1 hour for dissolving)
2.5x Biotin labeling buffer	25 mM Tris (pH 7.4) 2.5 mM EDTA
3.5x Bis-Tris buffer	1.25 M Bis-Tris (pH set to 6.7 with HCl) stored at 4℃
Bis-Tris separation gel	8-12% (v/v) acrylamide:bisacrylamide solution (37.5:1) 0.05% (v/v) APS 1x Bis-Tris buffer (3.5x) 0.01% TEMED
Bis-Tris stacking gel	4% (v/v) acrylamide:bisacrylamide solution (37.5:1) 0.05% (v/v) APS 1x Bis-Tris buffer (3.5x) 0.01% TEMED
Blocking solution for WB	5% (w/v) milk powder in TBS-T filtered via paper filter

	stored at -20℃
Bradford reagent	0.01% (w/v) Coomassie Brilliant Blue G250 4.75% ethanol 8.5% phosphoric acid filtered via paper filter stored at 4℃ in darkness
BSA/PBS for IP/ChIP	5 mg/ml BSA in PBS sterile-filtered (0.2 µm) stored at 4℃
ChIP elution buffer	1% SDS 0.1 M $NaHCO_3$ prepared freshly before usage
ChIP lysis buffer 1	10 mM Glycine 85 mM KCl 0.5% NP-40 5 mM PIPES (pH 8) Phosphatase and protease inhibitors stored at 4℃
ChIP lysis buffer 2	1% (w/v) Deoxycholic acid sodium salt 1 mM EDTA 150 mM NaCl 1% NP-40 Phosphatase and protease inhibitors 0.1% Sodium dodecyl sulfate (SDS) 10 mM Tris/HCl (pH 7.5) stored at 4℃
ChIP wash buffer 1	2 mM EDTA 150 mM NaCl 0.1% SDS 20 mM Tris/HCl (pH 8.1) 1% Triton X-100 stored at 4℃

ChIP wash buffer 2	2 mM EDTA 500 mM NaCl 0.1% SDS 20 mM Tris/HCl (pH 8.1) 1% Triton X-100 stored at 4℃
ChIP wash buffer 3	1% (w/v) Deoxycholate sodium salt (Na-DOC) 1 mM EDTA 250 mM LiCl 1% NP-40 10 mM Tris/HCl (pH 8.1) stored at 4℃
Deoxynucleotide triphosphates (dNTPs)	10 mM mix of dNTPs from Carl Roth (K039.2) stored at -20℃
6x DNA loading buffer	10 mM EDTA (pH 8.0) 0.2% (w/v) Orange G (Thermo Fisher Scientific) 40% (w/v) Sucrose
Doxycycline (1 mg/ml)	50 mg Doxycycline in 50 ml ethanol aliquoted stored at -20℃
Dynabeads washing solution A	100 mM NaOH 50 mM NaCl
Dynabeads washing solution B	100 mM NaCl
2x Dynabeads washing buffer	2 M NaCl 10 mM Tris (pH 7.5) 1 mM EDTA 0.1% (vv) Tween-20
Ethylenediaminetetraacetic acid (EDTA)	0.5 M
Formaldehyde	37% (v/v) formaldehyde from Carl Roth (4979.1) sterile-filtered (0.2 µM)
Glycine	1 M

	sterile-filtered (0.2 µM) stored at 4℃
IP buffer	0.5 mM EDTA 10% Glycerol 20 mM HEPES (pH 7.9) 200 mM NaCl 0.2% NP-40 stored at 4℃
6x Laemmli sample buffer	0.06% (w/v) Bromophenol blue 40.4% (v/v) Glycerol 12% (w/v) SDS 60 mM Tris/HCl (pH 6.8) after dissolving 9.3% (w/v) DTT was added aliquoted stored at -20℃
2x Lysis buffer for extraction of genomic DNA (gDNA)	20 mM EDTA (pH 8.0) 200 mM NaCl 1% (w/v) SDS 20 mM Tris-HCl (pH 8.0) finally diluted to 1x during gDNA preparation (screening samples) or already used as a 1x dilution (knock-in cell clone analyses)
20x MES running buffer	20 mM EDTA 1 M MES 2% (w/v) SDS 1 M Tris base stored at 4℃
1x MES running buffer	1x MES running buffer (20x) 5 mM sodium bisulfite stored at 4℃
Miniprep solution 1	200 mM NaOH 1% SDS
Miniprep solution 2	11.5% (v/v) acetic acid

	3 M CH_3COOK stored at 4℃
20x MOPS running buffer	20 mM EDTA 1 M MOPS 2% (w/v) SDS 1 M Tris base stored at 4℃
1x MOPS running buffer	1x MOPS running buffer (20x) 5 mM sodium bisulfite stored at 4℃
Polyethylenimine (PEI)	6 mM HCl 0.09% PEI sterile-filtered (0.2 µM) stored at 4℃ (darkness)
Phosphate-buffered saline (PBS)	2.7 mM KCl 1.76 mM KH_2PO_4 137 mM NaCl 10.1 mM Na_2HPO_4 autoclaved
Polybrene (Hexadimethrinbromide, 4 mg/ml)	4 mg polybrene in H_2O sterile-filtered (0.2 µM) aliquoted and stored at -20℃
Primary antibody solution (WB)	5% (w/v) BSA 0.02% NaN_3 in TBS-T
RIPA	0.1% (w/v) Deoxycholate sodium salt (Na-DOC) 1 mM EDTA 50 mM HEPES (pH 7.9) 140 mM NaCl 0.1% SDS 1% Triton X-100 sterile-filtered (0.2 µM)

	stored at 4℃
RNase A (10 mg/ml)	100 mg RNase A in 27 µl 3 M sodium acetate (pH 5.2) + 9 ml H_2O; 450 µl aliquots 30 min, 100℃ (DNase inactivation) + 50 µl 1 M Tris (pH 7.4) per aliquot stored at -20℃
Sodium Acetate	3 M (ph 5.2) sterile-filtered (0.2 µM)
Sodium bicarbonate ($NaHCO_3$)	1 M
Sodium Chloride (NaCl)	5 M
Sodium dodecyl sulfate (SDS)	10% (w/v)
50x TAE	2 M Tris (pH 8.0) 5.7% (v/v) acetic acid 50 mM EDTA (pH 8.0)
20x Transfer buffer	500 mM Bicine 500 mM Bis-Tris 0.1 mM Chlorobutanol 20.5 mM EDTA stored at 4℃
1x Transfer buffer	40% (v/v) methanol 1x dilution of transfer buffer (20x) stored at 4℃
Tris buffer	1 M (pH 6.8-7.4)
20x Tris-buffered saline (TBS)	2.8 M NaCl 500 mM Tris (pH 7.4)
Tris-buffered saline-Tween (TBS-T)	1x TBS (20x) 0.2% (v/v) Tween-20
1x Tris-EDTA (TE)	10 mM Tris (pH 7.4) 1 mM EDTA (pH 8.0)
Trypsin solution	5 mM EDTA 125 mM NaCl

	22.3 mM Tris (pH 7.4) 0.25% Trypsin

Table 4.5: List of solutions and buffers used.

4.6 Antibiotics and other small molecules

Item	Final concentration/amount	Manufacturer	Order number
Ampicillin	100 µg/ml (sterile-filtered)	Carl Roth	K029.2
Carbenicillin	100 µg/ml (sterile-filtered)	Carl Roth	6344.3
Doxycycline	1 µg/ml	Sigma-Aldrich	D9891-1G
EZ-Link HPDP-Biotin	0.2 µg	Thermo Fisher Scientific	#21341
Indole-3-acetic acid (IAA or auxin)	500 µM	Sigma-Aldrich	I5148-2G
Phosphatase Inhibitor Cocktail 2	1:1000	Sigma-Aldrich	P5726-5ML
Phosphatase Inhibitor Cocktail 3	1:1000	Sigma-Aldrich	P0044-5ML
Protease Inhibitor Cocktail	1:1000	Sigma-Aldrich	P8340-5ML
Puromycin	2-3 µg/ml	InvivoGen	ant-pr-1
RiboLock RNase Inhibitor	160 U/ml	Thermo Fisher Scientific	EO0381
4-thiouridine (4sU)	2 mM	Merck	T4509-250MG

Table 4.6: List of used small molecules.

4.7 Bacterial strains and bacterial culture medium with supplements

4.7.1 Bacterial strains

Name	Genetics	Purpose
XL1 Blue	*Escherichia coli*, recA1 endA1 gyrA96 thi-1 hsdR17 supE44 relA1 lac [F proAB lacIqZ∆M15 Tn10 (Tetr)]	For usual cloning purposes
Endura ElectroCompetent Cells (BioCat, #60242-2-LU)	*Escherichia coli*, recA13 supE44 ara-14 galK2 lacY1 proA2 rpsL20(StrR) xyl-5 λ– leu mtl-1 F– mcrB mrr hsdS20(rB–, mB–)	Transformation of genome-wide libraries

Table 4.7: List of bacterial strains used.

4.7.2 Bacterial culture media

Name	Ingredients
LB agar	LB medium 1.2% (w/v) Agar-Agar heated up until Agar-Agar was dissolved and cooled down to about 50℃, before antibiotics were added
LB medium	1% (w/v) NaCl 10% (w/v) Trypton/Pepton 0.5% (w/v) Yeast extract antibiotics were added freshly

Table 4.8: List of bacterial culture media used.

4.8 Kits, ladders, enzymes, beads

4.8.1 Kits

Kit	Manufacturer	Order number
CloneJET PCR Cloning Kit	Thermo Fisher Scientific	K1232
Experion DNA 1K Analysis Kit	Bio-Rad	700-7307
FastAP Thermosensitive Alkaline Phosphatase	Thermo Fisher Scientific	EF0654
GeneJET Gel Extraction Kit	Thermo Fisher Scientific	K0692
MaXtract high density tubes (200 x 1,5 ml)	Qiagen	129046
miRNeasy MiniKit (50)	Qiagen	217004
M-MLV Reverse Transcriptase	Promega	M1705
NEBNext Multiplex Oligos for Illumina (Dual Index Primers Set 1)	NEB	E7600S
NEBNext Poly(A) mRNA Magnetic Isolation Module	NEB	E7490
NEBNext rRNA Depletion Kit (Human/Mouse/Rat)	NEB	E6310
NEBNext Ultra II Directional RNA Library Prep Kit for Illumina	NEB	E7760
NGS Fragment High Sensitivity Analysis Kit, 1-6.000 bp	Agilent Technologies	DNF-474-0500
Phusion High-Fildelity DNA Polymerase	Thermo Fisher Scientific	F530L
PowerUp SYBR Green Master Mix	Thermo Fisher Scientific	A25742
PureLink HiPure Plasmid Maxiprep Kit	Thermo Fisher Scientific	K210007
Quant-iT RiboGreen RNA Assay Kit	Life Technologies GmbH	R11490
RNase-Free DNase Set (50)	Qiagen	79254
RNeasy MinElute Cleanup Kit (50)	Qiagen	74204
RNeasy Mini Kit (250)	Qiagen	74106
T4 DNA Ligase (5 U/µl)	Thermo Fisher Scientific	EL0014

Table 4.9: List of kits used.

4.8.2 Ladders and loading buffers

Ladder	Manufacturer	Order number
Color Prestained Protein Standard, Broad Range (11–245 kDa)	NEB	P7712
GeneRuler 1 kb Plus DNA Ladder	Thermo Fisher Scientific	SM1331
PageRuler Prestained Protein Ladder, 10 to 180 kDa	Thermo Fisher Scientific	26617

Table 4.10: List of DNA and protein ladders used.

4.8.3 Enzymes

Enzyme	Manufacturer	Order number
AgeI-HF	NEB	R3552L
BamHI-HF	NEB	R3136S
BbsI-HF	NEB	R3539L
BsmBI	NEB	R0580L
EcoRI-HF	NEB	R3101L
KpnI-HF	NEB	R3142L
MluI-HF	NEB	R3198L
NotI-HF	NEB	R3189L
Proteinase K (stock 10 mg/ml)	Carl Roth	7528.2
RNase A (stock 10 mg/ml)	Carl Roth	7156.1
SpeI-HF	NEB	R3133L
XhoI	NEB	R0146S
Trypsin (2.5%)	Thermo Fisher Scientific	15090-046
T4 PNK	NEB	M0201S

Table 4.11: List of enzymes used.

4.8.4 Beads

Beads	Manufacturer	Order number
Agencourt AMPure XP Beads	Beckman Coulter	A63881
Dynabeads MyOne Streptavidin T1	Thermo Fisher Scientific	65601
Dynabeads Protein A	Thermo Fisher Scientific	10002D
Dynabeads Protein G	Thermo Fisher Scientific	10004D

Table 4.12: List of beads used.

4.9 Nucleic acids

4.9.1 Oligos used for cloning

Primers needed to amplify the murine RiBi and RP promoters

The following table 4.13 lists the primer sequences used for PCRs to amplify promoter fragments of different lengths. For each gene, the corresponding "[...]_800_R" primer was always used as the reverse primer for all the amplifications of the corresponding gene promoter fragments.

Name	Sequence (5'-3')
EW_828_Repo_Rpl21_800_R	ttaACCGGTCTGGAAGATGGCTGCGG
EW_829_Repo_Rpl21_500_F	ccgACCGGTactgcatatgtggaatgacg
EW_831_Repo_mRpl22_800_F	ccgCTCGAGactgtgtctttgtttcaaaacca
EW_832_Repo_mRpl22_800_R	ttaACCGGTCGCCATGCTGAGCCCTA
EW_833_Repo_mRpl22_500_F	ccgCTCGAGtagtctgtttctgtttatgggactaac
EW_834_Repo_mRpl22_200_F	ccgCTCGAGctgccctttttcaggctgttat
EW_835_Repo_mRps17_800_F	ccgCTCGAGcatgaaagaaaagcccttggc
EW_836_Repo_mRps17_800_R	ttaACCGGTCTCCGGAGTCCACCACAAG
EW_837_Repo_mRps17_500_F	ccgCTCGAGcggaggcaaggcagatgta
EW_838_Repo_mRps17_200_F	ccgCTCGAGatctattgcagtgcctataaaaaaaga

EW_840_Repo_Rpl18_800_R	ttaACCGGTCATGATGGCGCCTCCTG
EW_841_Repo_Rpl18_500_F	ccgCTCGAGctcgggtgagagatctagtagga
EW_842_Repo_Rpl18_200_F	ccgCTCGAGccgggtcccagcccttt
EW_843_Repo_rrs1_800_F	ccgCTCGAGtgtgacaagacaaaaaaaccaacc
EW_844_Repo_rrs1_800_R	ttaACCGGTCATGGCTCTCGCTGCG
EW_845_Repo_rrs1_500_F	ccgCTCGAGatcacaggaacaaacaatggc
EW_846_Repo_rrs1_200_F	ccgCTCGAGccccacagcatgctgg
EW_847_Repo_tsr1_800_F	ccgCTCGAGgccgctccggcctg
EW_848_Repo_tsr1_800_R	ttaACCGGTCATTCTGCAGTCCACGTGTG
EW_849_Repo_tsr1_500_F	ccgCTCGAGgggtcgccgacatccg
EW_850_Repo_tsr1_200_F	ccgCTCGAGtccagagccggagccg
EW_851_Repo_fbl_800_F	ccgCTCGAGaggaggaacagaggcagaaac
EW_852_Repo_fbl_800_R	ttaACCGGTCATTACTGCGTTCTGGTCGC
EW_853_Repo_fbl_500_F	ccgCTCGAGgagatagctcagctgtgaagagaac
EW_854_Repo_fbl_200_F	ccgCTCGAGcttgtgataaaatttgccactctagg
EW_855_Repo_mRpl1_800_F	ccgCTCGAGggcagctgagacataacgga
EW_856_Repo_mRpl1_800_R	ttaACCGGTCGCCATGTTGACTGTTCCG
EW_857_Repo_mRpl1_500_F	ccgCTCGAGccgccttgggtggagg
EW_858_Repo_mRpl1_200_F	ccgCTCGAGaaagccattccccacccc

Table 4.13: List of primers used for cloning of the promoter fragments.

Primers needed to amplify the reporters

The following table 4.14 lists the primer sequences used for PCRs to amplify the fluorescent reporters used for testing the promoter fragments, for usage in the main screen and for usage in the endogenous screen. The template for tGFP was a plasmid from our clone collection (#167). A synthetic gBlock was ordered from IDT for tRFP-PESTmut and tGFP-PESTmut. The tRFP-PESTmut sequence served as a template for a mutagenesis PCR with the aim of mutating back the mutated PEST domain to the WT mODC PEST domain via an overlapping PCR with the primers indicated below. The EGFP-PEST sequence, however, was taken from the "pDECKO-mCherry-LDLR-GFPd2" plasmid, which was a kind gift from Florian Röhrig from AG Schulze in our department. A gBlock was ordered for the mScarlet-I-d2 knock-in construct. The 3' homology arm of

the HDR template for the endogenous knock-in into the *FBL* locus was generated via a PCR with the indicated primers below.

Name	Sequence (5'-3')	Fluorescent reporter
EW_823_tGFP_age_spe_F	taaACCGGTATGGAGAGCGACGAGAGC	tGFP
EW_824_tGFP_age_spe_R	ggACTAGTTTATTCTTCACCGGCATCTG	tGFP
EW_1048EGFPd2f	ccggACCGGTATGGTGAGCAA	EGFP-PEST
EW_1049EGFPd2r	ctagACTAGTCTACACATTGATCCTAGCAGAAGC	EGFP-PEST
EW_1070_mutagen_begin_tRFP_f	cagactgagtcggccggtggatc	mutagenesis primer to mutate PEST sequence back to the WT mODC sequence
EW_1071_mutagen_mid_PEST_r	CATCCTGCTCCTCCACCTCCGGC	mutagenesis primer to mutate PEST sequence back to the WT mODC sequence
EW_1072_mutagen_mid_PEST_f	GCCGGAGGTGGAGGAGCAGGATG	mutagenesis primer to mutate PEST sequence back to the WT mODC sequence
EW_1073_mutagen_end_PEST_r	ggcggatccgtcgacACTAGTTTAC	mutagenesis primer to mutate PEST sequence back to the WT mODC sequence
EW_1890_N-term_3Hom-hFbl_F	ggggtaccAAGCCAGGTCAGGCTGGGGTG	3' homology arm for *FBL* knock-in for second screen
EW_1891_N-term_3Hom-hFbl_R	cgGGATCCCGGAAAAGCTGGGATGCGGGA	3' homology arm for *FBL* knock-in for second screen

Table 4.14: List of primers used for cloning of the fluorescent reporters.

Primers needed to amplify the sgRNAs from genomic DNA obtained from the screening conditions

The following table 4.15 lists the primer sequences used for PCRs to amplify the fluorescent reporters used for testing the promoter fragments, for usage in the main screen and for usage in the endogenous screen. The template for tGFP was a plasmid from our clone collection (#167). A synthetic gBlock was ordered from IDT for tRFP-PESTmut and tGFP-PESTmut. The tRFP-PESTmut sequence served as a template for a mutagenesis PCR with the aim of mutating back the mutated PEST domain to the WT mODC PEST domain via an overlapping PCR with the primers indicated below. The EGFP-PEST sequence, however, was taken from the "pDECKO-mCherry-LDLR-GFPd2" plasmid, which was a kind gift from Florian Röhrig from AG Schulze in our department. A gBlock was ordered for the mScarlet-I-d2 knock-in construct. The 3' homology arm of the HDR template for the endogenous knock-in into the *FBL* locus was generated via a PCR with the indicated primers below.

Name	Sequence (5'-3')	Note
EW_1167_Gecko_PCR_1_f	ACACTCTTTCCCTACACGACGCTCTTCCGATCTCGAGCtcttGTGGAAAGGACGAAACACC*g	Used for the first PCR; the "*" at the end of the sequence marks a phosphorothioate linkage that was inserted to avoid oligo shortening by the exonuclease activity of the polymerase during PCR amplification
EW_1168_Gecko_PCR_1_r	GTGACTGGAGTTCAGACGTGTGCTCTTCCGATCTgccaattcccactcctttcaagac*c	Used for the first PCR; the "*" at the end of the sequence marks a phosphorothioate linkage that was inserted to avoid oligo shortening by the exonuclease activity of the polymerase during PCR amplification

Table 4.15: List of primers used for the two PCRs performed on genomic DNA of the sorted screening conditions, the screening plasmid library and the unsorted conditions from the screens.

Primers needed to amplify the homology arms for the HDR constructs

Name	Sequence (5'-3')
EW_1772_N-term_5'Hom-hRbm8a_F	ccggACCGGTttccagaagcagctctttatg
EW_1773_N-term_5'Hom-hRbm8a_R	gcgACGCGTctcgccttcgatcgagatc
EW_1774_N-term_3'Hom-hRbm8a_F	ccgGAATTCGCGGACGTGCTAGATCTTC
EW_1775_N-term_3'Hom-hRbm8a_R	ggACTAGTTCTCCCATTGTTCCTATGAG
EW_1890_N-term_3Hom-hFbl_F	ggggtaccAAGCCAGGTCAGGCTGGGGTG
EW_1891_N-term_3Hom-hFbl_R	cgGGATCCCGGAAAAGCTGGGATGCGGGA

Table 4.16: List of primers needed for the knock-in generation.

sgRNA sequences

Name	Sequence (5'-3')
EW_1076_sgRNA1_hMYC_antisense	CACCGAACGTTGAGGGGCATCGTCG
EW_1077_sgRNA1_hMYC_sense	AAACCGACGATGCCCCTCAACGTTC
EW_1078_sgRNA2_hMYC_sense	CACCGGCCGTATTTCTACTGCGACG
EW_1079_sgRNA2_hMYC_antisense	AAACCGTCGCAGTAGAAATACGGCC
EW_1080_sgRNA3_hMYC_sense	CACCGACAACGTCTTGGAGCGCCAG
EW_1081_sgRNA3_hMYC_antisense	AAACCTGGCGCTCCAAGACGTTGTC
EW_1082_sgRNA4_hMYC_antisense	CACCGCGCCGTCGTTGTCTCCCCGA
EW_1083_sgRNA4_hMYC_sense	AAACTCGGGGAGACAACGACGGCGC
EW_1092_sgRNA1_neg_sense	CACCGGCGAGGTATTCGGCTCCGCG
EW_1093_sgRNA1_neg_antisense	AAACCGCGGAGCCGAATACCTCGCC
EW_1094_sgRNA2_neg_sense	CACCGGCTTTCACGGAGGTTCGACG
EW_1095_sgRNA2_neg_antisense	AAACCGTCGAACCTCCGTGAAAGCC
EW_1096_sgRNA3_neg_sense	caccgATGTTGCAGTTCGGCTCGAT
EW_1097_sgRNA3_neg_antisense	aaacATCGAGCCGAACTGCAACATc

EW_1098_sgRNA1_tRFP_sense	CACCGGGCGAAGGCAAGCCCTACGA
EW_1099_sgRNA1_tRFP_antisense	AAACTCGTAGGGCTTGCCTTCGCCC
EW_1100_sgRNA2_tRFP_antisense	CACCGCACGCCCCCGTCTTCGTATG
EW_1101_sgRNA2_tRFP_sense	AAACCATACGAAGACGGGGGCGTGC
EW_1102_sgRNA3_tRFP_antisense	CACCGATGGTCTGGGTGCCCTCGTA
EW_1103_sgRNA3_tRFP_sense	AAACTACGAGGGCACCCAGACCATC
EW_1104_sgRNA4_tRFP_sense	CACCGATGCTGTACCCCGCTGACGG
EW_1105_sgRNA4_tRFP_antisense	AAACCCGTCAGCGGGGTACAGCATC
EW_1106_sgRNA1_EGFP_sense	CACCGGAGCTGGACGGCGACGTAAA
EW_1107_sgRNA1_EGFP_antisense	AAACTTTACGTCGCCGTCCAGCTCC
EW_1108_sgRNA2_EGFP_sense	CACCGAAGTTCAGCGTGTCCGGCGA
EW_1109_sgRNA2_EGFP_antisense	AAACTCGCCGGACACGCTGAACTTC
EW_1110_sgRNA3_EGFP_antisense	CACCGCGTCGCCGTCCAGCTCGACC
EW_1111_sgRNA3_EGFP_sense	AAACGGTCGAGCTGGACGGCGACGC
EW_2123_sg4-EGFP_sense_F	caccgCGCGCCGAGGTGAAGTTCGA
EW_2124_sg4-EGFP_sense_R	aaacTCGAACTTCACCTCGGCGCGc
EW_1380_sgAldoa_A3810_f	caccgTGACATCGCTCACCGCATTG
EW_1381_sgAldoa_A3810_r	aaacCAATGCGGTGAGCGATGTCAc
EW_1382_sgAldoa_B3811_f	caccgTCCCACCTGCTGGCAGATGC
EW_1383_sgAldoa_B3811_r	aaacGCATCTGCCAGCAGGTGGGAc
EW_1384_sgAldoa_B3810_f	caccgCCTTGCCCGGAGCCACAATG
EW_1385_sgAldoa_B3810_r	aaacCATTGTGGCTCCGGGCAAGGc
EW_1386_sgHspa8_B25037_f	caccgTATGTATTTACCTGCACCAT
EW_1387_sgHspa8_B25037_r	aaacATGGTGCAGGTAAATACATAc
EW_1388_sgHspa8_B25038_f	caccgACAGATGCCAAACGTCTGAT
EW_1389_sgHspa8_B25038_r	aaacATCAGACGTTTGGCATCTGTc
EW_1390_sgBud31_A7382_f	caccgTGATCTAGTTCATCCAACGT
EW_1391_sgBud31_A7382_r	aaacACGTTGGATGAACTAGATCAc
EW_1392_sgBud31_A7381_f	caccgCCCGAGTCTGAATGCAGCGT
EW_1393_sgBud31_A7381_r	aaacACGCTGCATTCAGACTCGGGc
EW_1394_sgCdc16_A9297_f	caccgCTCGGTGGTACTGCGCTGTG
EW_1395_sgCdc16_A9297_r	aaacCACAGCGCAGTACCACCGAGc

EW_1396_sgCdc16_B9299_f	caccgAAGGTAGCTTCACTCTCTCA
EW_1397_sgCdc16_B9299_r	aaacTGAGAGAGTGAAGCTACCTTc
EW_1398_sgEif4a3_B15846_f	caccgGCACGCTGCTGAATCGCTGA
EW_1399_sgEif4a3_B15846_r	aaacTCAGCGATTCAGCAGCGTGCc
EW_1400_sgEif4a3_A15855_f	caccgAATCTGCACCGCTAACTCCC
EW_1401_sgEif4a3_A15855_r	aaacGGGAGTTAGCGGTGCAGATTc
EW_1402_sgSfpq_B48080_f	caccgGTGCCATGCTGAGCAAAACG
EW_1403_sgSfpq_B48080_r	aaacCGTTTTGCTCAGCATGGCACc
EW_1404_sgSfpq_B48082_f	caccgGACTCCTCGCCCAGTCATTG
EW_1405_sgSfpq_B48082_r	aaacCAATGACTGGGCGAGGAGTCc
EW_1406_sgRpa1_A46093_f	caccgCCTCGATGGCCCCCTCGCTC
EW_1407_sgRpa1_A46093_r	aaacGAGCGAGGGGGCCATCGAGGc
EW_1408_sgRpa1_B46081_f	caccgCGGTACTTACAATGACCTGC
EW_1409_sgRpa1_B46081_r	aaacGCAGGTCATTGTAAGTACCGc
EW_1410_sgPlk1_B41511_f	caccgCCCCAGGTATACCTTGCTAG
EW_1411_sgPlk1_B41511_r	aaacCTAGCAAGGTATACCTGGGGc
EW_1412_sgPlk1_A41522_f	caccgGTCATTGAGCAACTCGTGAA
EW_1413_sgPlk1_A41522_r	aaacTTCACGAGTTGCTCAATGACc
EW_1414_sgEwsr1_A16779_f	caccgTGCATATGCAGTCTGCCCGT
EW_1415_sgEwsr1_A16779_r	aaacACGGGCAGACTGCATATGCAc
EW_1416_sgEwsr1_A16777_f	caccgCTGTACGCCTGCGGGGCAGT
EW_1417_sgEwsr1_A16777_r	aaacACTGCCCCGCAGGCGTACAGc
EW_1418_sgSsrp1_B51454_f	caccgGTCCACACCATCTTCCTGCG
EW_1419_sgSsrp1_B51454_r	aaacCGCAGGAAGATGGTGTGGACc
EW_1420_sgSsrp1_A51472_f	caccgTGACAGAAGGCATCTGGCGT
EW_1421_sgSsrp1_A51472_r	aaacACGCCAGATGCCTTCTGTCAc
EW_1422_sgRbm8a_B44842_f	caccgACCCAACAGCTGTTGAAGGT
EW_1423_sgRbm8a_B44842_r	aaacACCTTCAACAGCTGTTGGGTc
EW_1424_sgRbm8a_B44840_f	caccgACTCACCGGAGCCAAAGCCG
EW_1425_sgRbm8a_B44840_r	aaacCGGCTTTGGCTCCGGTGAGTc
EW_1784_sg1_sense_hRbm8a_f	CACCGgatctcgatcgaaggcgaga
EW_1785_sg1_sense_hRbm8a_r	AAACtctcgccttcgatcgagatcC

EW_1786_sg2_sense_hRbm8a_f	CACCGctcgatcgaaggcgagatgg
EW_1787_sg2_sense_hRbm8a_r	AAACccatctcgccttcgatcgagC
EW_1876_hFbl_sg1_antisense_F	CACCGCCCAGCCTGACCTGGCTTCA
EW_1877_hFbl_sg1_sense_R	AAACTGAAGCCAGGTCAGGCTGGGC
EW_1878_hFbl_sg2_sense_F	CACCGccagggctcgccATGAAGCC
EW_1879_hFbl_sg2_antisense_R	AAACGGCTTCATggcgagccctggC
EW_1906_sg1_mScarlet_sense_F	caccgGAACAGTACGAACGCTCCGA
EW_1907_sg1_mScarlet_sense_R	aaacTCGGAGCGTTCGTACTGTTCc
EW_1908_sg2_mScarlet_sense_F	caccgCTACAACGTCGACCGCAAGT
EW_1909_sg2_mScarlet_sense_R	aaacACTTGCGGTCGACGTTGTAGc
EW_2119_sg3-Scarlet_antis_F	caccgCTCGGGGTACAACCGCTCGG
EW_2120_sg3-Scarlet_antis_R	aaacCCGAGCGGTTGTACCCCGAGc
EW_2121_sg4-Scarlet_antis_F	caccgCTGGAGCCGTACATGAACTG
EW_2122_sg4-Scarlet_antis_R	aaacCAGTTCATGTACGGCTCCAGc

Table 4.17: List of primers used for cloning.

4.9.2 Primers used for Sanger sequencing

Name	Sequence (5'-3')
EW_1845_NAID-hRbm8a_Check_F	GCAACCAAGTCTGTTAGTTTCCTG
EW_1846_NAID-hRbm8a_Check_R	TCCTGCTCCACGCTGTCATAA
EW2365_NAID-hRbm8a_Check2_F	gattacaggcagggagtt
EW2366_NAID-hRbm8a_Check2_R	AGCTATCTCTGAACCCATTC
EW_1892_hFbl_Check_KI_F	CTGATTATTGGGGTGCTCGC
EW_1893_hFbl_Check_KI_R	CCCCAAATCTCCACTCCATCC

Table 4.18: List of primers used for Sanger sequencing of the endogenous knock-ins.

4.9.3 Plasmids

The following vectors were used for cloning or as libraries for the screens.

Name	Description	Purpose
FLAG-PolII-WT (#210)	from Addgene #35175	Co-IP with RBM8A
GeCKOv2 half-library A (#339)	amplified half-library A from the murine GeCKO v2 (Addgene 1000000052) library (in this thesis referred to as A1)	part of the screening library
GeCKOv2 half-library B.1 (#358)	amplified half-library B from the murine GeCKO v2 (Addgene 1000000052) library (in this thesis referred to as B1)	part of the screening library
GeCKOv2 half-library B.2 (#359)	amplified half-library B (this half-library was amplified twice) from the murine GeCKO v2 (Addgene 1000000052) library (in this thesis referred to as B2)	part of the screening library
Human CRISPR Knockout Pooled Library (Brunello)	amplified; from Addgene #73179	Genome-wide CRISPR library used for the endogenous screen; 2x 100 ng of the Addgene library were transformed and mixed, together with positive control sgRNAs targeting human MYC, EGFP and mScarlet-I; this library was used for the endogenous screen
pcDNA3	kind gift from AG Eilers in our department; from Invitrogen	used for cloning of HA-RBM8A (Co-IP experiment)
pCDNA3-GFP (#140)	from AG Eilers at our department	used as control plasmid for the Co-IP experiment

pDECKO-mCherry-LDLR-GFPd2	kind gift from Florian Röhrig (AG Schulze) of our department	used as template to amplify EGFP-PEST for further usage
pJET1.2/blunt	from Thermo Fisher Scientific (#K1232)	for cloning of HDR templates and gBlocks
pMD2.G	lentiviral envelope plasmid (Addgene #12259)	lentivirus production
pRRL	lentiviral vector with ampicillin and hygromycin resistance markers (similar backbone as Addgene #12252)	reporter constructs
psPAX2	lentiviral packaging plasmid (Addgene #12260)	lentivirus production
LentiCrispr v2	identical to Addgene #52961	sgRNAs
pX458	kind gift from Carina Maier (AG Schulze) from our department; see Addgene #48138	used for sgRNA cloning

Table 4.19: List of plasmids used.

4.9.4 qRT-PCR primers

Name	Sequence (5'-3')
EW_1020_tGFP_qPCR_F	CTACCACTTCGGCACCTACC
EW_1021_tGFP_qPCR_R	GTACTTCTCGATGCGGGTGT
EW_1046mActbqPCRF	ctaaggccaaccgtgaaaag
EW_1047mActbqPCRR	accagaggcatacagggaca

Table 4.20: List of used qRT-PCR primers.

4.9.5 ChIP-qPCR primers used after V5- and POL II-ChIPs

Name	Sequence (5'-3')
EW9-ch11-80MB-F	TTTTCTCACATTGCCCCTGT
EW10-ch11-80MB-R	TCAATGCTGTACCAGGCAAA
EW170_polr2a-1f	GGACGGTTGGAGAAGAAGG
EW171_polr2a-1r	TCCTGAACGGCAGAGGTTAC
EW_2224_Rps27L_START_F	CCGGAGCCCGATGTAAACAA
EW_2225_Rps27L_START_R	GCAGCTTCTATCCCGGAAGT
EW_2232_Rps13_START_F	CCAGAGCAGCCCAGAACATC
EW_2233_Rps13_START_R	CTTTCGTTGCCTGATCGCC
EW_2238_Rpl41_TSS1F	AACTTCGCCTTTCTCTCGGC
EW_2239_Rpl41_TSS1R	TGATGCTAAGTGCCGAGGTC
EW_2242_Rps23_TSS1F	CCCTTAAACCGGCCACAACA
EW_2243_Rps23_TSS1R	TGCGGTGCTTCTCTCTTTCG
EW2268_hB2M_TSS1_F	GAGATGTCTCGCTCCGTGG
EW2269_hB2M_TSS1_R	AGGGTAGGAGAGACTCACGC
EW2274_hHPRT1_TSS1_F	CTCAGGCGAACCTCTCGG
EW2275_hHPRT1_TSS1_R	CTGCTCAGGAGGAGGAAGC
EW2328_Rpl38_TSS1_F	TTTCGTCCTTTTCCCCGGTT
EW2329_Rpl38_TSS1_R	GCAGTGGATTGCCCCAGATT
EW2334_Rplp1_TSS1_F	CTGCGTATAGGCGCGAGA
EW2335_Rplp1_TSS1_R	CTAGTCGCCGGATGAAGTGA
EW2403_hTBP_TSS1_F	CATTATCAACGCGCGCCAG
EW2404_hTBP_TSS1_R	TGGGTCACTGCAAAGATCACT

Table 4.21: List of used ChIP-qPCR primers.

4.9.6 siRNAs

All siRNAs were purchased from GE Healthcare Dharmacon. The pools contain a mixture of four different siRNAs.

Target	Ordering number
ON-TARGETplus Mouse Aldoa (11674) siRNA - SMARTpool	L-061954-01-0005
ON-TARGETplus Non-targeting Pool	D-001810-10-50

Table 4.22: List of siRNAs used.

4.10 Cell lines

Cell line	Description	Source
HEK293TN	Human embryonic kidney cells, harboring a SV40 T-antigen and a neomycin resistance gene	ATCC
MEF	Immortalized murine embryonic fibroblasts	in-house preparation
T lymphoma$^{\text{MYC-Tet-Off}}$	Murine T lymphoma cells harboring a human MYC transgene, that can be switched off upon addition of Doxycycline	[Felsher and Bishop, 1999]

U2OS$^{\text{FBL-SCARLET;SFFV-GFP}}$	Human osteosarcoma cells with a one-allelic N-terminal knock-in of destabilized *mScarlet-I* and a Blasticidin resistance gene into the *FIBRILLARIN* locus directly after the start codon, most likely destroying *FBL* expression from that allele; the other allele contains a 5 bp-deletion starting 3 bp after the start codon	ATCC for parental cell line (knock-in performed by me)
U2OS$^{\text{N-AID-RBM8A}}$	Human osteosarcoma cells with an N-terminal homozygous knock-in of an AID- and a V5-tag and a Blasticidin resistance gene into the *RBM8A* locus	ATCC for parental cell line (knock-in performed by me)
3T3$^{\text{Fbl-GFP;Rpl18-RFP}}$	Murine NIH/3T3 cell line (embryonic fibroblasts), expressing EGFP-PEST under the control of an approx. 500 bp promoter fragment of the *Fibrillarin* gene and tRFP-PEST under the control of an approx. 500 bp promoter fragment of the *Ribosomal protein L18* gene	The parental NIH/3T3 cells were a kind gift from AG Gaubatz in Würzburg and the transgenes were inserted by me

3T3$^{Rpl18\text{-}GFP;Fbl\text{-}RFP}$	Murine NIH/3T3 cell line (embryonic fibroblasts), expressing EGFP-PEST under the control of an approx. 500 bp promoter fragment of the *Ribosomal protein L18* gene and tRFP-PEST under the control of an approx. 500 bp promoter fragment of the *Fibrillarin* gene	The parental NIH/3T3 cells were a kind gift from AG Gaubatz in Würzburg and the transgenes were inserted by me

Table 4.23: Cell lines used in this study. The cell lines were regularly tested to be negative for mycoplasms.

4.11 Cell culture media and supplements

Cell line	Medium	Manufacturer	Catalog number
All cell lines	Dulbecco's Modified Eagle Medium (DMEM) +	Thermo Fisher Scientific	41966052
(except	10% (v/v) Fetal Bovine Serum Advanced (or FBS from Biochrom) +	Capricorn Scientific (or Biochrom)	FBS-11A (or S 0115)
T lymphoma$^{MYC\text{-}Tet\text{-}Off}$)	1% (v/v) Penicillin/Streptomycin	Sigma-Aldrich	P4333-100ML
T lymphoma$^{MYC\text{-}Tet\text{-}Off}$	RPMI 1640 Medium (RPMI) +	Thermo Fisher Scientific	21875091

	10% (v/v) Fetal Bovine Serum Advanced (or FBS from Biochrom) +	Capricorn Scientific (or Biochrom)	FBS-11A (or S 0115)
	1% (v/v) Penicillin/Streptomycin +	Sigma-Aldrich	P4333-100ML
	1% (v/v) L-Glutamine +	Thermo Fisher Scientific	25030024
	1% (v/v) MEM Non-Essential Amino Acids Solution +	Thermo Fisher Scientific	11140-035
	50 µM 2-mercaptoethanol	Sigma-Aldrich	M7522-100ML

Table 4.24: Cell culture medium used in this study.

4.12 Other used cell culture media

Purpose	Medium	Manufacturer	Catalog number
Freezing medium	50% (v/v) Fetal Bovine Serum Advanced (or FBS from Biochrom) +	Capricorn Scientific (or Biochrom)	FBS-11A (or S 0115)
all cell lines (except	40% (v/v) Dulbecco's Modified Eagle Medium (DMEM) +	Thermo Fisher Scientific	41966052
(T lymphoma$^{MYC\text{-}Tet\text{-}Off}$)	10% (v/v) Dimethyl sulfoxide (DMSO)	Sigma-Aldrich	41640-1L-M

Freezing medium	90% (v/v) Fetal Bovine Serum Advanced (or FBS from Biochrom) +	Capricorn Scientific (or Biochrom)	FBS-11A (or S 0115)
(T lymphoma$^{MYC\text{-}Tet\text{-}Off}$)	10% (v/v) Dimethyl sulfoxide (DMSO)	Sigma-Aldrich	41640-1L-M
Transfection	Opti-MEM	Thermo Fisher Scientific	31985047
Transfection medium	Dulbecco's Modified Eagle Medium (DMEM) +	Thermo Fisher Scientific	41966052
	2% (v/v) Fetal Bovine Serum Advanced (or FBS from Biochrom)	Capricorn Scientific (or Biochrom)	FBS-11A (or S 0115)

Table 4.25: Cell culture medium used in this study for transfection and freezing of cells.

4.13 Primary antibodies

Target protein	Type	Application	Dilution or amount	Manufacturer	Catalog number
ALDOLASE A	monoclonal	western blot	1:3000	Santa Cruz	sc-390733 (lot H0117)
FLAG M2	monoclonal	western blot or IP	1:5000 or 2 µg	Sigma-Aldrich	F3165 (lot SLBQ7119V or SLCG2330)

GFP (B-2)	monoclonal	western blot	1:2000	Santa Cruz	sc-9996 (lot K2217)
HA-tag (C29F4)	monoclonal	western blot	1:5000	Cell Signaling	3724S (lot 10)
MYC-tag (9E10) for detection of TIR1	monoclonal	western blot	1:1000	made in-house	N/A
N/A	polyclonal, IgG control from mouse serum	ChIP control IgG	1.5 µg/IP	Sigma-Aldrich	I5381
N/A	polyclonal, IgG control from rabbit serum	ChIP control IgG	1.5 µg/IP	Sigma-Aldrich	I5006
POL II (pS2)	polyclonal	ChIP	3 µg	Abcam	ab5095 (lot GR3231908-7)
POL II (pS5) (CTD4H8)	monoclonal	ChIP	3 µg	Biolegend	MMS-128P
POL II (total) (A-10)	monoclonal	ChIP	3 µg	Santa Cruz	sc-17798 (lot L0418)
RBM8A	polyclonal	western blot	1:500 - 1:750	Sigma-Aldrich	HPA018403-100UL (lot A97138)
RPB2 (E-12)	monoclonal	western blot	1:1000	Santa Cruz	sc-166803 (lot G2117)
tRFP	polyclonal	western blot	1:2000	Evrogen	AB233 (lot 23301060466)
VINCULIN (CLONE*HVIN-1)	monoclonal	western blot	1:2000	Sigma-Aldrich	V9131-.5ML (lot 034M4809V or 89478)

V5-tag (D3H8Q)	monoclonal	western blot or ChIP	1:1000 or 1 µg/IP	Cell Signaling	13202S (lot 6)

Table 4.26: List of primary antibodies used.

4.14 Secondary antibodies

Target	Type	Application	Dilution	Manufacturer	Catalog number
Mouse IgG	monoclonal	western blot (Horseradish peroxidase (HRP)-conjugated)	1:7500	Thermo Fisher Scientific	10196124
Rabbit IgG	monoclonal	western blot (HRP-conjugated)	1:7500	Thermo Fisher Scientific	10794347
Mouse IgG (TrueBlot ULTRA)	polyclonal	western blot (HRP-conjugated) after IP	1:3000	Biomol	18-8817-33 (lot 37885 or 39899)
Rabbit IgG (TrueBlot)	polyclonal	western blot (HRP-conjugated) after IP	1:3000	Biomol	18-8816-33 (lot 40107)

Table 4.27: List of secondary antibodies used.

5 Methods

5.1 Cell biology

5.1.1 Splitting of cells

Cells were washed once with PBS, before 0.25% trypsin was added (1 ml per 10 cm dish, 2 ml per 15 cm dish). The cells were incubated at RT or 37℃ for a few minutes until all cells detached from the plate, before the digestion reaction was stopped by the addition of full medium in a ratio of about 1 (trypsin) to 10 (full medium). Subsequently, the cells were collected in a reaction tube and centrifuged at 200 x g, 4-5 min, RT before they were resuspended in full medium and partially seeded back onto a new plate.

5.1.2 Lentivirus production

Seeding and transfection

HEK293TN cells were counted with Casy or Neubauer chamber and 5×10^6 cells were seeded per 10 cm dish. If more virus was needed, more plates were transfected with the same plasmids and the supernatants were pooled later on. The day after seeding, transfection was performed with two different mixtures prepared in parallel (see table 5.1). As a side note, all produced viruses were second generation lentiviruses. This system consists of three plasmids:
a) one "transfer plasmid", that contains the sequences of interest (here: plasmid of interest),
b) one "envelope plasmid" (here: pMD2.G),
c) one "packaging plasmid" (here: psPAX2).
For more information, please check out the Addgene website[1].

[1] https://www.addgene.org/guides/lentivirus/#second-generation (October 22, 2021)

Transfection reaction per 10 cm plate	Ingredients	Volume
DNA mix	Opti-MEM	500 µl
	Plasmid of interest (1 µg/µl)	10 µl
	psPAX2 (1 µg/µl)	10 µl
	pMD2.G (1 µg/µl)	2.5 µl
PEI mix	Opti-MEM	500 µl
	PEI	30 µl

Table 5.1: List of the transfection reactions used for lentivirus production.

The transfection mixes were incubated at RT for 5 min, before the DNA mix was added to the PEI mix dropwise. After pipetting up and down, the reaction was incubated for 15 to 20 min at RT. Meanwhile, the HEK293TN cells were washed once with PBS before 5-6 ml of transfection medium (2% FCS/DMEM) were added. The transfection mix was added dropwise and the plates were gently swung to evenly distribute the transfection reagent on the plates. Afterwards, the plates were put into the incubator. About five to nine hours after transfection, medium was sucked off, cells were washed with PBS once and 5-6 ml of full medium were added to the cells, before putting them back into the incubator. Supernatant was harvested the next morning, the next evening and the morning afterwards. After each harvest, 5-6 ml of fresh full medium was added to the cells. Having harvested 15-18 ml of virus per dish, the cells were discarded and the virus supernatant was passed through a 0.45 µm filter. This filtered virus-containing supernatant was either directly used for infection, stored in the fridge for a couple of days before infection or flash-frozen in liquid nitrogen and stored at -80℃ for later use. In the latter case, it was thawed at RT or in the fridge before infection.

5.1.3 Lentiviral infection and selection

Viral transduction was performed by adding filtered viral supernatant to cells in full medium. Usually, a ratio of 1:1 (e.g. 5 ml of full medium + 5 ml of virus-containing supernatant) was chosen. Additionally, 8 µg/ml Polybrene (Hexadimethrinbromide) was added (for T cells, Protamine sulfate was used 1:1000 to facilitate infection. If necessary, multiple infections (but only one infection per day) were carried out.

5.1.4 Growth curve

To determine cell growth of the U2OS WT and U2OS$^{N\text{-}AID\text{-}RBM8A}$ cells, 150.000 cells were seeded in triplicates in 6-wells and treated with 500 µM auxin or equal volumes of solvent (H_2O). Medium, including auxin or H_2O, was changed daily. After two, four and six days, cells were counted with the Casy cell counter and reseeded (150.000 cells). A cumulative growth curve was calculated by dividing the counted cell number by the seeded cell number and multiplication of this result with the calculated cell number of the previous time point. A standard deviation of the triplicates was calculated and the data were plotted with R.

5.1.5 FACS

FACS analysis

To analyze cells via FACS, the cells were washed once with PBS before trypsinization with 0.5 ml (6 cm plates), 1 ml (10 cm plates) or 2 ml (15 cm plates) of 0.25% trypsin. Protein digestion with trypsin was stopped by the addition of about 5 to 10 ml of full medium. Cells were collected in a reaction tube and centrifuged at 200 x g, RT, for 4 to 5 minutes. The cells were then washed with PBS at least once and centrifuged again as previously described. Subsequently, the cells were resuspended in 2% FCS/PBS, resulting in a final concentration of cells of about $1 - 10 \times 10^6$ cells/ml. If cells were analyzed at the FACS machine of AG Rudel, the cells were additionally passed through a cell strainer to separate cells from each other, so that the formation of cell clumps is reduced. Cells were placed on ice until measurement and pipetted up and down or vortexed shortly before measurement. Experiment files and FCS files were exported in a 3.0/3.1 format and the data were analyzed with FlowJo v10.

Cell sorting

For cell sorting, cells were prepared as described in subsection 5.1.5 until resuspension in 2% FCS/PBS at a concentration of $1 - 10 \times 10^6$ cells/ml. For the screens, cells were resuspended in 10% FCS/PBS to avoid cell death due to starvation. The cells were then passed through a cell strainer to separate cells from each other, so that the formation of cell clumps is reduced. Cells were put on ice (inside a 50 ml reaction tube, if the cells

were still S2 material) until measurement and vortexed shortly before measurement. Cells were sorted into tubes (pooled sorting) or 96-well plates (single clone sorting) filled with full medium (2-3 ml or 150 µl, respectively) or 2x lysis buffer (screens). Full medium with 10% or 20% of FCS was used for single cell sorting to facilitate growth.

Barbara Bauer and Ryan Ramjan from our department were (helping in) sorting the cells. Experiment files and FCS files were exported in a 3.0/3.1 format and the data were analyzed with FlowJo v10.

5.1.6 Apoptosis measurement (Annexin V/PI-FACS)

To analyze apoptotic cells, Annexin V and propidium iodide (PI) were used as markers for apoptotic [Koopman et al., 1994] and necrotic/late apoptotic cells [Darzynkiewicz et al., 1992, Dive et al., 1992], respectively. 150.000 U2OS WT and the U2OS$^{N\text{-}AID\text{-}RBM8A}$ cells were seeded on 6 cm-dishes. The next day, medium was changed and 500 µM auxin or equal volumes of solvent (H_2O) were added to the cells. 48 hours later, the supernatant was transferred to a 15 ml reaction tube, cells were harvested by trypsinization and combined with their previously harvested supernatant. The cells were then centrifuged at 400 x g at 4 ℃ for 5 minutes. Afterwards, cells were washed with 5 ml of ice-cold PBS, centrifuged again and resuspended in 100 µl Annexin V binding buffer supplemented with 2 µl of Pacific Blue-conjugated Annexin V. The cells were incubated 15 min at RT in the dark before 400 µl of Annexin V binding buffer, supplemented with 9,86 ng/µl PI, was added. Cells were placed on ice and in darkness until FACS measurement. One additional sample, not labelled with Annexin V or PI, was used as an unstained control. An unstringent parental gate according to the forward and sideward scatter was set. Within this gate, four gates (Annexin V^-/PI^-, Annexin V^+/PI^-, Annexin V^-/PI^+ and Annexin V^+/PI^+) were set and the percentage of early apoptotic (Annexin V^+/PI^- cells) and late apoptotic (Annexin V^+/PI^+) cells was plotted.

5.1.7 Cycloheximide (CHX) assay

220.000 U2OS cells expressing SFFV-mSCARLET-I-d2 or SFFV-tRFP-PEST or SFFV-EGFP-PEST were seeded on a 6-well plate. Alternatively, 400.000 HEK cells expressing SFFV-tGFP or SFFV-tGFP-PESTmut were seeded on a 6-well plate. The next day, medium was changed and 10 µg/ml (U2OS) or 100 µg/ml (HEK) CHX, or EtOH solvent as a control, were added to the cells. For the last 8 hours of the longer time points for

U2OS cells, medium was again changed and fresh CHX or EtOH was added. Cells were harvested for FACS measurement (see subsubsection 5.1.5) at the indicated time points.

5.2 Molecular biology

5.2.1 Cloning

sgRNA design, phosphorylation and annealing

sgRNA sequences were either taken from the murine or human GeCKO v2 libraries (for validation experiments or the design of sgRNAs targeting human MYC for spike-in into the library used for the endogenous screen, respectively), designed manually (knock-ins) or designed with online tools, such as CHOPCHOP[2] (spiked-in sgRNAs used for the screens) or the sgRNA Designer tool from the Broad Institute[3] (spiked-in sgRNAs used for the screens). The design principle, however, was always the same. For each targeted locus, two reverse complementary strands of 20 bp were designed with the top strand containing a preceding 5' "CACCG" sequence and the bottom strand containing a preceding 5' "AAAC" sequence and a 3' "C". The two sgRNAs per locus were phosphorylated (see table 5.2) at 37℃ for 30 min prior to incubation at 95℃ for 5 min to inactivate the reaction.

Reagent	Volume/Amount
sgRNA top strand	10 µM
sgRNA bottom strand	10 µM
10x T4 ligation buffer (NEB or Thermo Fisher Scientific)	1x
T4 PNK (NEB)	5% (v/v)
ad H_2O	10 µl

Table 5.2: sgRNA phosphorylation reaction.

Annealing of the oligos was performed by placing the reaction tube at RT for about 20 min, so that the solution could cool down from 95℃ to RT. The phosphorylated and

[2]http://chopchop.cbu.uib.no/ (October 31, 2021)
[3]https://portals.broadinstitute.org/gpp/public/analysis-tools/sgrna-design (October 31, 2021)

annealed oligos were diluted 1:200 before ligation. 0.5 to 1 µl was usually used for the subsequent ligation reaction in a total volume of 20 µl.

Polymerase chain reaction (PCR) conditions used for cloning

A standard PCR reaction (see table 5.3) was performed on either about 20 ng of plasmid DNA or on about 100 ng of genomic DNA (gDNA).

PCR reagent	Volume/Amount
DNA	20 ng (plasmid) or 100 ng (gDNA)
5x HF or GC buffer	1x
dNTPs	0.2 mM
Forward primer	0.4 µM
Reverse primer	0.4 µM
DMSO	0 - 10%
Phusion	1% (v/v) of final volume
ad H_2O	50 µl

Table 5.3: PCR reaction.

The PCR cycling conditions for cloning reactions were chosen according to table 5.4.

Number of cycles	Temperature (°C)	Time (sec)
1	98	30
4	98	10
	55-72	10
	72	30 to 60 sec per kb
26 - 28	98	10
	55-72	10
	72	30 to 60 sec per kb
1	72	300
1	4	∞

Table 5.4: PCR cycling conditions.

Restriction digest

A restriction digest was performed on a PCR product or a plasmid according to table 5.5 and was incubated about one to six hours (about three hours in most cases) at the optimal temperature of the individual restriction enzymes (as indicated by the manufacturer). The enzymes were purchased from NEB and used with the CutSmart buffer, if there was no other buffer recommended by the company. Wherever applicable, high-fidelity enzymes were used.

Ingredient	Amount/Volume
CutSmart buffer	1x
DNA	10 to 30 µg
Restriction enzyme 1	1 to 3 µl
Optional: restriction enzyme 2	1 to 3 µl
Ad H_2O	50 µl

Table 5.5: Restriction digest reaction.

Digested DNA was loaded on an agarose gel (see section 5.2.1), gel-purified according to manufacturer's instructions with the GeneJET Gel Extraction Kit from Thermo Fisher Scientific, and subsequently used for ligation (see section 5.2.1) if digested with two enzymes. Single enzyme-digested vectors were first column- or gel-purified via the GeneJET Gel Extraction Kit from Thermo Fisher Scientific and then dephosphorylated by the addition of 1-2 µl FastAP Thermosensitive Alkaline Phosphatase (Thermo Fisher Scientific) and 1x AP reaction buffer and incubation at 37℃ for 10 minutes prior to heat-inactivation at 75℃ for 5 min. The dephosphorylated vectors were again gel-purified before ligation.

Agarose gel electrophoresis

1% ethidium bromide was added to 1%-2% agarose in 1x TAE buffer in a dilution of 1:50.000. The liquid mixture solidified in an gel apparatus with a comb. The solidified gel was transferred to a chamber filled with 1x TAE. The samples were loaded and the gel run was performed at 150 V for about 1 h. The DNA was made visible under UV light and bands of the correct sizes were cut for cloning, when gel-purification was needed. Images were analyzed with ImageJ.

Ligation

For sgRNA cloning, phosphorylated, annealed and diluted oligos (see section 5.2.1) were ligated with either BbsI-digested pX458 or BsmBI-digested LentiCrispr v2. Non-sgRNA cloning was performed using the pRRL vector, the pcDNA3 vector (Co-IP experiment) or the pJET vector.

Cloning into pJET was performed according to manufacturer's instructions, whereas ligation into pRRL or pcDNA3 or into the vectors for sgRNA cloning was performed according to table 5.6.

Ingredient	Amount/Volume
Vector	about 50-200 ng; usually 1 µl
Insert	molar ratio of insert to vector about 3:1 - 5:1
T4 DNA Ligase Buffer (Thermo Fisher Scientific)	1x
T4 DNA Ligase (Thermo Fisher Scientific)	1 µl
Ad H_2O	20 µl

Table 5.6: Ligation reaction.

Ligation (and a religation control without insert) was performed at 16℃ over night or for 2-4 hours with subsequent incubation at RT for 30 min in the latter case. The ligation reaction was then either used directly for transformation or frozen at -20℃ and thawed on ice before transformation.

Transformation

Transformation for usual cloning purposes was performed by thawing chemically competent XL1-blue bacteria on ice and addition of 10 µl of the ligation reaction to 50 µl of bacteria. Mixing was performed by snipping against the wall of the reaction tube. After an incubation on ice for 10 to 30 min, heat shock was performed at 42℃ for 45 sec in a water bath. Afterwards, the tube was put on ice for 3 min, before 500 µl LB medium without antibiotics was added. The transformed bacteria were shaken at 37℃ for 45-60 min. The cells were pelleted at 845 x g for 2 min, the supernatant was removed mostly with the left-over having been used to resuspend the bacteria and plate them on an LB-agar plate with the corresponding antibiotics. Instead of ampicillin, carbenicillin was

used in most cases to reduce satellite colony formation. The plates were incubated over night at 37℃. The next day, the plates were wrapped in Parafilm and incubated at 4℃ up to one month until further usage.

Small-scale plasmid preparation (Miniprep)

A small-scale plasmid amplification and preparation was performed the following way: with a pipette tip a bacterial colony was taken from transformed bacteria on an LB agar plate, that contained antibiotics (see subsubsection 5.2.1), and transferred to 3 ml of LB medium with appropriate antibiotics in a 14 ml reaction tube. This bacterial culture was shaken over night at 37℃ (or 30℃ for lentiviral plasmids) with a loosely capped lid. The next day, 1 ml of the culture was used for plasmid preparation, whilst the rest was kept at 4℃ with a closed lid. The 1 ml was transferred to a 1.5 ml reaction tube and centrifuged for 5 min at 950 x g at RT. 700 µl of the supernatant were discarded and the rest was used to resuspend the bacterial pellet. 300 µl of basic Miniprep solution 1 was added to lyse the cells and the solution was mixed by inversion. After 5 minutes of incubation at RT, 300 µl of acidic Miniprep solution 2 was added to stop lysis. The solution was mixed by inversion, incubated for 5 min at RT and centrifuged for 5 min at 13.000 x g at RT. 800 µl of the supernatant were transferred to a new 1.5 ml reaction tube, 600 µl of isopropanol were added to the supernatant and the solution was vortexed intensively. Afterwards, centrifugation for 10 min at 13.000 x g at 4℃ was performed and the pellet was washed twice with 950 to 1000 µl of 70% EtOH with "5 min, 13.000 x g, 4℃" centrifugation steps in between. EtOH was removed completely and the pellet was dried with an open lid at RT, before it was resuspended in 50 µl of Tris-EDTA (TE) buffer, supplemented with 5 µg of RNase A. Plasmid DNA was stored at -20℃.

Large-scale plasmid preparation (Maxiprep)

A large-scale plasmid amplification and preparation was performed the following way: 1 ml of a small-scale plasmid liquid culture (see subsubsection 5.2.1) was transferred into 200 ml of LB medium with appropriate antibiotics and grown over night at 37℃ (or 30℃ for lentiviral plasmids). The culture was centrifuged at 9605 x g, 4℃, for 30 min (JLA-16.250 rotor, Beckman Coulter centrifuge). The pellet was either frozen at -20℃ until maxiprep or used directly for large-scale plasmid preparation. The bacterial pellet was resuspended, lysed, precipitated, loaded onto the equilibrated column,

washed and eluted according to manufacturer's (PureLink HiPure Plasmid Maxiprep Kit) instructions, with the exception of the centrifugation step for precipitation, which was performed at 9605 x g, RT, for 30 min (JLA 16.250 rotor, Beckman Coulter centrifuge). After elution, 10.5 ml of isopropanol was added to the eluate and mixed well. The mixture was incubated for at least 20 min at 4℃ and centrifuged at 9605 x g, 4℃, for 30 min (JA-25.50 or JA-20 rotor, Beckman Coulter centrifuge). The supernatant was discarded and the DNA pellet was transferred to a new 1.5 ml reaction tube with 950 µl of 70 % EtOH. After centrifugation at 20.817 x g for 5 min at 4℃, the pellet was again washed with 70 % EtOH and centrifuged as before and dried at RT with an open lid, before it was resuspended in water to reach a final concentration of 1 mg/ml. DNA concentration was measured by UV/VIS spectrophotometry using NanoDrop 1000 and purity was determined by the ratio of absorbance of 260 nm over 280 nm, which should be in the range of 1.8 to 2.0 for DNA samples. Plasmid DNA was stored at -20℃.

5.2.2 Protein lysis

Protein lysis was performed by washing of the cells with ice-cold PBS twice and subsequent lysis in RIPA buffer (up to 0.5 ml for a 10 cm plate and 700 µl to 1 ml for a 15 cm plate), which was freshly supplemented with protease and phosphatase inhibitors (1:1000). Cells were scraped off the plates, collected in a 1.5 ml reaction tube and incubated on a rotating wheel at 4℃ for 20 min, before the lysed cells were centrifuged at 20.817 x g for 10 min at 4℃. The supernatant was transferred into a new 1.5 ml reaction tube on ice and either flash-frozen in liquid notrogen and stored at -80℃ (and thawed again later on on ice) or used directly for protein quantification via BCA (see section 5.2.3).

5.2.3 Protein quantification via the bicinchoninic acid (BCA) assay

1.5 µl of samples in RIPA buffer or RIPA buffer alone as a background reference or 1.5 µl of a serial dilution of a BSA-standard were pipetted in triplicates into a 96-well plate and 150 µl of a mix of BCA Solution A and BCA Solution B (50:1) were added per well. After incubation at 37℃ for 15 min, light absorption was measured (after removal of the plate lid) at the multiplate absorbance spectrometer. The plate was shaken once for 5 sec at 780 rpm and absorbance was measured at 550 nm. Protein concentration

could be calculated after subtraction of the background absorption and in relation to the standard curve.

5.2.4 Protein quantification via the Bradford assay

As an alternative to the BCA assay, the Bradford assay was used for the Co-IP experiments. 1.5 µl of samples in RIPA buffer or RIPA buffer alone as a background reference or 1.5 µl of a serial dilution of a BSA-standard were pipetted in triplicates into a 96-well plate and 150 µl of Bradford Solution, as well as 1.95 mM NaCl were added per well. Light absorption was measured (after removal of the plate lid) at the multiplate absorbance spectrometer. The plate was shaken once for 5 sec at 780 rpm and absorbance was measured at 630 nm. Protein concentration could be calculated after subtraction of the background absorption and in relation to the standard curve.

5.2.5 Sodium dodecyl-sulfate polyacrylamide gel electrophoresis (SDS-PAGE) and western blot

SDS-PAGE

Gels were casted with the Mini-PROTEAN Tetra Cell system from Bio-Rad. An 8-12% acrylamide separation gel (see section 4.5) was poured inbetween two glass plates (that were cleaned with 70% ethanol before) and covered with isopropanol. After solidification at RT, isopropanol was removed and the separation gel was covered with stacking gel (see section 4.5). A comb was inserted and the solution solidified at RT. For both, separation and stacking gel, APS and TEMED were added shortly before casting to start the polymerization reaction. The solidified gels including the comb were stored at 4℃ for up to two weeks in a moist paper tissue before usage.

The protein samples were prepared for gel loading by the addition of Laemmli buffer (6x) to a final concentration of 1x Laemmli buffer. All the samples that were compared to each other were diluted to the same final concentration and each sample was boiled to 95℃ for 5 min, shortly vortexed and spinned down before loading. A maximum of 20 µl per sample was loaded per gel pocket with a Hamilton pipette. 3 to 10 µl of the PageRuler Prestained Protein Ladder was used in most cases, which was replaced by the Broad Range marker, when POL II was blotted. Almost always, MOPS running

buffer was used to run the gel, but MES running buffer was occasionally used for proteins with a size of less than 30 kDa. The gel was run at 80 V until the protein samples started to separate within the separation gel, before the voltage was increased to 120 V.

Transfer and blocking of the membrane

After sufficient separation of the proteins, the gel was rinsed in 1x transfer buffer and placed on a PVDF membrane, which was activated with methanol for at least 30 seconds and subsequently rinsed in 1x transfer buffer beforehand. Two whatman papers were placed behind the gel and three whatman papers were placed behind the membrane. This set up was placed between two filter sponges in a blotting cassette. Air bubbles were removed from each "sandwich" layer in between. The Peqlab blotting system was filled with 1x transfer buffer and the sandwich cassette was inserted together with a magnetic stir bar. Transfer was performed at 400 mA for 3 hours at 4℃ under stirring conditions. After the transfer of the proteins onto the membrane, the membrane was rinsed in TBS-T and incubated in blocking solution for 1 h at RT.

Antibody staining, washing and signal detection

After blocking, the membrane was rinsed in TBS-T and cut horizontally into pieces according to the expected sizes of the proteins of interest. The membrane pieces were incubated with their corresponding primary antibodies in 5 ml of primary antibody solution in a 50 ml reaction tube over night at 4℃ on a rotating wheel.

The next day, the mebrane pieces were washed six times in TBS-T for 5 min and subsequently incubated in secondary HRP-coupled antibody (TrueBlot antibodies were used for IP experiments) in blocking solution at RT for 1 h on a rotating wheel (in a 50 ml reaction tube) or on a shaker. The membrane pieces were again washed six times with TBS-T for 5 min each.

Protein detection was performed at the LAS-4000 mini Fuji machine by the addition of equal volumes of the two substrate components from the Immobilon Western HRP Substrate kit. Pictures were analyzed with the Multi Gauge software and quantification was performed with the ImageStudio Lite software and normalization to a loading control.

5.2.6 Exogenous (co-)immunoprecipitation ((Co-)IP)

Seeding and transfection

3.5×10^6 HEK cells were seeded per 10 cm plate. 24 hours later, transfection was performed as described in subsubsection 5.1.2 with the difference, that the DNA mix consisted of 250 µl Optimem and 10 µg total DNA (5 µg of each overexpression construct or 5 µg of HA-tagged RBM8A together with a control plasmid leading to GFP overexpression). The PEI mix consisted of 250 µl Optimem mixed with 25 µl of PEI. 17 h after transfection, the cells were washed once with PBS and full medium was added.

Harvest

24 h after transfection, the cells were harvested. To this end, the HEK cells were first washed once in ice cold PBS and lysed by the addition of 700 µl IP buffer, freshly supplemented with protease and phosphatase inhibitors. The lysates were incubated for at least 30 min at 4℃ on a rotating wheel and centrifuged twice at full speed for 10 min at 4℃. The supernatant was aliquoted according to the number of subsequent IP reactions and flash-frozen in liquid nitrogen and stored at -80℃ until further usage.

Immunoprecipitation (IP)

The evening before the day of IP, the anti-FLAG antibody was coupled to a Dynabeads A/G mixture. To this end, 10 µl of Dynabeads A were mixed with 10 µl of Dynabeads G per IP reaction. This mixture was washed three times with 1 ml of ice-cold BSA-PBS (5 mg/ml) with the use of a magnetic rack and alternating mixing conditions (pipetting or invertion with subsequent short spin down at 4℃). The beads were resuspended in BSA-PBS using the same volume, that was used before the washing steps. 2 µg of FLAG-antibody per IP were added to the beads in a final volume of 800 µl BSA-PBS and the antibody was coupled to the beads over night at 4℃ on a rotating wheel.

At the day of IP, the lysates were thawed in almost ice-cold water and kept on ice afterwards. The beads containing the coupled FLAG-antibody were washed twice with 1 ml BSA-PBS and then once with 1 ml IP buffer, before they were again resuspended in the initial volume of 20 µl per IP in IP buffer. Equal amounts of lysates, as determined

by the Bradford assay (see subsection 5.2.4), were added per 20 µl of beads. 1% input was kept to estimate enrichment of FLAG-tagged POL II after IP. Immunoprecipitation was performed for three hours at 4 ℃ on a rotating wheel. The beads were then washed four times with IP buffer and proteins were eluted by the addition of 40 µl 2x Laemmli buffer per IP and incubation at 37 ℃ with 450 rpm shaking for 30 min. The samples were boiled at 95 ℃ for 5 min and shortly spinned down, before the eluate was separated from the beads by a magnetic rack. The input samples were filled up to 40 µl with 2x Laemmli buffer, denatured at 95 ℃ for 5 min and shortly spinned down. 10 µl per sample or input were loaded on a gel, separated via SDS-PAGE and subsequently analysed by western blot (see subsection 5.2.5).

5.3 Genomics

5.3.1 Screens

Amplification of the genome-wide plasmid libraries

The Mouse CRISPR Knockout Pooled Library (GeCKO v2) and the Human CRISPR Knockout Pooled Library (Brunello) were ordered from Addgene (catalog numbers 1 000000052 and 73179, respectively). 100-200 ng of each (half-)library (1 x 100 ng for the GeCKO v2 A half-library, 2 x 100 ng for the GeCKO v2 B half-library and 2 x 100 ng for the Brunello library) were transformed and amplified in bacteria in order to amplify the amount of DNA. To this end, SOC medium was first pre-warmed to RT and Lucigen electrocompetent bacteria were thawed on ice. 100 ng of the library (2 µl) were pipetted into a pre-chilled 1.5 ml reaction tube. 25 µl of bacteria were added, everything was mixed by carefully pipetting up and down and then placed on ice for a couple of minutes, before it was transferred to the bottom of a pre-chilled electroporation cuvette on ice. The production of air bubbles was tried to be avoided as much as possible at this point. Electroporation was performed using the Ec1 program (1.8 kV) of a Bio-Rad GenePulser electroporator. Immediately after electroporation, 973 µl of pre-warmed SOC medium was added to the cuvette, gently mixed with the electroporated bacteria and transferred to a 14 ml reaction tube. An additional ml of SOC medium was used to obtain the remaining bacteria from the cuvette and was combined with the 1 ml, that was taken before. These 2 ml were shaken in the 37 ℃ room for 1 hour. Meanwhile, 2x 5 (Brunello library) or 9-10 (for each GeCKO v2 half-library) 24.5 cm^2 square-shaped

LB-Ampicillin (LB-Amp) plates and one 10 cm LB-Amp or LB-Carbenicillin (LB-Carb) plate were pre-warmed at 37℃ for 1 hour. 1/200 of the solution was diluted 1/1000 and 20 µl of this were plated on the 10 cm LB-Amp/-Carb plate. Equal volumes of the remaining transformed bacteria were plated on the 24.5 cm^2 square-shaped LB-Amp plates. The plates were incubated upside down at 32℃ over night for at least 12 hours. The next day, transformation efficiency was calculated from the 10 cm LB-Amp/-Carb plate by dividing the number of counted colonies by the dilution factor 0.00001 to obtain colony-forming units (cfu) per 0.1 µg of transformed DNA. 10 ml of LB medium were added per 24.5 cm^2 square-shaped LB-Amp plate to enable collection of the bacteria from the plate. Additional 5 ml were added per plate to collect the remaining bacteria. Bacteria, that were obtained from the same electroporation reaction were pooled during harvest and a maxiprep was performed (see subsubsection 5.2.1), but two to five maxi columns were used instead of one for each (half-)library. These split maxipreps were pooled again at the end when the pellets were resuspended in water.

Libraries used for the different screens

The library for the pre-screen consisted of the amplified GeCKO half-libraries (about 75-80 %) and of spiked-in sgRNA controls (about 20-25 %; 3 sgRNAs against EGFP; 4 sgRNAs against tRFP and one non-targeting sgRNA).

The library for the main screen consisted of the amplified GeCKO half-libraries (the B half-library was about 1.2-fold overrepresented over the A half-library) and of spiked-in positive controls (about 0.07% of library; 3 sgRNAs against EGFP; 4 sgRNAs against tRFP).

The library for the endogenous screen consisted of the two independent amplifications of the Brunello library and spiked-in controls (0.25 ng of each of four different sgRNAs targeting human MYC or EGFP or mScarlet-I, respectively).

Virus titer estimation

Virus was produced from the final plasmid libraries used for the screens (for details with regard to virus production, please refer to section 5.1.2). Frozen virus was used for the screens. To estimate virus titer, 1×10^6 3T3$^{\text{Fbl-GFP;Rpl18-RFP}}$ or 1.5×10^6 U2OS$^{\text{FBL-SCARLET;SFFV-GFP}}$ were seeded per 15 cm dish one day prior to infection. The

next day, the cells were infected with 5 ml/0.5 ml (3T3) or 6 ml/3 ml/1.5 ml/0.5 ml (U2OS) of virus produced from the respective libraries. One plate of uninfected cells was used as a killing control. For details regarding infection, please refer to section 5.1.3. The next day, the infected cells were split 1:6 or 1:8 on 2 x 15 cm dishes. Two days after transfection, half of the plates were selected with 2 µg/ml of Puromycin for the following two days, with a medium exchange and fresh Puromycin treatment every day, until they were counted. By counting the cells that survived selection and the cells before selection, the MOI was estimated by additionally taking into account the likelihood of multiple infections[4]. For the pioneer screen an MOI of about 1, for the main screen an MOI of about 0.5 and for the endogenous screen an MOI of about 0.3 was used.

Screening procedure

Cells were expanded and seeded on 15 cm plates ($1 - 1.5 \times 10^6$ 3T3$^{\text{Fbl-GFP;Rpl18-RFP}}$ or 1.5×10^6 U2OS$^{\text{FBL-SCARLET;SFFV-GFP}}$ cells). The next day, cells were infected with the respective libraries at an MOI between 0.2 and 0.5 for the two main screens. The MOI for the pioneer screen was much higher (about 1). Before infection, $0.5‰$ of one sgRNA targeting EGFP and of one sgRNA targeting mScarlet-I were spiked-in at the viral level for the endogenous screen replicates. Triplicates were performed for the two main screens with a redundancy of about 167 per replicate for the main screen and about 200-330 for the endogenous screen replicates. One day after infection cells were split, whilst redundancy was kept. Two days after infection, selection with Puromycin started (3 µg/ml for NIH/3T3 cells and 2 µg/ml for U2OS cells). The cells that survived Puromycin selection incorporated the sequences between the two long terminal repeats (LTRs) of the vector into their genome, thus expressing (i) the Cas9 protein via a constitutive promoter, (ii) one of the sgRNAs from the genome-wide library and (iii) the selection marker. That way, in each individual cell, one specific gene was knocked out. Cells were kept under selection for four days and were split in between to avoid 100% confluency. Splitting always occurred in a way that redundancy was kept. Six days post infection, cells were harvested by washing with PBS, centrifugation and resuspension in 10%FCS/PBS with a final cell concentration of about 5 x 10^6 cells/ml. Cells were passed through a cell strainer to avoid clump formation and kept on ice until FACS sorting. Sorting was performed into four different fractions for the main screen

[4] https://www.transomic.com/cms/Transomic/media/Homepage/FAQ%20Guidelines/CRISPR/FAQ-Why-calculate-the-MOI.pdf (November 07, 2021)

(low green/mid-to-high red fluorescence (GFP down); low red/mid-to-high green fluorescence (RFP down); high green and red fluorescence (both up); low green and red fluorescence (both down)) and two different fractions for the endogenous screen (low red/median green fluorescence (Scarlet down); high red/median green fluorescence (Scarlet up)). 500.000 WT cells were lysed in 2x lysis buffer per sorted condition and the cells were sorted into the same tubes. After sorting, 2x lysis buffer was diluted to 1x with 10% FCS/PBS or PBS and 100 µg/ml RNase A was added to each sample. The same amount of cells that were analyzed by FACS, were harvested as the "unsorted" fractions in 1x lysis buffer and 100 µg/ml RNase A. These lysed cells were stored at -20℃ until genomic DNA extraction.

Genomic DNA extraction of the screening samples

The lysates from the screening samples (with about 2×10^6 cells per ml of lysis buffer) were first sonified with a Branson sonifier (1 pulse at 20% amplitude for 5 sec) with 1 ml per 15 ml reaction tube at a time. This 1 ml was transferred afterwards to a 2 ml reaction tube, 1 volume of phenol/chloroform/isoamylacohol was added and the mixture was vortexed vigorously. Afterwards, the samples were centrifuged at 12.000 x g at RT for 20 min. About 900 µl of the upper phase was transferred to a new reaction tube and again 1 ml of phenol/chloroform/isoamylacohol was added, vortexed and centrifuged at 12.000 x g at RT for 20 min. About 750 µl of the upper phase were transferred to a new reaction tube and 0.1 volumes of 3 M sodium acetate and 1 volume of isopropanol was added, as well as 75 µg/ml Glycoblue. The samples were vortexed or inverted and stored at RT for 2 h or at -20℃ over night or until further usage and afterwards centrifuged at 12.000 x g for 30 min at 4℃ or RT. The pellet was washed twice with 950 µl 70% EtOH by vortexing and centrifugation at 12.000 x g for 5 min at RT. Afterwards, the pellet was air-dried and resuspended in water. The concentration was adjusted to 1 mg/ml. DNA was stored at -20℃.

Library preparation of the screening samples

Two PCRs were needed to generate the libraries from the plasmid or genomic DNAs. Enough reactions were performed from the unsorted material and the plasmid library material, to ensure that redundancy is kept and no bottleneck is introduced at these steps. From the sorted samples, the whole material was used in PCR reactions. The

following tables list the PCR conditions for both PCRs. The primers used can be found in table 4.15. Several PCR reactions were performed per condition. A semi-quantitative PCR was performed for each sample in order to determine the number of cycles needed to yield sufficient amounts of product, which could be visualized on an agarose gel, whilst at the same time avoiding over-amplification by choosing a cycle number, where the plateau phase was not yet reached.

PCR reagent	Volume/Amount
DNA	1 ng (plasmid) or 3 µg (gDNA) or 1 µl of the first PCR reaction
5x GC buffer	1x
dNTPs	0.2 mM
Forward primer	0.2 µM
Reverse primer	0.2 µM
DMSO	2%
Phusion	2% (v/v) of final volume
ad H_2O	50 µl

Table 5.7: PCR reaction for library preparation of screening samples.

Number of cycles	Temperature (°C)	Time (sec)
1	98	120
x	98	20
	60	20
	72	20
1	72	300
1	4	∞

Table 5.8: PCR cycling conditions for amplification of screening samples. x = varying number of cycles, that needed to be determined beforehand with a semi-quantitative PCR.

The second PCRs were gel-purified and analyzed on the Fragment Analyzer or the Experion. Subsequently, the samples were mixed equimolarly and loaded onto the NextSeq 500 for NGS sequencing. Again, redundancy was kept.

5.3.2 Knock-in cell line generation

Design and generation of the homology arms and the sgRNAs for the knock-ins

For the knock-in, a homology-directed repair template had to be generated, which was transfected later on in combination with an sgRNA, that targeted close to the start codon. The genomic sequence was received from the UCSC Genome Browser[5]). For the *RBM8A* knock-in, the 5' and 3' homology arms were designed to have a length of about 500 bp before and after the start codon, respectively. The PCRs for the homology arms were performed according to the protocol in section **??**. The 5' homology arm PCR was then purified, digested with AgeI and MluI and gel-purified. The 3' homology arm PCR was purified, digested with EcoRI and SpeI and gel-purified. The AID-tag, together with the V5-tag and the Blasticidin resistance marker, were received by MluI/EcoRI digestion of plasmid #621 from our clone collection, which was generated by Ashwin Narain in our group. A triple ligation reaction into pJet was performed over night and frozen the next day (see section 5.2.1). Subsequently, transformation, miniprep and maxiprep of the resulting HDR plasmid were performed (see section 5.2.1). For the *FBL* knock-in, the 5' homology arm (125 bp) was ordered as a gBlock. Directly adjacent to it, mScarlet-I-d2, followed by a GSG-P2A linker, a Blasticidin resistance gene and a SV40 late poly(A) signal were added and ordered within the same gBlock. The gBlock was cloned into pJet and the 3' homology arm was generated by PCR according to section 5.2.1 and cloned into the previously generated plasmid containing the gBlock.

The sgRNAs were designed manually in a way that the cut would be close to the start codon. The sgRNAs were phosphorylated, annealed and ligated into pX458 (Addgene #48138) for the *RBM8A* and the *FBL* knock-ins (see section 5.2.1).

[5]https://genome.ucsc.edu/ (October 26, 2021)

Transfection

200.000 U2OS cells were seeded per 10 cm plate and transfected the next day according to table 5.9.

Transfection reaction per 10 cm plate	Ingredients	Volume
DNA mix	Opti-MEM DNA	700 µl 9 µg
PEI mix	Opti-MEM PEI	700 µl 30 µl

Table 5.9: List of the transfection reactions used for transfection of the HDR template and the sgRNAs needed to generate the knock-in cell lines.

After 10 min of incubation at RT of the mixed DNA and PEI reactions, the DNA mix was added to the PEI mix dropwise and pipetted up and down. This transfection mix was then incubated for 20 min at RT. Meanwhile, cells were washed once with PBS and 6 ml of transfection medium was added, before the transfection mixture was added to the cells. The plates were swung gently and placed into the incubator. Medium was changed to full medium about six hours after transfection after one washing step with PBS.

Selection and clone "picking"

One or two days after transfection, the cells were split and about 3 to 4 days after transfection, selection with 7.5 µg/ml of Blasticidin was started. The medium with antibiotics was refreshed every 2-3 days until the killing control plate was dead, with no cell splitting in between. Cell from the condition, where the HDR template and the sgRNA were transfected, were split in various dilutions (ranging from 1:5 or lower to 1:1000) on 15 cm plates and Colonies were picked several days later from a dilution plate where clones were well separable and big enough to survive transfer (they could be seen without a microscope). For colony "picking", cells were washed once with PBS, before metal cloning rings (autoclaved) were pressed in vaseline (autoclaved) and placed around the individual cell colonies. 50 µl of trypsin were put into each cloning ring and incubated for about 20 min. The trypsinized cells were then transferred into a 24-well plate filled with 1 ml of medium per well.

Genomic DNA extraction to analyze knock-in event

The clones were analyzed for the knock-in event by extraction of genomic DNA and a subsequent PCR with primers targeting sequences close to the designed homology arms of the locus of interest. While splitting the clones, a fraction of it was spinned down at 200 x g for 4 min at RT and the pellet was either frozen at -20℃ or directly used for extraction of gDNA. To this end, 500 µl 1x lysis buffer and 4 µl Proteinase K were added per sample and pipetted up and down. The lysed cells were incubated at 37℃ for 2 h on a rotating wheel. 250 µl of a saturated sodium chloride solution was added and the samples were vortexed for about 20 sec and subsequently incubated on ice for 10 min. After centrifugation at 5000 x g for 10 min at 4℃, the supernatant was transferred into a new reaction tube and supplemented with 15 µg Glycoblue and 650 µl isopropanol. The tube was inverted, incubated for 15 min at RT and centrifuged at full speed for 10 min. The pellet was washed twice with 150 µl 70% ethanol and 5 min of centrifugation at RT at maximum speed. The pellet was air-dried and resuspended in 15 µl water. Genomic DNA was stored at -20℃ and a PCR was performed to check, whether the knock-in event occurred.

5.3.3 Chromatin immunoprecipitation (ChIP)

Seeding, treatment and harvest

1.6 x 10^6 cells were plated per 15 cm dish. The next day, the cells were treated with 500 µM auxin or solvent (H_2O) for 6 h, before one plate was counted and 1 % formaldehyde was added to the cells on the other plates. These plates were smoothly shaken and fixation was stopped by the addition of 111 mM glycine, followed by about 5 min of incubation at RT while the plates were smoothly shaken. From now on it was worked on ice. Cells were washed twice in ice-cold PBS and scraped off in 1 ml of ice-cold PBS, freshly supplemented with protease and phosphatase inhibitors. The suspension of up to 10 plates were pooled in one reaction tube and centrifuged at 470 x g for 15 - 20 min at 4℃. The cells were lysed in 3 ml ChIP lysis buffer 1, freshly supplemented with protease and phosphatase inhibitors, per 10 plates. Cell lysis was performed for 20 min on ice and nuclei were collected by centrifugation at 470 x g for 15 - 20 min at 4℃. The pellets were flash-frozen in liquid nitrogen and stored at -80℃ until further usage.

Sonication

The nuclei of 5 - 7 plates were resuspended in 1 ml ChIP lysis buffer 2, freshly supplemented with protease and phosphatase inhibitors. After 10 min of incubation on ice, 1 ml of each lysate was transferred into a Covaris tube and sonicated for 50 min at 7℃. Afterwards, the samples were kept on ice, until sonication efficiency was validated.

To check for sonication efficiency, 25 µl before and after sonication were separated and decrosslinked by the serial addition of 258.8 µl 1x TE buffer, 163 mM NaCl and 40.7 µg/ml RNase A and incubation at 37℃ for 1 h and then over night at 65℃ with shaking at 750 - 800 rpm. The next day, 4 mM EDTA and 200 µg/ml proteinase K were added and the samples were incubated for 2 h at 45℃ with shaking at 700 rpm. DNA was isolated via phenol/chloroform extraction. To this end, 1 volume of phenol/chloroform/isoamylacohol was added and the mixture was vortexed for 5 min. Afterwards, the samples were centrifuged at full speed at RT for 5 min. The upper phase was transferred to a new reaction tube and 15 µg Glycoblue, as well as 30 µl of 3 M sodium acetate (pH 5.2) and 1 ml ice-cold 100% EtOH were added sequentially. The samples were inverted and incubated at -20℃ for at least 30 min and afterwards centrifuged at full speed for 20 min at 4℃ or RT. The pellet was washed twice with 700 µl ice-cold 70% EtOH by vortexing and centrifugation at full speed for 10 min at 4℃. Afterwards, the pellet was air-dried at RT and resuspended in 25 µl TE buffer. 10 µl were loaded on a 2% agarose gel and sonication efficiency was checked (fragment sizes should have been below 500 bp).

After fragment size determination, the lysates, which were kept on ice at 4℃ until then, were either sonicated again or centrifuged at 20.817 x g for 20 min at 4℃ and the supernatant was kept for IP.

Chromatin-Immunoprecipitation

15 µl Dynabeads A were mixed with 15 µl Dynabeads G per IP. Beads were washed three times with 1 ml BSA/PBS (see subsection 5.2.6). Beads were resuspended in 400 µl BSA/PBS per IP and 3 µg of antibody were added per IP. The antibodies were incubated with the beads over night at 4℃ on a rotating wheel. Beads were then washed again three times with 1 ml BSA/PBS as before and resuspended in 30 µl BSA/PBS per IP.

Two to four aliquots of 1% input chromatin were taken out of the lysates. From the remainder, as much chromatin as would correspond to one 15 cm plate, was added to the beads and incubated over night on a rotating wheel at 4℃. Beads were washed three times each for 5 min at 4℃ with 950 µl of ChIP wash buffer 1 first, then ChIP wash buffer 2, followed by ChIP wash buffer 3. Beads were then washed once with 950 µl pre-cooled TE buffer, while the reaction tube was changed within the last washing step. Beads were shortly spinned down and the remainder of TE buffer was removed before elution with 150 µl ChIP elution buffer was performed by incubation on a rotating wheel at RT for 15 min. This elution was repeated once and the eluates were merged. The 1% input samples were also filled up to 300 µl with elution buffer.

Samples (also input) were reverse crosslinked and DNA was extracted via phenol/chloroform extraction as described in subsubsection 5.3.3, but using 42.8 mM Tris buffer instead of TE buffer, 171 mM NaCl and 61 µg/ml RNase A and later 5.2 mM EDTA and 149 µg/ml proteinase K. After phenol/chloroform extraction, DNA was resuspended in 500 µl H_2O and stored at -20℃.

ChIP-qPCR

Samples were run in technical triplicates with 5 µl DNA and 4.5 µl of PowerUp SYBR Green Master Mix and 0.5 µM primer mix per well. The used primers can be found in table 4.21. The 96-well plate was sealed with a transparent foil and the run conditions were the following:

Number of cycles	Temperature (℃)	Time (sec)
1	50	120
	95	120
40	95	3
	60	30
1	95	15
	60	60
	rise to 95℃ with +0.3℃ steps	
	95	15

Table 5.10: ChIP-qPCR cycling conditions.

ChIP efficiency was calculated as enrichment over 1% input. For this, the cycle threshold (C_T) value of the sample was subtracted from the C_T of the corresponding input sample for each well individually, leading to the ΔC_T value. The relative expression was then calculated like this: $2^{\Delta C_T}$. Afterwards, the mean and the standard deviation of the technical triplicates of the relative expression values was calculated and displayed.

5.4 Transcriptomics

5.4.1 RNA extraction for qRT-PCR analysis of the reporters

RNA extraction was performed with the RNeasy Mini Kit according to manufacturer's instructions, including on-column DNAse I digestion. However, to completely remove RPE buffer before elution, the column was centrifuged twice in inverted orientations of the reaction tubes at full speed for 3 min each and elution was performed with 30 µl of water. RNA was stored at -80℃.

5.4.2 cDNA synthesis for qRT-PCR analysis of the reporters

2x 2 µg of RNA were diluted in H_2O and 400 ng/ml of random primers (Sigma/Roche, #11034731001) in a final volume of 20 µl per sample. The solutions were incubated at 65℃ for 1 min and then immediately transferred to ice and incubated for 2 min. 78 µl of cDNA master mix were added to the samples. This master mix consisted of the following ingredients:

Ingredient	µl/sample
5x MLV buffer	20
Ribolock RNase Inhibitor	0.4
RNase-free water	55.1
10 mM dNTP mix	2.5

Table 5.11: Master mix used for cDNA synthesis per sample.

2 µl of M-MLV reverse transcriptase was added to half of the samples. The second half was used as a negative control, where the reverse transcriptase was replaced by water.

These 100 µl per sample were incubated for 10 min at 23℃, followed by incubation for 50 min at 37℃ and 15 min at 70℃. The sample was filled up with water to 1 ml final volume. cDNA was stored at -20℃.

5.4.3 quantitative real-time PCR (qRT-PCR) for analysis of the reporters

10 µl of cDNA or the corresponding negative control sample were pipetted in triplicates into a 96-well plate. 10 µl of master mix (1 µl primer pair (10 µM each) mixed with 9 µl of PowerUp SYBR Green Master Mix) were added per well and the samples were run with the following conditions:

Number of cycles	Temperature (℃)	Time (sec)
1	50	120
	95	120
40	95	3
	60	30
1	95	15
	60	60
	rise to 95℃ with +0.3℃ steps	
	95	15

Table 5.12: qRT-PCR cycling conditions.

The $\Delta\Delta C_T$ method was used to calculate relative expression values.

5.4.4 RNA sequencing (RNA-Seq)

Seeding, transfection of siRNAs, and harvest

0.8 x 10^6 $3T3^{Fbl\text{-}GFP;Rpl18\text{-}RFP}$ cells or NIH/3T3 cells were seeded on 10 cm plates. About 20 to 24 hours later, siRNAs were transfected the following way: for each plate, 7 µl RNAiMAX were mixed with 513 µl Optimem and 7 µl siRNA (20 µM stock) were mixed with 513 µl Optimem. These two transfection reactions were mixed and incubated for 35 min at RT. Meanwhile, cells were washed once with PBS and medium was changed to 5 ml transfection medium (2%FCS/DMEM). The transfection mix was then added to

the cells and the plates were gently swung and put into the incubator. 10 hours later, cells were washed once with PBS, before full medium was added. The next day, 1x 10^6 cells per condition were splitted on 10 cm plates. About 48 h after transfection, one plate was counted, one was harvested for WB analysis and triplicates were harvested for RNA-Seq in RLT buffer.

Library preparation

RNA was extracted with the RNeasy Mini Kit according to manufacturer's instructions. RNA concentration was measured with the Nanodrop and RNA quality was measured on the Fragment Analyzer. Library was prepared with the NEBNext Poly(A) mRNA Magnetic Isolation Module and the NEBNext Ultra II Directional RNA Library Prep Kit for Illumina according to manufacturer's instructions. The library was again run on a Fragment Analyzer and mixed equimolarly for Illumina sequencing.

5.4.5 Generation of 4-thiouridine-labeled T cell spike-in

160 $\times$ 10^6 T lymphoma cells were split onto four falcons, each with 40 $\times$ 10^6 cells in 10 ml of medium. 2 mM 4sU was added per falcon and they were incubated (standing and loosely capped) in the incubator for 24 minutes. After 10 minutes the falcons were inverted once. The cells were spinned down at about 200xg for 4 min at RT. After 30 minutes of total 4sU labeling time, medium was sucked off and cells were lysed in 5 ml of QIAzol per tube. 1 ml aliquots were generated in 1.5 ml reaction tubes, flash-frozen in liquid nitrogen and stored at -80℃.

5.4.6 4-thiouridine sequencing (4sU-Seq)

Seeding

4 $\times$ 10^6 U2OS WT cells (infected with TIR1) were seeded per 15 cm dish in triplicates (for +IAA and +4sU treatment). One additional plate was seeded and used for WB later on (+ IAA, - 4sU) and another plate was used as a "-4sU" condition, which should result in no pull down of RNA later on. Moreover, 4 $\times$ 10^6 U2OS$^{N\text{-}AID\text{-}RBM8A}$ cells (infected with TIR1) were seeded per 15 cm dish in triplicates for each of the conditions (+/- IAA, +4sU). From these cells additional plates used for WB were seeded as well (+/-IAA).

4sU as well as the samples including 4sU-labeled RNA were protected from light as much as possible during the whole procedure.

Treatment

The WT cells were treated with auxin (500 µM) and the U2OS$^{N\text{-}AID\text{-}RBM8A}$ cells were treated with auxin (500 µM) or the same volume of H_2O for a total of six hours and labeled with 4sU (2 mM) for the last 15 minutes prior to harvest with each of the treatments happening via a medium change.

Harvest

Cells were harvested for WB through washing with PBS twice and lysis in 800 µl RIPA buffer (per plate), freshly supplemented with protease and phosphatase inhibitors (1:1000). For more details, please refer to section 5.2.2.

RNA was harvested by aspiration of the medium and subsequent addition of 2.1 ml of QIAzol. Care was taken so that QIAzol covered the whole plate. A cell scraper cleaned in Millipore water was used to scrape cells from the plate. The lysates were triturated about 10 times before they were transferred into a 15 ml reaction tube, flash-frozen in liquid nitrogen and stored at -80℃.

Total RNA extraction

The lysates were thawed at RT and 100 µl of in-house made T cell spike-in (please refer to section 5.4.5 for details on the generation of the spike-in) was added to each "+4sU" sample. The mixture was then split onto three 1.5 ml reaction tubes (but later on distributed onto two columns only) and triturated about 10 times with a pipette and a 0.6 x 30 mm needle on top of a 1 ml tip. 140 µl chloroform was added and the sample was vortexed for about 15 seconds. Further steps were performed according to manufacturer's instructions (miRNeasy mini kit) with the exception, that 500 µl of RWT buffer was used before and after DNase I digestion and centrifugation was performed for 1 - 3 min each. RNA was eluted in 30 µl per column, resulting in a total volume of 60 µl per sample. After measurement of the concentration, I by accident added 120 µl

of water to all the samples, thus diluting it too much. To concentrate it, I precipitated the RNA.

RNA precipitation

15 µg of GlycoBlue, 20 µl of 3 M sodium acetate (sterile-filtered) and 500 µl of ice-cold 100% EtOH were added sequentially and the solution was vortexed. This mixture was then placed at -20℃ for 1 hour and centrifuged at full speed for 30 min at 4℃ to precipitate the RNA. The pellet was washed twice with 0.5 ml ice-cold 75% EtOH and centrifuged in between at full speed at 4℃ for 48 min and 10 min, respectively. EtOH was removed, the reaction tube was spinned down at full speed for 10 sec, so that the remaining EtOH could be completely removed. The pellet was air-dried and resuspended in 40 µl H_2O.

Biotin-labeling and pull down of labeled RNA

42 µg (replicate 1) or 46 µg (replicates 2 and 3) of RNA were used for biotinylation and pull down of biotinylated RNA. To this end, RNA was first denatured at 65℃ for 5 min, followed by 10 min on ice, before 100 µl of biotin labeling buffer (2.5x) and 0.2 µg (50 µl) of biotin-HPDP-DMF was added. The reaction was mixed by rigorous vortexing for at least 15 sec and incubated for 2 h on a shaker at RT with vortexing steps in between every 15 min. 250 µl chloroform/isoamylacohol (24:1) was added, the samples were vortexed twice for 10 sec and loaded onto MaXtract high density tubes (the tubes were centrifuged at RT, 14.000xg, 30sec before). The samples were centrifuged at 14.000xg for 5 min at 4℃ and the upper phase (about 240 µl) was transferred into a new 1.5 ml low-binding microcentrifuge tube. These tubes were also used for all the following steps until usage of the RNeasy MinElute cleanup kit.

15 µg GlycoBlue was added, the solution was briefly vortexed and RNA was precipitated by the sequential addition of 24 µl 5 M NaCl and 220 µl ice-cold isopropanol, followed by vortexing and incubation at RT for 5 min, before centrifugation was performed at 20.000xg for 20 min at 4℃. The pellet was washed twice with 500 µl of ice-cold 75% EtOH, followed by centrifugation at 20.000xg at 4℃ for 10 min. EtOH was completely removed, the pellet was dried at RT and resuspended in 100 µl H_2O. 50 µl of properly mixed MyOne Streptavidin T1 Dynabeads per sample were washed twice with an equal volume of Dynabeads washing solution A and once with Dynabeads washing solution

B with the help of a magnetic rack. The beads were then resuspended in 100 µl of Dynabeads washing buffer (2x) per sample. These 100 µl beads were then mixed with 100 µl RNA obtained from the previous step and incubated on a rotating wheel at RT for 15 min. The beads with the attached biotinylated RNA were washed four times with 1x Dynabeads washing buffer with the help of a magnetic rack. The beads were resuspended in 100 µl of freshly prepared 100 mM DTT and incubated at RT for 5 min on a rotation wheel to elute the RNA. After a quick spin-down and a separation on a magnetic rack, the RNA-containing supernatant was transferred to a new 1.5 ml reaction tube and cleaned up using the RNeasy MinElute cleanup kit according to manufacturer's instructions. The pulled down RNA was stored at -80°C and the concentration was measured with the Quant-iT RiboGreen RNA assay kit. To this end, 5 µl of Ribogreen reagent were mixed with 10 ml 1x TE first. 200 µl of it was added to a standard dilution, which was generated by using a 2 ng/µl stock C solution in 1x TE, that was serially diluted to obtain 40/20/10/5/2.5/1.25 pg/µl RNA standards in 200 µl 1x TE final volume. 1 µl of the RNA sample from the 4sU-Seq experiment was then mixed with 249 µl 1x TE and 250 µl of the previously diluted Ribogreen RNA reagent. 190 µl of each sample or standard were pipetted into a 96-well plate in duplicates and measured at the Tecan (480 nm excitation/520 nm emission).

Library preparation

Library was prepared starting from 105 ng RNA per sample in 12 µl total volume with the NEBNext rRNA Depletion Kit according to manufacturer's instructions using a 5x dilution of the adaptors and 11 PCR cycles. The number of PCR cycles needed was determined via a qPCR that was performed on 9 µl of the PCR reaction (meanwhile the other half was left on ice) mixed with 1 µl of 10x SYBR Green in DMSO. A mock control (a sample for which water was used instead of RNA at the beginning of the library preparation procedure) and a water control (water with PCR enzyme mix and primers) were also measured via qPCR in a sealed 96-well plate. The cycle number where all samples are within the linear phase (as seen in a muliple component plot) was used for the PCR during library preparation. The libraries were measured on a Fragment Analyzer (diluted in 0.1x TE buffer) and equimolarly mixed for sequencing on a NextSeq 500 from Illumina.

5.5 Bioinformatics

5.5.1 Model-based Analysis of Genome-wide CRISPR/Cas9 Knockout (MAGeCK) for analysis of the screens

Fastq files for the individual lanes per sample were merged using cat. To remove adapters and only retain sgRNA sequences, reads were processed with cutadapt (v1.18) [Martin, 2011]. Trimming was performed in two passes, using first the command line argument `-g CGAAACACCG` and in a second step the command line argument `-a GTTTTAGAGC`. Reads were aligned to sgRNA sequences using bowtie2 (v2.3.4) [Langmead and Salzberg, 2012] in stranded mode through the use of the command line parameter `--norc`. Following sorting of reads with samtools (v1.9) [Li et al., 2009], reads were assigned to sgRNAs using the MAGeCK (v0.5.7) [Li et al., 2014] `count` command. Enrichment was calculated using MAGeCK `test` in positive selection mode and with "total" as normalization strategy, through the use of the command line arguments

`--norm-method total --sort-criteria pos`.

5.5.2 Statistics and plotting

Unless otherwise indicated, statistics were performed in R. Where applicable, p values were corrected for multiple testing using the Benjamini-Hochberg FDR method.

Plots were generated using the ggplot2 and eulerr libraries for R.

6 Results

Parts of this thesis have been submitted for publication as a journal article.

The overall aim of the PhD project was the identification of new transcriptional regulators of ribosome biogenesis. Corresponding genes are represented in the form of a ribosome biogenesis (RiBi) gene and a ribosomal protein (RP) gene in this thesis. The base for this overall goal was a genome-wide knockout reporter screen in a cell clone that expresses two reporters: (i) a green fluorescent protein under the control of a ribosome biogenesis gene promoter and (ii) a red fluorescence protein under the control of a ribosomal protein gene promoter (see figure 6.1).

By the use of a genome-wide CRISPR knockout library, I aimed to identify proteins that are needed for the transcriptional regulation of RiBis and/or RPs via the effect of such a knockout on fluorescent reporter expression: if a transcriptional regulator of RiBis is targeted by one of the guide RNAs of the library, then in this very cell green fluorescence would decline, since the reporter is expressed under the control of a RiBi promoter. Red fluorescence, however, which is under the control of a ribosomal protein promoter, would not get affected. Along this line, guide RNAs that target proteins important for RP expression, but not RiBi expression, would lead to less red fluorescence, though unchanged green fluorescence. Additionally, in case repressors of RiBi and RP expression would be targeted by guide RNAs, the fluorescence of both fluorescent reporters should increase and if activators of both processes are targeted, this should lead to a decrease in fluorescence of both reporters. All of these fractions can be sorted and compared to an "unsorted" fraction of cells for their enrichment of specific guide RNAs. For a successful screen, several questions needed to be considered first:

(i) Which exact fluorescent reporters shall be used?
(ii) Which exact promoters should be chosen for the expression of the reporters?
(iii) Is the whole procedure in principle, but especially the sorting approach, sufficient to be able to enrich for positive controls as a measure for the applicability of the screening setup?

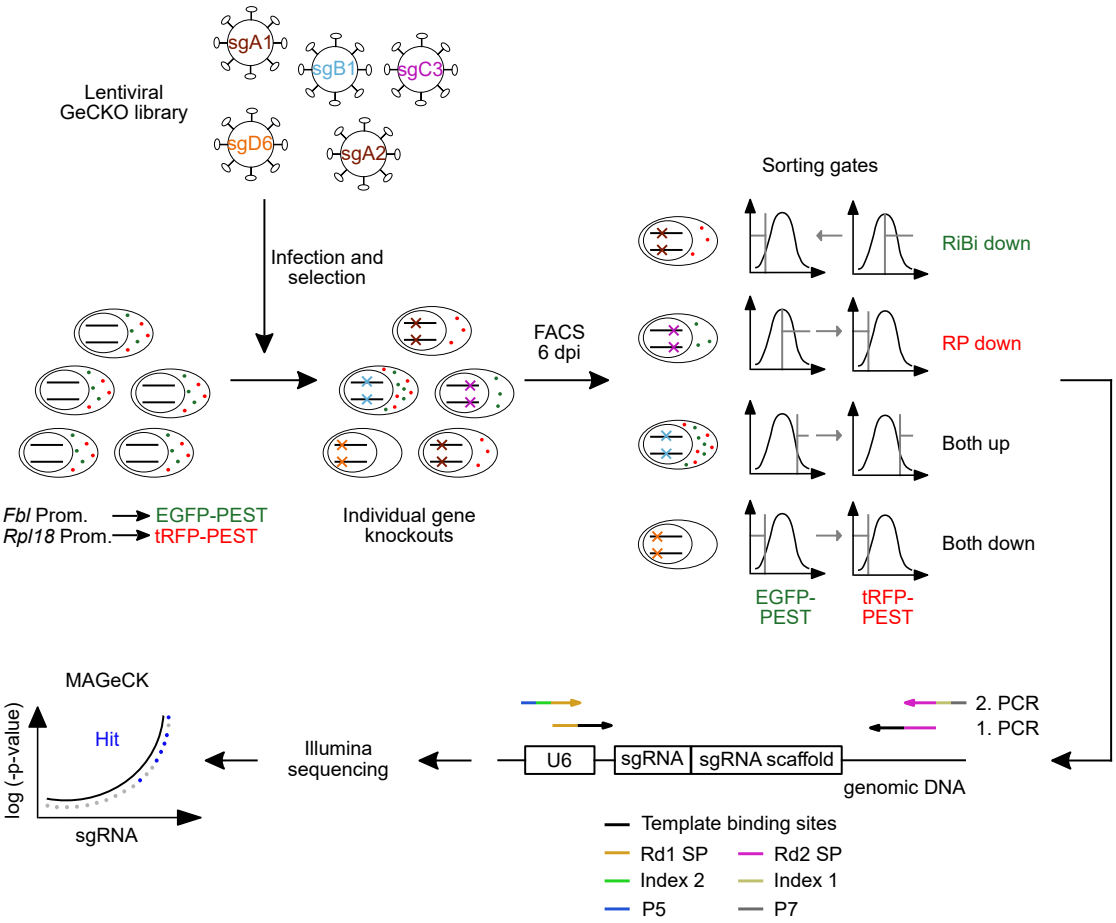

Figure 6.1: Scheme of the genome-wide CRISPR/Cas9 screen in NIH/3T3 cells. The 3T3$^{\text{Fbl-GFP;Rpl18-RFP}}$ cell line, which expresses EGFP-PEST under the control of an approx. 500 bp promoter fragment of the *Fibrillarin* (*Fbl*) gene and tRFP-PEST under the control of an approx. 500 bp promoter fragment of the *Ribosomal protein L18* (*Rpl18*) gene, was infected with Cas9 and a genome-wide sgRNA library. Six days after infection and selection, the cells were sorted for the indicated populations: Cells that displayed high red fluorescence, but low green fluorescence, were sorted as the "GFP/RiBi down" condition. Cells that showed high green fluorescence, but low red fluorescence, were sorted as the "RFP/RP down" condition. Cells that presented high or low green and red fluorescence were sorted into the "both up" or "both down" fractions, respectively. Genomic DNA was extracted and the sgRNA loci were amplified via two PCRs. With the first PCR the read sequencing primer sequences (Rd1 SP and Rd2 SP) were introduced and with the second PCR the indices, which distinguish the different samples during sequencing, were introduced. The second PCR was also used to introduce the sequences needed for binding to the flow cell (P5 and P7). The gel-purified libraries were then used for Illumina sequencing and the screen was analyzed with the bioinformatic "model-based analysis of genome-wide CRISPR-Cas9 knockout" (MAGeCK) tool [Li et al., 2014]. Prom. = promoter, dpi = days post infection, RiBi = ribosome biogenesis, RP = ribosomal protein, U6 = U6 promoter, sgRNA = single guide RNA.

6.1 Selection of suitable fluorescent proteins as reporters for the screen

The fluorescent reporters needed to fulfill two criteria:
i) They had to be as stable as needed to reach enough fluorescence intensity above background at steady state, meaning their degradation time needed to be slower than their maturation time.
ii) At the same time, the reporters had to be as unstable as possible, so that their intensity can change rapidly upon transcriptional alterations.

I started by testing the applicability of turboGFP (tGFP), a bright green fluorescent protein [Evdokimov et al., 2006]. To analyze its stability, I performed a cycloheximide (CHX) assay, which revealed a half-life of more than 24 hours (see figure 6.2A). To reduce stability, I fused a mutated version of the PEST domain of murine ornithine decarboxylase (mODC) to tGFP. The wild type (WT) PEST domain of the mODC protein was already used previously to destabilize fluorescent proteins, such as tGFP [Evdokimov et al., 2006] or enhanced GFP (EGFP) [Li et al., 1998], thus reducing the half-life of each of the two green fluorescent proteins to about 2 hours [Evdokimov et al., 2006, Li et al., 1998]. In their publication, Li et al. also used a triple mutant of the PEST domain (E428A/E430A/E431A) that decreased the half-life of EGFP even more [Li et al., 1998]. I thus used this mutant PEST domain and fused it to tGFP, which hereafter is called tGFP-PESTmut. This fusion resulted in a reduction of the protein half-life to about 1.5 hours (see figure 6.2B) and a concomitant reduction in fluorescence intensity (see figure 6.2C - compare *Fbl*_800-tGFP with *Fbl*_800-tGFP-PESTmut). However, this reduction in fluorescence intensity, in combination with the fact, that all the tested ribosomal protein gene or ribosome biogenesis gene promoter fragments used to drive reporter expression were much weaker than the spleen focus forming virus (SFFV) promoter (see figure 6.2C - compare SFFV-tGFP with *Fbl*_800-tGFP-PESTmut; also see figure 6.3), yielded in no detectable fluorescence.

The search for a more suitable fluorescent reporter ended in testing of the more commonly used green fluorescent protein "enhanced GFP" (EGFP). In contrast to tGFP it is only a weak dimer, which might improve maturation and thus fluorscence intensity when expression is driven by weak promoters. EGFP was fused to the WT PEST mODC domain instead of the mutated one, to regain some stability. Indeed, the half-life of this fusion protein was only about 4 hours (see figure 6.2D). Without further testing, this

WT mODC domain was also fused to turboRFP (tRFP-PEST), which was subsequently used as the second reporter (see figure 6.1).

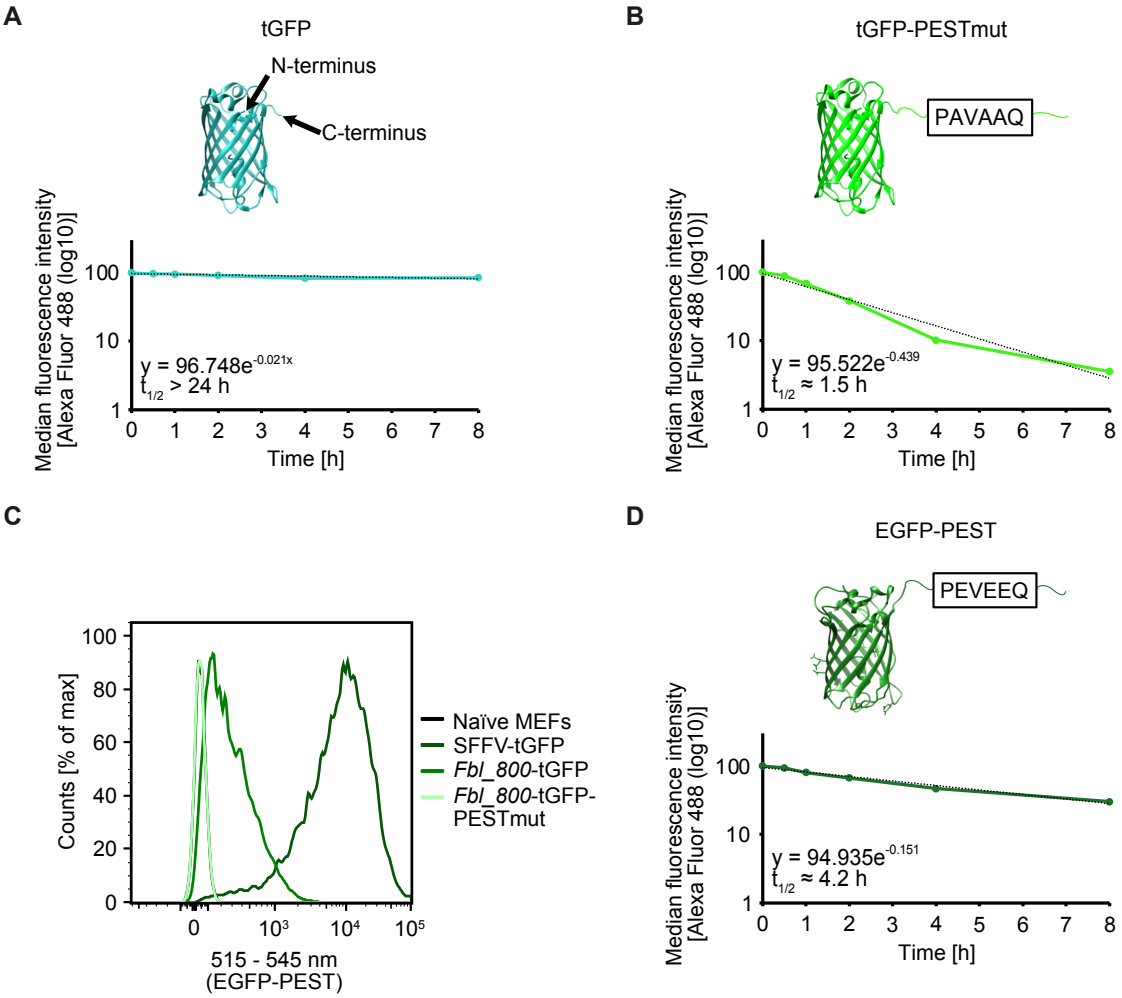

Figure 6.2: Stability differences between the green fluorescent reporter alternatives. (A) Monomeric structure of tGFP from [Evdokimov et al., 2006] (RCSB 2G6Y) and CHX (100 µg/ml) assay on HEK cells expressing SFFV-driven tGFP. Single experiment. tGFP = turbo green fluorescent protein. (B) Monomeric structure of tGFP from [Evdokimov et al., 2006] (RCSB 2G6Y), that was manually extended by a scheme of the murine PEST domain of the ornithine decarboxylase (ODC) protein. The triple alanine mutations within the PEST sequence are indicated. Lower subpanel shows the CHX (100 µg/ml) assay on HEK cells expressing SFFV-driven tGFP-PESTmut. Single experiment. tGFP-PESTmut = triple mutated (E428A/E430A/E431A) PEST domain from the murine ODC protein fused to tGFP. (C) Murine embryonic fibroblast (MEF) cells infected with the indicated reporter constructs were analyzed via FACS for their green fluorescence intensity. Single experiment. Naïve MEFs = uninfected MEFs, SFFV = spleen focus forming virus promoter, *Fbl_800* = *Fibrillarin* promoter fragment of approx. 800 bp. (D) Structure of EGFP from [Arpino et al., 2012] (RCSB 4EUL), that was manually extended by a scheme of the murine PEST domain of ODC. For a better comparison with (B), the WT amino acids of the sequence mutated in (B) is depicted. Lower subpanel shows the CHX (10 µg/ml) assay on U2OS cells expressing SFFV-driven EGFP-PEST. Single experiment. EGFP-PEST = PEST domain from the murine ODC protein fused to EGFP. (A) and (B) and (D) h = hours, $t_{1/2}$ = half-life.

6.2 Selection of suitable promoter sequences for reporter cell line generation

More than 200 ribosome biogenesis factors and about 80 ribosomal proteins do exist in mammalian cells. Several of them were tested prior to the screen, whether they meet a set of criteria that needed to be fulfilled by the promoters in order to be considered suitable for the screen:
(i) The promoter fragments should be functional in the sense that they lead to a decent expression of the reporter.
(ii) The promoter fragments were also tested for their changes in activity upon reduction of the transcription factor MYC, a well known regulator of ribosome biogenesis [van Riggelen et al., 2010, Lorenzin et al., 2016]. To this end, I made use of a murine T lymphoma$^{\text{MYC-Tet-Off}}$ cell line [Felsher and Bishop, 1999] that expresses a human MYC transgene under the control of a tetracycline-dependent promoter, which is switched off upon addition of doxycycline (Dox). MYC-dependent target gene expression is shut down accordingly, thus enabling the quantification of the promoter fragment-dependent expression of the reporter transcripts via quantitative real-time PCR (qRT-PCR).

As mentioned above, there are more than 200 ribosome biogenesis genes and about 80 ribosomal protein genes. Before I started my thesis, possible gene promoters were preselected by Elmar Wolf. He firstly ranked the genes according to their expression changes (fold change) induced by MYC depletion in U2OS and T lymphoma$^{\text{MYC-Tet-Off}}$ cells. Secondly, since the occurrence of E-boxes might well contribute to a possible differential regulation of RiBis and RPs (see introduction subsection 3.4.2), the presence (RiBi) or absence (RP) of a canonical E-box sequence in the MYC-bound promoter region was also included as a selection parameter. Thirdly, ChIP-Seq data were used to additionally filter for genes for which the majority of the called MYC peak(s) was located in front of the start codon, since all cis-regulatory elements located after the start codon would be lost when the fluorescent reporter,instead of the RiBi/RP gene, is following the promoter. I tested the activity of a selection of promoters fulfilling the aforementioned parameters in quantitative real-time polymerase chain reaction (qRT-PCR) experiments and included different lengths of the promoter fragments to investigate the minimum length needed to drive most efficient reporter expression. Accordingly, figure 6.3 shows an array of murine ribosome biogenesis gene promoter fragments (*Fbl*, *Rrs1*, *Tsr1*) and ribosomal protein gene promoter fragments (*Rpl18*, *Mrpl22*, *Mrpl1*, *Mrps17*, *Rpl21*) of different lengths, that induce the expression of tGFP-PESTmut.

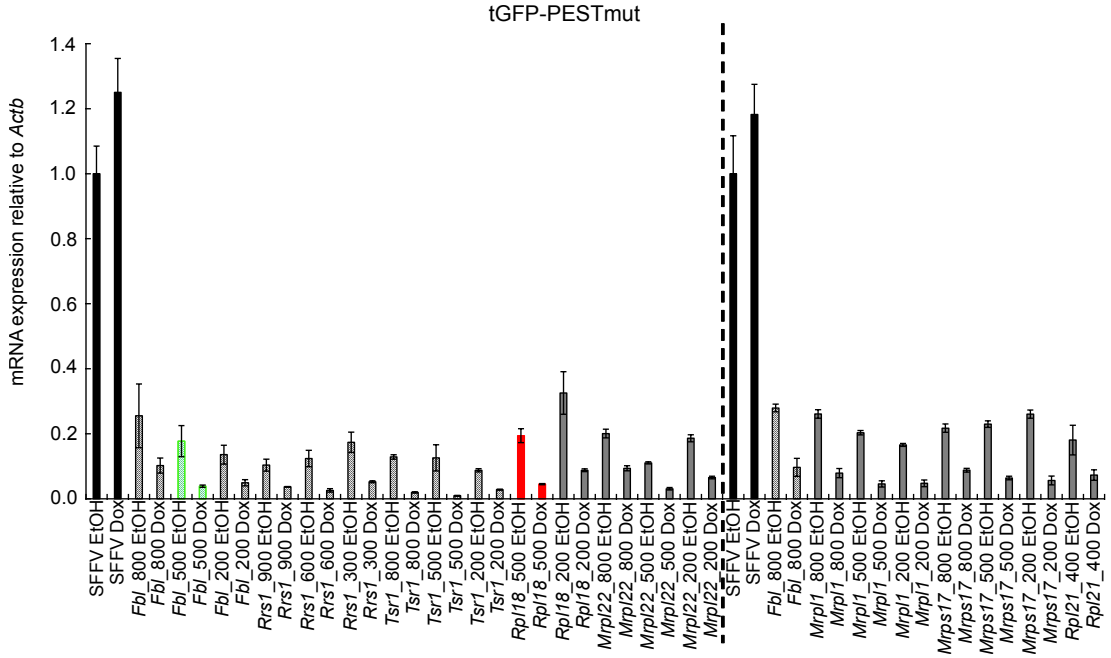

Figure 6.3: Responsiveness of different promoters to MYC depletion. T lymphoma$^{\text{MYC-Tet-Off}}$ cells were infected with the indicated reporter constructs. The indicated names are corresponding to the gene promoter and the variable length (in bp) of the promoter fragment, always ending in front of the start codon of the gene. The bars of the SFFV-promoter construct are shown in black, the ones of the RiBi gene promoter constructs are gray-shaded or green and the bars representing the RP gene promoter constructs are filled gray or red. The green and red promoters were chosen for further usage in the screen. Expression was analyzed normalized to *β-Actin*. The dashed line separates the two plates that were run on the quantitative real-time PCR cycler. Representative experiment from a duplicate (for some promoters triplicate) experiment.

Compared to the SFFV-driven expression of tGFP-PESTmut, all the tested promoter fragments showed much weaker promoter activity (compare the EtOH conditions of the promoter constructs with the EtOH condition of the SFFV construct in figure 6.3). In contrast to the SFFV construct, the tested promoters exhibited reduced activity upon MYC depletion (Doxycycline treatment), indicating, that all the tested promoter fragments are functional and possess cis-regulatory elements responsible for a change in activity upon MYC withdrawal. A trade-off between high absolute induction of reporter expression and high responsiveness to MYC depletion yielded in the choice of the 564 bp long promoter fragment (fold change Dox/EtOH: 0.219320619) of the *Fibrillarin* (*Fbl*) gene as a representative promoter for RiBi genes. The 569 bp promoter fragment (fold change Dox/EtOH: 0.232656381) of the *Ribosomal protein L18* (*Rpl18*) gene was chosen as a representative promoter for RP genes.

MYC-binding at the *Fbl* and the *Rpl18* promoters and MYC-dependent (Dox condition) regulation of the respective genes in T lymphoma$^{\text{MYC-Tet-Off}}$ cells are depicted in figure

6.4. In this figure, a browser track picture from ChIP-Seq data (subpanel A) [Walz et al., 2014] and RNA-Seq data (subpanel B) from Sarah Dötsch, a former master student in our working group, are shown.

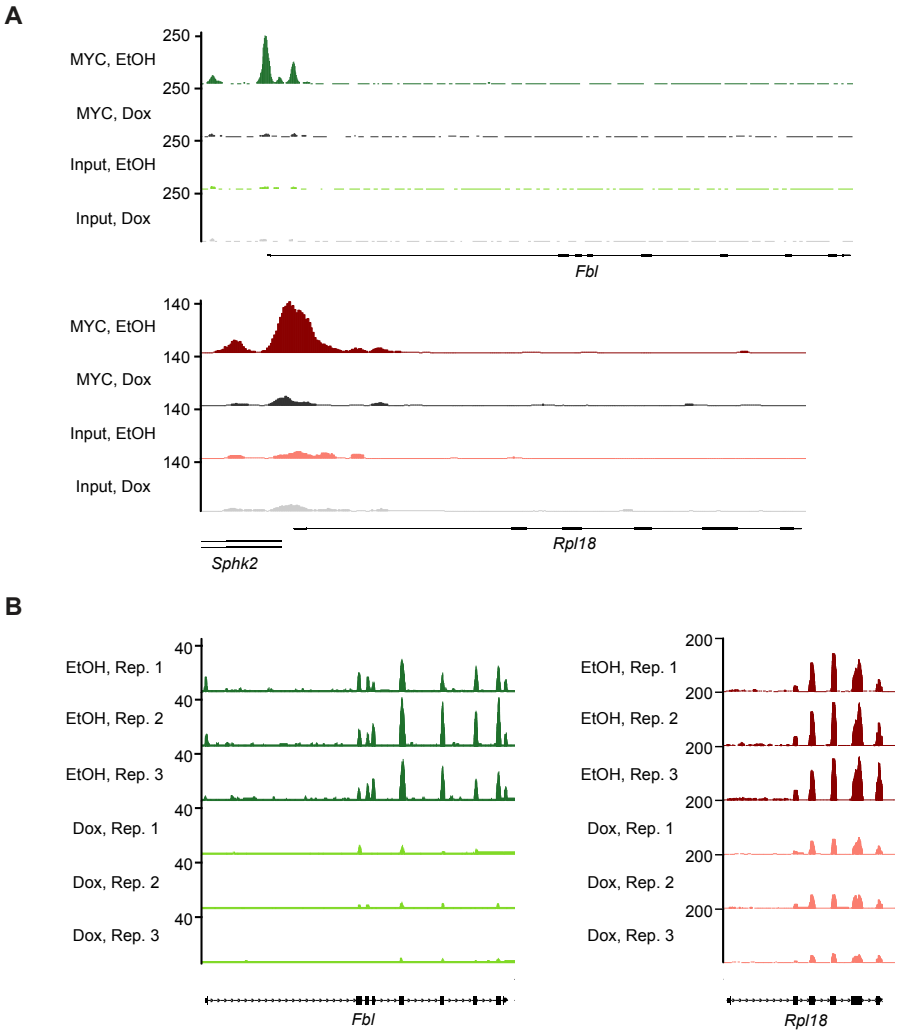

Figure 6.4: MYC-binding (A) and MYC-dependent regulation (B) of the endogenous *Fbl* and *Rpl18* genes in T lymphoma$^{\text{MYC-Tet-Off}}$ cells. (A) Data from [Walz et al., 2014]. (B) Data from Sarah Dötsch, a former master student in our laboratory. (A) and (B) Dox = doxycycline treated cells (MYC is switched off). EtOH = control treatment with EtOH.

With the above tested tools in hand, a NIH/3T3 cell clone with enough fluorescence intensity could be generated, that expressed EGFP-PEST under the control of the approx. 500 bp *Fbl* promoter fragment and tRFP-PEST under the control of the approx. 500 bp *Rpl18* promoter fragment (see figure 6.5). The clone was called "3T3$^{\text{Fbl-GFP;Rpl18-RFP}}$".

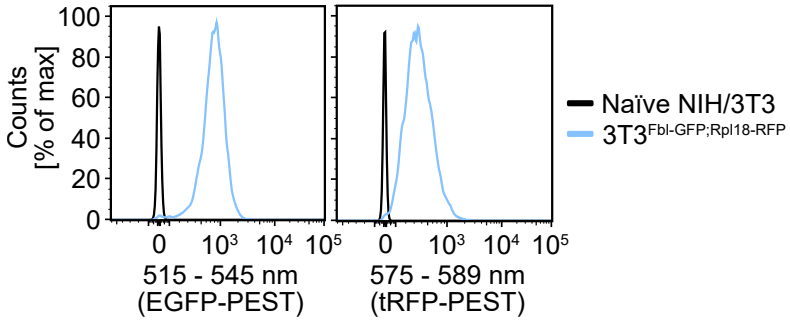

Figure 6.5: FACS profile of the screening cell line 3T3$^{\text{Fbl-GFP;Rpl18-RFP}}$. 3T3$^{\text{Fbl-GFP;Rpl18-RFP}}$ is a murine NIH/3T3 cell line, that expresses EGFP-PEST under the control of the approx. 500 bp *Fbl* promoter fragment and tRFP-PEST under the control of the approx. 500 bp *Rpl18* promoter fragment. The plots were generated with FlowJo v10. The x-axis represents fluorescence intensity and is divided into 256 bins. The y-axis represents the number of cells in % of the fluorescence intensity bin with the highest amount of cells. Naïve NIH/3T3 = uninfected NIH/3T3 cells, which were used as a reference for background fluorescence.

6.3 Identification of experimental conditions by a small scale pioneer screen

6.3.1 Plasmid library amplifications and distribution of the sgRNAs within the amplified plasmid libraries

For the screen, we decided to use the "Mouse CRISPR Knockout Pooled Library" (GeCKO v2), which is provided by the Zhang laboratory via Addgene. This murine, genome-wide knockout library targets more than 20.000 genes whilst at the same time including six sgRNAs per gene, in contrast to other libraries that contain only four or five (e.g. the "Brie" library from the Root and Doench laboratory). The more sgRNAs per gene are used, the more robust the screen becomes towards non-functional sgRNAs or sgRNAs with off-target effects that may confound results. The library contains a total of 129.209 different sgRNAs, split into two half-libraries with 2 $\times$ 1000 non-targeting sgRNAs. The GeCKO v2 half-libraries were amplified via electroporation and large-scale plasmid preparation from bacteria prior to use. Subsequently, the amplified libraries were sequenced and analyzed for sgRNA distribution. Half-library A was amplified once (A1) with a calculated mean redundancy of 604, meaning that on average each sgRNA is represented 604 times. Half-library B was amplified twice (B1 and B2) with calculated redundancies of 559 and 143, respectively. Figure 6.6 shows, that the sgRNAs in the two B half-libraries were distributed almost identically, with more than 1900 sgRNAs being not represented at all in both libraries (see density curve at "-3" on the x-axis). Library A1 showed a similar distribution pattern, but in contrast to the two B

half-libraries, only about 500 to 600 sgRNAs were not represented in this library.

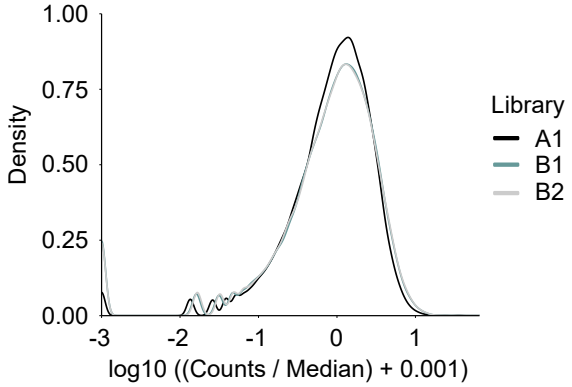

Figure 6.6: Distribution of the guide RNAs around the median of each individual amplified half-library from the murine GeCKO v2 library. The read count of each sgRNA was divided by the median count for each half-library and a pseudocount of 0.001 was added. A density plot of the log10 transformed data was plotted for the amplified half-libraries.

6.3.2 Testing of the suitability of designed sgRNAs targeting *EGFP-PEST* or *tRFP-PEST* for their usability as functional positive controls in the screen

After amplification, the "A"- and the two "B"-GeCKO v2 half-libraries were mixed. Additionally, positive control sgRNA spike-in would be needed, which should surely become enriched in the different sorted fractions of the screen. Direct targeting of the fluorescent reporters with sgRNAs should effectively abolish fluorescence in a time-dependent manner and should also result in an enrichment of cells containing these sgRNAs in the respective sorted conditions, e.g. an sgRNA targeting *EGFP-PEST* should result in a decrease of "green" fluorescence, but should not decrease tRFP-PEST expression. A cell harboring such an sgRNA should therefore be sorted into the "GFP/RiBi down" fraction. To test the suitability of using *EGFP*- and *tRFP*-targeting guide RNAs as positive controls, a time-course experiment was performed: the $3T3^{Fbl\text{-}GFP;Rpl18\text{-}RFP}$ cell clone was infected with either a control guide RNA or an sgRNA targeting *EGFP* or *tRFP* and three or five days after infection and selection, the cells were analyzed for their reporter expression by FACS. Figure 6.7 shows, that these two positive control sgRNAs were capable of effectively reducing EGFP-PEST (green line) or tRFP-PEST (red line) expression, respectively, in a time-dependent manner (compare subfigures 6.7A (three days after transduction of the sgRNAs) and B (five days after transduction of the sgRNAs)). The non-targeting sgRNA (gray line), however, did not reduce expression of any

of the reporters, which can be seen in the comparison with uninfected cells (compare gray and blue lines).

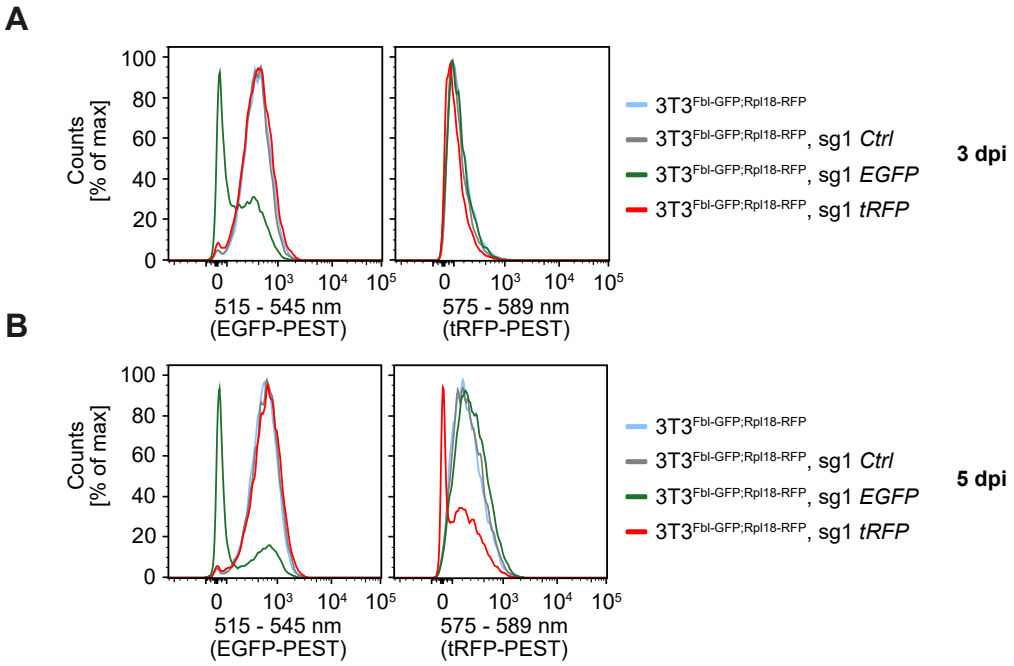

Figure 6.7: sgRNAs targeting *EGFP* or *tRFP* effectively reduce expression of the respective fluorescent reporter in a time-dependent manner. Three days (A) or five days (B) after infection and (at least started) selection of the screening cell line $3T3^{Fbl\text{-}GFP;Rpl18\text{-}RFP}$ with sgRNAs targeting *EGFP* or *tRFP*. Single experiment.

Finally, several of these positive control sgRNAs (three sgRNAs targeting *EGFP*, four sgRNAs targeting *tRFP*) and one non-targeting sgRNA were spiked into the library mix, leading to a library that contained about 20 % to 25 % of spiked-in controls. The spiked-in non-targeting control sgRNA was one of the 1000 control guide RNAs that were already included in the GeCKO v2 library and served as an additional "spike-in" control to ensure, that there was no unspecific enrichment of a spiked-in sgRNA in a certain condition simply due to its mere abundance.

6.3.3 Screening procedure of the pioneer screen and library preparation for next-generation sequencing (NGS)

In order to avoid ribosome imbalance-induced apoptosis in the screen, a time point for sorting, that is as short as possible, but as long as necessary to result in an efficient downregulation of the reporters, needed to be chosen. From the experiment shown in figure 6.7, a possible enrichment of the positive control sgRNAs already after four days

Processed events	GFP/Ribi down	RFP/RP down	Both down	Both up
7 x 10^6	74989 (1.07%)	70151 (1.00%)	305298 (4.36%)	5480 (0.08%)

Table 6.1: Sorted events for the individual fractions of the pioneer screen. The percentage indicates the number of sorted cells in percent of all processed events.

was suspected. I thus used the library mentioned above in a pioneer screen to establish the protocol and to determine whether the sorting approach is in principle capable of enriching the positive controls in the right fractions. Virus was produced from the library mix and the $3T3^{Fbl\text{-}GFP;Rpl18\text{-}RFP}$ cell line was infected. Four days after infection and selection, the cells were sorted into the following four conditions: "GFP/RiBi down", "RFP/RP down", "Both down" and "Both up" (see sorting scheme in figure 6.1). The amount of sorted cells per condition is shown in table 6.1. Half of the cells were lysed without being sorted and served as the "Unsorted" fraction over which the enrichment of the guide RNAs in the sorted fractions was calculated.

Genomic DNA was extracted and a PCR protocol was established to amplify the guides. During the first PCR, the sequences required for binding of the second PCR primers were introduced. The guide RNAs could be amplified from the unsorted condition and the sorted conditions, except for "both up" (see lanes 7 - 11 of figure 6.8A; the corresponding water controls were loaded in lanes 2 - 5). The second PCR (see figure 6.8B) was required to introduce the indices needed to distinguish the different samples after sequencing. It should be noted here, that a second PCR on one of the water controls of the first PCR, resulted in a product as well (lane 6 in figure 6.8B), but was of lower molecular size than the other samples (compare lane 6 with lanes 2 - 5 in figure 6.8B) and a new water control for this PCR did not result in an amplified product (lane 7 in figure 6.8B). We thus continued with next-generation sequencing (NGS).

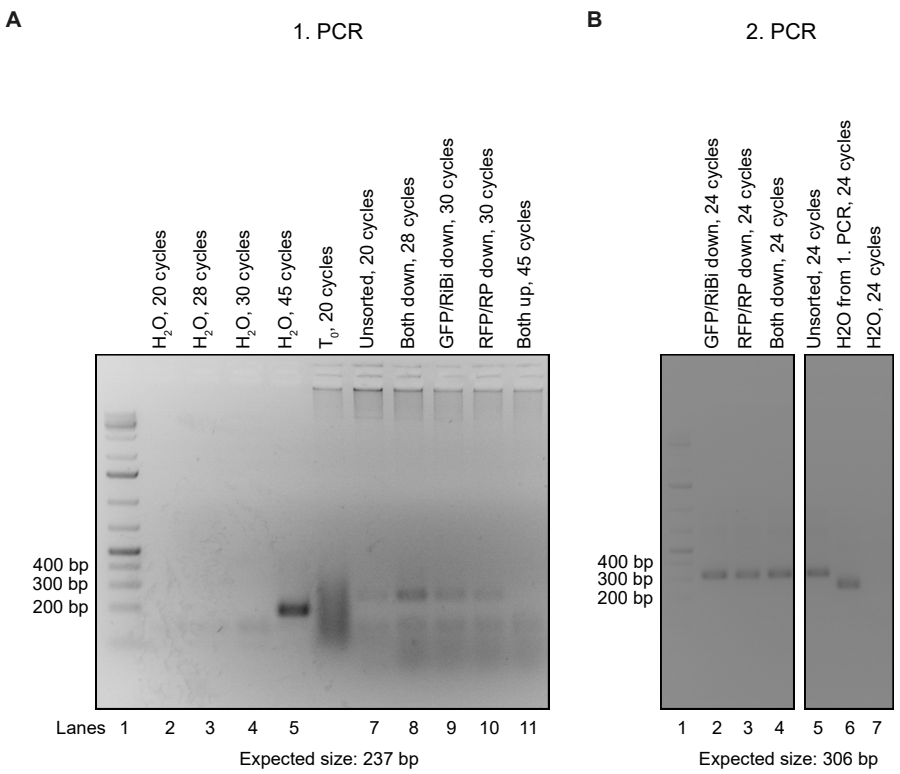

Figure 6.8: Sequencing library generation of the pioneer screening samples. (A) Amplification of the guide RNAs from the different sorted conditions and "unsorted" during the first PCR. A product of 237 base pairs (bp) was generated. It included the sgRNA sequence and the binding sites for the sequencing primers. T_0 was a sample collected two days after infection, but was used with another genomic DNA extraction protocol. This sample was thus excluded from further analyses. (B) The second PCR introduced the indices, which specify the sample, and the binding sites for the flow cell. The generated second PCR products had the expected size of 306 bp.

6.3.4 Positive control sgRNAs were specifically depleted or enriched in the different sorted conditions

As seen in figure 6.8A, lane 11, the library preparation of the "both up" condition failed and thus was excluded from further analyses with the bioinformatic tool called "Model-based Analysis of Genome-wide CRISPR-Cas9 Knockout" (MAGeCK) [Li et al., 2014]. This pioneer screen was performed to see, whether the positive control sgRNAs were enriched in the respective fractions. Figure 6.9 shows the enrichment or depletion of the positive control sgRNAs (three sgRNAs targeting EGFP, colored in shades of green, and four guide RNAs targeting tRFP, colored in shades of red) in the different sorted fractions, relative to their abundance in the unsorted condition. Moreover, the spiked-in non-targeting control sgRNA (gray) and the rest of the sgRNAs, which belong to the GeCKO library (black) are shown. There were slight changes in the amount of the individual control sgRNAs between plasmid library and the unsorted condition,

probably displaying subtle bottlenecks introduced by the virus production and/or during infection and selection. As expected, the sgRNAs targeting *EGFP* were enriched in the "GFP/RiBi down" condition, but were depleted in the "RFP/RP down" condition. The opposite effect could be observed with the guide RNAs targeting *tRFP*. The non-targeting control sgRNA was not enriched in either of the sorted conditions. Moreover, the overall abundance of the sgRNAs of the GeCKO library did not change. In the both down condition, no clear enrichment was observed, which is expected, since the likelihood of sorting a cell that was infected with an *EGFP*- and a *tRFP*-targeting sgRNA at the same time, which would then lead to a loss of expression of both reporters and an enrichment of the positive control sgRNAs in this condition, was rather low.

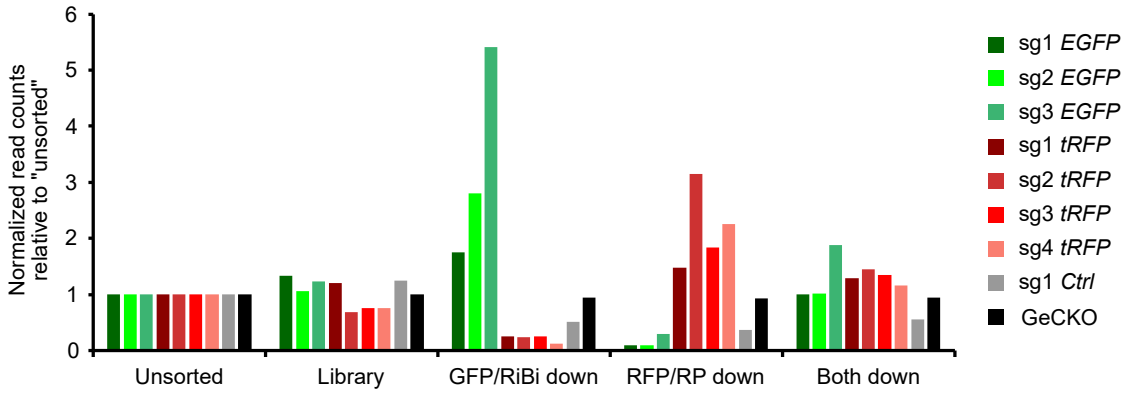

Figure 6.9: Enrichment and depletion of spiked-in control sgRNAs from the pioneer screen in the expected sorted conditions. Analysis of the normalized read counts of the spiked-in positive control sgRNAs, the non-targeting control sgRNA and the sgRNAs from the GeCKO library in the different conditions of the pioneer screen relative to unsorted.

All in all, this pioneer screen revealed, that with the established protocol we are able to enrich the positive controls in the respective fractions. Nevertheless, the effects of knockouts of genes regulating reporter expression are expected to be weaker than the effects of a knockout of the reporter itself. Four days might thus be a too short time point for the screen, since even some positive control sgRNAs will not yet have led to a marked decrease in reporter expression and would thus probably only mildly enrich in the respective fractions (see figures 6.7 and 6.9, e.g. sg1 *tRFP*). Having these data in mind, we decided to wait for six days after infection, until the cells would be sorted in the main screen.

6.4 Identification of regulators of ribosome biogenesis by a genome-wide CRISPR/Cas9 reporter screen

6.4.1 Screening procedure of the reporter screen

The objective of the thesis was to find new transcriptional regulators of RiBi and RP expression. To this end, we performed a genome-wide CRISPR/Cas9 knockout screen as depicted in figure 6.1. The ratio of the A and B half-library mix was adjusted according to the read distribution in the pioneer screen to reach a more equal distribution of the two half-libraries. The positive control sgRNAs (three targeting EGFP and four targeting tRFP) were spiked in to a much lesser extent than in the pre-screen, so that about 0.07% of the library reads were originating from the positive control sgRNAs. An MOI of about 0.5 was used for infection and six days after infection and selection, the cells were harvested for FACS sorting. The screen was performed in triplicates. Table 6.2 summarizes the amount of processed and sorted cells for each replicate. Please note the huge difference between the number of sorted cells in the "both down" condition compared to all other fractions although the gates were in principle not set less stringent. This observation suggests, that most cells with low fluorescence intensity of one reporter usually also just lowly express the other reporter and that only very few cells show differential reporter expression. The same amount of cells that were processed at the FACS machine were also used for the "unsorted" population.

Replicate	Processed events	GFP/Ribi down	RFP/RP down	Both down	Both up
1	30 x 10^6	93997 (0.31%)	35225 (0.12%)	1826322 (6.09%)	50095 (0.17%)
2	35 x 10^6	170617 (0.49%)	100878 (0.29%)	708784 (2.03%)	112701 (0.32%)
3	60 x 10^6	234826 (0.39%)	64424 (0.11%)	1351632 (2.25%)	186609 (0.31%)

Table 6.2: Sorted events from the individual conditions of the screen per replicate. The percentage indicates the number of sorted cells in percent of all processed events.

Genomic DNA was isolated next, and sgRNAs were amplified via two sequential PCRs. The second PCR was then gel-purified and sequenced.

6.4.2 Quality measurements reveal strong enrichment of the positive control sgRNAs in the respective sorted conditions and similarities between the recovered sgRNAs within the triplicates of each screening condition

All analyses, from the fastq-files to the ranked gene lists, were performed with MAGeCK [Li et al., 2014]. For these analyses and many follow-up screen-related bioinformatic analyses, I received help from Sören Lukassen (Charité/BIH, Berlin). To get a first impression of the sgRNA distribution in the different conditions and replicates, we performed a principal component analysis on the normalized sgRNA read counts from all conditions (see figure 6.10A). The plasmid library clustered well with the unsorted conditions. From the sorted conditions, "both down" was most similar to "unsorted" or the plasmid library. "Both down" was also similar to "both up" and "GFP/RiBi down". The "RFP/RP down" sorted cell population differed most from the other conditions. This condition also showed the widest variability within the individual replicates, but all in all the PCA suggested a decent correlation between the different replicates of each condition. At the same time, the PCA suggested sgRNA distribution changes in the sorted populations compared to the unsorted condition.

As a supplement to the PCA analysis, a kernel density plot does not only give insights into how similar or dissimilar the conditions and individual replicates are in principle, but gives a detailed overview of the underlying distribution of the sgRNAs. Since a positive-selection screen was performed, only a small population of specific guide RNAs was expected to be enriched in each condition, but many, if not most, of the sgRNAs should be depleted in the sorted fractions. The kernel density plot (see figure 6.10B) indicates, that the plasmid library and the unsorted conditions showed an even distribution of the sgRNAs with very few depleted or lowly abundant sgRNAs (bottom middle and right subpanels with an additional focus on the left side of the x-axis). When analyzing the sorted conditions, "both down" was the fraction with the lowest amount of depleted sequences (see figure 6.10B, bottom left subpanels). In the "GFP/RiBi down", "RFP/RP down" and "both up" conditions, more sgRNAs were depleted, most prominently visible in replicate 1 of the "RFP/RP down" condition (see figure 6.10B, top subpanels). Whilst some sgRNAs were depleted, others were enriched in the sorted conditions compared to the unsorted condition, as can be seen by a broadening and flattening of the main peak at around 100 counts (see figure 6.10B).

Along this line, a quantitative measure of inequality of sgRNA distribution is the Gini

index, a number between 0 and 1 with 0 representing perfect equal distribution of all guide RNAs and 1 representing a scenario, where all the recovered sequences would come from a single sgRNA. The Gini index was plotted above each kernel density plot. In the library and the unsorted conditions, an equal distribution was expected, with very few guide RNAs being underrepresented or even not present at all. "Library" and "unsorted" possessed the lowest Gini indices (ranging from 0.438 for the library to about 0.46 in the unsorted conditions; see figure 6.10B, bottom middle and right subpanels). Since many of the sgRNAs were depleted in the first replicate of the "RFP/RP down" condition, with the least amount of recovered sgRNAs this condition showed the highest Gini index value. Generally, the sorted conditions showed higher Gini indices than the unsorted condition or the plasmid library, indicating a less equal distribution of the different sgRNA sequences.

From these observations, another question arose: were the guide RNAs that could be recovered from each sample (thus ignoring the guide RNAs that had no counts), similar among the replicates of the same condition? The stronger the overlap of sgRNAs that are recovered in the different replicates of each individual condition, the more likely it would be to identify reliable hits, since the guide RNAs would have been reproducibly enriched. To this end, I plotted proportional Venn diagrams for each condition (see figure 6.10C). The overlap of all three replicates of each sorted condition was at least 30 %, more than expected by chance. Concretely, the overlap was 1.47 times higher than expected by chance for "GFP/RiBi down", 1.62 times higher than expected by chance for "RFP/RP down" and 1.6 times higher than expected by chance for "both up". The overlap from the "both down" replicates was only 1.1 times higher than expected by chance and the overlap of the replicates of the "unsorted" population was 1.03 times higher than expected by chance, already indicating, that the degree of information that can be gained from the analysis of the "both down" condition, might be lower than the one coming from the other conditions.

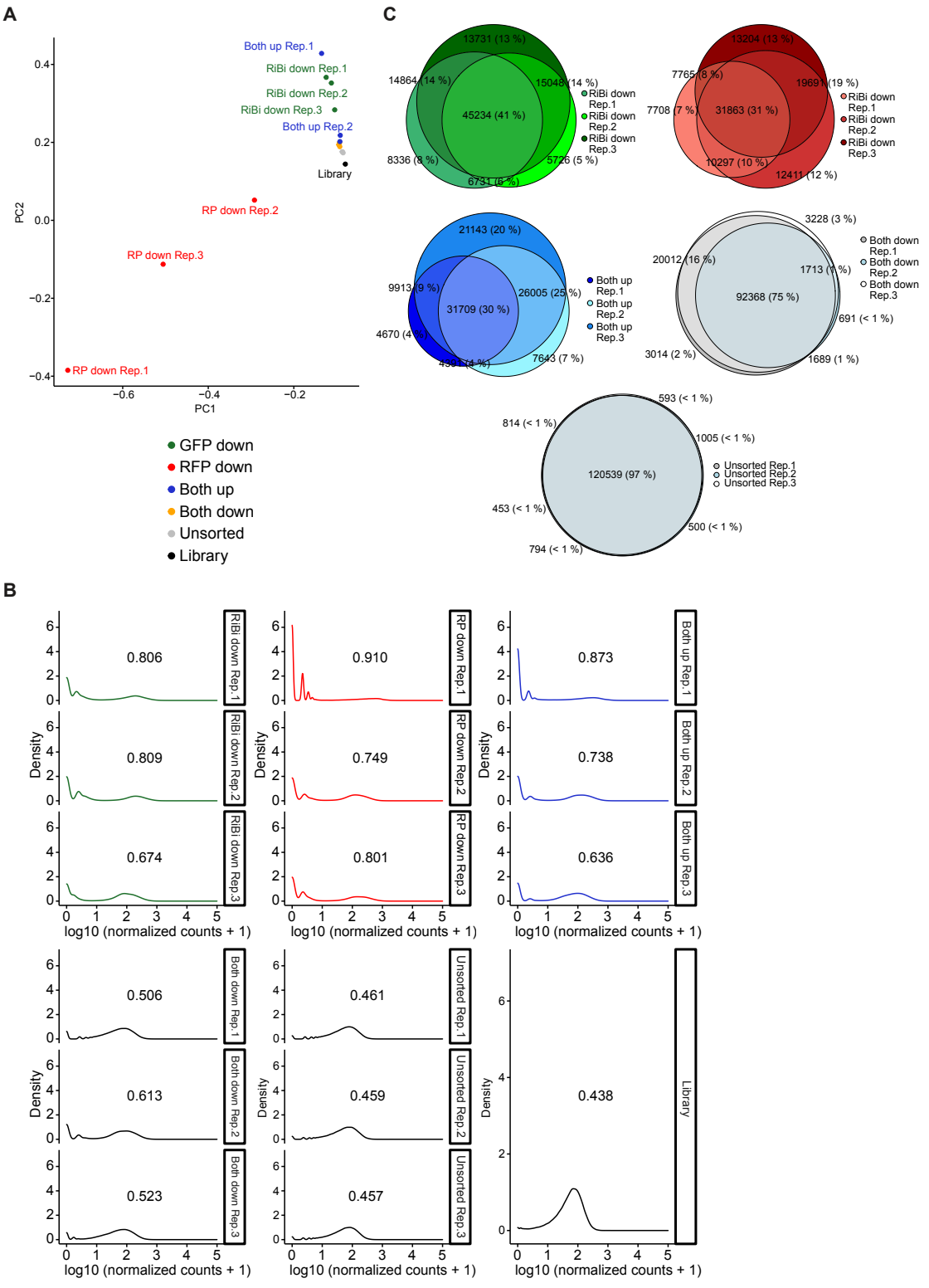

Figure 6.10: Quality measurements of the screen reveal similarities between the different replicates of each condition (A), depletion and enrichment of many guide RNAs (B) and a good overlap of guide RNAs recovered from the different replicates of each condition (C). (A) Principal component analysis (PCA) on the normalized read counts of all the sorted conditions, unsorted and the plasmid library from all three replicates. (B) Kernel density plots of the normalized read counts of all the sorted conditions, unsorted and the plasmid library from all three replicates. A pseudocount of 1 was added to the normalized read counts and the result was log10 transformed. The Gini indices were written above each Kernel density curve. (C) Venn diagrams of the overlap of sgRNAs, that were recovered per replicate of each (un)sorted condition. The overlap between all three replicates was more than expected by chance (as calculated by multiplication of the recovered normalized sgRNAs per replicate divided by the square of the total number of sgRNAs in the library), especially for "GFP/RiBi down", "RFP/RP down" and "both up".

Finally, we analyzed the enrichment of the positive control guide RNAs in all of the conditions (see figure 6.11). There was a strong increase in the amount of recovered control sgRNAs in the expected fractions, for example guide RNAs against EGFP were enriched in the conditions, where I sorted cells with high red and low green fluorescence and sgRNAs targeting tRFP were enriched strongly in the condition, where cells showing high green and low red fluorescence were sorted. Moreover, although hardly seen in this figure, the positive control guide RNAs additionally tended to be depleted from the "both up" condition, in line with our expectations, that sorting for very high levels of fluorescence should counterselect for guide RNAs that lead to a knockout of the fluorescence reporter.

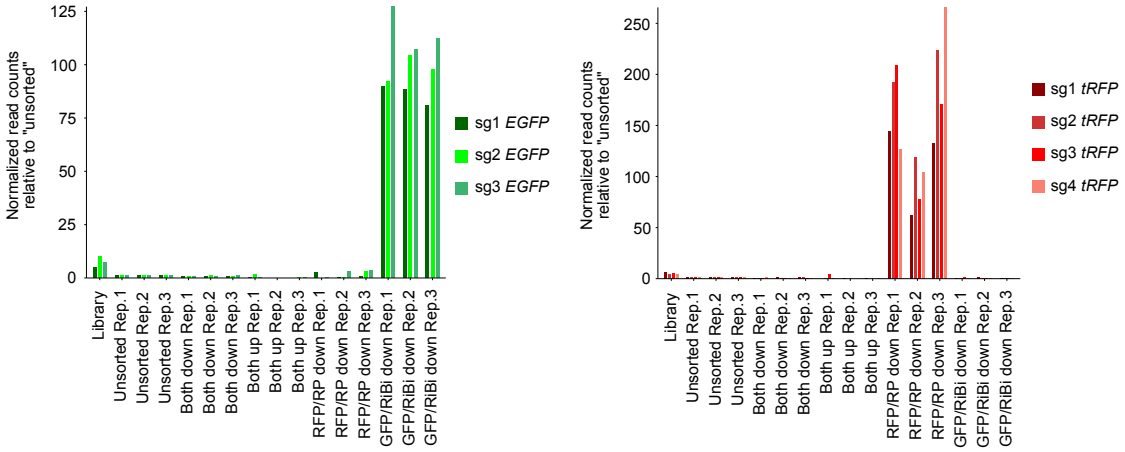

Figure 6.11: Distribution of sgRNAs targeting EGFP or tRFP among the different conditions of the screen. Analysis of the normalized read counts of the positive control sgRNAs in the different conditions of the screen.

6.4.3 Enriched genes from the different sorted conditions of the screen

We then had a look at the genes that were enriched in the different sorted conditions in comparison to "unsorted". When analyzing the genes of the condition in which we expected to find activators of ribosome biogenesis and ribosomal protein gene expression ("both down" list), we noticed no significant enrichment of hits (false discovery rate (FDR) < 0.05; see table 6.3). A possible explanation for this might be, that many cells might have been sorted although they did not harbor sgRNAs that specifically led to a downregulation of RiBi or RP genes (and thus of the reporters), but contained sgRNAs that were generally affecting "healthiness" of cells or which integrated into a genomic environment, for example into an essential gene locus, which was disastrous for the cells. Both scenarios might lead to a reduced expression of the reporters, although the

guides recovered from these cells would just reflect "background noise".

Rank	Gene	Protein	logFC	FDR
1	*Recql4*	ATP-dependent DNA helicase Q4	0.70734	0.909674
2	*Cdh13*	Cadherin-13	0.11177	0.909674
3	*Lrp5*	Low-density lipoprotein receptor-related protein 5	0.69146	0.909674
4	*Senp1*	Sentrin-specific protease 1	0.44218	0.909674
5	*4930432M17Rik*	Submitted name: RIKEN cDNA 4930432M17 gene	0.1137	0.909674
6	*Itga11*	Integrin alpha-11	0.45477	0.909674
7	*Olfr585*	Olfactory receptor	0.48003	0.909674
8	*Uqcrc1*	Cytochrome b-c1 complex subunit 1, mitochondrial	0.34867	0.909674
9	*Olfr186*	Olfactory receptor 186	1.1352	0.909674
10	*Fgf1*	Fibroblast growth factor 1	0.55612	0.909674
11	*Ttll11*	Tubulin polyglutamylase TTLL11	0.16918	0.909674
12	*Slc17a1*	Sodium-dependent phosphate transport protein 1	0.22087	0.909674
13	*Zbtb24*	Zinc finger and BTB domain-containing protein 24	-0.041356	0.909674
14	*Chst7*	Carbohydrate sulfotransferase 7	0.76199	0.909674
15	*Olfr126*	Olfactory receptor	0.66091	0.909674
16	*Commd10*	COMM domain-containing protein 10	0.045828	0.909674
17	*Sgcg*	Gamma-sarcoglycan	0.38126	0.909674
18	*Tmem57* (or *Maco1*)	Transmembrane protein 57 (or Macoilin)	0.34791	0.909674
19	*Wdr11*	WD repeat-containing protein 11	0.3805	0.909674
20	*Prkd1*	Serine/threonine-protein kinase D1	0.59261	0.909674
21	*Tmem108*	Transmembrane protein 108	0.32829	0.909674
22	*Fmr1*	Synaptic functional regulator FMR1	-0.49756	0.909674

23	*Pinlyp*	phospholipase A2 inhibitor and Ly6/PLAUR domain-containing protein	0.3397	0.909674
24	*mmu-mir-669d-2* (or *Mir669d-2*)		0.67509	0.909674
25	*Zfp608*	Submitted name: Zinc finger protein 608	0.75495	0.909674

Table 6.3: Positively enriched genes from the "both down" condition of the genome-wide CRISPR-Cas9 knockout screen. The genes represent the top 25 scoring genes from the condition sorted for low EGFP-PEST (RiBi promoter) and low tRFP-PEST (RP promoter) fluorescence intensity. The ranked gene list, together with the log fold change (logFC) and the false discovery rate (FDR) were obtained using the bioinformatic tool MAGeCK [Li et al., 2014] and the "Protein" column information was obtained from "www.uniprot.org".

As opposed to the "both down" condition, several significantly enriched genes were found in the condition sorted for high EGFP-PEST as well as high tRFP-PEST reporter expression ("both up"). The list of candidate genes was remarkably enriched for genes that encode constituents of the proteasome (10 out of 14 significantly enriched genes; see all gene names starting with "Psm[...]" in table 6.4). Since disruption of the proteasome would increase cellular protein amounts significantly, an increase of the EGFP-PEST and tRFP-PEST reporters was indeed expected in cells expressing sgRNAs targeting proteasomal components. Although their appearance as hits in the condition where we wanted to find repressors of RiBis and RPs, proved, that the sorting approach was indeed working, it became clear that our hit lists would not only contain (transcriptional) regulators of ribosome biogenesis processes, but also genes that are involved in the regulation of the fluorescent reporters itself. The other four significantly enriched genes were *Pabpn1*, *Sap18*, *Zcchc11* and *Ewsr1*, which are discussed later.

Rank	Gene	Protein	logFC	FDR
1	*Psmd6*	26S proteasome non-ATPase regulatory subunit 6	2.7237	0.000825
2	*Psmc5*	26S proteasome regulatory subunit 8	2.8954	0.000825
3	*Psmd11*	26S proteasome non-ATPase regulatory subunit 11	2.7376	0.000825

4	*Psmc4*	26S proteasome regulatory subunit 6B	2.313	0.000825
5	*Pabpn1*	Polyadenylate-binding protein 2	2.1401	0.000825
6	*Psmb4*	Proteasome subunit beta type-4	2.1495	0.000825
7	*Psmb1*	Proteasome subunit beta type-1	1.7014	0.021924
8	*Psmb7*	Proteasome subunit beta type-7	-1.7966	0.025371
9	*Psmd3*	26S proteasome non-ATPase regulatory subunit 3	0.73305	0.026953
10	*Sap18*	Histone deacetylase complex subunit SAP18	1.2639	0.027228
11	*Zcchc11* (or *Tut4*)	Zinc finger CCHC domain-containing protein 11 (or Terminal uridylyltransferase 4)	2.2489	0.033753
12	*Psma4*	Proteasome subunit alpha type-4	1.7334	0.034653
13	*Ewsr1*	RNA-binding protein EWS	1.3086	0.034653
14	*Psmb6*	Proteasome subunit beta type-6	0.52107	0.04703
15	*Psmd14*	26S proteasome non-ATPase regulatory subunit 14	1.9102	0.065017
16	*Kcnk9*	Potassium channel subfamily K member 9	1.6672	0.08323
17	*Snip1*	Smad nuclear-interacting protein 1	1.1429	0.138905
18	*Cdc73*	Parafibromin	0.58369	0.179043
19	*Alyref2*	Submitted name: RNA and export factor binding protein 2	1.1187	0.22698
20	*Ankrd28*	Serine/threonine-protein phosphatase 6 regulatory ankyrin repeat subunit A	1.0975	0.235599
21	*Cercam*	Inactive glycosyltransferase 25 family member 3	1.0908	0.235599
22	*Tmem159*	Lipid droplet assembly factor 1	0.17253	0.270125
23	*mmu-mir-6376* (or *Mir6376*)		1.4368	0.22698

24	*Atg4b*	Cysteine protease ATG4B	0.84943	0.276657
25	*Olfr1424*	Olfactory receptor	1.0803	0.276657

Table 6.4: Positively enriched genes from the "both up" condition of the genome-wide CRISPR-Cas9 knockout screen. The genes represent the top 25 scoring genes from the condition sorted for high EGFP-PEST (RiBi promoter) and high tRFP-PEST (RP promoter) fluorescence intensity. The ranked gene list, together with the log fold change (logFC) and the false discovery rate (FDR) were obtained using the bioinformatic tool MAGeCK [Li et al., 2014] and the "Protein" column information was obtained from "www.uniprot.org".

We then analyzed the enriched genes of the condition, where cells with high expression of the *Fbl*-driven EGFP-PEST reporter and a concurrent low expression of the *Rpl18*-driven tRFP-PEST reporter were sorted. Besides the positive control gene *tRFP*, which was the top hit, there was only one additional significantly enriched gene, Adrm1, a proteasomal ubiquitin receptor.

Rank	Gene	Protein	logFC	FDR
1	*tRFP*	turbo red fluorescent protein	7.014	0.002475
2	*Adrm1*	Proteasomal ubiquitin receptor ADRM1	3.2209	0.002475
3	*Depdc1a*	DEP domain-containing protein 1A	1.119	0.222772
4	*Vhl*	von Hippel-Lindau disease tumor suppressor	0.89249	0.491337
5	*H60b*	Histocompatibility antigen 60b	-0.29663	0.757426
6	*Olfr799*	Olfactory receptor	1.2109	0.948588
7	*Pygb*	Glycogen phosphorylase, brain form	0.77045	0.948588
8	*E130012A19Rik* (or *Epop*)	Elongin BC and Polycomb repressive complex 2-associated protein	1.0993	0.948588
9	*Vmn2r30*	Submitted name: Vomeronasal 2, receptor 30	0.83429	0.948588
10	*A230065H16Rik* (or *Lbhd2*)	Submitted name: LBH domain-containing 2	-0.53777	0.948588
11	*Champ1*	Chromosome alignment-maintaining phosphoprotein 1	-1.7772	0.948588
12	*Sult4a1*	Sulfotransferase 4A1	0.68461	0.948588

13	*Gm5544*	Submitted name: Predicted gene, EG433632	1.0355	0.948588
14	*Ppfibp1*	Liprin-beta-1	-0.85748	0.948588
15	*Syne1*	Nesprin-1	-1.0322	0.948588
16	*Adap1*	Submitted name: Adap1 protein	0.55248	0.948588
17	*Tha1*	Submitted name: L-threonine aldolase	-0.83895	0.948588
18	*Cwf19l2*	CWF19-like protein 2	-0.63088	0.948588
19	*mmu-mir-3074-1* (or Mir3074-1)		0.82883	0.948588
20	*Gstm2*	Glutathione S-transferase Mu 2	0.89832	0.948588
21	*Abcb1a*	ATP-dependent translocase ABCB1	1.0043	0.948588
22	*Tbrg1*	Transforming growth factor beta regulator 1	1.0004	0.948588
23	*Lipc*	Hepatic triacylglycerol lipase	1.151	0.948588
24	*Mettl16*	RNA N6-adenosine-methyltransferase METTL16	-4.6332	0.948588
25	*Nipa2*	Magnesium transporter NIPA2	1.0266	0.948588

Table 6.5: Positively enriched genes from the "RFP/RP down" condition of the genome-wide CRISPR-Cas9 knockout screen. The genes represent the top 25 scoring genes from the condition sorted for constant or high EGFP-PEST (RiBi promoter), but low tRFP-PEST (RP promoter) fluorescence intensity. The ranked gene list, together with the log fold change (logFC) and the false discovery rate (FDR) were obtained using the bioinformatic tool MAGeCK [Li et al., 2014] and the "Protein" column information was obtained from "www.uniprot.org" and "www.ncbi.nlm.nih.gov".

Our focus, however, was lying on the genes, that were enriched in the condition, where cells with high expression of the *Rpl18*-driven tRFP-PEST reporter and a concomitant low expression of the *Fbl*-driven EGFP-PEST reporter were sorted. The positive control gene *Egfp* was ranked second. The top ranking gene was *Aldolase A* (*Aldoa*), a glycolytic enzyme. Other metabolic enzymes were not found to be significantly enriched. Validation experiments for this hit are described in section 6.5.2. Several genes involved in the general transcription process were among the top scoring genes, for example POL II subunits *Polr2[...]*, *Ssrp1* (a member of the FACT chromatin remodeling complex) or *Cpsf3l* (a subunit of the Integrator complex, which is involved in transcription and RNA processing). GPN1, which is required for the import of RPB1 and

RPB2, the two largest subunits of POL II, into the nucleus [Forget et al., 2010], is also a transcription-associated hit. Moreover, many spliceosomal or spliceosome-associated hits are enriched among the top-ranked genes, such as *Bud31* and *Rbm22*, as well as two of the exon junction complex (EJC) members, namely *Eif4a3* and *Rbm8a*. Additionally, members of the anaphase promoting complex/cyclosome (APC/C) are also among the top ranked genes, for example *Cdc16*, *Anapc1* and at least four additional subunits or APC/C-associated factors, which are not shown anymore in table 6.6, but are still scoring within the top 50 genes.

Rank	Gene	Protein	logFC	FDR
1	*Aldoa*	Fructose-bisphosphate aldolase A	3.2833	0.000381
2	*Egfp*	enhanced green fluorescent protein	6.5042	0.000381
3	*Hspa8*	Heat shock cognate 71 kDa protein	3.5377	0.000381
4	*Bud31*	Protein BUD31 homolog	3.5657	0.000381
5	*Polr2l*	DNA-directed RNA polymerases I, II, and III subunit RPABC5	2.709	0.000381
6	*Polr2e*	DNA-directed RNA polymerases I, II, and III subunit RPABC1	2.5822	0.000381
7	*Cdc16*	Cell division cycle protein 16 homolog	2.5678	0.000381
8	*Eif4a3*	Eukaryotic initiation factor 4A-III	2.6534	0.000381
9	*Polr2c*	DNA-directed RNA polymerase II subunit RPB3	3.1384	0.000381
10	*Polr2h*	DNA-directed RNA polymerases I, II, and III subunit RPABC3	2.4026	0.000381
11	*Anapc1*	Anaphase-promoting complex subunit 1	2.2172	0.000381
12	*Eif4a1*	Eukaryotic initiation factor 4A-I	2.7656	0.000381
13	*Gm21637* (or *Gm5926*)	Submitted name: Predicted gene 5926	2.6418	0.000381
14	*Sfpq*	Splicing factor, proline- and glutamine-rich	1.8375	0.003182

15	*Rpa1*	Replication protein A 70 kDa DNA-binding subunit	1.2269	0.01021
16	*Plk1*	Serine/threonine-protein kinase PLK1	1.5814	0.01021
17	*Itgav*	Integrin alpha-V	1.5507	0.015434
18	*Cpsf3l* (or *Ints11*)	Integrator complex subunit 11	1.7228	0.017327
19	*Ewsr1*	RNA-binding protein EWS	1.8731	0.019566
20	*Uba1*	Ubiquitin-like modifier-activating enzyme 1	1.55	0.019566
21	*Krt19*	Keratin, type I cytoskeletal 19	1.2569	0.019566
22	*Ssrp1*	FACT complex subunit SSRP1	-0.15156	0.025878
23	*Rbm8a*	RNA-binding motif protein 8A	2.0989	0.026609
24	*Gpn1*	GPN-loop GTPase 1	-0.87054	0.026609
25	*Rbm22*	Pre-mRNA-splicing factor RBM22	1.0593	0.040198

Table 6.6: Positively enriched genes from the "GFP/RiBi down" condition of the genome-wide CRISPR-Cas9 knockout screen. The genes represent the top 25 scoring genes from the condition sorted for constant or high tRFP-PEST (RP promoter), but low EGFP-PEST (RiBi promoter) fluorescence intensity. The ranked gene list, together with the log fold change (logFC) and the false discovery rate (FDR) were obtained using the bioinformatic tool MAGeCK [Li et al., 2014] and the "Protein" column information was obtained from "www.uniprot.org" and "www.ncbi.nlm.nih.gov".

6.5 Validation experiments of candidate genes revealed by the genome-wide CRISPR/Cas9 reporter screen

6.5.1 Summary of FACS validation experiments

For validation experiments, I focused on the genes that were enriched in the GFP/RiBi down condition, because it contained many significantly enriched genes of which several were clearly associated with transcription-related processes. Accordingly, the likelihood of finding new genes associated with a transcriptional regulation of RiBis and RPs was expected to be highest for this condition. I cloned individual sgRNAs from the GeCKO v2 library, produced virus, infected the $3T3^{Fbl\text{-}GFP;Rpl18\text{-}RFP}$ cell clone and analyzed reporter expression by FACS six days after infection and selection. With FlowJo, the median EGFP-PEST reporter expression was analyzed for each sample.

The background fluorescence was subtracted from this value and the result was divided by the non-targeting control sgRNA signal after background subtraction (formula: $\frac{MFI\ sgTarget - MFI\ naïve\ cells}{MFI\ sg1\ Ctrl - MFI\ naïve\ cells}$). These ratio values were plotted as individual data points from different experiments in figure 6.12 (dark blue data points).

Expression of *Aldoa*, *Hspa8* and of at least one of the tested *Bud31*, *Eif4a3* and *Rbm8a* sgRNAs, resulted in a substantial downregulation of EGFP-PEST reporter expression. The profiles for *Aldoa* and *Rbm8a* are shown in figure 6.14 and 6.20 and will be discussed in sections 6.5.2 and 6.5.3, respectively. Examples of the FACS profiles of *Hspa8*, *Bud31* and *Eif4a3* knockout are shown in figure 6.13. *Sfpq*-targeting sgRNAs were an exception, because the *Sfpq* knockout from two out of four experiments resulted in a strong downregulation of green fluorescence intensity, but in a bimodal manner (see figure 6.13), resulting in an underestimation of the effect shown in figure 6.12A.

The sgRNAs targeting *Aldoa*, *Hspa8*, one sgRNA targeting *Eif4a3* and one sgRNA targeting *Rbm8a*, were not only reducing EGFP-PEST, but also tRFP-PEST expression (see figures 6.12B). The sgRNAs targeting *Bud31* and *Sfpq*, however, only led to a minor downregulation of tRFP-PEST expression, if at all (see figures 6.12B and 6.13). Knockout of some of the candidate genes, such as *Rpa1*, *Plk1* and *Ssrp1*, apparently upregulated reporter expression, but this effect was also observed for some replicates of the control sgRNAs, such as empty vector (EV) or sgRNAs targeting tRFP (when examining green fluorescence intensity).

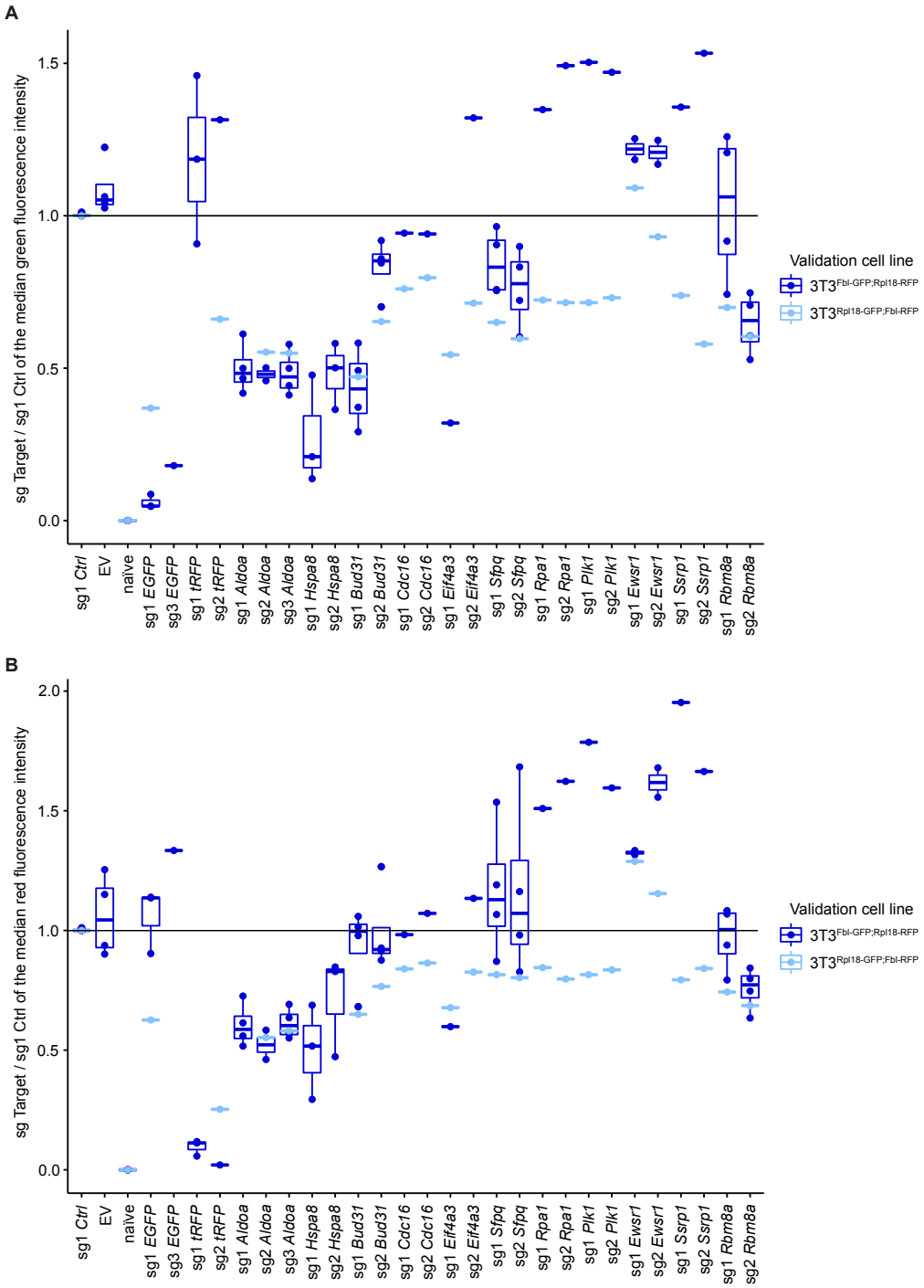

Figure 6.12: Median green (A) and red (B) fluorescence intensity of each tested candidate gene-targeting sgRNA relative to a non-targeting control, tested in the screening cell line 3T3$^{\text{Fbl-GFP;Rpl18-RFP}}$ (dark blue) and the swapped reporter cell line 3T3$^{\text{Rpl18-GFP;Fbl-RFP}}$ (light blue). Median fluorescence intensity (MFI) was calculated by the FlowJo v10 software. The background MFI value of the naïve NIH/3T3 cells was subtracted from "sg1 *Ctrl*", a non-targeting control sgRNA and from each individual candidate gene-targeting sgRNA. The resulting MFI value of each candidate gene-targeting sgRNA was then divided by the calculated MFI value of "sg1 *Ctrl*", thus centering the non-targeting control at 1. Each dot in the plot represents one replicate, the line represents the median value of the replicates and the upper and lower horizontal lines of the boxplot represent the 75th and 25th percentile, respectively. The black line at "1" represents the MFI value of the non-targeting control reference used for calculation.

We then wanted to know, whether the observed effects were dependent on the specific representative promoters used to drive reporter expression, or whether the reporter itself was determining the observed effects. In other words, would a knockout of *Bud31* for example, only regulate ribosome biogenesis genes, but not ribosomal protein genes, because figure 6.12 shows a specific downregulation of EGFP-PEST, but not tRFP-PEST upon *Bud31* knockout? An alternative hypothesis would be, that EGFP-PEST is less stable than tRFP-PEST, which may lead to a stronger downregulation of EGFP-PEST than of tRFP-PEST, although both of them are regulated similarly strong on a transcriptional level. To investigate this further, we swapped the reporters and generated a NIH/3T3 cell line expressing *Rpl18* promoter-driven EGFP-PEST and *Fbl* promoter-driven tRFP-PEST. There was a tendency, that the reporter was the stronger determinant for the observed effects than the promoters driving the reporters, since instead of tRFP-PEST being downregulated in conditions, where EGFP-PEST was previously more downregulated, it was again EGFP-PEST, that was downregulated stronger than tRFP-PEST (see figure 6.12, compare light blue data points from subfigure A with dark blue data points from subfigure B and vice versa for comparison of the same promoter driving different reporters), suggesting, that there may be no completely specific regulator of only RiBi genes or RP genes, respectively, among the tested candidates. However, replicates of the swapped reporter cell line would still be needed to finally prove this point.

In summary, the FACS validation experiments of some candidate genes of the "GFp/RiBi down" list indicate, that some of them indeed downregulated RiBi- or RP-promoter dependent expression of the reporters and may thus be regulators of RiBis and RPs, but there is no clear indication, that specific regulators may be among them.

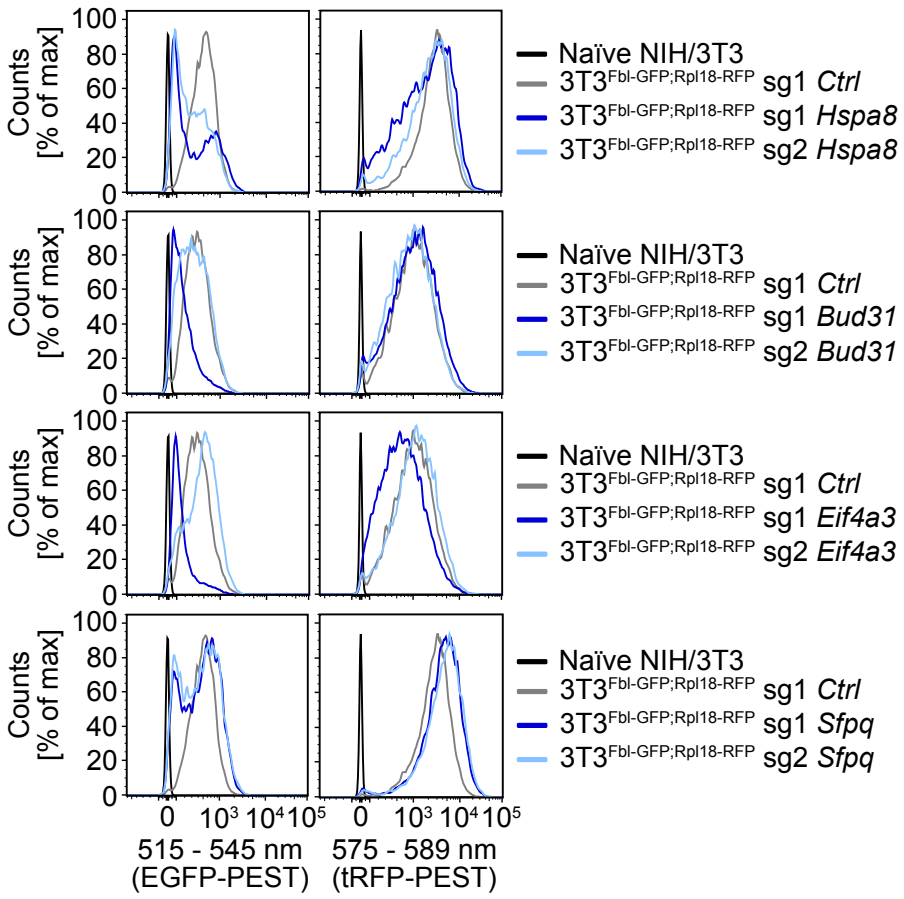

Figure 6.13: Representative replicate of validation experiment FACS profiles of candidate genes displaying a reduction of EGFP-PEST (sgRNAs targeting *Hspa8*, *Bud31*, *Eif4a3* and *Sfpq*) and tRFP-PEST (sgRNAs targeting *Hspa8*, and *Eif4a3*) expression. Six days after infection and selection of the screening cell line $3T3^{Fbl\text{-}GFP;Rpl18\text{-}RFP}$. sg1 *Ctrl* was a non-targeting control guide used as a reference for "unperturbed" fluorescence. The x-axis represents fluorescence intensity and is divided into 256 bins. The y-axis represents the number of cells in % of the fluorescence intensity bin with the highest amount of cells. Naïve NIH/3T3 cells are non-fluorescent cells, which were used as a reference for background fluorescence.

6.5.2 ALDOLASE A (ALDOA) is a regulator of ribosome biogenesis and other growth genes

Aldoa, encoding a glycolytic enzyme, was the top scoring gene of the screening condition, in which I sorted for low EGFP-PEST fluorescence. Moreover, knockout of *Aldoa* with three different sgRNAs resulted in a reproducible and prominent downregulation of the reporters in the validation experiments (see figure 6.12). The FACS profile of one of the replicates of these validation experiments is shown in figure 6.14.

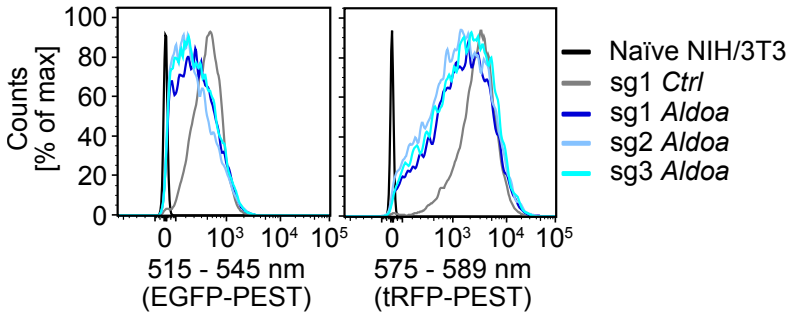

Figure 6.14: ***Aldoa* knockout reduces the expression of *Fbl*-promoter-driven EGFP-PEST and *Rpl18*-promoter-driven tRFP-PEST.** FACS analysis of three different sgRNAs (sg1 *Aldoa*, sg2 *Aldoa* and sg3 *Aldoa*) targeting *Aldoa*. Six days after infection and selection of the screening cell line $3T3^{Fbl\text{-}GFP;Rpl18\text{-}RFP}$. sg1 *Ctrl* was a non-targeting control guide used as a reference for "unperturbed" fluorescence. The x-axis represents fluorescence intensity and is divided into 256 bins. The y-axis represents the number of cells in % of the fluorescence intensity bin with the highest amount of cells. Naïve NIH/3T3 cells are non-fluorescent cells, which were used as a reference for background fluorescence. A representative experiment from quadruplicate experiments is shown.

The above results made *Aldoa* a promising candidate for further investigation. Several research questions arose from the observations described above:

1.) Figures 6.12 and 6.14 suggest, that EGFP-PEST expression may be regulated stronger than tRFP-PEST expression. May this reflect a possible stronger regulation of RiBis than RPs or could it simply be, that this effect is a result of different fluorescent reporter stabilities?
2.) Does ALDOA depletion regulate RiBi/RP mRNA expression?
3.) Are there potentially also other genes, that are downregulated upon ALDOA depletion, which may support ribosome biogenesis and associated cellular programs such as growth and proliferation?

The following experiments were performed in order to answer the aforementioned questions:

1.) The swapped reporter cell line was infected with sgRNAs targeting *Aldoa* and analyzed by FACS six and seven days post infection and selection (see figure 6.15). In case

of a stronger RiBi regulation, it would be expected, that tRFP-PEST is downregulated stronger than EGFP-PEST in this cell line. Instead, EGFP-PEST was downregulated stronger (see figure 6.15), at least seven days after infection. All these experiments suggested, that ALDOA may regulate RPs and RiBis in a similar manner.

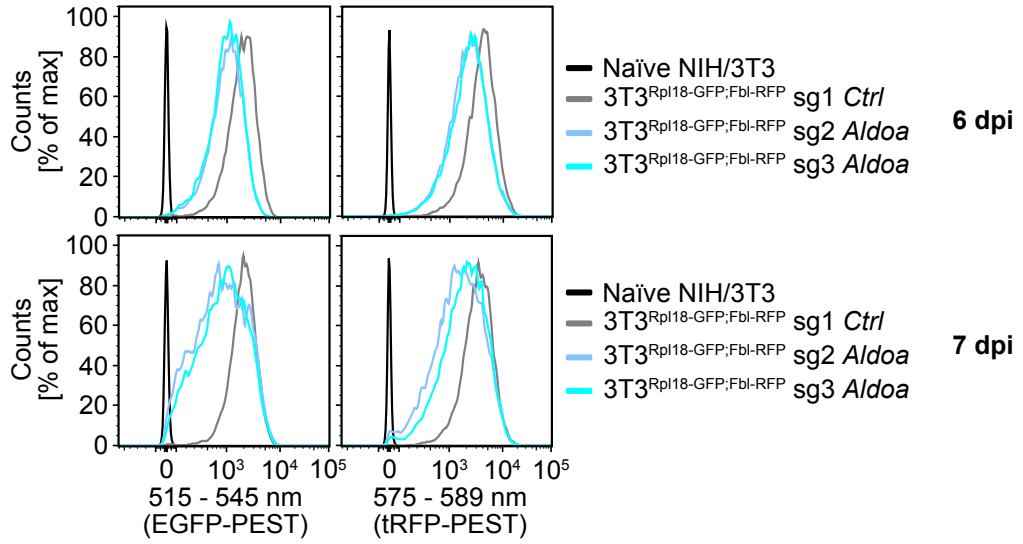

Figure 6.15: ***Aldoa*** **knockout reduces the expression of** ***Rpl18*****-promoter-driven EGFP-PEST and** ***Fbl*****-promoter-driven tRFP-PEST in the swapped reporter cell line 3T3$^{\text{Rpl18-GFP;Fbl-RFP}}$ in a similar manner as in the screening cell line 3T3$^{\text{Fbl-GFP;Rpl18-RFP}}$.** FACS analysis of two different sgRNAs (sg2 *Aldoa* and sg3 *Aldoa*) targeting *Aldoa*. Six or seven days after infection and selection of the swapped reporter cell line 3T3$^{\text{Rpl18-GFP;Fbl-RFP}}$. sg1 *Ctrl* was a non-targeting control guide used as a reference for "unperturbed" fluorescence. The x-axis represents fluorescence intensity and is divided into 256 bins. The y-axis represents the number of cells in % of the fluorescence intensity bin with the highest amount of cells. Naïve NIH/3T3 cells are non-fluorescent cells, which were used as a reference for background fluorescence. Single experiments.

2.) To investigate, whether ALDOA depletion may indeed influence transcription of RiBis and RPs, I performed an RNA-Seq experiment with a more acute depletion of ALDOA. An *Aldoa*-targeting siRNA pool of four different siRNAs was used for transfection of the screening cell line and of parental NIH/3T3 cells. Two days after transfection, the cells were harvested and an RNA-Seq library was prepared, sequenced and analyzed. Additionally, a western blot of this experiment was performed to determine depletion efficiency of ALDOA, EGFP-PEST and tRFP-PEST. Figure 6.16 shows, that ALDOA was depleted by 89 % in NIH/3T3 or 96 % in the screening cell line 3T3$^{\text{Fbl-GFP;Rpl18-RFP}}$ (left panel). Notably, the screening cell line expressed more ALDOA than the parental cell line. The protein levels of the fluorescent reporters reduced to about 60 % and 50 % of the control levels for EGFP-PEST (middle panel) and tRFP-PEST (right panel), respectively.

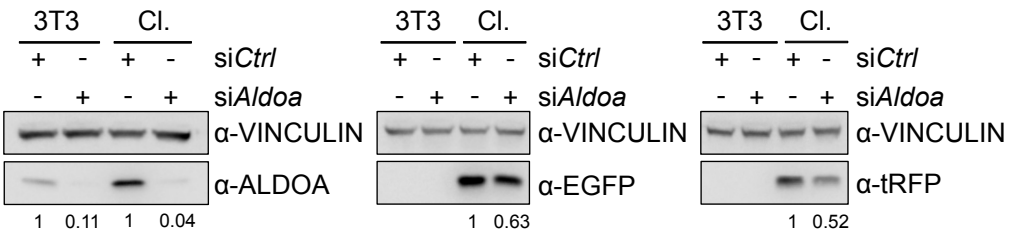

Figure 6.16: Western blot confirmation of an *Aldoa* knockdown (left panel) and a concomitant reduction in the amount of *Fbl*-promoter-driven EGFP-PEST (middle panel) and *Rpl18*-promoter-driven tRFP-PEST (right panel). Knockdown was achieved with a pool of four different siRNAs targeting *Aldoa* (si*Aldoa*). A pool of four non-targeting siRNAs was used as a control (si*Ctrl*). Proteins (from a single plate per condition) were harvested two days after siRNA transfection of the screening cell line $3T3^{Fbl\text{-}GFP;Rpl18\text{-}RFP}$ or the parental NIH/3T3 cell line. The numbers below the blots show the quantification of the ALDOA, EGFP-PEST or tRFP-PEST signal from each condition as a ratio over the VINCULIN signal. From these normalized values, the ratio of si*Aldoa* over si*Ctrl* is shown.

We were wondering whether the observed slight downregulation of the reporters upon ALDOA depletion may point towards a regulation of ribosomal protein genes and ribosome biogenesis genes by ALDOA. It should be noted here, that Apoorva Baluapuri from our research group analyzed the RNA-Seq, with me continuing bioinformatic analyses from the step of the generated count/differential gene expression tables. A gene set enrichment analysis (GSEA) was performed to receive an overview about the regulated gene sets upon ALDOA depletion. Many ribosome biogenesis gene sets were significantly depleted upon ALDOA withdrawal (see figure 6.17, marked by a green color). In fact, about 15 - 17 % of RiBis (from the gene ontology term "ribosome biogenesis") and 5 % of RP genes (from the GO term "structural constituent of ribosome") were significantly downregulated upon *Aldoa* depletion.

Gene set	Size	NES NIH/3T3	FDR q-val NIH/3T3	NES clone	FDR q-val clone	
GO_SMALL_NUCLEOLAR_RIBONUCLEOPROTEIN_COMPLEX	18	2.1853144	0.001130826	2.0970075	0.002615791	Ribosome biogenesis
GO_NUCLEOLAR_PART	59	2.2197106	0.001168273	1.5689712	0.13662	
REACTOME_RNA_POL_I_TRANSCRIPTION	66	1.8910435	0.006228365	1.3431001	0.23115598	
GO_RRNA_MODIFICATION	22	1.9367964	0.011522155	1.8776871	0.027191823	
GO_SNORNA_BINDING	24	1.8422132	0.02100726	1.6179396	0.10880591	
GO_ORGANELLAR_LARGE_RIBOSOMAL_SUBUNIT	27	1.762142	0.03128555	1.4326866	0.23856024	
GO_DNA_REPLICATION	183	2.546264	0	2.4270575	0	DNA replication
REACTOME_DNA_REPLICATION	170	2.6369953	0	2.333908	0	
REACTOME_ASSEMBLY_OF_THE_PRE_REPLICATIVE_COMPLEX	58	2.427513	0	2.0436342	0.001293203	
KAUFFMANN_DNA_REPLICATION_GENES	124	2.2196612	1.46E-04	1.957434	0.003346821	
GO_REPLICATION_FORK	58	2.0220816	0.006845257	1.9969682	0.008458413	
CHANG_CYCLING_GENES	128	2.67821	0	2.5979111	0	Cell cycle, meiosis, mitosis, chromosome segregation
ISHIDA_E2F_TARGETS	48	2.5405579	0	2.3439233	0	
BENPORATH_PROLIFERATION	126	2.4537847	0	2.0675912	0.001027586	
REACTOME_CELL_CYCLE_MITOTIC	283	2.4489732	0	2.2243552	6.76E-05	
CHICAS_RB1_TARGETS_GROWING	181	2.401499	0	2.0971758	7.83E-04	
GO_CELL_CYCLE_PHASE_TRANSITION	229	1.9100454	0.012645539	1.8784251	0.027889965	
REACTOME_MRNA_SPLICING	104	2.0330553	0.001503416	1.6695826	0.042361237	Splicing
KEGG_SPLICEOSOME	119	1.9616904	0.003091115	1.4145603	0.16712098	
GO_SPLICEOSOMAL_SNRNP_ASSEMBLY	33	2.0717127	0.004589809	1.6983364	0.07640976	
GO_PRECATALYTIC_SPLICEOSOME	21	2.0395813	0.006129047	1.7196851	0.06949566	
GO_SMALL_NUCLEAR_RIBONUCLEOPROTEIN_COMPLEX	58	2.0008543	0.007748592	1.491723	0.19077446	
GO_STEROL_BIOSYNTHETIC_PROCESS	32	2.4604068	0	2.2509563	3.28E-04	Metabolism
GO_STEROID_BIOSYNTHETIC_PROCESS	66	2.0949416	0.003603926	1.6868297	0.08089521	
GO_DEOXYRIBONUCLEOTIDE_METABOLIC_PROCESS	29	1.9609123	0.010335812	2.1248212	0.001661136	
GO_ANAPHASE_PROMOTING_COMPLEX_DEPENDENT_CATABOLIC_PROCESS	70	1.9051967	0.013002473	1.43008	0.2380279	
GO_PYRIMIDINE_CONTAINING_COMPOUND_CATABOLIC_PROCESS	23	1.7470267	0.035091735	2.1251347	0.00182725	
GO_CELLULAR_AMINO_ACID_BIOSYNTHETIC_PROCESS	67	1.6863447	0.052462712	1.4177126	0.24692611	
KAUFFMANN_DNA_REPAIR_GENES	209	2.0694098	0.001152273	2.2588038	2.97E-05	DNA repair
REACTOME_DNA_REPAIR	98	1.9531186	0.003430406	1.8546187	0.009563755	
GO_DNA_SYNTHESIS_INVOLVED_IN_DNA_REPAIR	67	2.0022895	0.007792062	2.147493	0.001659682	
GO_RECOMBINATIONAL_REPAIR	67	1.9436613	0.01072685	1.9172723	0.021425257	
GO_DAMAGED_DNA_BINDING	57	1.9444892	0.010853311	1.8641348	0.030589039	
GO_DOUBLE_STRAND_BREAK_REPAIR	143	1.824018	0.022654733	1.8222797	0.040547214	
REACTOME_TRANSCRIPTION	172	1.7701166	0.017532501	1.3438666	0.23071864	Transcription
REACTOME_RNA_POL_II_TRANSCRIPTION	90	1.6302946	0.04772672	1.3841656	0.19057691	

Figure 6.17: Selection of representative significantly enriched gene sets in si*Ctrl* vs. si*Aldoa* in NIH/3T3 cells and the 3T3$^{Fbl\text{-}GFP;Rpl18\text{-}RFP}$ cell clone used for the screen. A gene set enrichment analysis (GSEA) was performed on the read-normalized and expression filtered read counts of the triplicate RNA-Seq experiment of si*Ctrl* vs. si*Aldoa*. RNA was harvested two days after transfection of NIH/3T3 and 3T3$^{Fbl\text{-}GFP;Rpl18\text{-}RFP}$ cells. All C5 (ontology) and C2 (curated) gene sets from the MSigDB collection version 6.2 were used for the GSEA analysis. Representative gene sets that were significantly (FDR q-value < 0.25) enriched in si*Ctrl* of both cell lines are shown, grouped by color. GO = gene ontology, FDR = false discovery rate, NES = normalized enrichment score, size = size of the indicated gene set.

When analyzing the heatmap of the GO term "ribosome biogenesis" (see figure 6.18A), it became clear, that the genes were similarly regulated within the replicates of each condition (si*Ctr* or si*Aldoa*), with many RiBi genes being downregulated upon ALDOA depletion. It should be noted here, that the GO term "ribosome biogenesis" also contained some ribosomal protein genes, but many of them were not as prominently downregulated upon ALDOA depletion. However, when discriminating cytosolic and mitochondrial ribosomal protein genes, many of the latter were also significantly downregulated upon ALDOA depletion (see figure 6.18B; genes with a blue color code), although this effect was less pronounced than for the RiBi genes. A browser track picture and the normalized read counts of an example RiBi (*Rpp40*) and RP gene (*Mrpl55*) are shown in figure 6.19.

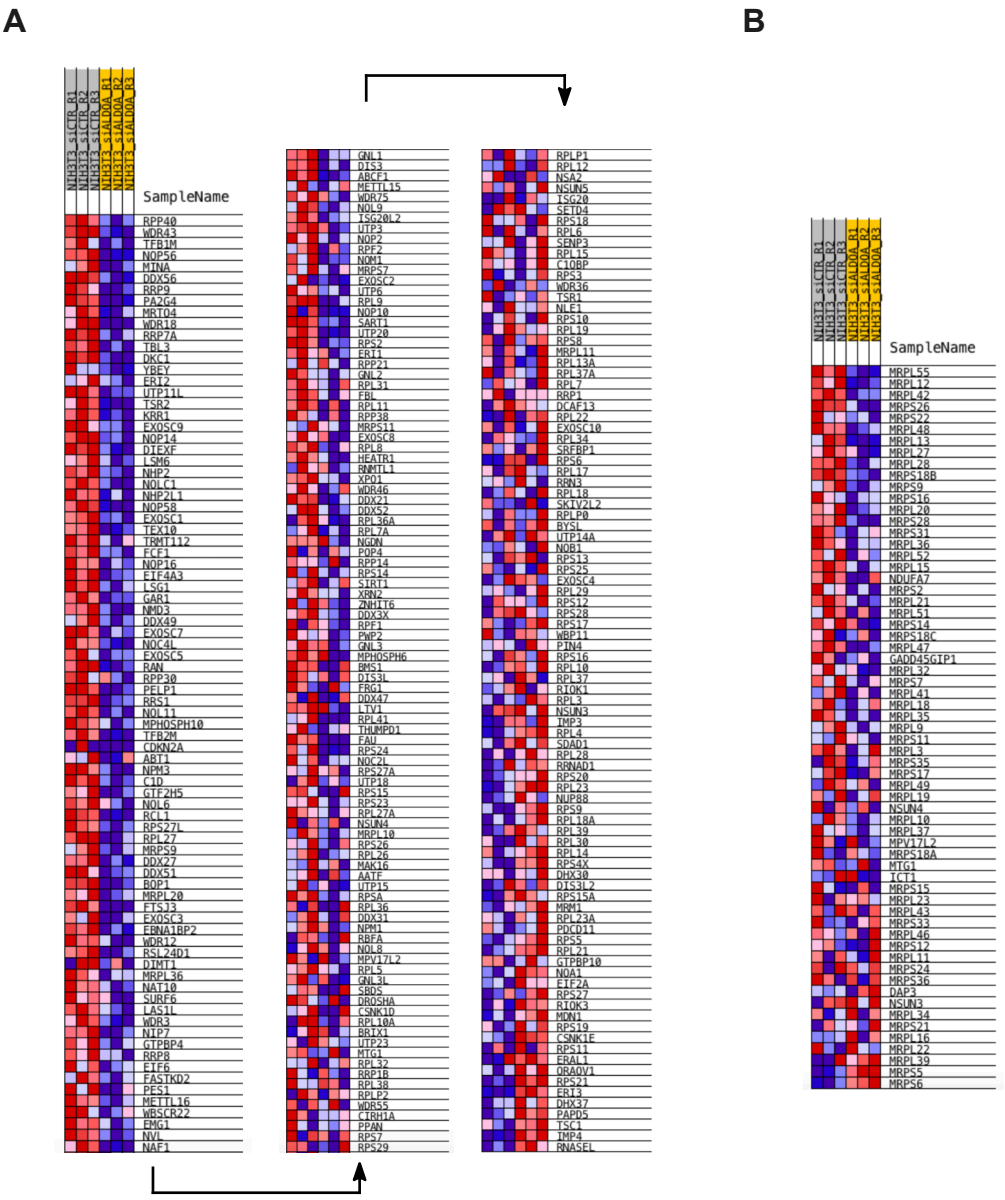

Figure 6.18: GSEA analysis of the GO terms "GO_RIBOSOME_BIOGENESIS" (left) and "GO_ORGANELLAR_RIBOSOME" (right) reveal a downregulation of many RiBis and MRPs upon ALDOA depletion in NIH/3T3 cells. MSigDB collection C5.all.v6.2.symbols.gmt was used for GSEA analysis of the read-normalized read counts from the RNA-Seq performed on NIH/3T3 cells. The depicted heatmap on the left is divided into three parts with the arrows indicating, that the list continues from left to right. Shown is the GSEA output for the GO term "GO_RIBOSOME_BIOGENESIS" on the left. This GO term was at rank 30, with an FDR q-value of 0.007593089 and an NES of 2.0060995. On the right, the heatmap of the GO term "GO_ORGANELLAR_RIBOSOME" (rank 57, NES 1.91, FDR q-value 0.013) from the GSEA output is depicted. Values range from few (blue) to many (red) read counts.

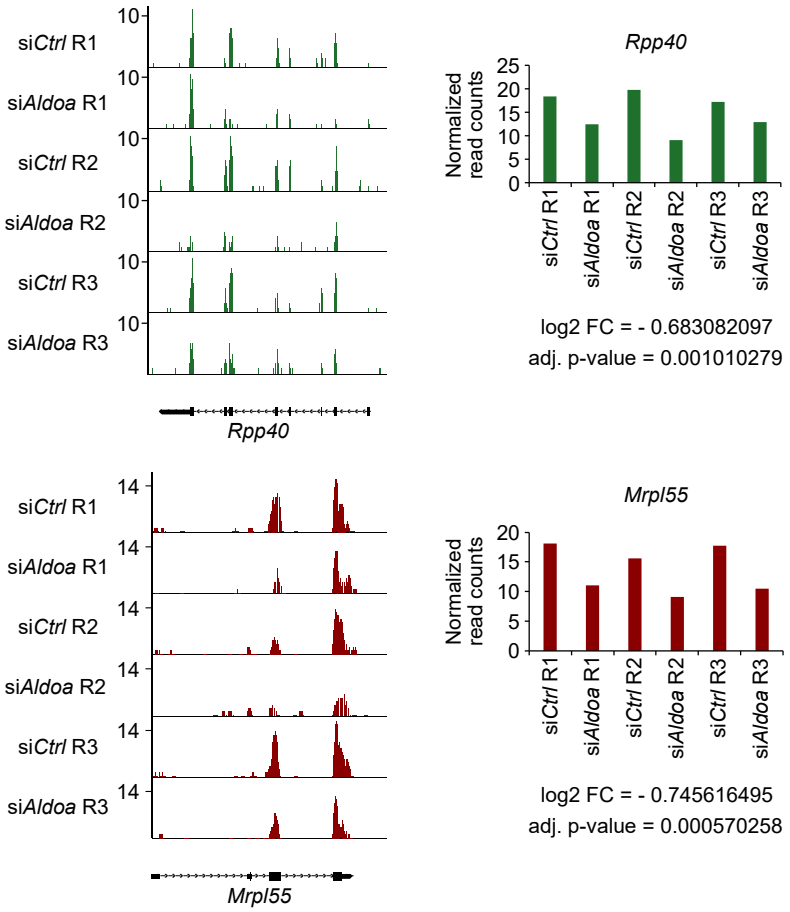

Figure 6.19: Browser track pictures (left) and normalized read counts (right) for a RiBi (*Rpp40*) and an MRP (*Mrpl55*) gene, that are downregulated upon ALDOA depletion with siRNAs are shown. See also figure 6.18.

3.) Following up the previous observations, the question arose, which other genes are downregulated upon ALDOA depletion. The GSEA analysis revealed, that in addition to ribosome biogenesis-associated genes, many more growth- and proliferation-associated genes were significantly downregulated upon *Aldoa* knockdown, for example genes involved in DNA replication, cell cycle, splicing, biosynthetic processes, DNA repair and transcription (see figure 6.17).

In summary, ALDOA depletion reduced reporter expression and led to a significant downregulation of ribosome biogenesis genes and other proliferation-associated gene sets. Our screening approach therefore indeed identified a new regulator of growth genes.

6.5.3 RNA-BINDING MOTIF PROTEIN 8A (RBM8A) regulates ribosomal protein gene expression

In addition to *Aldoa* as the top scoring gene in the condition sorted for low Fbl-driven EGFP-PEST reporter expression, there were also several spliceosome-associated proteins that scored in this condition and the validation experiments, such as *Hspa8*, *Bud31*, *Sfpq*, *Eif4a3* and *Rbm8a* (see figures 6.6 and 6.12). Two of them, *Rbm8a* and *Eif4a3*, encode members of the exon junction complex (EJC), that is placed about 20 to 24 bp upstream of an exon-exon junction after splicing [Hir et al., 2000], thus influencing downstream fates of mRNA molecules, for example their degradation via the nonsense-mediated mRNA decay (NMD) pathway [Gehring et al., 2005]. In addition to the regulation of post-transcriptional processes, the EJC was shown to bind to chromatin and influence transcription [Akhtar et al., 2019]. We thus decided to investigate a possible role of one of the pre-EJC members (*Rbm8a*) in the regulation of ribosome biogenesis genes and/or ribosomal protein genes. Two of the validation experiments are shown in figure 6.20. For this experiment, the screening cell line $3T3^{\text{Fbl-GFP;Rpl18-RFP}}$ was infected with viruses containing two different sgRNAs targeting *Rbm8a* or a control sgRNA. The cells were analyzed by FACS six days post infection and selection.

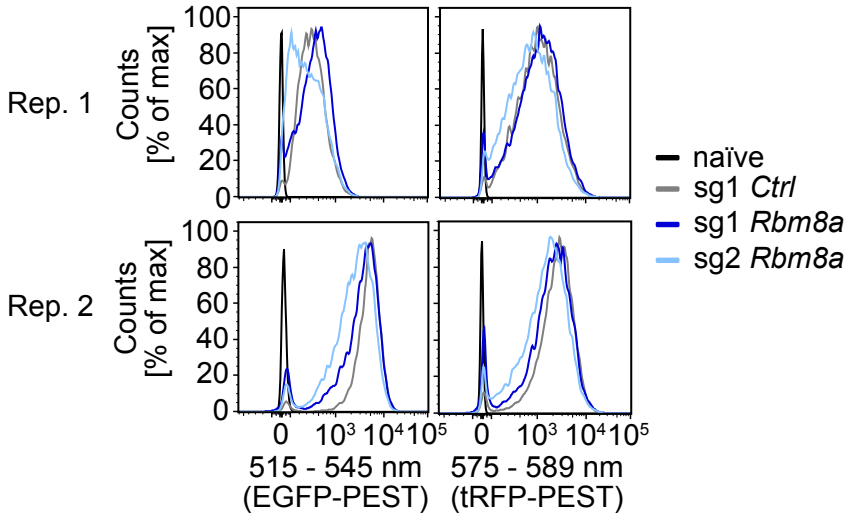

Figure 6.20: ***Rbm8a* knockout reduces the expression of *Fbl*-promoter-driven EGFP-PEST and mildly affects the expression of *Rpl18*-promoter-driven tRFP-PEST.** Fluorescent-activated cell sorting (FACS) analysis of two different sgRNAs (sg1 *Rbm8a* and sg2 *Rbm8a*) targeting *Rbm8a*, six days after infection and selection of the screening cell line $3T3^{\text{Fbl-GFP;Rpl18-RFP}}$. sg1 *Ctrl* was a non-targeting control guide used as a reference for "unperturbed" fluorescence. The plots were generated with FlowJo v10. The x-axis represents fluorescence intensity and is divided into 256 bins. The y-axis represents the number of cells in % of the fluorescence intensity bin with the highest amount of cells. Naïve cells are non-fluorescent NIH/3T3 cells, which were used as a reference for background fluorescence. Two representative experiments from a quadruplicate experiment are shown.

As seen in figure 6.20, mainly *Fbl*-driven EGFP-PEST fluorescence intensity decreased with at least one of the two sgRNAs targeting *Rbm8a*, whereas the effect on tRFP-PEST fluorescence was less prominent. Interestingly, a specific downregulation of green fluorescence was also observed when the promoters driving green and red fluorescent reporter expression were exchanged in the 3T3$^{\text{Rpl18-GFP;Fbl-RFP}}$ cell line (see figure 6.21), thus pointing either towards a post-transcriptional regulation of EGFP-PEST or a possible regulation of both, RiBis and RPs, by RBM8A. The seemingly specific effect on Rpl18-driven green fluorescence might then have come from different reporter stabilities that led to a faster decrease of EGFP-PEST fluorescence than of Fbl-driven tRFP-PEST fluorescence.

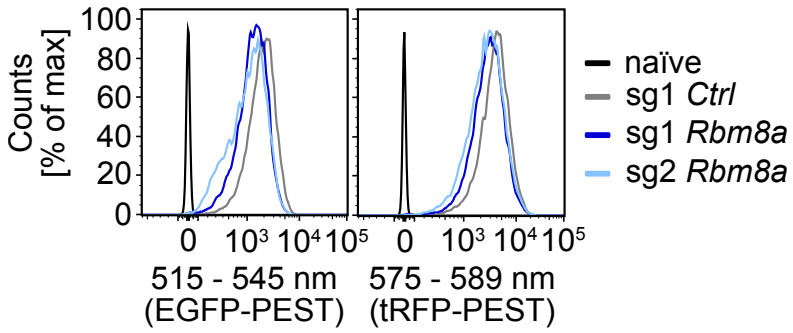

Figure 6.21: ***Rbm8a* knockout reduces the expression of *Rpl18*-promoter-driven EGFP-PEST and *Fbl*-promoter-driven tRFP-PEST.** FACS analysis of two different sgRNAs (sg1 *Rbm8a* and sg2 *Rbm8a*) targeting *Rbm8a*, six days after infection and selection of the 3T3$^{\text{Rpl18-GFP;Fbl-RFP}}$ cell line, in which the reporters were swapped compared to the screening cell line 3T3$^{\text{Fbl-GFP;Rpl18-RFP}}$. sg1 *Ctrl* was a non-targeting control guide used as a reference for "unperturbed" fluorescence. The plots were generated with FlowJo v10. The x-axis represents fluorescence intensity and is divided into 256 bins. The y-axis represents the number of cells in % of the fluorescence intensity bin with the highest amount of cells. Naïve cells are non-fluorescent NIH/3T3 cells, which were used as a reference for background fluorescence. Single experiment.

To investigate whether RBM8A directly influences transcription of ribosome biogenesis-related genes, I made use of a system that combines rapid target protein degradation (within a few hours) with subsequent nascent RNA sequencing to identify genes whose transcription is directly and immediately affected by the degradation of the targeted protein. To this end, I generated a cell line in which RBM8A can be acutely depleted by the addition of auxin/indole-3-acetic acid (IAA). Auxin is a plant hormone that is important for growth (see review [Teale et al., 2006]) and binds Aux/IAA transcriptional repressors and the F-box transport inhibitor response 1 (TIR1) protein within the SCF$^{\text{TIR1}}$ E3 ligase complex, thus exploiting the ubiquitin machinery to degrade Aux/IAA transcriptional repressors [Dharmasiri et al., 2005, Kepinski and Leyser, 2005, Nishimura et al., 2009]. Nishimura and colleagues applied this system to different eukaryotic non-plant cells, where they tagged a protein of interest (POI) with an "auxin-inducible degron" (AID)-tag, overexpressed the E3-ligase TIR1 and added auxin, which resulted in POI-

specific protein degradation [Nishimura et al., 2009]. I used this tool by endogenously and homozygously knocking a V5-tag and an AID-tag at the N-terminus of *RBM8A* in human bone osteosarcoma epithelial (U2OS) cells (figure 6.22A). To this end, sgRNAs cutting close to the start codon, as well as a homology-directed repair (HDR) template were designed. The HDR template contained the approx. 500 bp upstream and downstream sequences around the start codon, which were amplified by PCR on genomic DNA extracted from U2OS cells. Moreover, the HDR template contained a Blasticidin resistance gene for selection, separated from the V5- and AID-tag by a glycine-serine-glycine spacer and a porcine teschovirus-1 2A self-cleaving peptide (GSG-P2A) sequence, which ensures proper "cleavage" of the Blasticidin resistance gene from tagged RBM8A. Moreover, a flexible linker was designed between the AID tag and RBM8A. The HDR template and one sgRNA were transfected into U2OS cells and the cells were selected with Blasticidin. For more details about the knock-in generation, please refer to methods subsection 5.3.2. After selection and sparse seeding of cells, the generated clones were analyzed by a PCR that spanned the homology construct in order to ensure integration at the right locus and with the correct sequence. The PCR was analyzed on an agarose gel (figure 6.22B) and sequenced (figure 6.22C).

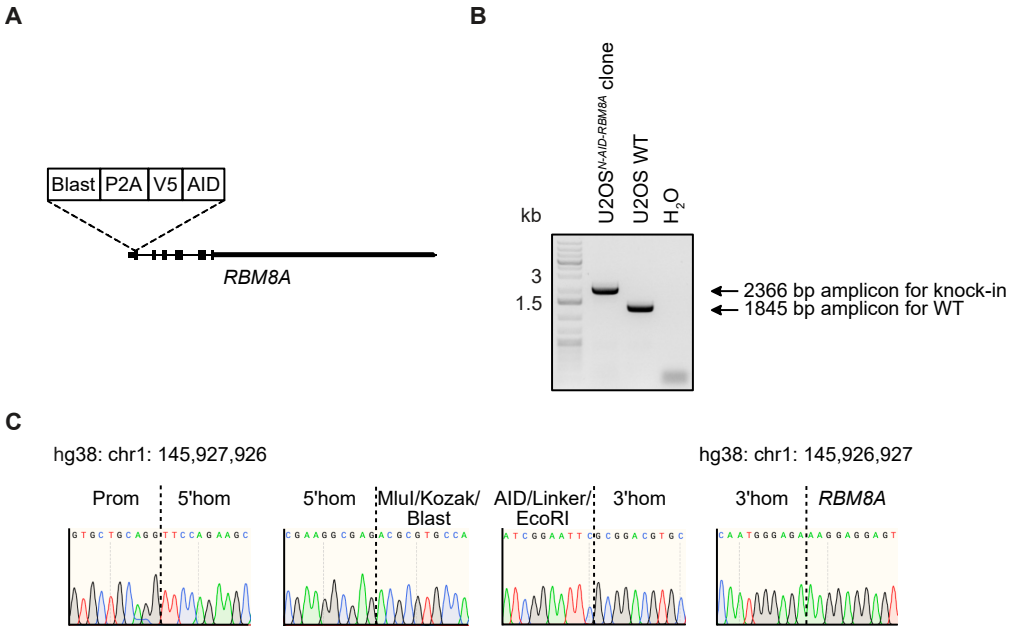

Figure 6.22: Design, generation and validation of a homozygous N-AID-RBM8A knock-in clone. (A) Schematic of the knock-in design. Blast = Blasticidin, P2A = porcine teschovirus-1 2A self-cleaving peptide, V5 = V5-tag, AID = Auxin-inducible degron tag. (B) Agarose gel of the N-terminal *AID-RBM8A* (N-AID-RBM8A) knock-in clone, analyzed via PCR for its genomic status in comparison to WT U2OS cells. kb = kilobase pairs, WT = wild type. (C) Sanger sequencing of a PCR product of the U2OS$^{N\text{-}AID\text{-}RBM8A}$ clone. Prom = Promoter, 5'hom/3'hom = 5' or 3' homology arm, MluI/EcoRI = restriction sites, Kozak = Kozak sequence, hg38 = the human reference genome hg38, chr = chromosome.

TIR1 was expressed in the chosen clone after viral infection and a time-course experiment of auxin treatment, resulting in a gradual depletion of N-AID-RBM8A, was performed (see figure 6.23). Wild type U2OS cells contained untagged RBM8A (lane 1). Protein samples of the N-AID-RBM8A clone were loaded in lanes 2 to 8. Due to the the V5- and the AID-tag, a shift in size can be observed for RBM8A (prominent lower band). The weak upper RBM8A band may correspond to a fusion protein of tagged RBM8A with Blasticidin, indicating incomplete P2A function. Upon expression of TIR1 in the cell clone, some reduction in RBM8A protein levels can be observed (compare lanes 2 and 3). Upon auxin addition, the RBM8A protein levels declined to background levels within six hours of treatment. An RBM8A- (upper part) and a whole membrane V5- (lower part) blot are shown (see figure 6.23). The staining with an anti-RBM8A antibody was needed to validate the homozygosity of the knock-in and to rule out the existence of possible shorter isoforms of the protein, that may not be tagged and could result in insufficient RBM8A degradation.

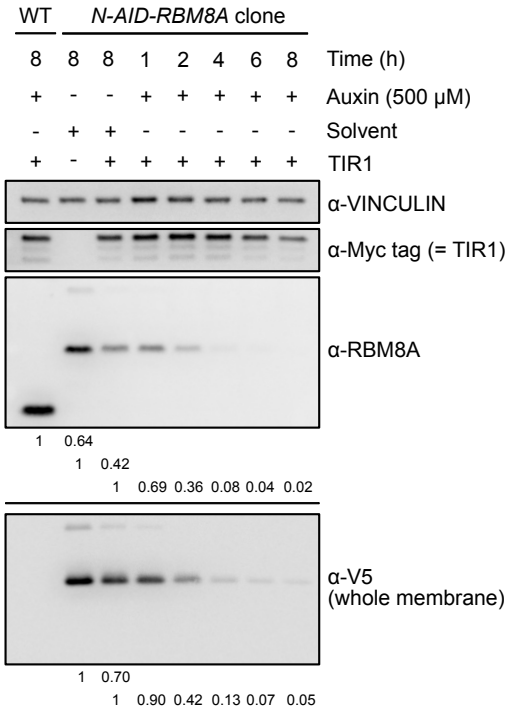

Figure 6.23: N-AID-RBM8A levels rapidly decrease upon addition of auxin. The U2OS$^{N\text{-}AID\text{-}RBM8A}$ clone was infected with virus encoding the F-box transport inhibitor response 1 (TIR1) protein and treated with auxin for different time periods. WT cells expressing TIR1 and treated with auxin served as a reference for RBM8A expression levels and as a reference for the expected size shift of tagged RBM8A in the clone. The numbers below the blots show the quantification of the RBM8A signal from each condition as a ratio over the VINCULIN signal. From these normalized values, the ratio over the respective control condition is shown. The values for the V5-blot are generated as the ones for the RBM8A blot, but without normalization to VINCULIN, since it was a whole membrane blot without staining of VINCULIN. RBM8A and V5 quantifications are based on the more prominent lower band only. Single experiment.

Figures 6.22 and 6.23 demonstrate, that I established a knock-in cell line for the rapid degradation of endogenous RBM8A, which subsequently was utilized to study the direct effects of RBM8A depletion on nascent RNA levels. To this end, I labeled nascent RNA with 4-thiouridine (4sU), a uridine analog, for 15 minutes at the end of six hours of RBM8A depletion with auxin, precipitated the nascent transcripts, prepared a library and sequenced it via next-generation sequencing (NGS). The depletion of RBM8A in this experiment was confirmed by western blot (see figure 6.24).

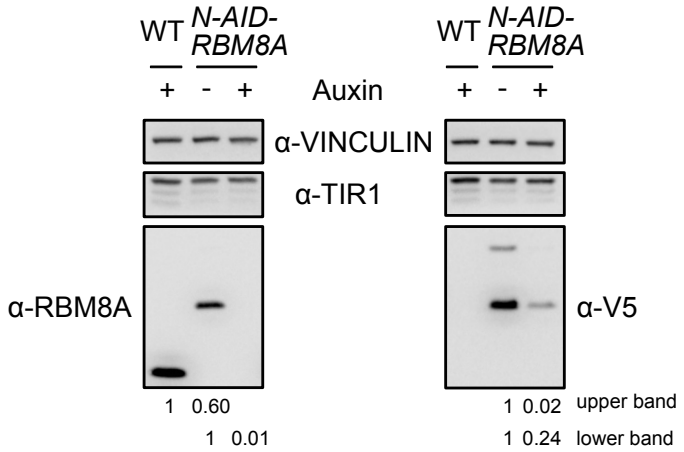

Figure 6.24: Confirmation of RBM8A depletion in the 4sU-Seq experiment. The U2OS$^{N\text{-}AID\text{-}RBM8A}$ clone expressing F-box transport inhibitor response 1 (TIR1) was treated with auxin for six hours. WT TIR1-expressing cells treated with auxin served as a control condition. The numbers below the blots show the quantification of the RBM8A/V5 signal from each condition as a ratio over the VINCULIN signal. From these normalized values, the ratio over the respective control condition is shown. The quantifications are based on the more prominent lower band only. One additional plate from the triplicate 4sU-Seq experiment was used for protein isolation and western blot analysis.

Pranjali Bhandare from our research group analyzed the 4sU-Seq experiment. The analyses downstream of count/differential gene expression tables, however, were performed by myself. To get an idea about the regulated gene sets upon RBM8A depletion, I performed a gene set enrichment analysis (GSEA) which revealed a striking downregulation of ribosomal protein gene-driven pathways upon RBM8A depletion (see figure 6.25).

NAME	SIZE	NES	FDR q-val
GO_CYTOSOLIC_RIBOSOME	88	3,0165856	0
REACTOME_EUKARYOTIC_TRANSLATION_ELONGATION	85	3,0523145	0
GO_STRUCTURAL_CONSTITUENT_OF_RIBOSOME	132	2,8310425	0
KEGG_RIBOSOME	81	3,0158296	0
GO_RIBOSOMAL_SUBUNIT	146	2,7585342	0
GO_RIBOSOME	178	2,583265	0
GO_RIBOSOME_ASSEMBLY	43	2,3562496	0
GO_CYTOPLASMIC_TRANSLATION	80	2,3334236	0
GO_POLYSOMAL_RIBOSOME	29	2,2172413	7,13E-04
GO_RIBOSOME_BIOGENESIS	219	2,0601096	0,007084056
REACTOME_TRANSLATION	231	2,289699	8,12E-05
BILANGES_SERUM_RESPONSE_TRANSLATION	26	2,0647135	0,001808807

Figure 6.25: Ribosomal protein gene sets are downregulated upon RBM8A depletion. Gene set enrichment analysis (GSEA) of a triplicate 4-thiouridine (4sU)-Seq experiment of the U2OS$^{N\text{-}AID\text{-}RBM8A}$ TIR1-expressing cell clone +/- auxin and of WT TIR1-expressing U2OS cells treated with auxin. RNA was harvested six hours after auxin treatment, incl. 15 minutes of 4sU labeling at the end of the six hours. All C5 (ontology) and C2 (curated) gene sets from version 7.1 were used for the GSEA analysis. Shown is a small collection of the gene sets that were significantly (FDR q-value < 0.25) enriched in WT cells or U2OS$^{N\text{-}AID\text{-}RBM8A}$ cells without auxin treatment, respectively, over RBM8A depleted cells. GO = gene ontology, FDR = false discovery rate, NES = normalized enrichment score, size = size of the indicated gene set.

Upon closer inspection it became clear, that especially cytosolic ribosomal protein genes (CRPs) drive the significantly enriched gene sets in the comparison of +/- RBM8A depletion (figures 6.25 and 6.26 (left panel)). Upon RBM8A depletion, the mean nascent transcript levels of CRPs were reduced by about 27% compared to the clone without RBM8A depletion and by about 20% compared to WT cells treated with auxin (figure 6.26, left and right panel, respectively). MRPs and RiBis on the other hand, were largely unaffected by acute RBM8A depletion (see figure 6.26, left panel).

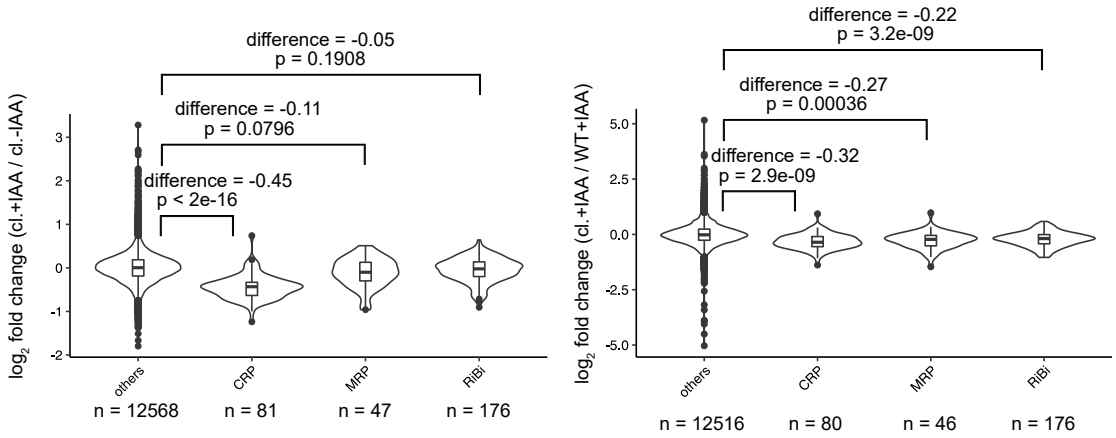

Figure 6.26: RBM8A depletion reduces nascent transcript levels of cytosolic ribosomal protein genes (CRPs) and potentially also of ribosome biogenesis genes. Violinplots of the log2 fold change of the indicated comparisons. FC = fold change, n = number of genes within the corresponding gene set, CRP = cytosolic ribosomal protein genes, MRP = mitochondrial ribosomal protein genes, RiBi = ribosome biogenesis genes, others = all other genes which do not fall into the category "CRP", "MRP" or "RiBi". CRPs and MRPs were extracted from the GO term "GO:0003735 Structural constituent of ribosome". The RiBi genes were extracted from the GO term "GO: 0042254 Ribosome biogenesis". Genes overlapping with the CRP or MRP gene sets were removed from the RiBi gene set. Differences and p-values were calculated with a two-sided Dunnett's test.

Additionally, sustained RBM8A withdrawal led to a strong decrease in cell number (see figure 6.27A) and induction of apoptosis as determined by Annexin V/PI-FACS (see figure 6.27B), consistent with literature [Ishigaki et al., 2016].

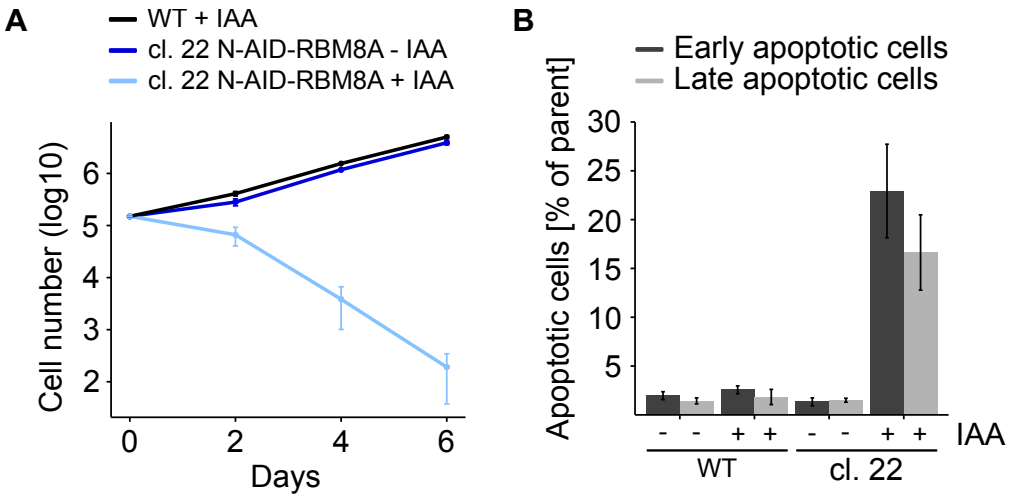

Figure 6.27: RBM8A depletion leads to a drastic decrease in cell number (A), most likely due to apoptosis (B). (A) Logarithmic (log10) growth curve of WT TIR1-expressing U2OS cells treated with auxin and the U2OS$^{N\text{-}AID\text{-}RBM8A}$ cell clone +/- auxin in triplicates. Error bars represent the standard deviation of the triplicates. (B) Annexin V/PI-FACS of WT TIR1-expressing U2OS cells and the U2OS$^{N\text{-}AID\text{-}RBM8A}$ cell clone +/- auxin in triplicates. 48 h auxin treatment. Early apoptotic cells were cells with high Annexin V, but low propidium iodide (PI) signal. Late apoptotic cells were cells with high Annexin V and propidium iodide (PI) signal. Error bars represent the standard deviation of the triplicates.

As an attempt to further understand the potential direct role of RBM8A in the regulation of CRPs specifically, we wanted to know, whether RBM8A directly binds to CRP promoters. Chromatin-immunoprecipitation experiments (see figure 6.28) revealed, that V5-tagged RBM8A could readily be detected at these loci (*RPL41*, *RPS27L*, *RPL38*, *RPLP1*), but also at "housekeeping gene" promoters that were not significantly regulated in the 4sU-Seq experiment (*HPRT1*, *TBP*, *B2M*, *POLR2A*). Surprisingly, RBM8A could also be immunoprecipitated from a gene-free region (intergenic region). This signal appeared to be specific, however, since i) it was reduced to background levels upon auxin treatment and ii) there was no enrichment of RBM8A-bound DNA from these loci from WT cells, indicating that the V5-antibody does not recognize chromatin unspecifically. Additionally, the non-specific Immunoglobulin G (IgG) control did also not enrich these loci above background levels.

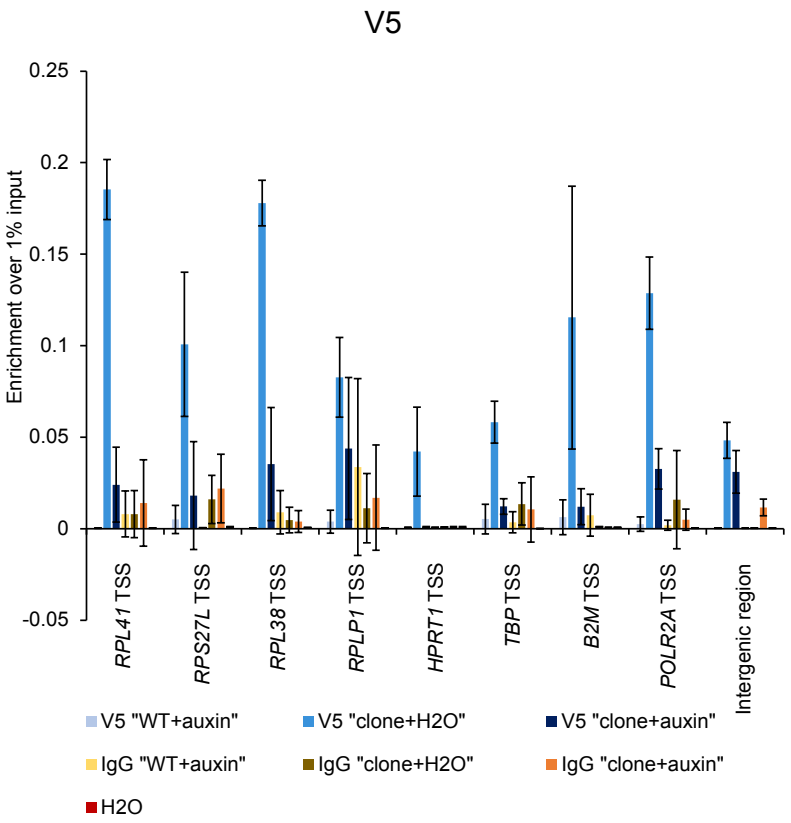

Figure 6.28: Chromatin-immunoprecipitation of V5-tagged RBM8A reveals broad binding of RBM8A to chromatin. Different ribosomal protein genes (*RPL41*, *RPS27L*, *RPL38*, *RPLP1*), that were significantly depleted upon RBM8A withdrawal in the 4sU-Seq experiment, as well as non-significantly regulated "housekeeping genes" (*HPRT1*, *TBP*, *B2M*, *POLR2A*) and a gene desert on chromosome 11 (intergenic region) were analyzed for their enrichment over input in the indicated conditions. 500 µM auxin or water were added for six hours to U2OS$^{N\text{-}AID\text{-}RBM8A}$ TIR1-expressing cells or WT TIR1-expressing U2OS cells and RBM8A was chromatin-immunoprecipitated with a V5 antibody. A representative experiment from three independent replicates (duplicates for WT) is shown. Primers were chosen to amplify a region roughly - 50 bp to + 150 bp around the transcriptional start site (TSS). The error bars represent the standard deviation of the technical triplicates of the depicted experiment.

Given the apparent broad chromatin-binding affinity of RBM8A, we wondered how ribosomal protein genes could be specifically affected by RBM8A loss. Could it be, that RBM8A binds directly to POL II, thereby potentially influencing POL II's function during the transcription cycle, somehow specifically at ribosomal protein genes? Along this line, we first wanted to analyze whether RBM8A binds POL II directly and performed co-immunoprecipitation (Co-IP) experiments after overepression of HA-tagged RBM8A and FLAG-tagged RPB1, the largest subunit of POL II, in human embryonic kidney (HEK) cells. Indeed, when immunoprecipitating FLAG-tagged RPB1, I could co-immunoprecipitate HA-tagged RBM8A (see figure 6.29; compare lane 3 and 4). RPB2 is a well known interaction partner of RPB1 and served as a positive control for the Co-IP.

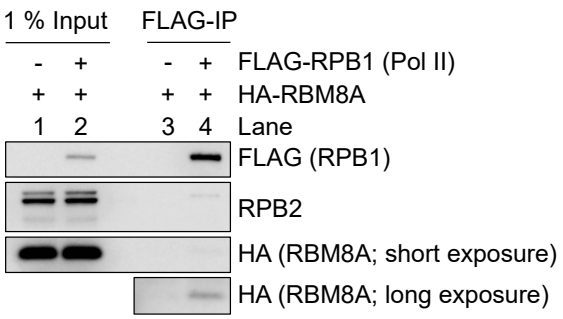

Figure 6.29: Exogenous Co-IP of HA-RBM8A with FLAG-RPB1, the largest subunit of POL II. HEK cells were transfected with HA-RBM8A and FLAG-RPB1 or with HA-RBM8A and a GFP-expressing control vector. 24 hours after transfection, the cells were harvested and IP was performed with an anti-FLAG antibody. Western blot analysis was performed with anti-FLAG, anti-RPB2 and anti-HA antibodies. RPB2 served as a positive control interaction partner of RPB1. Representative experiment from a triplicate experiment is shown.

After having confirmed the interaction of RBM8A with POL II, we wanted to know whether RBM8A might also influence the amount of total POL II or elongating POL II around the transcription start site (TSS). To study this, I immunoprecipitated chromatin-engaged total POL II and elongating POL II (serine 2-phosphorylated POL II). Figure 6.30a shows, that upon acute depletion of RBM8A with auxin, there was no significant difference in neither the amount of total, nor the amount of serine 2-phosphorylated POL II (pS2-POL II). This was also true for the *RPS27L* locus, which is one of the very few exceptions of RPs showing significant upregulation in reponse to RBM8A depletion.

I also analyzed selected genes for pS5-POL II-binding, a marker for initiating POL II [Komarnitsky et al., 2000], using ChIP (figure 6.30b). To this end, I tested one RP gene that was significantly downregulated in the 4sU-Seq experiment only in the RBM8A depleted condition (*RPL41*), one RP gene that was significantly downregulated not only in the Rbm8a depleted condition, but also in the comparison clone without auxin to WT (*RPS23*) and one RP gene that was not significantly regulated at all (*RPS13*). With regard to chippable pS5-POL II at the aforementioned loci, there was no difference observable, suggesting that not only transcription elongation, but also initiation is not directly affected by RBM8A withdrawal at all the different loci investigated, ranging from "housekeeping genes" to regulated and apparently non-regulated ribosomal protein genes.

Thus, how RBM8A directly influences ribosomal protein gene expression, needs further investigation and could not be finally determined within the scope of this thesis.

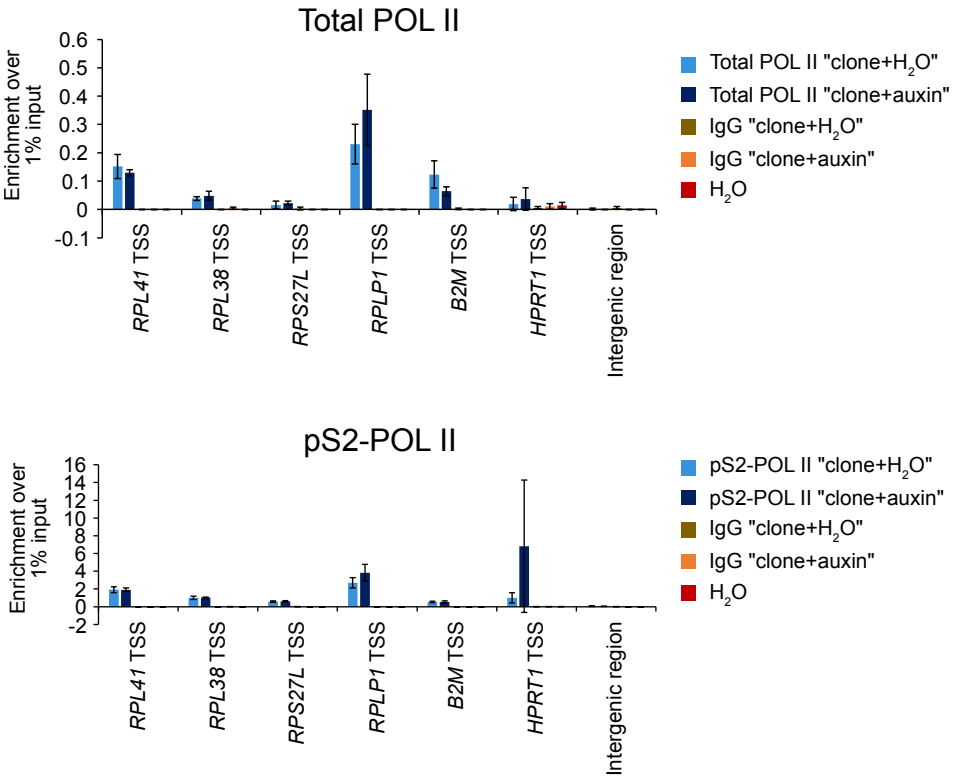

(a) Total/pS2-POL II levels are unchanged upon acute RBM8A depletion at the tested CRP (and housekeeping) genes. Different ribosomal protein genes (*RPL41*, *RPL38*, *RPS27L*, *RPLP1*), that were significantly depleted upon RBM8A withdrawal in the 4sU-Seq experiment, and non-significantly regulated "housekeeping genes" (*B2M*, *HPRT1*) were analyzed for their enrichment in the indicated conditions. 500 µM auxin was added for six hours and total or pS2-POL II was chromatin-immunoprecipitated. Representative experiment from two independent replicates is shown. Primers were chosen to amplify a region roughly - 50 bp to + 150 bp around the TSS. The error bars represent the standard deviation of the technical triplicates of the depicted experiment.

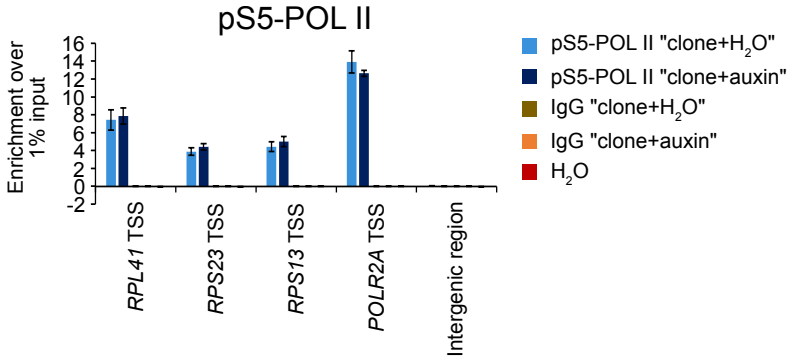

(b) pS5-POL II levels are unchanged upon acute RBM8A depletion at the tested CRP (and housekeeping) genes. Different ribosomal protein genes (*RPL41*, *RPS23*, *RPS13*) and one "housekeeping gene" (*POLR2A*) were analyzed for their enrichment in the indicated conditions. 500 µM auxin was added for six hours and pS5-POL II was chromatin-immunoprecipitated. Single experiment. Primers were chosen to amplify a region roughly - 50 bp to + 150 bp around the TSS. The error bars represent the standard deviation of the technical triplicates of the experiment.

Figure 6.30: Total/pS2/pS5-POL II levels are unchanged upon acute RBM8A depletion at the tested CRP (and housekeeping) genes. U2OS$^{N\text{-}AID\text{-}RBM8A}$ TIR1-expressing cells were used. The intergenic region was a gene desert on chromosome 11.

6.6 Genome-wide CRISPR-Cas9 screen utilizing the endogenous *FBL* promoter to drive reporter expression

Although some promising hits were discovered in the screen, some partially unexpected problems occurred, that confounded the results:

i) Although tested beforehand in T lymphoma cells, the promoter fragments might not have been able to unfold their full regulatory capacity. The reporter constructs used had been integrated randomly into the genome and only contained roughly 500 bp of the region directly 5' of the start codon. It is well imaginable, that additional regulatory regions further upstream may contribute to the full regulating potential. Additionally, some cis-regulatory sequences might become relevant only within the supposed, endogenous location in the genome. Moreover, topologically associating domains (TADs) may form to facilitate transcription at RP and RiBi genes in dependence of surrounding chromatin features. All of these potential problems might have led to fewer hits that could be identified.
ii) tRFP-PEST seemed to be way more stable than EGFP-PEST, leading to a shift of the hits from an expected occurence in the "both down" list to the "GFP/RiBi down list".

To overcome these issues, we wanted to repeat the screen with an improved design that tried to counteract the aforementioned obstacles.

i) We decided to endogenously knock-in a reporter directly after the start codon. With this strategy we could make use of the full regulatory capacity with the exception of potential cis-regulatory elements that are present after the start codon. However, we did not want to use a C-terminal knock-in strategy in order to avoid splicing factors etc. to appear as hits again. Moreover, we wanted to use a heterozygous cell clone instead of a homozygous one to reduce the risk of ribosome imbalance-induced cell death. At the knock-in allele, a poly(A) site was inserted in order to stop transcription and avoid a possible fusion protein of the RiBi/RP gene, the reporter and Blasticidin (see figure 6.31A). I generated a knock-in cell line at the endogenous *FBL* locus in human U2OS cells, since this is one of the best characterized cell lines in our research group from which we had many genomics and transcriptomics data available that helped us to decide which human RiBi/RP gene to choose. *FBL* and *RPL36* (but the latter is not further discussed in this thesis) were chosen for the knock-ins, because they were among the most strongly downregulated genes within their group (RiBi or RP,

respectively) upon MYC depletion in U2OS cells with only very little MYC binding after the start codon [Lorenzin et al., 2016].

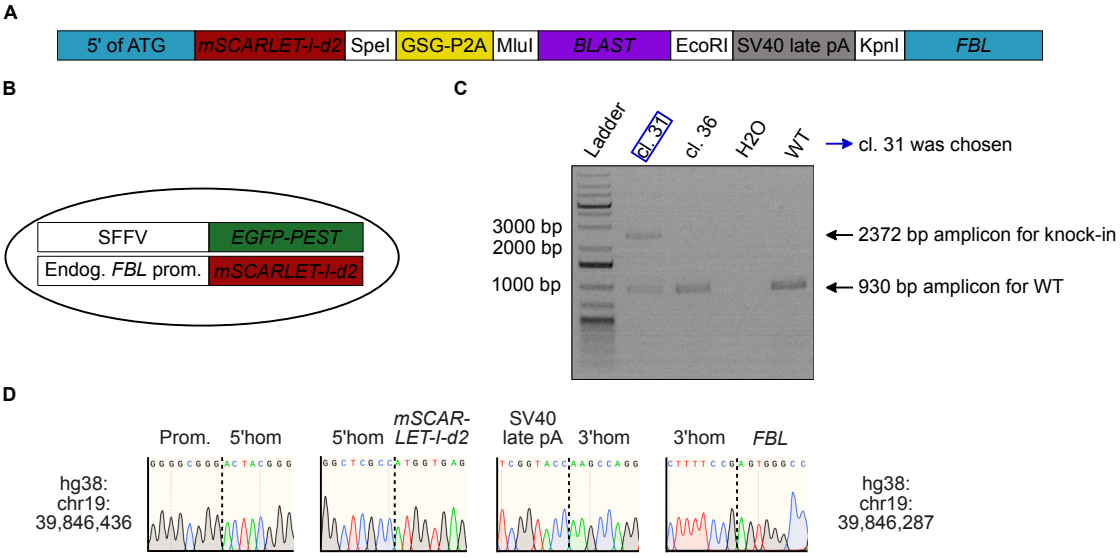

Figure 6.31: Design (A and B), generation and validation (C and D) of a clone (cl. 31) with a heterozygous mScarlet-I-d2 knock-in, at the N-terminus of the endogenous *FBL* gene with a concomitant disruption of the *FIBRILLARIN* gene according to the design scheme. (A) Scheme of the knock-in design. ATG = Start codon, GSG-P2A = porcine teschovirus-1 2A self-cleaving peptide and a preceding glycine-serine-glycine (GSG) linker (amino acid sequence: GSGATNFSLLKQAGDVEENPGP), Blast = Blasticidin, SV40 late pA = simian virus 40 late polyadenylation signal, SpeI/MluI/EcoRI/KpnI = restriction recognition sites, *FBL* = *FIBRILLARIN* gene. (B) Scheme of the final cell clone driving EGFP-PEST expression from an SFFV promoter and heterozygous mSCARLET-I-d2 expression from one of the endogenous *FBL* promoters. SFFV = spleen focus-forming virus, Endog. = endogenous, prom. = promoter. (C) Agarose gel of different clones, analyzed via PCR for their genomic status. The picked clone number 31 was heterozygous for the knock-in, but harbored a 5 bp deletion on the "WT" allele. Cl. = clone, WT = wild type. (D) Sanger sequencing of the PCR product from clone 31. 5'hom = 5' homology arm, 3'hom = 3' homology arm, hg38 = the human reference genome 38, chr = chromosome.

ii) We noticed that general transcription-associated processes were enriched in the "GFP/RiBi down" list, although they were expected to occur in the "both down" list. Such a result could be explained by different reporter stabilities. To investigate this hypothesis, I performed a CHX-assay on tRFP-PEST. This experiment confirmed the higher stability of tRFP-PEST in comparison to EGFP-PEST (compare figure 6.32, left panel, with figure 6.2D) with a measured half-life of more than 24 hours for tRFP-PEST and 4 hours for EGFP-PEST, respectively. To reduce the stability differences between the green and red fluorescent reporters in another screen, I decided to replace tRFP-PEST by another red fluorescent protein. mScarlet-I-PEST (hereafter called mScarlet-I-d2) was tested in a CHX-assay (figure 6.32, right panel) and used instead of tRFP-PEST as a reporter driven by the endogenous *FBL* promoter, since its half-life was only about 13 hours. EGFP-PEST driven by the SFFV promoter was used as a ribosome biogenesis-independent reporter system within the same cells (see figure 6.31B). We

used the more stable mScarlet-I-d2 protein as the reporter for RiBi regulation and the less stable green fluorescent protein as a "counter" reporter to avoid the enrichment of general transcription-associated genes in the screen, because when cells are sorted for low red and high green fluorescence, an enrichment of hits leading to a decrease of the less stable green fluorescence first, such as POL II, could thus be excluded.

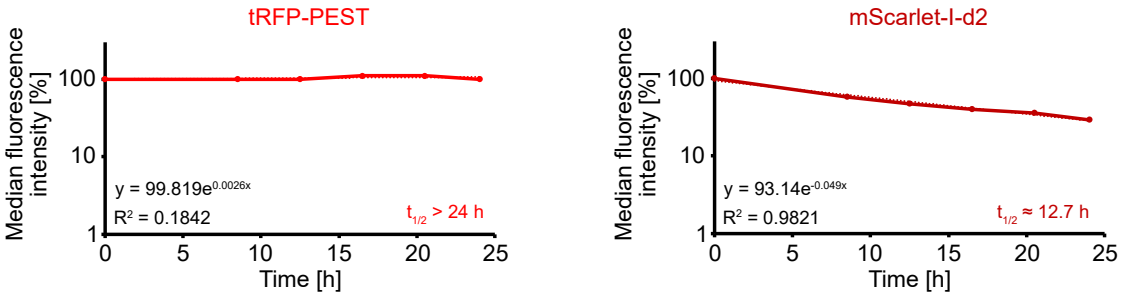

Figure 6.32: Cycloheximide (CHX) assay reveals major differences in the stabilities of the indicated red fluorescent proteins. U2OS cell lines driving the expression of the indicated proteins under the control of an SFFV promoter were treated with 10 µg/ml CHX for a maximum of 24 hours and fluorescence was measured by FACS. Analysis was performed with FlowJo v10 and the median fluorescence intensity in percent of the fluorescence intensity at 0 h is depicted. Single experiment. R^2 = coefficient of determination, $t_{1/2}$ = half-life.

Having decided about the general design of the cell lines I wanted to generate, I transfected and selected the cells, picked individual clones, isolated their genomic DNA and performed a PCR to identify heterozygous clones. Clone 31, also called U2OS$^{\text{FBL-SCARLET;SFFV-GFP}}$, was chosen for further experiments (see figures 6.31C and D).

With this cell line I repeated the former screen, but sorted different populations than previously: "mScarlet-I-d2/RiBi down" and "mScarlet-I-d2/RiBi up" with high green and low green fluorescence as a counter gate, respectively. When analyzing this screen, only the mScarlet positive control was significantly enriched in the "mScarlet-I-d2/RiBi down" list (see table 6.7) and no significant enrichment of genes was found in the "mScarlet-I-d2/RiBi up" condition. This screen therefore did not reveal new transcriptional regulators of RiBi genes.

Rank	Gene	Protein	logFC	FDR
1	*SCARLET*	mScarlet-I-d2	3.6137	0.00495
2	*PAQR9*	Membrane progestin receptor epsilon	1.4892	0.823484
3	*KMT2B*	Histone-lysine N-methyltransferase 2B	1.1238	0.823484
4	*DAZAP2*	DAZ-associated protein 2	1.4306	0.823484
5	*ETHE1*	Persulfide dioxygenase ETHE1, mitochondrial	1.5092	0.823484
6	*LSR*	Lipolysis-stimulated lipoprotein receptor	0.84191	0.823484
7	*ZCWPW2*	Zinc finger CW-type PWWP domain protein 2	1.5141	0.823484
8	*IGFBPL1*	Insulin-like growth factor-binding protein-like 1	1.3619	0.823484
9	*CHTF18*	Chromosome transmission fidelity protein 18 homolog	1.0365	0.823484
10	*AKR1B1*	Aldo-keto reductase family 1 member B1	1.422	0.823484
11	*TRAPPC8*	Trafficking protein particle complex subunit 8	-2.0282	0.823484
12	*DDX6*	Probable ATP-dependent RNA helicase DDX6	1.0801	0.823484
13	*PSMC2*	26S proteasome regulatory subunit 7	0.97202	0.823484
14	*TBC1D19*	TBC1 domain family member 19	0.38292	0.823484
15	*IMPA1*	Inositol monophosphatase 1	1.3269	0.823484
16	*ZCCHC2*	Zinc finger CCHC domain-containing protein 2	1.5274	0.823484
17	*CRB1*	Protein crumbs homolog 1	0.24147	0.823484
18	*MTF2*	Metal-response element-binding transcription factor 2	0.95358	0.823484
19	*SLC39A2*	Zinc transporter ZIP2	1.1236	0.823484

20	*EIF3K*	Eukaryotic translation initiation factor 3 subunit K	0.72398	0.823484
21	*SFTPA2*	Pulmonary surfactant-associated protein A2	-0.56167	0.823484
22	*DEFB115*	Beta-defensin 115	1.1898	0.823484
23	*TRAF4*	TNF receptor-associated factor 4	0.6555	0.823484
24	*FBXO42*	F-box only protein 42	0.92179	0.823484
25	*KLF11*	Krueppel-like factor 11	1.1406	0.823484

Table 6.7: Positively enriched genes from the "mScarlet-I-d2/RiBi down" condition of the endogenous genome-wide CRISPR-Cas9 knockout screen. The "Protein" column information was obtained from "www.uniprot.org".

7 Discussion

To my knowledge, no certain differential transcriptional regulator of RiBi or RP genes has been identified in mammals so far. Some screens, that were performed to find regulators of ribosome biogenesis, read-out changes in nucleolar size [**?**] or nuclei number [Farley-Barnes et al., 2018]. Other screens identified proteins involved in ribosome subunit biogenesis [Wild et al., 2010, Badertscher et al., 2015] or pre-rRNA processing [Tafforeau et al., 2013]. However, none of these screens specifically aimed to identify new transcriptional regulators of ribosome biogenesis factors or ribosomal proteins. Our screening design theoretically allowed the identification of such differential regulators of RiBi and RP genes in the "GFP/RiBi down" and "RFP/RP down" lists, respectively.

We used fluorescent reporters driven by a RiBi (*Fbl*) or an RP (*Rpl18*) promoter to identify new transcriptional and potentially even differential regulators of these processes in an unbiased, genome-wide screen.

7.1 Detailed discussion about the screening results

In the main screen, four conditions were sorted:
(i) low expression of *Fbl*-driven EGFP-PEST and low expression of *Rpl18*-driven tRFP-PEST ("both down")
(ii) high expression of *Fbl*-driven EGFP-PEST and high expression of *Rpl18*-driven tRFP-PEST ("both up")
(iii) median to high expression of *Fbl*-driven EGFP-PEST and low expression of *Rpl18*-driven tRFP-PEST ("RFP down")
(iv) low expression of *Fbl*-driven EGFP-PEST and median to high expression of *Rpl18*-driven tRFP-PEST ("GFP down").

According to the sorting strategy, the following kinds of candidate genes were expected to be enriched in the respective sorted samples:
(i) activators of RiBi and RP gene expression
(ii) repressors of RiBi and RP gene expression

(iii) activators of RP gene expression
(iv) activators of RiBi gene expression.

It became apparent, that the "both down" condition did not include any significantly enriched genes. Reasons may be, that many sgRNAs potentially target essential processes of cells, leading to apoptosis which may have influenced fluorescence intensity of cells. Thus, it could have been the case, that many cells were sorted in this condition due to a general downregulation of cellular processes. Alternatively, since the guide RNAs integrated randomly into the genome, with a preference of lentiviral integrations into genes [Yang et al., 2008], it is well imaginable, that sgRNAs integrated into essential genes. This integration might have rendered that particular gene unfunctional, potentially influencing cell viability and reporter expression as described above. All of these effects might have led to the sorting of many cells harboring sgRNAs, that only indirectly influenced reporter expression, thus influencing statistical enrichment of truly positive hits.

The "RFP down" condition revealed only one significantly enriched gene (apart from the positive control), *Adrm1*, a proteasomal ubiquitin receptor. Although not shown in this thesis, I could validate, that it was a very specific regulator of tRFP-PEST, even after swapping of the reporters. Thus, although the mechanisms are not clear, it seems likely, that it is not a specific transcriptional regulator or RP genes.

Significant candidate genes were mainly found in the "both up" and the "GFP/RiBi down" condition with a clear enrichment of transcription-associated processes in the "GFP/RiBi down" condition. Thus, only hits from this condition were further analyzed in this thesis. However, the "both up" condition may have harbored promising candidates as well. The observed enrichment of proteasomal subunits in this list indicated, that the screen was in principle able to connect the genotypic information to the phenotype which was sorted, since an inhibition of protein degradation would lead to an accumulation of the reporters with a concomitant increase in fluorescence intensity. Nevertheless, since we wanted to identify new transcriptional modulators of ribosome biogenesis, these genes were excluded from further analyses. Other potentially promising, significantly enriched genes in the "both up" condition were for example (i) PABPN1, (ii) ZCCHC11 and (iii) EWSR1, which will be discussed in more detail: (i) PABPN1 is suggested to bind to POL II during transcription [Bear et al., 2003] and gets assembled on the emerging poly(A) tail [Bear et al., 2003], whose length it controls [**?**]. PABPN1 hyperadenylates transcripts, which promotes their nuclear decay [Bresson and Conrad, 2013]. However, PABPN1 depletion does not generally affect mRNA levels, but leads

to an accumulation of some long non-coding RNAs (lncRNAs), such as snoRNA host genes [Beaulieu et al., 2012]. It may thus well be, that ribosome biogenesis is affected upon PABPN1 depletion. The reason, why PABPN1 scored in our screen, is not fully clear, though. Does PABPN1 influence the transcription of snoRNAs which may feed back to *Fbl*- and *Rpl18* promoter-driven transcription? Alternatively, is PABPN1 required for efficient polyadenylation of the reporters, which may influence reporter transcript stability and thus possibly also translation efficiency, with all of these effects being independent of a regulation of ribosome biogenesis? Further studies would be needed to investigate whether PABPN1 may be a possible new regulator of ribosome biogenesis. (ii) ZCCHC11, which is also called TUT4, is a terminal uridylyl transferase, that uridylates the $7S_B$ rRNA [Pirouz et al., 2019], which provides a link to ribosome biogenesis. (iii) The protein EWSR1 was shown to be important for nucleolar integrity [Abraham et al., 2020] and was additionally identified as a pre-rRNA processing factor in human cells [Tafforeau et al., 2013].

Finally, the main focus of this thesis was lying on the candidate genes obtained from the "GFP/RiBi down" condition. Initially, specific activators of RiBi genes were expected to be enriched in this condition. Validation experiments revealed, however, that a knockout of many candidate genes reduced expression of both reporters, at least to some extent. Even if a knockout of some of the hits apparently specifically downregulated EGFP-PEST expression, such as *Bud31* or *Sfpq*, a repetition of the validation experiments in a swapped reporter cell line revealed, that the reporter itself was a stronger determinant of fluorescence intensity changes after knockout than the promoters driving the reporters. This effect could be explained by the differential stability of tRFP-PEST and EGFP-PEST. Depending on the sorting time point, a hit that actually regulates both, RiBis and RPs, might thus be captured as a seemingly specific regulator of EGFP-PEST/RiBis, although tRFP-PEST fluorescent changes are just delayed. The stability differences thus led to an enrichment of sgRNAs targeting factors, that regulated the expression of EGFP-PEST and tRFP-PEST in this condition. But which of them might be potential new transcriptional regulators of RiBi and RP genes? This study focused mainly on *Aldoa* and *Rbm8a*, but what about the other significantly enriched genes from the "GFP/RiBi down" condition? Are some of them already described as potential modulators of ribosome biogenesis? Were some of them found in other published screens that aimed to find proteins with a previously unknown role in ribosome biogenesis?

7.2 Identification of potential regulators of ribosome biogenesis, which were also identified in published screens

When comparing the candidate genes, indeed some overlap becomes apparent. Knockdown of members of the FACT complex, for example, reduces nucleolar size, whereas knockdown of the SIN3-histone deacetylase complex increased nucleolar size [**?**]. These data are in line with the results of our reporter screen, in which *Ssrp1*, a member of the FACT complex, scored in the "GFP/RiBi down condition" and *Sap18*, a member of the SIN3-repressive complex, scored in the "both up" condition.

Interestingly, depletion of two POL II subunits were found to reduce the number of nucleoli to one, with *Polr2e* and *Polr2j3* being the corresponding genes [Farley-Barnes et al., 2018]. Moreover, *Polr2e* and *Polr2h* scored in a screen searching for new pre-rRNA processing factors [Tafforeau et al., 2013] and were strong hits in our screen as well (table 6.6).

Eif4a3, a member of the EJC, also scored in our screen and in screens, that identified regulators of ribosome subunit biogenesis [Wild et al., 2010] and pre-rRNA processing [Tafforeau et al., 2013]. Splicing-associated factors, such as *Bud31*, *Eif4a3* and *Sfpq* were found in a screen, that identified proteins regulating human 40S ribosomal subunit biogenesis [Badertscher et al., 2015] and were also found in our screen. Nevertheless, splicing factors could very indirectly influence ribosome biogenesis, for example by missplicing/-processing of snoRNAs, that are mostly located in introns, thus influencing ribosome biogenesis via a post-transcriptional mechanism.

In summary, many of the candidate genes we identified were also identified in other screens and may be (direct) transcriptional regulators of ribosome biogenesis.

7.3 Other potential new regulators of ribosome biogenesis among the significantly enriched genes from the different sorted screening conditions

One candidate gene of the "GFP/RiBi down" condition, that could be validated as a regulator of both reporters, was *Hspa8*. The protein encoded by this gene is HSC70, a constitutively expressed chaperone of the HSP70 family [Stricher et al., 2013, Finka et al., 2015]. Interestingly, three copies of *Snord14*, which encode the U14 small nucleolar RNA (snoRNA), are located in introns of *Hspa8* [Liu and Maxwell, 1990]. It is well imaginable, that a knockout of *Hspa8* may lead to limiting amounts of U14 snoRNA, which may result in impaired rRNA methylation [Dunbar and Baserga, 1998] and potentially dysregulated ribosome biogenesis. In yeast, it could already be shown, that impaired ribosome biogenesis feeds back to the transcription of ribosomal proteins, limiting their production [Albert et al., 2019]. Potentially, similar effects may have been captured in our reporter screen.

Besides a potential effect on the encoded U14 snoRNA, a knockout of the *Hspa8* gene also affects HSC70 protein levels. Might the encoded HSC70 protein also have functions in ribosome biogenesis? An indicator for this hypothesis may be, that snoRNAs are often located within introns of genes with a function in ribosome biogenesis [Sollner-Webb, 1993]. Moreover, HSC70 interacts with HCF-1 [Wysocka et al., 2003] and SP1 [Gunther et al., 2000], both of which are transcription factors implicated in the regulation of ribosome biogenesis [Popay et al., 2021, Nosrati et al., 2014, Rajput et al., 2016]. As a side note, both of these transcription factors scored within the top 2 % of the "GFP/RiBi down" condition of our screen. Whether the interaction of HSPA8 with SP1 and HCF-1 is functionally important for the regulation of ribosome biogenesis, though, remains to be investigated.

The "GFP/RiBi down" hit list also included several genes involved in (alternative) splicing, such as *Bud31*, *Rbm22* and the two EJC members *Eif4a3* and *Rbm8a*.

Knockout of *Bud31* resulted in a strong downregulation of green fluorescence, whereas red fluorescence was only minorly affected, with a similar picture being observed in the swapped reporter cell line, although the sum of these experiments might point towards a potential stronger regulation of ribosome biogenesis genes than of ribosomal protein genes (see figure 6.12), in case the reporter regulation reflects the level of RiBi and RP gene regulation. In the amoeba *Dictyostelium discoideum*, Bud31 localizes to

the nucleolus [Catalano and O'Day, 2015] and influences 40S maturation [Badertscher et al., 2015]. Whether *Bud31* has a (extra-spliceosomal) role in ribosome biogenesis in mammals, however, remains to be investigated in the future.

A specific downregulator of *Fbl*-driven EGFP-PEST fluorescence, displaying a bimodal pattern upon knockout (see figure 6.12 and 6.13), was *Sfpq*. SFPQ (also called PSF) is a DNA- and RNA-binding protein [Zhang et al., 1993, Patton et al., 1993] involved in splicing and transcription among other processes [Patton et al., 1993, Hirose et al., 2013, Dong et al., 2007]. Moreover, SFPQ was identified as a potential downstream phospho-target of the AKT-mTOR-p70 S6K-signaling cascade among many other proteins with known functions in ribosome biogenesis [Piazzi et al., 2019]. Further evidence for a potential role of SFPQ in ribosome biogenesis can be found in a publication from Roepcke et al., which showed, that SFPQ binds to ribosomal protein gene promoters and influences their transcription in dependence of the position of the bound sequence element relative to the TSS [Roepcke et al., 2011]. A detailed investigation of the mechanisms of SFPQ regulating RPs and potentially also RiBis, remains open. Nevertheless, an involvement of SFPQ as a transcriptional regulator of ribosome biogenesis seems likely, when combining our screening results with published data.

7.4 Subunits shared between all three RNA polymerases as potential anchor point for regulators of ribosome biogenesis

One additional striking observation was the occurrence of several polymerase subunits among the top scoring genes in the "GFP/RiBi down" condition. Five polymerase subunits are shared between all three RNA polymerases: *Polr2e*, *Polr2f*, *Polr2h*, *Polr2l* and *Polr2k* [Barba-Aliaga et al., 2021, Turowski and Boguta, 2021]. Four of them are ranked within the top 30 genes enriched in the GFP/RiBi down condition. Generally, all polymerase subunits scored within the 24th percentile, but were not significantly depleted in the unsorted condition compared to the library (data not shown).

Most likely, the polymerase subunits scored high, because transcription was shut down, but the cells did not undergo apoptosis yet. Instead, polymerase subunit knockout likely resulted in a stronger decrease of green fluorescence than red fluorescence due to different reporter stabilities. Accordingly, cells were sorted into the GFP/RiBi down condition.

Nevertheless, the higher scoring of subunits shared between all three polymerases may also point towards the possibility of a crosstalk between POL I/POL III-dependent transcription and POL II-dependent transcription. Might proteins exist, that can bind to these shared subunits and regulate ribosome biogenesis via a coordinated influence on all three polymerases?

Indeed, the yeast protein Bud27 was shown to interact with all three RNA polymerases via the shared subunits RPB5 and RPB10 [Mirón-García et al., 2013]. It influences the transcription of Pol I-, II- and III-target genes, regulates the processing of rRNA and globally affects RiBi and RP transcript levels [Martínez-Fernández et al., 2020]. The human homologue of yeast Bud27 is URI. It was also shown to bind RPB5. Moreover, it is regulated downstream of mTOR signaling, thereby influencing transcription of genes involved in cell growth [Gstaiger et al., 2003].

Notably, further evidence for an existing general crosstalk between all three polymerases was found in a study, where POL I transcriptional deregulation impacted on the transcriptional output of all other ribosomal components in yeast [Laferté et al., 2006].

Taken together, albeit the occurrence of the polymerase subunits in the GFP/RiBi down condition could simply reflect transcriptionally inactive cells, it might still be, that the shared polymerase subunits may be important anchor points for proteins regulating ribosome biogenesis.

In summary, all of the above mentioned genes indicate, that the screen was indeed able to identify general regulators of ribosome biogenesis. Future investigation is needed to identify how many of these newly identified modulators of ribosome biogenesis are direct transcriptional effectors.

7.5 ALDOA as a new regulator of ribosome biogenesis

After all, the top hit of the "GFP/RiBi down" condition was *Aldoa*, an enzyme involved in glycolysis in the cytoplasm. ALDOA is a glycolytic enzyme that catalyzes the reversible conversion of D-Fructose-1,6-bisphosphate (F1,6-BP) to D-glyceraldehyde-3-phosphate (G3P) and dihydroxyacetone phosphate (DHAP) in the cytoplasm [van Riggelen et al., 2010].

However, since the main objective of the screen was the identification of new transcriptional regulators of RiBis and RPs, localization to the nucleus confers a prerequisite for

a direct role of any hit in the transcriptional regulation of those genes. With regard to the localization of ALDOA, literature suggests, that it can indeed also translocate into the nucleus in dependence of nutrient availability, cell density and other stimuli [Mamczur et al., 2013]. Strikingly, many other glycolytic enzymes were also found in the nucleus (reviewed in [Ronai, 1993, Boukouris et al., 2016, Yu and Li, 2016]) and diverse moonlighting functions (meaning additional, non-enzymatic functions) were identified for many of them [Boukouris et al., 2016]. HK2, for instance, translocates to the nucleus to regulate gene expression upon external stimuli [De La Cera et al., 2002, Ahuatzi et al., 2004, Neary and Pastorino, 2010].

May ALDOA have a similar role and activate RiBi/RP gene expression upon growth signals? As already mentioned above, ALDOA can shuttle between the cytoplasm and the nucleus [Mamczur et al., 2013]. Moreover, there are already first indications for a possible direct involvement of ALDOA in ribosome biogenesis. It binds the POL III complex [Cieśla et al., 2014] and enhances the association of POL III with its target genes [Cieśla et al., 2014]. Moreover, ALDOA can directly bind DNA [Ronai et al., 1992].

All of these insights made ALDOA interesting for further investigations in the direction of a potential new role of ALDOA in the transcriptional regulation of RiBis and RPs. Our FACS validation experiments measuring the change in reporter expression after knockout of candidate genes revealed, that ALDOA was a regulator of both fluorescent reporters and follow up experiments confirmed, that ribosome biogenesis gene sets, e.g. many RiBis and MRPs, were downregulated upon *Aldoa* knockdown in an RNA-Seq experiment. CRPs were not significantly affected, which is in contrast to the regulation suggested by the FACS experiments, although different timings could explain these discrepancies. Additionally, many of the downregulated gene sets upon *Aldoa* depletion are comprised of genes important for proliferating cells, such as genes involved in cell cycle progression, splicing, metabolism, DNA repair and transcription.

These findings raised the question, whether ALDOA might directly bind to these genes, thereby regulating their expression. Within this thesis, no clear answer to this question was found, but possible mechanisms will be discussed.

One hypothesis would be, that ALDOA may bind directly to the promoters and modulate expression of genes by interacting with POL II (see figure 7.1A). Hints for this model come from proteomics studies, which indicated an interaction of ALDOA with POL II [Pineda et al., 2015] and from studies that showed, that ALDOA is able to bind to DNA [Ronai et al., 1992].

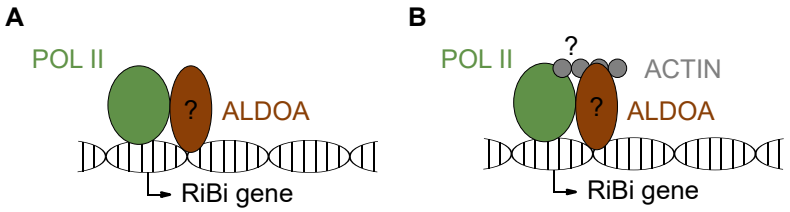

Figure 7.1: Models for possible mechanisms of a direct transcriptional regulation of RiBi (and potentially also RP) gene expression by ALDOA. (A) ALDOA may directly bind DNA and/or may interact with POL II at these sites, possibly modulating POL II activity. The question mark indicates that ALDOA binding at these promoters was not yet investigated and therefore remains purely speculative. (B) Similar to (A), but interaction with and/or regulation of POL II may be modulated by ALDOA together with ACTIN.

Alternatively or additionally, modulation of gene expression by ALDOA could depend on its actin-binding activity. ALDOA was found to bind to F-actin in the cytoplasm [Kusakabe et al., 1997]. Interestingly, both actin [Falahzadeh et al., 2015] and ALDOA [Mamczur et al., 2013] are also present in the nucleus. Moreover, actin exhibits an important function in POL I-, POL II-, and POL III-mediated transcription [Philimonenko et al., 2004, Hu et al., 2004, Hofmann et al., 2004, Percipalle, 2012] and ALDOA was shown to modulate POL III-mediated transcription [Cieśla et al., 2014]. But could it also modulate POL II-mediated transcription? Connecting these observations, the hypothesis would be, that ALDOA may bind RiBi and potentially also RP genes and modulates their expression together with actin (see figure 7.1B). This hypothesis may also be strengthened by the finding, that ALDOA's nuclear localization correlates with cell proliferation [Mamczur et al., 2013] and ribosome biogenesis is an important prerequisite for proliferation. Along this thought, an inhibitor of ALDOA and of the interaction of ALDOA with actin, UM0112176, prevents ALDOA's nuclear localization and inhibits cell proliferation [Gizak et al., 2019]. All these data make it tempting to speculate, that ALDOA might bind actin not only in the cytoplasm, but potentially also in the nucleus, and that this may pose a mechanism of direct transcriptional regulation of ribosome biogenesis genes by ALDOA.

However, further investigation is needed to address whether ALDOA directly regulates ribosome biogenesis by binding to chromatin, thereby influencing transcriptional output. ChIP or ChIP-Seq experiments could be performed, to investigate whether ALDOA binds to RiBi and potentially (some) RP genes. Moreover, with an *AID-Aldoa* cell line, 4sU-Seq could be performed to identify genes that are acutely and directly regulated by ALDOA.

Nevertheless, ALDOA could also indirectly regulate RiBi genes on a transcriptional level with some of the possible scenarios being discussed here. It was shown, that ALDOA

is a component of the vacuolar H^+-ATPases (V-ATPases) [Lu et al., 2001], which are proton pumps involved in acidification of different intracellular compartments [Forgac, 2007]. ALDOA is important for the assembly and activity of these V-ATPases [Lu et al., 2001, 2004, 2007]. ALDOA depletion disassembles V-ATPases, leading to an activation of AMPK [Zhang et al., 2017], which in turn may inactivate mTORC1 [Inoki et al., 2006, Gwinn et al., 2008], a key regulator or growth and proliferation and an inducer of anabolic pathways [Laplante and Sabatini, 2012]. The gene sets downregulated upon *Aldoa*-KD (figure 6.17) would therefore be at least partially in line with an effect of *Aldoa*-KD on mTORC1 signaling.

Along this line, mTORC1 promotes nucleotide biosynthesis [Robitaille et al., 2013, Ben-Sahra et al., 2013, 2016] and a reduction of nucleotide biosynthesis due to mTORC1 inactivation would strongly impact ribosome biogenesis, one of the most nucleotide- and energy-demanding processes of a cell [Mayer and Grummt, 2006].

On the other hand, rapamycin, an inhibitor of mTORC1 activity [Schmelzle and Hall, 2000], was shown to lead to the transcriptional repression of CRPs, but not MRPs in yeast [Cardenas et al., 1999]. In contrast, our results reveal, that *Aldoa* KD decreases primarily RiBi genes and to a lesser extent MRPs, but not CRPs, at least at the time point used for the analysis.

To summarize, the observed downregulation of ribosome biogenesis processes may not only be driven by potential effects of *Aldoa* depletion on the mTORC1 pathway or other indirect effects. There is also the potential of a direct involvement of ALDOA in the transcriptional regulation of ribosome biogenesis-related genes.

7.6 RBM8A as a direct transcriptional regulator of (cytosolic) ribosomal protein genes

Besides *Aldoa*, *Rbm8a* was another hit obtained from the condition sorted for high *Rpl18*-driven red fluorescence and low *Fbl*-driven green fluorescence. It is part of the EJC, that is placed about 24 bp upstream of exon-exon junctions on mRNAs after splicing and influences several fates of mRNAs downstream of transcription, such as splicing, mRNA localization, translation efficiency and NMD [Hir et al., 2015]. The EJC is removed from mRNAs by the first translating ribosome [Hir et al., 2015]. Strikingly, not only *Rbm8a* scored as a significant hit; *Eif4a3*, another core member of the EJC also scored significantly in our screen.

We got interested in studying the EJC, because of the following observation: knockdown (KD) of the EJC leads to dysregulated splicing of mRNAs [Akhtar et al., 2019, Wang et al., 2014]. Deregulated splicing may strongly influence gene expression. However, primarily the expression of genes containing larger introns is influenced by KD of EJC components [Akhtar et al., 2019], but interestingly our reporter constructs did not contain introns at all. Thus, deregulated reporter expression due to missplicing should therefore not lead to the observed downregulation of the reporters.

Could instead transcription be directly affected by RBM8A loss? It is known, that the EJC binds to promoters [Roy Choudhury et al., 2016, Akhtar et al., 2019] and associates with POL II [Chuang et al., 2019, Akhtar et al., 2019]. Binding to chromatin and POL II is mediated by RNA [Akhtar et al., 2019]. However, chromatin-binding also occurs at least partially independent of RNA-binding [Roy Choudhury et al., 2016].

Although a direct role of RBM8A in transcription is not well studied yet and basically consists of isolated reports, one mechanism of how the EJC regulates transcription, could already be shown: the interaction of EJC components with POL II influences POL II promoter-proximal pausing [Akhtar et al., 2019], with a KD of the EJC leading to Pol II pause-release, premature elongation and dysregulated splicing of mRNAs [Akhtar et al., 2019, Wang et al., 2014]. However, a clear connection between these data and our results can not readily be made.

To further investigate a possible role of RBM8A in transcription and its regulation of RiBi/RP genes, we developed a system that enabled us to acutely deplete RBM8A within a few hours and combined this tool with nascent RNA sequencing. We could show, that long-term RBM8A depletion leads to apoptosis, in line with literature [Ishigaki et al., 2016]. Acute RBM8A depletion mainly reduced the nascent transcript levels of cytosolic ribosomal protein genes. Hints towards a role of RBM8A in the regulation of RPs can also be found in the literature. Lin and colleagues found out, that ribosomal and other proliferation-associated genes are functionally associated with RBM8A in hepatocellular carcinoma [Lin et al., 2019]. Moreover, mice haploinsufficient for individual components of the EJC show dysregulated transcription of ribosomal proteins in the developing brain during embryogenesis [Mao et al., 2016] and *magoh* mutant Zebrafish embryos show a downregulation of ribosomal proteins [Gangras et al., 2020], suggesting, that the regulation of ribosomal components is also occurring upon long-term RBM8A depletion, in addition to the effect we have seen in our 4sU-Seq experiment.

A direct regulation of CRPs might be explainable by an acute drop in RBM8A binding to the respective promoters, but other housekeeping genes, that were not significantly regulated upon acute RBM8A depletion in our 4sU-Seq experiment, also showed a similar reduction in V5-tagged RBM8A levels. We were wondering, whether instead of RBM8A levels at the respective promoters, POL II levels (total, elongating or initiating) could be altered upon RBM8A depletion, which may indicate different transcription rates. However, although we could show, that RBM8A interacts with POL II, consistent with literature [Chuang et al., 2019, Akhtar et al., 2019], this interaction did not seem to influence POL II levels at the CRP promoters or any other promoter tested.

Within this thesis we could therefore not find a mechanism explaining the observed downregulation of CRPs upon acute RBM8A depletion, but some possible explanations are discussed. Several screens have been performed during the last years, that aimed to identify new regulators of ribosome biogenesis [Wild et al., 2010, **?**, Tafforeau et al., 2013, Badertscher et al., 2015]. In three of these screens, *Eif4a3*, another component of the EJC, was one of the hits identified to be important for ribosome biogenesis [Wild et al., 2010, Tafforeau et al., 2013, Badertscher et al., 2015]. Moreover, these screens identified several proteins known to be involved in the DNA damage response (DDR) as potential new regulators of ribosome biogenesis. More and more evidence for a crosstalk between ribosome biogenesis and the DDR pathway has been revealed over the last years, as reviewed in [Ogawa and Baserga, 2017]. Along this line, SP1, a well-known transcription factor involved in ribosome biogenesis [Nosrati et al., 2014], is recruited to DNA damage foci and needed for DNA damage repair [Beishline et al., 2012]. Interestingly, transcription and DDR are strongly intertwined processes, with transcription increasing the likelihood of DNA damage [Marnef et al., 2017], and efficient DDR depending on transcriptional activity [Fong et al., 2013]. Active genes tend to accumulate more DNA damage in their promoters [Marnef et al., 2017]. Since RPs are strongly transcribed genes, it seems likely, that DDR factors are present at the respective promoters. RBM8A also plays a role in DDR signaling and interacts with several well-characterized DDR proteins, such as KU70, KU80 or TRIM28 [Chuang et al., 2019]. Could there be a link between the transcriptional regulation of highly active ribosomal protein genes by RBM8A to DNA damage in their promoters? Could RBM8A be especially important for DNA damage repair at the respective promoters and might unrepaired DNA damage lead to reduced transcription of RP genes?

All in all, there are several indications, that RBM8A, potentially within its role as a core EJC component, is involved in the regulation of ribosome biogenesis, but how exactly RBM8A directly influences the transcription of ribosomal protein genes remains un-

known. The broad chromatin-binding affinity of RBM8A, combined with the missing effect on POL II CTD phosphorylation upon acute RBM8A depletion, raises the alternative hypothesis of a potential role of RBM8A in regulating gene expression via DDR signaling, which might be particularly important for genes that are as strongly expressed as ribosomal components.

7.7 Response to proteotoxic stress as an example for the benefits of specific transcriptional regulators of RiBis and RPs

In summary, this thesis identified several proteins involved in ribosome biogenesis. However, it is not clear, whether differential transcriptional regulators of RiBis and RPs could really be deciphered within this thesis and requires further investigation.

Nevertheless, there are strong indications that, and reasons why, cells may have developed differential regulators of RiBi and RP genes. The occurrence of at least partially different transcription factor binding sites in the promoters of RiBi (E-boxes) [Brown et al., 2008] and RP (SP1, GABP, YY1) [Perry, 2005] genes suggests, that these two sets of genes may be differentially regulated at times. Under certain circumstances it may be beneficial for cells to counterbalance an over- or underproduction of specific components of ribosome biosynthesis, for example upon proteotoxic stress. A proliferating cell produces large amounts of ribosomal components [Mayer and Grummt, 2006]. However, protein biosynthesis is a very error-prone process. In fact, about one third of freshly generated proteins are defective ribosomal products (DRiPs), that are degraded by the proteasome immediately after their synthesis [Schubert et al., 2000]. An increased demand of protein synthesis, for example during growth or proliferation, may thus overload the proteasome with DRiPs, leading to an aggregation of defective proteins and the subsequent induction of proteotoxic stress [Cenci and Sitia, 2007]. Insoluble aggregates of ribosomal proteins can feedback to ribosomal protein gene transcription via sequestration of the RP-specific transcription factor Ifh1 in yeast [Albert et al., 2019].

Although such a mechanism was not yet described in mammals, it is well imaginable, that similar feedback mechanisms exist. Using such mechanisms, cells would profit from a repertoire of RiBi-/RP-specific transcription factors, which are regulated differently upon varying kinds of ribosome imbalance-inducing stresses. Like this, expres-

sion of RPs or RiBis could be fine-tuned in response to an over- or undersupply of their gene products. At the same time, global regulators of ribosome biogenesis, like MYC, are needed to generally and rapidly induce or restrict ribosome production.

7.8 Outlook

Although many putative regulators of ribosome biogenesis could be identified in our screen, several problems occurred, which masked or confounded the results, so that many potential hits could probably not be identified. To circumvent some of these problems, such as differential reporter stability, missing chromatin-environment or sub-optimal promoter length, a second screen was performed which should theoretically improve or abolish the aforementioned problems. However, no significant hit could be found in this screen. One possible explanation might be, that four sgRNAs per gene is more prone to outliers than the usage of six sgRNAs, resulting in less confident candidate genes. Nevertheless, the cell line, that contains mSCARLET-I-d2 knocked in into the endogenous *FBL* locus, as well as the cell line with the knock-in into the endogenous *RPL36* locus, could be used for a subscreen of hits from the first screen to directly see, whether a gene is needed for RiBi or RP expression only.

Moreover, a subscreen with a transcriptional read-out, e.g. an siRNA screen in NIH/3T3 cells with subsequent qRT-PCRs on RiBi and RP genes, could be performed for the most promising hits to further narrow down the set of genes, so that high-confidence transcriptional regulators of these processes can be obtained. Using a non-reporter cell line for this validation experiment would harbor the benefit of testing the hits in an independent cell line to exclude clonal effects. Such an experiment would also shed light on the differential regulation of CRPs and MRPs, that we, for example, observed upon *Aldoa* or *Rbm8a* depletion. Are these two gene sets generally regulated differently? To my knowledge, differential regulators of MRPs and CRPs have not yet been described.

All in all, this thesis identified new regulators of ribosome biogenesis, but more research needs to be done on the obtained hits to clarify whether they regulate RiBi and RP genes via direct or indirect mechanisms.

Bibliography

K. J. Abraham, N. Khosraviani, J. N. Y. Chan, A. Gorthi, A. Samman, D. Y. Zhao, M. Wang, M. Bokros, E. Vidya, L. A. Ostrowski, R. Oshidari, V. Pietrobon, P. S. Patel, A. Algouneh, R. Singhania, Y. Liu, V. T. Yerlici, D. D. D. Carvalho, M. Ohh, B. C. Dickson, R. Hakem, J. F. Greenblatt, S. Lee, A. J. R. Bishop, and K. Mekhail. Nucleolar RNA polymerase II drives ribosome biogenesis. *Nature 2020 585:7824*, 585 (7824):298–302, jul 2020. ISSN 1476-4687. doi: 10.1038/s41586-020-2497-0. URL https://www.nature.com/articles/s41586-020-2497-0.

M. D. Abràmoff. Image Processing with ImageJ.

D. Ahuatzi, P. Herrero, T. de la Cera, and F. Moreno. The Glucose-regulated Nuclear Localization of Hexokinase 2 in Saccharomyces cerevisiae Is Mig1-dependent *. *Journal of Biological Chemistry*, 279(14):14440–14446, apr 2004. ISSN 0021-9258. doi: 10.1074/JBC.M313431200. URL http://www.jbc.org/article/S0021925819641207/fulltexthttp://www.jbc.org/article/S0021925819641207/abstracthttps://www.jbc.org/article/S0021-9258(19)64120-7/abstract.

J. Akhtar, N. Kreim, F. Marini, G. Mohana, D. Brüne, H. Binder, and J.-Y. Roignant. Promoter-proximal pausing mediated by the exon junction complex regulates splicing. *Nature Communications*, 10(1), dec 2019. doi: 10.1038/S41467-019-08381-0. URL /pmc/articles/PMC6355915//pmc/articles/PMC6355915/?report=abstracthttps://www.ncbi.nlm.nih.gov/pmc/articles/PMC6355915/.

B. Albert, I. C. Kos-Braun, A. K. Henras, C. Dez, M. P. Rueda, X. Zhang, O. Gadal, M. Kos, and D. Shore. A ribosome assembly stress response regulates transcription to maintain proteome homeostasis. *eLife*, 8, may 2019. doi: 10.7554/ELIFE.45002.

A. Amsterdam, K. C. Sadler, K. Lai, S. Farrington, R. T. Bronson, J. A. Lees, and N. Hopkins. Many Ribosomal Protein Genes Are Cancer Genes in Zebrafish. *PLoS Biology*, 2(5), 2004. doi: 10.1371/JOURNAL.PBIO.0020139. URL /pmc/articles/PMC406397//pmc/articles/PMC406397/?report=abstracthttps://www.ncbi.nlm.nih.gov/pmc/articles/PMC406397/.

A. Arabi, S. Wu, K. Ridderstr®ale, H. Bierhoff, C. Shiue, K. Fatyol, S. Fahlén, P. Hydbring, O. Söderberg, I. Grummt, L.-G. Larsson, and A. P. H. Wright. c-Myc associates

with ribosomal DNA and activates RNA polymerase I transcription. *Nature Cell Biology 2005 7:3*, 7(3):303–310, feb 2005. ISSN 1476-4679. doi: 10.1038/ncb1225. URL https://www.nature.com/articles/ncb1225.

J. Armistead and B. Triggs-Raine. Diverse diseases from a ubiquitous process: The ribosomopathy paradox. *FEBS Letters*, 588(9):1491–1500, may 2014. ISSN 1873-3468. doi: 10.1016/J.FEBSLET.2014.03.024. URL https://onlinelibrary.wiley.com/doi/full/10.1016/j.febslet.2014.03.024https://onlinelibrary.wiley.com/doi/abs/10.1016/j.febslet.2014.03.024https://febs.onlinelibrary.wiley.com/doi/10.1016/j.febslet.2014.03.024.

J. A. J. Arpino, P. J. Rizkallah, and D. D. Jones. Crystal Structure of Enhanced Green Fluorescent Protein to 1.35 ®A Resolution Reveals Alternative Conformations for Glu222. *PLOS ONE*, 7(10):e47132, oct 2012. ISSN 1932-6203. doi: 10.1371/JOURNAL.PONE.0047132. URL https://journals.plos.org/plosone/article?id=10.1371/journal.pone.0047132.

J. D. Arroyo, A. A. Jourdain, S. E. Calvo, C. A. Ballarano, J. G. Doench, D. E. Root, and V. K. Mootha. A Genome-wide CRISPR Death Screen Identifies Genes Essential for Oxidative Phosphorylation. *Cell metabolism*, 24(6):875, dec 2016. ISSN 19327420. doi: 10.1016/J.CMET.2016.08.017. URL /pmc/articles/PMC5474757//pmc/articles/PMC5474757/?report=abstracthttps://www.ncbi.nlm.nih.gov/pmc/articles/PMC5474757/.

L. Badertscher, T. Wild, C. Montellese, L. T. Alexander, L. Bammert, M. Sarazova, M. Stebler, G. Csucs, T. U. Mayer, N. Zamboni, I. Zemp, P. Horvath, and U. Kutay. Genome-wide RNAi Screening Identifies Protein Modules Required for 40S Subunit Synthesis in Human Cells. *Cell Reports*, 13(12):2879–2891, dec 2015. ISSN 2211-1247. doi: 10.1016/J.CELREP.2015.11.061.

M. Barba-Aliaga, P. Alepuz, and J. E. Pérez-Ortín. Eukaryotic RNA Polymerases: The Many Ways to Transcribe a Gene. *Frontiers in Molecular Biosciences*, 0:207, apr 2021. ISSN 2296-889X. doi: 10.3389/FMOLB.2021.663209.

M. Barna, A. Pusic, O. Zollo, M. Costa, N. Kondrashov, E. Rego, P. H. Rao, and D. Ruggero. Suppression of Myc oncogenic activity by ribosomal protein haploinsufficiency. *Nature*, 456(7224):971, dec 2008. doi: 10.1038/NATURE07449. URL /pmc/articles/PMC2880952//pmc/articles/PMC2880952/?report=abstracthttps://www.ncbi.nlm.nih.gov/pmc/articles/PMC2880952/.

D. G. Bear, N. Fomproix, T. Soop, B. Björkroth, S. Masich, and B. Daneholt. Nuclear poly(A)-binding protein PABPN1 is associated with RNA polymerase II during transcription and accompanies the released transcript to the nuclear pore. *Experimental Cell Research*, 286(2):332–344, jun 2003. ISSN 0014-4827. doi: 10.1016/S0014-4827(03)00123-X.

Y. B. Beaulieu, C. L. Kleinman, A.-M. Landry-Voyer, J. Majewski, and F. Bachand. Polyadenylation-Dependent Control of Long Noncoding RNA Expression by the Poly(A)-Binding Protein Nuclear 1. *PLOS Genetics*, 8(11):e1003078, nov 2012. ISSN 1553-7404. doi: 10.1371/JOURNAL.PGEN.1003078. URL https://journals.plos.org/plosgenetics/article?id=10.1371/journal.pgen.1003078.

K. Beishline, C. M. Kelly, B. A. Olofsson, S. Koduri, J. Emrich, R. A. Greenberg, and J. Azizkhan-Clifford. Sp1 Facilitates DNA Double-Strand Break Repair through a Nontranscriptional Mechanism. *Molecular and Cellular Biology*, 32(18):3790, sep 2012. doi: 10.1128/MCB.00049-12. URL /pmc/articles/PMC3430196//pmc/articles/PMC3430196/?report=abstracthttps://www.ncbi.nlm.nih.gov/pmc/articles/PMC3430196/.

I. Ben-Sahra, J. J. Howell, J. M. Asara, and B. D. Manning. Stimulation of de novo pyrimidine synthesis by growth signaling through mTOR and S6K1. *Science*, 339 (6125):1323–1328, mar 2013. doi: 10.1126/SCIENCE.1228792.

I. Ben-Sahra, G. Hoxhaj, S. J. H. Ricoult, J. M. Asara, and B. D. Manning. mTORC1 induces purine synthesis through control of the mitochondrial tetrahydrofolate cycle. *Science*, 351(6274):728–733, feb 2016. doi: 10.1126/SCIENCE.AAD0489. URL https://www.science.org/doi/abs/10.1126/science.aad0489.

T. K. Blackwell, L. Kretzner, E. M. Blackwood, R. N. Eisenman, and H. Weintraub. Sequence-Specific DNA Binding by the c-Myc Protein. *Science*, 250(494):1149–1151, nov 1990. doi: 10.1126/SCIENCE.2251503. URL https://www.science.org/doi/abs/10.1126/science.2251503.

D. F. Bogenhagen, S. Sakonju, and D. D. Brown. A control region in the center of the 5S RNA gene directs specific initiation of transcription: II. The 3' border of the region. *Cell*, 19(1):27–35, jan 1980. ISSN 0092-8674. doi: 10.1016/0092-8674(80)90385-2.

A. E. Boukouris, S. D. Zervopoulos, and E. D. Michelakis. Metabolic Enzymes Moonlighting in the Nucleus: Metabolic Regulation of Gene Transcription. *Trends in Biochemical Sciences*, 41(8):712–730, aug 2016. ISSN 0968-0004. doi: 10.1016/J.TIBS.2016.05.013. URL http://www.cell.

com/article/S0968000416300561/fulltexthttp://www.cell.com/article/S0968000416300561/abstracthttps://www.cell.com/trends/biochemical-sciences/abstract/S0968-0004(16)30056-1.

T. Bratkovič, J. Božič, and B. Rogelj. Functional diversity of small nucleolar RNAs. *Nucleic Acids Research*, 48(4):1627–1651, feb 2020. ISSN 0305-1048. doi: 10.1093/NAR/GKZ1140. URL https://academic.oup.com/nar/article/48/4/1627/5673630.

S. M. Bresson and N. K. Conrad. The Human Nuclear Poly(A)-Binding Protein Promotes RNA Hyperadenylation and Decay. *PLOS Genetics*, 9(10):e1003893, oct 2013. ISSN 1553-7404. doi: 10.1371/JOURNAL.PGEN.1003893. URL https://journals.plos.org/plosgenetics/article?id=10.1371/journal.pgen.1003893.

S. J. Brown, M. D. Cole, and A. J. Erives. Evolution of the holozoan ribosome biogenesis regulon. *BMC Genomics 2008 9:1*, 9(1):1–13, sep 2008. ISSN 1471-2164. doi: 10.1186/1471-2164-9-442. URL https://bmcgenomics.biomedcentral.com/articles/10.1186/1471-2164-9-442.

S. Bursac, M. C. Brdovcak, G. Donati, and S. Volarevic. Activation of the tumor suppressor p53 upon impairment of ribosome biogenesis. *Biochimica et Biophysica Acta (BBA) - Molecular Basis of Disease*, 1842(6):817–830, jun 2014. ISSN 0925-4439. doi: 10.1016/J.BBADIS.2013.08.014.

K. J. Campbell and R. J. White. MYC Regulation of Cell Growth through Control of Transcription by RNA Polymerases I and III. *Cold Spring Harbor Perspectives in Medicine*, 4(5), jan 2014. doi: 10.1101/CSHPERSPECT.A018408. URL /pmc/articles/PMC3996375//pmc/articles/PMC3996375/?report=abstracthttps://www.ncbi.nlm.nih.gov/pmc/articles/PMC3996375/.

D. Canella, V. Praz, J. H. Reina, P. Cousin, and N. Hernandez. Defining the RNA polymerase III transcriptome: Genome-wide localization of the RNA polymerase III transcription machinery in human cells. *Genome Research*, 20(6):710, jun 2010. doi: 10.1101/GR.101337.109. URL /pmc/articles/PMC2877568//pmc/articles/PMC2877568/?report=abstracthttps://www.ncbi.nlm.nih.gov/pmc/articles/PMC2877568/.

M. E. Cardenas, N. S. Cutler, M. C. Lorenz, C. J. D. Como, and J. Heitman. The TOR signaling cascade regulates gene expression in response to nutrients. *Genes & Development*, 13(24):3271, dec 1999. doi: 10.1101/GAD.13.24.3271.

URL /pmc/articles/PMC317202//pmc/articles/PMC317202/?report=abstracthttps://www.ncbi.nlm.nih.gov/pmc/articles/PMC317202/.

A. Catalano and D. H. O'Day. Evidence for nucleolar subcompartments in Dictyostelium. *Biochemical and Biophysical Research Communications*, 456(4):901–907, jan 2015. ISSN 0006-291X. doi: 10.1016/J.BBRC.2014.12.050.

S. Cenci and R. Sitia. Managing and exploiting stress in the antibody factory. *FEBS Letters*, 581(19):3652–3657, jul 2007. ISSN 1873-3468. doi: 10.1016/J.FEBSLET.2007.04.031. URL https://onlinelibrary.wiley.com/doi/full/10.1016/j.febslet.2007.04.031https://onlinelibrary.wiley.com/doi/abs/10.1016/j.febslet.2007.04.031https://febs.onlinelibrary.wiley.com/doi/10.1016/j.febslet.2007.04.031.

C. Chauvin, V. Koka, A. Nouschi, V. Mieulet, C. Hoareau-Aveilla, A. Dreazen, N. Cagnard, W. Carpentier, T. Kiss, O. Meyuhas, and M. Pende. Ribosomal protein S6 kinase activity controls the ribosome biogenesis transcriptional program. *Oncogene*, 33(4):474–483, 2014. ISSN 09509232. doi: 10.1038/onc.2012.606.

T.-W. Chuang, C.-C. Lu, C.-H. Su, P.-Y. Wu, S. Easwvaran, C.-C. Lee, H.-C. Kuo, K.-Y. Hung, K.-M. Lee, C.-Y. Tsai, and W.-Y. Tarn. The RNA Processing Factor Y14 Participates in DNA Damage Response and Repair. *iScience*, 13: 402–415, mar 2019. ISSN 2589-0042. doi: 10.1016/J.ISCI.2019.03.005. URL http://www.cell.com/article/S2589004219300719/fulltexthttp://www.cell.com/article/S2589004219300719/abstracthttps://www.cell.com/iscience/abstract/S2589-0042(19)30071-9.

M. Cieśla, J. Mierzejewska, M. Adamczyk, A. K. Ö. Farrants, and M. Boguta. Fructose bisphosphate aldolase is involved in the control of RNA polymerase III-directed transcription. *Biochimica et Biophysica Acta (BBA) - Molecular Cell Research*, 1843(6): 1103–1110, jun 2014. ISSN 0167-4889. doi: 10.1016/J.BBAMCR.2014.02.007.

S. Cory and J. M. Adams. A very large repeating unit of mouse DNA containing the 18S, 28S and 5.8S rRNA genes. *Cell*, 11(4):795–805, aug 1977. ISSN 0092-8674. doi: 10.1016/0092-8674(77)90292-6.

M.-S. Dai, R. Sears, and H. Lu. Feedback Regulation of c-Myc by Ribosomal Protein L11. *http://dx.doi.org/10.4161/cc.6.22.4895*, 6(22):2735–2741, nov 2007. doi: 10.4161/CC.6.22.4895. URL https://www.tandfonline.com/doi/abs/10.4161/cc.6.22.4895.

N. Danilova and H. T. Gazda. Ribosomopathies: how a common root can cause a tree of pathologies. *Disease Models & Mechanisms*, 8(9):1013–1026, sep 2015. ISSN 1754-8403. doi: 10.1242/DMM.020529.

Z. Darzynkiewicz, S. Bruno, G. D. Bino, W. Gorczyca, M. A. Hotz, P. Lassota, and F. Traganos. Features of apoptotic cells measured by flow cytometry. *Cytometry*, 13(8):795–808, jan 1992. ISSN 1097-0320. doi: 10.1002/CYTO.990130802. URL https://onlinelibrary.wiley.com/doi/full/10.1002/cyto.990130802https://onlinelibrary.wiley.com/doi/abs/10.1002/cyto.990130802https://onlinelibrary.wiley.com/doi/10.1002/cyto.990130802.

T. De La Cera, P. Herrero, F. Moreno-Herrero, R. S. Chaves, and F. Moreno. Mediator Factor Med8p Interacts with the Hexokinase 2: Implication in the Glucose Signalling Pathway of Saccharomyces cerevisiae. *Journal of Molecular Biology*, 319(3):703–714, jun 2002. ISSN 0022-2836. doi: 10.1016/S0022-2836(02)00377-7.

N. Dharmasiri, S. Dharmasiri, and M. Estelle. The F-box protein TIR1 is an auxin receptor. *Nature 2005 435:7041*, 435(7041):441–445, may 2005. ISSN 1476-4687. doi: 10.1038/nature03543. URL https://www.nature.com/articles/nature03543.

C. Dive, C. D. Gregory, D. J. Phipps, D. L. Evans, A. E. Milner, and A. H. Wyllie. Analysis and discrimination of necrosis and apoptosis (programmed cell death) by multiparameter flow cytometry. *Biochimica et Biophysica Acta (BBA) - Molecular Cell Research*, 1133(3):275–285, feb 1992. ISSN 0167-4889. doi: 10.1016/0167-4889(92)90048-G.

X. Dong, J. Sweet, J. R. G. Challis, T. Brown, and S. J. Lye. Transcriptional Activity of Androgen Receptor Is Modulated by Two RNA Splicing Factors, PSF and p54nrb. *Molecular and Cellular Biology*, 27(13):4863–4875, jul 2007. doi: 10.1128/MCB.02144-06. URL https://journals.asm.org/journal/mcb.

D. A. Dunbar and S. J. Baserga. The U14 snoRNA is required for 2'-O-methylation of the pre-18S rRNA in Xenopus oocytes. *RNA*, 4(2):195, feb 1998. URL /pmc/articles/PMC1369608/?report=abstracthttps://www.ncbi.nlm.nih.gov/pmc/articles/PMC1369608/.

J. C. Ellis, D. D. Brown, and J. W. Brown. The small nucleolar ribonucleoprotein (snoRNP) database. *RNA*, 16(4):664, apr 2010. doi: 10.1261/RNA.1871310. URL /pmc/articles/PMC2844615//pmc/articles/PMC2844615/?report=abstracthttps://www.ncbi.nlm.nih.gov/pmc/articles/PMC2844615/.

A. G. Evdokimov, M. E. Pokross, N. S. Egorov, A. G. Zaraisky, I. V. Yampolsky, E. M. Merzlyak, A. N. Shkoporov, I. Sander, K. A. Lukyanov, and D. M. Chudakov. Structural basis for the fast maturation of Arthropoda green fluorescent protein. *EMBO reports*, 7(10):1006–1012, aug 2006. ISSN 1469-3178. doi: 10.1038/SJ.EMBOR.7400787. URL https://www.embopress.org/doi/full/10.1038/sj.embor.7400787https://www.embopress.org/doi/abs/10.1038/sj.embor.7400787.

K. Falahzadeh, A. Banaei-Esfahani, and M. Shahhoseini. The Potential Roles of Actin in The Nucleus. *Cell Journal (Yakhteh)*, 17(1):7, mar 2015. doi: 10.22074/CELLJ.2015.507. URL /pmc/articles/PMC4393673//pmc/articles/PMC4393673/?report=abstracthttps://www.ncbi.nlm.nih.gov/pmc/articles/PMC4393673/.

K. I. Farley-Barnes, K. L. McCann, L. M. Ogawa, J. Merkel, Y. V. Surovtseva, and S. J. Baserga. Diverse Regulators of Human Ribosome Biogenesis Discovered by Changes in Nucleolar Number. *Cell Reports*, 22(7):1923–1934, feb 2018. ISSN 2211-1247. doi: 10.1016/J.CELREP.2018.01.056. URL http://www.cell.com/article/S2211124718301050/fulltexthttp://www.cell.com/article/S2211124718301050/abstracthttps://www.cell.com/cell-reports/abstract/S2211-1247(18)30105-0.

A. M. Fedoriw, J. Starmer, D. Yee, and T. Magnuson. Nucleolar Association and Transcriptional Inhibition through 5S rDNA in Mammals. *PLoS Genetics*, 8(1):1002468, jan 2012. doi: 10.1371/JOURNAL.PGEN.1002468. URL /pmc/articles/PMC3261910//pmc/articles/PMC3261910/?report=abstracthttps://www.ncbi.nlm.nih.gov/pmc/articles/PMC3261910/.

D. W. Felsher and J. Bishop. Reversible Tumorigenesis by MYC in Hematopoietic Lineages. *Molecular Cell*, 4(2):199–207, aug 1999. ISSN 1097-2765. doi: 10.1016/S1097-2765(00)80367-6. URL http://www.cell.com/article/S1097276500803676/fulltexthttp://www.cell.com/article/S1097276500803676/abstracthttps://www.cell.com/molecular-cell/abstract/S1097-2765(00)80367-6.

A. Finka, S. K. Sharma, and P. Goloubinoff. Multi-layered molecular mechanisms of polypeptide holding, unfolding and disaggregation by HSP70/HSP110 chaperones. *Frontiers in Molecular Biosciences*, 0(JUN):29, jun 2015. ISSN 2296-889X. doi: 10.3389/FMOLB.2015.00029.

Y. W. Fong, C. Cattoglio, and R. Tjian. The Intertwined Roles of Transcription and Repair Proteins. *Molecular cell*, 52(3):291, nov 2013. doi: 10.1016/J.MOLCEL.2013.10.018. URL /pmc/articles/PMC3919531//pmc/articles/PMC3919531/?report=abstracthttps://www.ncbi.nlm.nih.gov/pmc/articles/PMC3919531/.

M. Forgac. Vacuolar ATPases: rotary proton pumps in physiology and pathophysiology. *Nature Reviews Molecular Cell Biology 2007 8:11*, 8(11):917–929, nov 2007. ISSN 1471-0080. doi: 10.1038/nrm2272. URL https://www.nature.com/articles/nrm2272.

D. Forget, A.-A. Lacombe, P. Cloutier, R. Al-Khoury, A. Bouchard, M. Lavallée-Adam, D. Faubert, C. Jeronimo, M. Blanchette, and B. Coulombe. The Protein Interaction Network of the Human Transcription Machinery Reveals a Role for the Conserved GTPase RPAP4/GPN1 and Microtubule Assembly in Nuclear Import and Biogenesis of RNA Polymerase II. *Molecular & Cellular Proteomics : MCP*, 9(12):2827, 2010. doi: 10.1074/MCP.M110.003616. URL /pmc/articles/PMC3002788//pmc/articles/PMC3002788/?report=abstracthttps://www.ncbi.nlm.nih.gov/pmc/articles/PMC3002788/.

N. H. Freese, D. C. Norris, and A. E. Loraine. Integrated genome browser: visual analytics platform for genomics. *Bioinformatics (Oxford, England)*, 32(14):2089–2095, jul 2016. ISSN 1367-4811. doi: 10.1093/BIOINFORMATICS/BTW069. URL https://pubmed.ncbi.nlm.nih.gov/27153568/.

P. Gallant and D. Steiger. Myc's secret life without Max. *http://dx.doi.org/10.4161/cc.8.23.10088*, 8(23):3848–3853, dec 2009. ISSN 15514005. doi: 10.4161/CC.8.23.10088. URL https://www.tandfonline.com/doi/abs/10.4161/cc.8.23.10088.

P. Gangras, T. L. Gallagher, M. A. Parthun, Z. Yi, R. D. Patton, K. T. Tietz, N. C. Deans, R. Bundschuh, S. L. Amacher, and G. Singh. Zebrafish rbm8a and magoh mutants reveal EJC developmental functions and new 3'UTR intron-containing NMD targets. *PLOS Genetics*, 16(6):e1008830, jun 2020. ISSN 1553-7404. doi: 10.1371/JOURNAL.PGEN.1008830. URL https://journals.plos.org/plosgenetics/article?id=10.1371/journal.pgen.1008830.

N. H. Gehring, J. B. Kunz, G. Neu-Yilik, S. Breit, M. H. Viegas, M. W. Hentze, and A. E. Kulozik. Exon-Junction Complex Components Specify Distinct Routes of Nonsense-Mediated mRNA Decay with Differential Cofactor Requirements. *Molecular Cell*, 20 (1):65–75, oct 2005. ISSN 1097-2765. doi: 10.1016/J.MOLCEL.2005.08.012.

N. R. Genuth and M. Barna. Heterogeneity and specialized functions of translation machinery: from genes to organisms. *Nature Reviews Genetics 2018 19:7*, 19(7): 431–452, may 2018. ISSN 1471-0064. doi: 10.1038/s41576-018-0008-z. URL https://www.nature.com/articles/s41576-018-0008-z.

A. Gilles, L. Frechin, K. Natchiar, G. Biondani, O. von Loeffelholz, S. Holvec, J.-L. Malaval, J.-Y. Winum, B. P. Klaholz, and J.-F. Peyron. Targeting the Human 80S Ribosome in Cancer: From Structure to Function and Drug Design for Innovative Adjuvant Therapeutic Strategies. *Cells 2020, Vol. 9, Page 629*, 9(3):629, mar 2020. doi: 10.3390/CELLS9030629. URL https://www.mdpi.com/2073-4409/9/3/629/htmhttps://www.mdpi.com/2073-4409/9/3/629.

A. Gizak, J. Wiśniewski, P. Heron, P. Mamczur, J. Sygusch, and D. Rakus. Targeting a moonlighting function of aldolase induces apoptosis in cancer cells. *Cell Death & Disease 2019 10:10*, 10(10):1–16, sep 2019. ISSN 2041-4889. doi: 10.1038/s41419-019-1968-4. URL https://www.nature.com/articles/s41419-019-1968-4.

N. Gomez-Roman, C. Grandori, R. N. Eisenman, and R. J. White. Direct activation of RNA polymerase III transcription by c-Myc. *Nature 2003 421:6920*, 421(6920):290–294, jan 2003. ISSN 1476-4687. doi: 10.1038/nature01327. URL https://www.nature.com/articles/nature01327.

I. L. Gonzalez and J. E. Sylvester. Complete Sequence of the 43-kb Human Ribosomal DNA Repeat: Analysis of the Intergenic Spacer. *Genomics*, 27(2):320–328, may 1995. ISSN 0888-7543. doi: 10.1006/GENO.1995.1049.

C. Grandori, N. Gomez-Roman, Z. A. Felton-Edkins, C. Ngouenet, D. A. Galloway, R. N. Eisenman, and R. J. White. c-Myc binds to human ribosomal DNA and stimulates transcription of rRNA genes by RNA polymerase I. *Nature Cell Biology 2005 7:3*, 7 (3):311–318, feb 2005. ISSN 1476-4679. doi: 10.1038/ncb1224. URL https://www.nature.com/articles/ncb1224.

S. S. Grewal, L. Li, A. Orian, R. N. Eisenman, and B. A. Edgar. Myc-dependent regulation of ribosomal RNA synthesis during Drosophila development. *Nature Cell Biology 2005 7:3*, 7(3):295–302, feb 2005. ISSN 1476-4679. doi: 10.1038/ncb1223. URL https://www.nature.com/articles/ncb1223.

M. Gstaiger, B. Luke, D. Hess, E. J. Oakeley, C. Wirbelauer, M. Blondel, M. Vigneron, M. Peter, and W. Krek. Control of Nutrient-Sensitive Transcription Programs by the

Unconventional Prefoldin URI. *Science*, 302(5648):1208–1212, nov 2003. doi: 10.1126/SCIENCE.1088401. URL https://www.science.org.

M. Gunther, M. Laithier, and O. Brison. A set of proteins interacting with transcription factor Sp1 identified in a two-hybrid screening. *Molecular and Cellular Biochemistry 2000 210:1*, 210(1):131–142, 2000. ISSN 1573-4919. doi: 10.1023/A:1007177623283. URL https://link.springer.com/article/10.1023/A:1007177623283.

D. M. Gwinn, D. B. Shackelford, D. F. Egan, M. M. Mihaylova, A. Mery, D. S. Vasquez, B. E. Turk, and R. J. Shaw. AMPK Phosphorylation of Raptor Mediates a Metabolic Checkpoint. *Molecular Cell*, 30(2):214–226, apr 2008. ISSN 1097-2765. doi: 10.1016/J.MOLCEL.2008.03.003. URL http://www.cell.com/article/S109727650800169X/fulltexthttp://www.cell.com/article/S109727650800169X/abstracthttps://www.cell.com/molecular-cell/abstract/S1097-2765(08)00169-X.

K. M. Hannan, Y. Brandenburger, A. Jenkins, K. Sharkey, A. Cavanaugh, L. Rothblum, T. Moss, G. Poortinga, G. A. McArthur, R. B. Pearson, and R. D. Hannan. mTOR-Dependent Regulation of Ribosomal Gene Transcription Requires S6K1 and Is Mediated by Phosphorylation of the Carboxy-Terminal Activation Domain of the Nucleolar Transcription Factor UBF†. *Molecular and Cellular Biology*, 23(23):8862–8877, dec 2003. doi: 10.1128/MCB.23.23.8862-8877.2003. URL https://journals.asm.org/journal/mcb.

A. K. Henras, C. Plisson-Chastang, M.-F. O'Donohue, A. Chakraborty, and P.-E. Gleizes. An overview of pre-ribosomal RNA processing in eukaryotes. *Wiley Interdisciplinary Reviews. RNA*, 6(2):225, mar 2015. doi: 10.1002/WRNA.1269. URL /pmc/articles/PMC4361047//pmc/articles/PMC4361047/?report=abstracthttps://www.ncbi.nlm.nih.gov/pmc/articles/PMC4361047/.

H. L. Hir, E. Izaurralde, L. E. Maquat, and M. J. Moore. The spliceosome deposits multiple proteins 20–24 nucleotides upstream of mRNA exon–exon junctions. *The EMBO Journal*, 19(24):6860, dec 2000. doi: 10.1093/EMBOJ/19.24.6860. URL /pmc/articles/PMC305905//pmc/articles/PMC305905/?report=abstracthttps://www.ncbi.nlm.nih.gov/pmc/articles/PMC305905/.

H. L. Hir, J. Saulière, and Z. Wang. The exon junction complex as a node of post-transcriptional networks. *Nature Reviews Molecular Cell Biology 2015 17:1*, 17(1):41–54, dec 2015. ISSN 1471-0080. doi: 10.1038/nrm.2015.7. URL https://www.nature.com/articles/nrm.2015.7.

T. Hirose, G. Virnicchi, A. Tanigawa, T. Naganuma, R. Li, H. Kimura, T. Yokoi, S. Nakagawa, M. Bénard, A. H. Fox, and G. Pierron. NEAT1 long noncoding RNA regulates transcription via protein sequestration within subnuclear bodies. *https://doi.org/10.1091/mbc.e13-09-0558*, 25(1):169–183, oct 2013. doi: 10.1091/MBC.E13-09-0558. URL https://www.molbiolcell.org/doi/abs/10.1091/mbc.e13-09-0558.

W. A. Hofmann, L. Stojiljkovic, B. Fuchsova, G. M. Vargas, E. Mavrommatis, V. Philimonenko, K. Kysela, J. A. Goodrich, J. L. Lessard, T. J. Hope, P. Hozak, and P. de Lanerolle. Actin is part of pre-initiation complexes and is necessary for transcription by RNA polymerase II. *Nature Cell Biology 2004 6:11*, 6(11):1094–1101, oct 2004. ISSN 1476-4679. doi: 10.1038/ncb1182. URL https://www.nature.com/articles/ncb1182.

H. Hu and X. Li. Transcriptional regulation in eukaryotic ribosomal protein genes. *Genomics*, 90(4):421–423, oct 2007. ISSN 0888-7543. doi: 10.1016/J.YGENO.2007.07.003.

P. Hu, S. Wu, and N. Hernandez. A role for β-actin in RNA polymerase III transcription. *Genes & Development*, 18(24):3010, dec 2004. doi: 10.1101/GAD.1250804. URL /pmc/articles/PMC535912//pmc/articles/PMC535912/?report=abstracthttps://www.ncbi.nlm.nih.gov/pmc/articles/PMC535912/.

V. Iadevaia, R. Liu, and C. G. Proud. mTORC1 signaling controls multiple steps in ribosome biogenesis. *Seminars in Cell & Developmental Biology*, 36:113–120, dec 2014. ISSN 1084-9521. doi: 10.1016/J.SEMCDB.2014.08.004.

K. Inoki, H. Ouyang, T. Zhu, C. Lindvall, Y. Wang, X. Zhang, Q. Yang, C. Bennett, Y. Harada, K. Stankunas, C.-y. Wang, X. He, O. A. MacDougald, M. You, B. O. Williams, and K.-L. Guan. TSC2 Integrates Wnt and Energy Signals via a Coordinated Phosphorylation by AMPK and GSK3 to Regulate Cell Growth. *Cell*, 126 (5):955–968, sep 2006. ISSN 0092-8674. doi: 10.1016/J.CELL.2006.06.055. URL http://www.cell.com/article/S0092867406010166/fulltexthttp://www.cell.com/article/S0092867406010166/abstracthttps://www.cell.com/cell/abstract/S0092-8674(06)01016-6.

Y. Ishigaki, Y. Nakamura, T. Tatsuno, M. Hashimoto, T. Shimasaki, K. Iwabuchi, and N. Tomosugi. Depletion of RNA-binding protein RBM8A (Y14) causes cell cycle deficiency and apoptosis in human cells:. *https://doi.org/10.1177/1535370213494646*, 238(7):889–897, nov 2016. doi: 10.1177/1535370213494646. URL https:

//journals.sagepub.com/doi/10.1177/1535370213494646?url_ver=Z39.88-2003&rfr_id=ori%3Arid%3Acrossref.org&rfr_dat=cr_pub++0pubmed.

H. Ji, G. Wu, X. Zhan, A. Nolan, C. Koh, A. D. Marzo, H. M. Doan, J. Fan, C. Cheadle, M. Fallahi, J. L. Cleveland, C. V. Dang, and K. I. Zeller. Cell-Type Independent MYC Target Genes Reveal a Primordial Signature Involved in Biomass Accumulation. *PLOS ONE*, 6(10):e26057, 2011. ISSN 1932-6203. doi: 10.1371/JOURNAL.PONE.0026057. URL https://journals.plos.org/plosone/article?id=10.1371/journal.pone.0026057.

P. Jorgensen, J. L. Nishikawa, B. J. Breitkreutz, and M. Tyers. Systematic identification of pathways that couple cell growth and division in yeast. *Science*, 297(5580):395–400, jul 2002. doi: 10.1126/SCIENCE.1070850. URL https://www.science.org.

P. Jorgensen, I. Rupeš, J. R. Sharom, L. Schneper, J. R. Broach, and M. Tyers. A dynamic transcriptional network communicates growth potential to ribosome synthesis and critical cell size. *Genes & Development*, 18 (20):2491, oct 2004. doi: 10.1101/GAD.1228804. URL /pmc/articles/PMC529537//pmc/articles/PMC529537/?report=abstracthttps://www.ncbi.nlm.nih.gov/pmc/articles/PMC529537/.

R. N. Judson, A. M. Tremblay, P. Knopp, R. B. White, R. Urcia, C. De Bari, P. S. Zammit, F. D. Camargo, and H. Wackerhage. The Hippo pathway member Yap plays a key role in influencing fate decisions in muscle satellite cells. *Journal of Cell Science*, 125(24):6009–6019, dec 2012. ISSN 0021-9533. doi: 10.1242/JCS.109546.

T. Kantidakis, B. A. Ramsbottom, J. L. Birch, S. N. Dowding, and R. J. White. mTOR associates with TFIIIC, is found at tRNA and 5S rRNA genes, and targets their repressor Maf1. *Proceedings of the National Academy of Sciences of the United States of America*, 107(26):11823–11828, jun 2010. ISSN 10916490. doi: 10.1073/PNAS.1005188107/-/DCSUPPLEMENTAL. URL https://www.pnas.org/content/107/26/11823https://www.pnas.org/content/107/26/11823.abstract.

S. Kepinski and O. Leyser. The Arabidopsis F-box protein TIR1 is an auxin receptor. *Nature 2005 435:7041*, 435(7041):446–451, may 2005. ISSN 1476-4687. doi: 10.1038/nature03542. URL https://www.nature.com/articles/nature03542.

O. Kitahara, Y. Furukawa, T. Tanaka, C. Kihara, K. Ono, R. Yanagawa, M. E. Nita, T. Takagi, Y. Nakamura, and T. Tsunoda. Alterations of Gene Expression during Colorectal

Carcinogenesis Revealed by cDNA Microarrays after Laser-Capture Microdissection of Tumor Tissues and Normal Epithelia. *Cancer Research*, 61(9), 2001.

P. Komarnitsky, E.-J. Cho, and S. Buratowski. Different phosphorylated forms of RNA polymerase II and associated mRNA processing factors during transcription. *Genes & Development*, 14(19):2452–2460, oct 2000. ISSN 0890-9369. doi: 10.1101/GAD.824700. URL http://genesdev.cshlp.org/content/14/19/2452.fullhttp://genesdev.cshlp.org/content/14/19/2452http://genesdev.cshlp.org/content/14/19/2452.abstract.

R. Kominami, Y. Urano, Y. Mishima, and M. Muramatsu. Organization of ribosomal RNA gene repeats of the mouse. *Nucleic Acids Research*, 9(14):3219–3233, jul 1981. ISSN 0305-1048. doi: 10.1093/NAR/9.14.3219. URL https://academic.oup.com/nar/article/9/14/3219/1136923.

G. Koopman, C. P. Reutelingsperger, G. A. Kuijten, R. M. Keehnen, S. T. Pals, and M. H. Van Oers. Annexin V for Flow Cytometric Detection of Phosphatidylserine Expression on B Cells Undergoing Apoptosis. *Blood*, 84(5):1415–1420, sep 1994. ISSN 0006-4971. doi: 10.1182/BLOOD.V84.5.1415.1415.

J. Kufel and P. Grzechnik. Small Nucleolar RNAs Tell a Different Tale. *Trends in Genetics*, 35(2):104–117, feb 2019. ISSN 0168-9525. doi: 10.1016/J.TIG.2018.11.005. URL http://www.cell.com/article/S0168952518302038/fulltexthttp://www.cell.com/article/S0168952518302038/abstracthttps://www.cell.com/trends/genetics/abstract/S0168-9525(18)30203-8.

T. Kusakabe, K. Motoki, and K. Hori. Mode of Interactions of Human Aldolase Isozymes with Cytoskeletons. *Archives of Biochemistry and Biophysics*, 344(1):184–193, aug 1997. ISSN 0003-9861. doi: 10.1006/ABBI.1997.0204.

A. Laferté, E. Favry, A. Sentenac, M. Riva, C. Carles, and S. Chédin. The transcriptional activity of RNA polymerase I is a key determinant for the level of all ribosome components. *Genes & Development*, 20(15):2030, aug 2006. doi: 10.1101/GAD.386106. URL /pmc/articles/PMC1536055//pmc/articles/PMC1536055/?report=abstracthttps://www.ncbi.nlm.nih.gov/pmc/articles/PMC1536055/.

B. Langmead and S. L. Salzberg. Fast gapped-read alignment with Bowtie 2. *Nature Methods 2012 9:4*, 9(4):357–359, mar 2012. ISSN 1548-7105. doi: 10.1038/nmeth.1923. URL https://www.nature.com/articles/nmeth.1923.

M. Laplante and D. M. Sabatini. mTOR Signaling in Growth Control and Disease. *Cell*, 149(2):274–293, apr 2012. ISSN 0092-8674. doi: 10.1016/J.CELL.2012.03.017. URL http://www.cell.com/article/S0092867412003510/fulltexthttp://www.cell.com/article/S0092867412003510/abstracthttps://www.cell.com/cell/abstract/S0092-8674(12)00351-0.

H. Lempiäinen and D. Shore. Growth control and ribosome biogenesis. *Current Opinion in Cell Biology*, 21(6):855–863, dec 2009. ISSN 0955-0674. doi: 10.1016/J.CEB.2009.09.002.

H. Lempiäinen, A. Uotila, J. Urban, I. Dohnal, G. Ammerer, R. Loewith, and D. Shore. Sfp1 Interaction with TORC1 and Mrs6 Reveals Feedback Regulation on TOR Signaling. *Molecular Cell*, 33(6):704–716, mar 2009. ISSN 1097-2765. doi: 10.1016/J.MOLCEL.2009.01.034. URL http://www.cell.com/article/S1097276509000999/fulltexthttp://www.cell.com/article/S1097276509000999/abstracthttps://www.cell.com/molecular-cell/abstract/S1097-2765(09)00099-9.

H. Li, B. Handsaker, A. Wysoker, T. Fennell, J. Ruan, N. Homer, G. Marth, G. Abecasis, and R. Durbin. The Sequence Alignment/Map format and SAMtools. *Bioinformatics*, 25(16):2078, aug 2009. ISSN 13674803. doi: 10.1093/BIOINFORMATICS/BTP352. URL /pmc/articles/PMC2723002//pmc/articles/PMC2723002/?report=abstracthttps://www.ncbi.nlm.nih.gov/pmc/articles/PMC2723002/.

H. Li, Y. Yang, W. Hong, M. Huang, M. Wu, and X. Zhao. Applications of genome editing technology in the targeted therapy of human diseases: mechanisms, advances and prospects. *Signal Transduction and Targeted Therapy 2020 5:1*, 5(1):1–23, jan 2020. ISSN 2059-3635. doi: 10.1038/s41392-019-0089-y. URL https://www.nature.com/articles/s41392-019-0089-y.

S. H.-J. Li, M. Nofal, L. R. Parsons, J. D. Rabinowitz, and Z. Gitai. Monitoring mammalian mitochondrial translation with MitoRiboSeq. *Nature Protocols 2021 16:6*, 16(6):2802–2825, may 2021. ISSN 1750-2799. doi: 10.1038/s41596-021-00517-1. URL https://www.nature.com/articles/s41596-021-00517-1.

W. Li, H. Xu, T. Xiao, L. Cong, M. I. Love, F. Zhang, R. A. Irizarry, J. S. Liu, M. Brown, and X. S. Liu. MAGeCK enables robust identification of essential genes from genome-scale CRISPR/Cas9 knockout screens. *Genome Biology 2014 15:12*, 15(12):1–12, dec 2014. ISSN 1474-760X. doi: 10.1186/

S13059-014-0554-4. URL https://genomebiology.biomedcentral.com/articles/10.1186/s13059-014-0554-4.

X. Li, X. Zhao, Y. Fang, X. Jiang, T. Duong, C. Fan, C.-C. Huang, and S. R. Kain. Generation of Destabilized Green Fluorescent Protein as a Transcription Reporter *. *Journal of Biological Chemistry*, 273(52):34970–34975, dec 1998. ISSN 0021-9258. doi: 10.1074/JBC.273.52.34970. URL http://www.jbc.org/article/S0021925818371709/fulltexthttp://www.jbc.org/article/S0021925818371709/abstracthttps://www.jbc.org/article/S0021-9258(18)37170-9/abstract.

Y. Lin, R. Liang, Y. Qiu, Y. Lv, J. Zhang, G. Qin, C. Yuan, Z. Liu, Y. Li, D. Zou, and Y. Mao. Expression and gene regulation network of RBM8A in hepatocellular carcinoma based on data mining. *Aging (Albany NY)*, 11 (2):423, jan 2019. doi: 10.18632/AGING.101749. URL /pmc/articles/PMC6366983//pmc/articles/PMC6366983/?report=abstracthttps://www.ncbi.nlm.nih.gov/pmc/articles/PMC6366983/.

S. I. Lippman and J. R. Broach. Protein kinase A and TORC1 activate genes for ribosomal biogenesis by inactivating repressors encoded by Dot6 and its homolog Tod6. *Proceedings of the National Academy of Sciences*, 106(47): 19928–19933, nov 2009. ISSN 0027-8424. doi: 10.1073/PNAS.0907027106. URL https://www.pnas.org/content/106/47/19928https://www.pnas.org/content/106/47/19928.abstract.

J. Liu and E. S. Maxwell. Mouse U14 snRNA is encoded in an intron of the mouse cognate hsc70 heat shock gene. *Nucleic Acids Research*, 18(22):6565, nov 1990. doi: 10.1093/NAR/18.22.6565. URL /pmc/articles/PMC332611/?report=abstracthttps://www.ncbi.nlm.nih.gov/pmc/articles/PMC332611/.

H. Lodish, A. Berk, S. L. Zipursky, P. Matsudaira, D. Baltimore, and J. Darnell. Processing of rRNA and tRNA. 2000. URL https://www.ncbi.nlm.nih.gov/books/NBK21729/.

F. Lorenzin, U. Benary, A. Baluapuri, S. Walz, L. A. Jung, B. von Eyss, C. Kisker, J. Wolf, M. Eilers, and E. Wolf. Different promoter affinities account for specificity in MYC-dependent gene regulation. *eLife*, 5(JULY), jul 2016. doi: 10.7554/ELIFE.15161.

M. Lu, L. S. Holliday, L. Zhang, W. A. Dunn, and S. L. Gluck. Interaction between Aldolase and Vacuolar H+-ATPase: EVIDENCE FOR DIRECT COUPLING OF GLYCOLYSIS TO THE ATP-HYDROLYZING PROTON PUMP. *Journal of Biological*

Chemistry, 276(32):30407–30413, aug 2001. ISSN 0021-9258. doi: 10.1074/JBC.M008768200.

M. Lu, Y. Y. Sautin, L. S. Holliday, and S. L. Gluck. The Glycolytic Enzyme Aldolase Mediates Assembly, Expression, and Activity of Vacuolar H+-ATPase. *Journal of Biological Chemistry*, 279(10):8732–8739, mar 2004. ISSN 0021-9258. doi: 10.1074/JBC.M303871200.

M. Lu, D. Ammar, H. Ives, F. Albrecht, and S. L. Gluck. Physical Interaction between Aldolase and Vacuolar H+-ATPase Is Essential for the Assembly and Activity of the Proton Pump. *Journal of Biological Chemistry*, 282(34):24495–24503, aug 2007. ISSN 0021-9258. doi: 10.1074/JBC.M702598200.

P. Mamczur, A. Gamian, J. Kolodziej, P. Dziegiel, and D. Rakus. Nuclear localization of aldolase A correlates with cell proliferation. *Biochimica et Biophysica Acta (BBA) - Molecular Cell Research*, 1833(12):2812–2822, dec 2013. ISSN 0167-4889. doi: 10.1016/J.BBAMCR.2013.07.013.

H. Mao, J. J. McMahon, Y.-H. Tsai, Z. Wang, and D. L. Silver. Haploinsufficiency for Core Exon Junction Complex Components Disrupts Embryonic Neurogenesis and Causes p53-Mediated Microcephaly. *PLOS Genetics*, 12(9):e1006282, sep 2016. ISSN 1553-7404. doi: 10.1371/JOURNAL.PGEN.1006282. URL https://journals.plos.org/plosgenetics/article?id=10.1371/journal.pgen.1006282.

A. Marnef, S. Cohen, and G. Legube. Transcription-Coupled DNA Double-Strand Break Repair: Active Genes Need Special Care. *Journal of Molecular Biology*, 429(9):1277–1288, may 2017. ISSN 0022-2836. doi: 10.1016/J.JMB.2017.03.024.

M. Martin. Cutadapt removes adapter sequences from high-throughput sequencing reads. *EMBnet.journal*, 17(1):10–12, may 2011. ISSN 2226-6089. doi: 10.14806/EJ.17.1.200. URL http://journal.embnet.org/index.php/embnetjournal/article/view/200/479http://journal.embnet.org/index.php/embnetjournal/article/view/200.

V. Martínez-Fernández, A. Cuevas-Bermúdez, F. Gutiérrez-Santiago, A. I. Garrido-Godino, O. Rodríguez-Galán, A. Jordán-Pla, S. Lois, J. C. Triviño, J. de la Cruz, and F. Navarro. Prefoldin-like Bud27 influences the transcription of ribosomal components and ribosome biogenesis in Saccharomyces cerevisiae. *RNA*, 26(10):1360–1379, oct 2020. ISSN 1355-8382. doi: 10.1261/RNA.075507.120. URL http://rnajournal.cshlp.org/content/26/10/1360.fullhttp:

//rnajournal.cshlp.org/content/26/10/1360http://rnajournal.cshlp.org/content/26/10/1360.abstract.

C. Mayer and I. Grummt. Ribosome biogenesis and cell growth: mTOR coordinates transcription by all three classes of nuclear RNA polymerases. *Oncogene 2006 25:48*, 25(48):6384–6391, oct 2006. ISSN 1476-5594. doi: 10.1038/sj.onc.1209883. URL https://www.nature.com/articles/1209883.

O. Meyuhas. Synthesis of the translational apparatus is regulated at the translational level. *European Journal of Biochemistry*, 267(21):6321–6330, nov 2000. ISSN 1432-1033. doi: 10.1046/J.1432-1327.2000.01719.X. URL https://onlinelibrary.wiley.com/doi/full/10.1046/j.1432-1327.2000.01719.xhttps://onlinelibrary.wiley.com/doi/abs/10.1046/j.1432-1327.2000.01719.xhttps://febs.onlinelibrary.wiley.com/doi/10.1046/j.1432-1327.2000.01719.x.

M. C. Mirón-García, A. I. Garrido-Godino, V. García-Molinero, F. Hernández-Torres, S. Rodríguez-Navarro, and F. Navarro. The Prefoldin Bud27 Mediates the Assembly of the Eukaryotic RNA Polymerases in an Rpb5-Dependent Manner. *PLOS Genetics*, 9(2):e1003297, feb 2013. ISSN 1553-7404. doi: 10.1371/JOURNAL.PGEN.1003297. URL https://journals.plos.org/plosgenetics/article?id=10.1371/journal.pgen.1003297.

P. B. Moore and T. A. Steitz. The Roles of RNA in the Synthesis of Protein. *Cold Spring Harbor Perspectives in Biology*, 3(11), nov 2011. doi: 10.1101/CSHPERSPECT.A003780. URL /pmc/articles/PMC3220363//pmc/articles/PMC3220363/?report=abstracthttps://www.ncbi.nlm.nih.gov/pmc/articles/PMC3220363/.

S. T. Mullineux and D. L. Lafontaine. Mapping the cleavage sites on mammalian pre-rRNAs: Where do we stand? *Biochimie*, 94(7):1521–1532, jul 2012. ISSN 0300-9084. doi: 10.1016/J.BIOCHI.2012.02.001.

S. K. Nair and S. K. Burley. X-Ray Structures of Myc-Max and Mad-Max Recognizing DNA: Molecular Bases of Regulation by Proto-Oncogenic Transcription Factors. *Cell*, 112(2):193–205, jan 2003. ISSN 0092-8674. doi: 10.1016/S0092-8674(02)01284-9. URL http://www.cell.com/article/S0092867402012849/fulltexthttp://www.cell.com/article/S0092867402012849/abstracthttps://www.cell.com/cell/abstract/S0092-8674(02)01284-9.

H. Nakhoul, J. Ke, X. Zhou, W. Liao, S. X. Zeng, and H. Lu. Ribosomopathies: Mechanisms of Disease. *Clinical Medicine Insights: Blood Disorders*, 7:7, aug 2014. doi: 10.4137/CMBD.S16952. URL /pmc/articles/PMC4251057//pmc/articles/PMC4251057/?report=abstracthttps://www.ncbi.nlm.nih.gov/pmc/articles/PMC4251057/.

A. Narla and B. L. Ebert. Ribosomopathies: human disorders of ribosome dysfunction. *Blood*, 115(16):3196–3205, apr 2010. ISSN 0006-4971. doi: 10.1182/BLOOD-2009-10-178129. URL http://ashpublications.org/blood/article-pdf/115/16/3196/1325052/zh801610003196.pdf.

S. K. Natchiar, A. G. Myasnikov, H. Kratzat, I. Hazemann, and B. P. Klaholz. Visualization of chemical modifications in the human 80S ribosome structure. *Nature 2017 551:7681*, 551(7681):472–477, nov 2017. ISSN 1476-4687. doi: 10.1038/nature24482. URL https://www.nature.com/articles/nature24482.

C. L. Neary and J. G. Pastorino. Nucleocytoplasmic shuttling of hexokinase II in a cancer cell. *Biochemical and Biophysical Research Communications*, 394(4):1075–1081, apr 2010. ISSN 0006-291X. doi: 10.1016/J.BBRC.2010.03.129.

K. Nishimura, T. Fukagawa, H. Takisawa, T. Kakimoto, and M. Kanemaki. An auxin-based degron system for the rapid depletion of proteins in nonplant cells. *Nature Methods 2009 6:12*, 6(12):917–922, nov 2009. ISSN 1548-7105. doi: 10.1038/nmeth.1401. URL https://www.nature.com/articles/nmeth.1401.

N. Nosrati, N. R. Kapoor, and V. Kumar. Combinatorial action of transcription factors orchestrates cell cycle-dependent expression of the ribosomal protein genes and ribosome biogenesis. *The FEBS Journal*, 281(10):2339–2352, may 2014. ISSN 1742-4658. doi: 10.1111/FEBS.12786. URL https://febs.onlinelibrary.wiley.com/doi/full/10.1111/febs.12786https://febs.onlinelibrary.wiley.com/doi/abs/10.1111/febs.12786https://febs.onlinelibrary.wiley.com/doi/10.1111/febs.12786.

L. M. Ogawa and S. J. Baserga. Crosstalk between the nucleolus and the DNA damage response. *Molecular bioSystems*, 13(3):443, 2017. doi: 10.1039/C6MB00740F. URL /pmc/articles/PMC5340083//pmc/articles/PMC5340083/?report=abstracthttps://www.ncbi.nlm.nih.gov/pmc/articles/PMC5340083/.

J. G. Patton, E. B. Porro, J. Galceran, P. Tempst, and B. Nadal-Ginard. Cloning and characterization of PSF, a novel pre-mRNA splicing factor. *Genes & Development*, 7(3):393–406, mar 1993. ISSN 0890-9369. doi: 10.1101/

GAD.7.3.393. URL http://genesdev.cshlp.org/content/7/3/393http://genesdev.cshlp.org/content/7/3/393.abstract.

A. Pecoraro, M. Pagano, G. Russo, and A. Russo. Ribosome Biogenesis and Cancer: Overview on Ribosomal Proteins. *International Journal of Molecular Sciences 2021, Vol. 22, Page 5496*, 22(11):5496, may 2021. doi: 10.3390/IJMS22115496. URL https://www.mdpi.com/1422-0067/22/11/5496/htmhttps://www.mdpi.com/1422-0067/22/11/5496.

P. Percipalle. Co-transcriptional nuclear actin dynamics. *http://dx.doi.org/10.4161/nucl.22798*, 4(1):43–52, 2012. doi: 10.4161/NUCL.22798. URL https://www.tandfonline.com/doi/abs/10.4161/nucl.22798.

D. Perina, M. Korolija, M. Roller, M. Harcet, B. Jelicic, A. Miko, and H. etkovi. Over-represented localized sequence motifs in ribosomal protein gene promoters of basal metazoans. *Genomics*, 98(1):56–63, jul 2011. ISSN 0888-7543. doi: 10.1016/J.YGENO.2011.03.009.

R. P. Perry. The architecture of mammalian ribosomal protein promoters. *BMC Evolutionary Biology*, 5:15, feb 2005. doi: 10.1186/1471-2148-5-15. URL /pmc/articles/PMC554972//pmc/articles/PMC554972/?report=abstracthttps://www.ncbi.nlm.nih.gov/pmc/articles/PMC554972/.

V. V. Philimonenko, J. Zhao, S. Iben, H. Dingová, K. Kyselá, M. Kahle, H. Zentgraf, W. A. Hofmann, P. de Lanerolle, P. Hozák, and I. Grummt. Nuclear actin and myosin I are required for RNA polymerase I transcription. *Nature Cell Biology 2004 6:12*, 6 (12):1165–1172, nov 2004. ISSN 1476-4679. doi: 10.1038/ncb1190. URL https://www.nature.com/articles/ncb1190.

L. Philippe, A. M. G. van den Elzen, M. J. Watson, and C. C. Thoreen. Global analysis of LARP1 translation targets reveals tunable and dynamic features of 5' TOP motifs. *Proceedings of the National Academy of Sciences*, 117(10):5319–5328, mar 2020. ISSN 0027-8424. doi: 10.1073/PNAS.1912864117. URL https://www.pnas.org/content/117/10/5319https://www.pnas.org/content/117/10/5319.abstract.

M. Piazzi, A. Bavelloni, A. Gallo, I. Faenza, and W. L. Blalock. Signal Transduction in Ribosome Biogenesis: A Recipe to Avoid Disaster. *International Journal of Molecular Sciences*, 20(11), jun 2019. doi: 10.3390/IJMS20112718. URL /pmc/articles/PMC6600399//pmc/articles/PMC6600399/?report=abstracthttps://www.ncbi.nlm.nih.gov/pmc/articles/PMC6600399/.

G. Pineda, Z. Shen, C. P. De Albuquerque, E. Reynoso, J. Chen, C. C. Tu, W. Tang, S. Briggs, H. Zhou, and J. Y. Wang. Proteomics studies of the interactome of RNA polymerase II C-terminal repeated domain. *BMC Research Notes*, 8(1):616, oct 2015. ISSN 17560500. doi: 10.1186/S13104-015-1569-Y. URL /pmc/articles/PMC4627417//pmc/articles/PMC4627417/?report=abstracthttps://www.ncbi.nlm.nih.gov/pmc/articles/PMC4627417/.

M. Pirouz, M. Munafò, A. G. Ebrahimi, J. Choe, and R. I. Gregory. Exonuclease Requirements for Mammalian Ribosomal RNA Biogenesis and Surveillance. *Nature structural & molecular biology*, 26(6):490, jun 2019. doi: 10.1038/S41594-019-0234-X. URL /pmc/articles/PMC6554070//pmc/articles/PMC6554070/?report=abstracthttps://www.ncbi.nlm.nih.gov/pmc/articles/PMC6554070/.

T. M. Popay, J. Wang, C. M. Adams, G. C. Howard, S. G. Codreanu, S. D. Sherrod, J. A. McLean, L. R. Thomas, S. L. Lorey, Y. J. Machida, A. M. Weissmiller, C. M. Eischen, Q. Liu, and W. P. Tansey. Myc regulates ribosome biogenesis and mitochondrial gene expression programs through its interaction with host cell factor–1. *eLife*, 10:1–39, 2021. doi: 10.7554/ELIFE.60191.

P. Rajput, V. Pandey, and V. Kumar. Stimulation of ribosomal RNA gene promoter by transcription factor Sp1 involves active DNA demethylation by Gadd45-NER pathway. *Biochimica et Biophysica Acta (BBA) - Gene Regulatory Mechanisms*, 1859(8):953–963, aug 2016. ISSN 1874-9399. doi: 10.1016/J.BBAGRM.2016.05.002.

F. A. Ran, P. D. Hsu, J. Wright, V. Agarwala, D. A. Scott, and F. Zhang. Genome engineering using the CRISPR-Cas9 system. *Nature Protocols 2013 8:11*, 8(11): 2281–2308, oct 2013. ISSN 1750-2799. doi: 10.1038/nprot.2013.143. URL https://www.nature.com/articles/nprot.2013.143.

A. M. Robitaille, S. Christen, M. Shimobayashi, M. Cornu, L. L. Fava, S. Moes, C. Prescianotto-Baschong, U. Sauer, P. Jenoe, and M. N. Hall. Quantitative phosphoproteomics reveal mTORC1 activates de novo pyrimidine synthesis. *Science*, 339(6125):1320–1323, mar 2013. doi: 10.1126/SCIENCE.1228771.

S. Roepcke, S. Stahlberg, H. Klein, M. H. Schulz, L. Theobald, S. Gohlke, M. Vingron, and D. J. Walther. A tandem sequence motif acts as a distance-dependent enhancer in a set of genes involved in translation by binding the proteins NonO and SFPQ. *BMC Genomics 2011 12:1*, 12(1):1–15, dec 2011. ISSN 1471-2164. doi: 10.1186/1471-2164-12-624. URL https://bmcgenomics.biomedcentral.com/articles/10.1186/1471-2164-12-624.

Z. Ronai. Glycolytic enzymes as DNA binding proteins. *International Journal of Biochemistry*, 25(7):1073–1076, jul 1993. ISSN 0020-711X. doi: 10.1016/0020-711X(93)90123-V.

Z. Ronai, R. Robinson, S. Rutberg, P. Lazarus, and M. Sardana. Aldolase-DNA interactions in a SEWA cell system. *Biochimica et Biophysica Acta (BBA) - Gene Structure and Expression*, 1130(1):20–28, feb 1992. ISSN 0167-4781. doi: 10.1016/0167-4781(92)90456-A.

F. J. Rosario, T. L. Powell, M. B. Gupta, L. Cox, and T. Jansson. mTORC1 Transcriptional Regulation of Ribosome Subunits, Protein Synthesis, and Molecular Transport in Primary Human Trophoblast Cells. *Frontiers in Cell and Developmental Biology*, 0:1301, nov 2020. ISSN 2296-634X. doi: 10.3389/FCELL.2020.583801.

S. Roy Choudhury, A. K. Singh, T. McLeod, M. Blanchette, B. Jang, P. Badenhorst, A. Kanhere, and S. Brogna. Exon junction complex proteins bind nascent transcripts independently of pre-mRNA splicing in Drosophila melanogaster. *eLife*, 5 (NOVEMBER2016), nov 2016. doi: 10.7554/ELIFE.19881.

S. Sakonju, D. F. Bogenhagen, and D. D. Brown. A control region in the center of the 5S RNA gene directs specific initiation of transcription: I. The 5' border of the region. *Cell*, 19(1):13–25, jan 1980. ISSN 0092-8674. doi: 10.1016/0092-8674(80)90384-0.

N. E. Sanjana, O. Shalem, and F. Zhang. Improved vectors and genome-wide libraries for CRISPR screening. *Nature Methods 2014 11:8*, 11(8):783–784, jul 2014. ISSN 1548-7105. doi: 10.1038/nmeth.3047. URL `https://www.nature.com/articles/nmeth.3047`.

T. Schmelzle and M. N. Hall. TOR, a Central Controller of Cell Growth. *Cell*, 103(2):253–262, oct 2000. ISSN 0092-8674. doi: 10.1016/S0092-8674(00)00117-3.

U. Schubert, L. C. Antón, J. Gibbs, C. C. Norbury, J. W. Yewdell, and J. R. Bennink. Rapid degradation of a large fraction of newly synthesized proteins by proteasomes. *Nature 2000 404:6779*, 404(6779):770–774, apr 2000. ISSN 1476-4687. doi: 10.1038/35008096. URL `https://www.nature.com/articles/35008096`.

A. Shibui-Nihei, Y. Ohmori, K. Yoshida, J. I. Imai, I. Oosuga, M. Iidaka, Y. Suzuki, J. Mizushima-Sugano, K. Yoshitomo-Nakagawa, and S. Sugano. The 5' terminal oligopyrimidine tract of human elongation factor 1A-1 gene functions as a transcriptional initiator and produces a variable number of Us at the transcriptional level. *Gene*, 311(1-2):137–145, jun 2003. ISSN 0378-1119. doi: 10.1016/S0378-1119(03)00583-3.

D. Shore, S. Zencir, and B. Albert. Transcriptional control of ribosome biogenesis in yeast: links to growth and stress signals. *Biochemical Society Transactions*, 49(4):1589–1599, aug 2021. ISSN 0300-5127. doi: 10.1042/BST20201136. URL /biochemsoctrans/article/49/4/1589/229230/Transcriptional-control-of-ribosome-biogenesis-in.

K. E. Sloan, A. S. Warda, S. Sharma, K.-D. Entian, D. L. J. Lafontaine, and M. T. Bohnsack. Tuning the ribosome: The influence of rRNA modification on eukaryotic ribosome biogenesis and function. *RNA Biology*, 14(9): 1138, sep 2017. doi: 10.1080/15476286.2016.1259781. URL /pmc/articles/PMC5699541//pmc/articles/PMC5699541/?report=abstracthttps://www.ncbi.nlm.nih.gov/pmc/articles/PMC5699541/.

C. M. Smith and J. A. Steitz. Sno Storm in the Nucleolus: New Roles for Myriad Small RNPs. *Cell*, 89(5):669–672, may 1997. ISSN 0092-8674. doi: 10.1016/S0092-8674(00)80247-0.

B. Sollner-Webb. Novel intron-encoded small nucleolar RNAs. *Cell*, 75(3):403–405, nov 1993. ISSN 0092-8674. doi: 10.1016/0092-8674(93)90374-Y.

F. Stricher, C. Macri, M. Ruff, and S. Muller. HSPA8/HSC70 chaperone protein. *http://dx.doi.org/10.4161/auto.26448*, 9(12):1937–1954, dec 2013. doi: 10.4161/AUTO.26448. URL https://www.tandfonline.com/doi/abs/10.4161/auto.26448.

L. Tafforeau, C. Zorbas, J. L. Langhendries, S. T. Mullineux, V. Stamatopoulou, R. Mullier, L. Wacheul, and D. L. Lafontaine. The Complexity of Human Ribosome Biogenesis Revealed by Systematic Nucleolar Screening of Pre-rRNA Processing Factors. *Molecular Cell*, 51(4):539–551, aug 2013. ISSN 1097-2765. doi: 10.1016/J.MOLCEL.2013.08.011.

W. D. Teale, I. A. Paponov, and K. Palme. Auxin in action: signalling, transport and the control of plant growth and development. *Nature Reviews Molecular Cell Biology 2006 7:11*, 7(11):847–859, sep 2006. ISSN 1471-0080. doi: 10.1038/nrm2020. URL https://www.nature.com/articles/nrm2020.

Ö. A. Teber, G. Gillessen-Kaesbach, S. Fischer, S. Böhringer, B. Albrecht, A. Albert, M. Arslan-Kirchner, E. Haan, M. Hagedorn-Greiwe, C. Hammans, W. Henn, G. K. Hinkel, R. König, E. Kunstmann, J. Kunze, L. M. Neumann, E. C. Prott, A. Rauch, H. D. Rott, H. Seidel, S. Spranger, M. Sprengel, B. Zoll, D. R. Lohmann, and D. Wieczorek. Genotyping in 46 patients with tentative diagnosis of Treacher

Collins syndrome revealed unexpected phenotypic variation. *European Journal of Human Genetics 2004 12:11*, 12(11):879–890, sep 2004. ISSN 1476-5438. doi: 10.1038/sj.ejhg.5201260. URL https://www.nature.com/articles/5201260.

C. C. Thoreen, L. Chantranupong, H. R. Keys, T. Wang, N. S. Gray, and D. M. Sabatini. A unifying model for mTORC1-mediated regulation of mRNA translation. *Nature 2012 485:7396*, 485(7396):109–113, may 2012. ISSN 1476-4687. doi: 10.1038/nature11083. URL https://www.nature.com/articles/nature11083.

Z. Turi, M. Lacey, M. Mistrik, and P. Moudry. Impaired ribosome biogenesis: mechanisms and relevance to cancer and aging. *Aging (Albany NY)*, 11 (8):2512, apr 2019. doi: 10.18632/AGING.101922. URL /pmc/articles/PMC6520011//pmc/articles/PMC6520011/?report=abstracthttps://www.ncbi.nlm.nih.gov/pmc/articles/PMC6520011/.

T. W. Turowski and M. Boguta. Specific Features of RNA Polymerases I and III: Structure and Assembly. *Frontiers in Molecular Biosciences*, 0:349, may 2021. ISSN 2296-889X. doi: 10.3389/FMOLB.2021.680090.

T. W. Turowski and D. Tollervey. Transcription by RNA polymerase III: insights into mechanism and regulation. *Biochemical Society Transactions*, 44(5):1367, oct 2016. doi: 10.1042/BST20160062. URL /pmc/articles/PMC5095917//pmc/articles/PMC5095917/?report=abstracthttps://www.ncbi.nlm.nih.gov/pmc/articles/PMC5095917/.

J. van Riggelen, A. Yetil, and D. W. Felsher. MYC as a regulator of ribosome biogenesis and protein synthesis. *Nature Reviews Cancer 2010 10:4*, 10(4):301–309, apr 2010. ISSN 1474-1768. doi: 10.1038/nrc2819. URL https://www.nature.com/articles/nrc2819.

S. Walz, F. Lorenzin, J. Morton, K. E. Wiese, B. von Eyss, S. Herold, L. Rycak, H. Dumay-Odelot, S. Karim, M. Bartkuhn, F. Roels, T. Wüstefeld, M. Fischer, M. Teichmann, L. Zender, C.-L. Wei, O. Sansom, E. Wolf, and M. Eilers. Activation and repression by oncogenic MYC shape tumour-specific gene expression profiles. *Nature 2014 511:7510*, 511(7510):483–487, jul 2014. ISSN 1476-4687. doi: 10.1038/nature13473. URL https://www.nature.com/articles/nature13473.

Z. Wang, V. Murigneux, and H. Le Hir. Transcriptome-wide modulation of splicing by the exon junction complex. *Genome Biology 2014 15:12*, 15(12):1–18, dec 2014. ISSN 1474-760X. doi: 10.1186/S13059-014-0551-7. URL https://genomebiology.biomedcentral.com/articles/10.1186/s13059-014-0551-7.

T. Wild, P. Horvath, E. Wyler, B. Widmann, L. Badertscher, I. Zemp, K. Kozak, G. Csucs, E. Lund, and U. Kutay. A Protein Inventory of Human Ribosome Biogenesis Reveals an Essential Function of Exportin 5 in 60S Subunit Export. *PLoS Biology*, 8(10):1000522, 2010. doi: 10.1371/JOURNAL.PBIO.1000522. URL /pmc/articles/PMC2964341//pmc/articles/PMC2964341/?report=abstracthttps://www.ncbi.nlm.nih.gov/pmc/articles/PMC2964341/.

T. N. Willig, N. Draptchinskaia, I. Dianzani, S. Ball, C. Niemeyer, U. Ramenghi, K. Orfali, P. Gustavsson, E. Garelli, A. Brusco, C. Tiemann, J. L. Pérignon, C. Bouchier, L. Cicchiello, N. Dahl, N. Mohandas, and G. Tchernia. Mutations in Ribosomal Protein S19 Gene and Diamond Blackfan Anemia: Wide Variations in Phenotypic Expression. *Blood*, 94(12):4294–4306, dec 1999. ISSN 0006-4971. doi: 10.1182/BLOOD.V94.12.4294.

J. Wysocka, M. P. Myers, C. D. Laherty, R. N. Eisenman, and W. Herr. Human Sin3 deacetylase and trithorax-related Set1/Ash2 histone H3-K4 methyltransferase are tethered together selectively by the cell-proliferation factor HCF-1. *Genes & Development*, 17(7):896–911, apr 2003. ISSN 0890-9369. doi: 10.1101/GAD.252103. URL http://genesdev.cshlp.org/content/17/7/896.fullhttp://genesdev.cshlp.org/content/17/7/896http://genesdev.cshlp.org/content/17/7/896.abstract.

R. Yamashita, Y. Suzuki, N. Takeuchi, H. Wakaguri, T. Ueda, S. Sugano, and K. Nakai. Comprehensive detection of human terminal oligo-pyrimidine (TOP) genes and analysis of their characteristics. *Nucleic Acids Research*, 36 (11):3707, jun 2008. doi: 10.1093/NAR/GKN248. URL /pmc/articles/PMC2441802//pmc/articles/PMC2441802/?report=abstracthttps://www.ncbi.nlm.nih.gov/pmc/articles/PMC2441802/.

J. Yang, J. Nie, X. Ma, Y. Wei, Y. Peng, and X. Wei. Targeting PI3K in cancer: mechanisms and advances in clinical trials. *Molecular Cancer 2019 18:1*, 18(1):1–28, feb 2019. ISSN 1476-4598. doi: 10.1186/S12943-019-0954-X. URL https://molecular-cancer.biomedcentral.com/articles/10.1186/s12943-019-0954-x.

S. H. Yang, P. H. Cheng, R. T. Sulivan, J. W. Thomas, and A. W. Chan. Lentiviral Integration Preferences in Transgenic Mice. *Genesis (New York, N.Y. : 2000)*, 46(12):711, 2008. ISSN 1526954X. doi: 10.1002/DVG.20435.

URL /pmc/articles/PMC4381762//pmc/articles/PMC4381762/?report=abstracthttps://www.ncbi.nlm.nih.gov/pmc/articles/PMC4381762/.

J. W. Yewdell. Not such a dismal science: the economics of protein synthesis, folding, degradation and antigen processing. *Trends in Cell Biology*, 11(7):294–297, jul 2001. ISSN 0962-8924. doi: 10.1016/S0962-8924(01)02030-X.

G. Yu, Y. Zhao, and H. Li. The multistructural forms of box C/D ribonucleoprotein particles. *RNA*, 24(12):1625, dec 2018. doi: 10.1261/RNA.068312.118. URL /pmc/articles/PMC6239191//pmc/articles/PMC6239191/?report=abstracthttps://www.ncbi.nlm.nih.gov/pmc/articles/PMC6239191/.

X. Yu and S. Li. Non-metabolic functions of glycolytic enzymes in tumorigenesis. *Oncogene 2017 36:19*, 36(19):2629–2636, oct 2016. ISSN 1476-5594. doi: 10.1038/onc.2016.410. URL https://www.nature.com/articles/onc2016410.

S. Zencir, D. Dilg, M. P. Rueda, D. Shore, and B. Albert. Mechanisms coordinating ribosomal protein gene transcription in response to stress. *Nucleic Acids Research*, 48(20):11408–11420, nov 2020. ISSN 0305-1048. doi: 10.1093/NAR/GKAA852. URL https://academic.oup.com/nar/article/48/20/11408/5934540.

C.-S. Zhang, S. A. Hawley, Y. Zong, M. Li, Z. Wang, A. Gray, T. Ma, J. Cui, J.-W. Feng, M. Zhu, Y.-Q. Wu, T. Y. Li, Z. Ye, S.-Y. Lin, H. Yin, H.-L. Piao, D. G. Hardie, and S.-C. Lin. Fructose-1,6-bisphosphate and aldolase mediate glucose sensing by AMPK. *Nature 2017 548:7665*, 548(7665):112–116, jul 2017. ISSN 1476-4687. doi: 10.1038/nature23275. URL https://www.nature.com/articles/nature23275.

L. Zhang, W. Zhou, V. E. Velculescu, S. E. Kern, R. H. Hruban, S. R. Hamilton, B. Vogelstein, and K. W. Kinzler. Gene Expression Profiles in Normal and Cancer Cells. *Science*, 276(5316):1268–1272, may 1997. ISSN 0036-8075. doi: 10.1126/SCIENCE.276.5316.1268. URL https://science.sciencemag.org/content/276/5316/1268https://science.sciencemag.org/content/276/5316/1268.abstract.

W. W. Zhang, L. X. Zhang, R. K. Busch, J. Farrés, and H. Busch. Purification and characterization of a DNA-binding heterodimer of 52 and 100 kDa from HeLa cells. *Biochemical Journal*, 290(1):267–272, feb 1993. ISSN 0264-6021. doi: 10.1042/BJ2900267. URL /biochemj/article/290/1/267/36132/Purification-and-characterization-of-a-DNA-binding.

H. Zhou and S. Huang. The complexes of mammalian target of rapamycin. *Current protein & peptide science*, 11(6):409, jul 2010. ISSN 13892037. doi: 10.2174/138920310791824093. URL /pmc/articles/PMC2928868//pmc/articles/PMC2928868/?report=abstracthttps://www.ncbi.nlm.nih.gov/pmc/articles/PMC2928868/.

List of Figures

List of Tables

8 Appendix

8.1 List of abbreviations

SI prefixes

c – centi
k – kilo
m – milli
n – nano
µ - micro

SI units and other units

A – ampere
d – day(s)
Da – Dalton
g – g force; also called “relative centrifugal force” (rcf)
h - hour
kg – kilogram
l – liter(s)
m – meter(s)
M – mol/l
min – minute(s) (time)
mol – mole
S – Svedberg unit(s)
sec – second(s)
U – unit(s)
V – volt
v/v – volume per volume
w/v – weight per volume

℃ – degree Celsius

Other abbreviations

AID – Auxin-inducible degron
Aldoa – Aldolase A
Amp – Ampicillin
APS – ammonium persulfate
BCA - bicinchoninic acid
Blast – Blasticidin
bp – base pair(s)
Carb – Carbenicillin
Cas9 – CRISPR-associated 9 nuclease
cfu – colony-forming units
ChIP – Chromatin-immunoprecipitation
Chr – chromosome
CHX – cycloheximide
Co-IP – Co-immunoprecipitation
CRISPR – clustered regularly interspaced short palindromic repeat
CRP – cytosolic ribosomal protein
crRNA – CRISPR RNA
CTD – C-terminal domain
CTR; Ctrl - control
DBA – Diamond-Blackfan anemia
DDR – DNA-damage response
DMF - Dimethylformamide
DMSO – Dimethyl sulfoxide
DNA – deoxyribonucleic acid
DOC – Deoxycholate
Dox – Doxycycline
dpi – days post infection
DRiP - defective ribosomal products
DSB – double-strand break
E. coli – *Escherichia coli*
EDTA - Ethylenediaminetetraacetic acid

eEF1A-1 – elongation factor 1A-1
EGFP – enhanced green fluorescent protein (variant of the initially isolated green fluorescent protein from Aequorea victoria)
EGFP-PEST – PEST domain from mODC fused to EGFP
EJC – exon junction complex
EtOH – Ethanol
EV - empty vector
f - forward
FACS – Fluorescence-activated cell sorting
Fbl – Fibrillarin
FBS – fetal bovine serum
FC – fold change
FCS – fetal calf serum
FDR - false discovery rate
FLAG - a protein tag
gDNA – genomic DNA
GeCKO – genome-wide CRISPR knockout
GSEA – gene set enrichment analysis
GO - gene ontology
GSG – glycine-serine-glycine
HA - hemagglutinin tag
HDR – homology-directed repair
HEK – human embryonic kidney
HeLa cells – Henrietta Lacks cells
HK2 – Hexokinase 2
HRP – Horseradish peroxidase
IAA – Indole-3-acetic acid
IgG – Immunoglobulin G
IP - immunoprecipitation
IRBC – impaired ribosome biogenesis checkpoint
KD – knockdown
KO – knockout
LARP1 - La-related protein 1
LB – Lysogeny broth
LTR – long terminal repeats
LTSM – localized tandem sequence motif
MAGeCK – model-based analysis of genome-wide CRISPR-Cas9 knockout

MEF - murine embryonic fibroblasts
mODC – murine ornithine decarboxylase
MOI – multiplicity of infection
MRP – mitochondrial ribosomal protein
mTORC1 – mammalian target of rapamycin complex 1
MYC - MYC proto-oncogene, BHLH Transcription Factor; name comes from “myelocytomatosis”
NaCl – Sodium chloride
NEB – New England Biolabs
NGS – next-generation sequencing
NMD – nonsense-mediated decay
o. n. – over night
PAGE - polyacrylamide-gelelectrophoresis
PAM - protospacer adjacent motif
PBS – phosphate buffered saline
PCR – polymerase chain reaction
PEST – a (usually destabilizing) protein domain/peptide sequence rich in proline (P), glutamic acid (E), serine (S) and threonine (T)
PI3K – phosphatidylinositol-3-kinase
POI - protein of interest
PolI – RNA Polymerase I
PolII – RNA Polymerase II
PolIII – RNA Polymerase III
pS2 – phospho-serine 2
pS5 – phospho-serine 5
P2A - porcine teschovirus-1 2A self-cleaving peptide
qRT-PCR – quantitative real-time reverse transcription polymerase chain reaction
rDNA – ribosomal DNA
rev; r - reverse
RiBi – ribosome biogenesis
RNA – ribonucleic acid
RP – ribosomal protein
Rpl – Ribosomal protein large subunit
rpm - rounds per minute
Rps – Ribosomal protein small subunit
rRNA – ribosomal RNA
RT – room temperature

SDS – sodium dodecyl sulfate
SFFV - spleen focus forming virus
sgRNA – single guide RNA
siRNA – small interfering RNA
snoRNA – small nucleolar RNA
snoRNP - small nucleolar ribonucleoprotein particle(s)
SV40 late pA - simian virus 40 late polyadenylation signal
S6K – S6 kinase
TAD – topologically associating domain
TAE – TRIS-acetic acid-EDTA
TALEN – transcription activator-like effector nuclease
TCS – Treacher-Collins syndrome
TE – Tris-EDTA
Tet-Off - transgene, that can be switched off by the addition of Doxycycline
TF – transcription factor
tGFP – turboGFP (variant of green fluorescent protein isolated from Pontellina plumata)
TIR1 - Transport inhibitor response 1 protein
tracrRNA – trans-activating RNA
tRFP – turboRFP (variant of a red fluorescent protein isolated from Entacmaea quadricolor)
tRFP-PEST - PEST domain from mODC fused to tRFP
TSS – transcription start site
UV - ultraviolet
U2OS – human bone osteosarcoma epithelial cells
WT – wild type
ZNF – zinc-finger (nuclease)
3'hom – 3' homology arm
4E-BP – 4E-binding protein
4sU – 4-thiouridine
5'hom – 5' homology arm
5' TOP – 5' terminal oligopyrimidine

8.2 Candidate gene lists from each screening condition

The complete candidate gene lists of the screening conditions showed in this thesis can be found on Zenodo with the following digital object identifier (DOI):
https://doi.org/10.5281/zenodo.5717228

In addition, the top and bottom 100 genes from each screening condition are listed below.

8.2.1 Top 100 positively enriched genes from the condition sorted for low expression of *Fbl*-driven EGFP-PEST and median to high expression of *Rpl18*-driven tRFP-PEST ("GFP down")

Rank	Gene	Number of sgRNAs	Good sgRNAs	LogFC	FDR
1	Aldoa	6	6	3.2833	0.000381
2	EGFP	3	3	6.5042	0.000381
3	Hspa8	6	5	3.5377	0.000381
4	Bud31	6	6	3.5657	0.000381
5	Polr2l	6	4	2.709	0.000381
6	Polr2e	5	3	2.5822	0.000381
7	Cdc16	6	6	2.5678	0.000381
8	Eif4a3	6	5	2.6534	0.000381
9	Polr2c	5	4	3.1384	0.000381
10	Polr2h	5	5	2.4026	0.000381
11	Anapc1	6	5	2.2172	0.000381
12	Eif4a1	6	5	2.7656	0.000381
13	Gm21637	6	4	2.6418	0.000381
14	Sfpq	6	5	1.8375	0.003182
15	Rpa1	6	3	1.2269	0.01021
16	Plk1	6	4	1.5814	0.01021
17	Itgav	6	4	1.5507	0.015434
18	Cpsf3l	6	5	1.7228	0.017327
19	Ewsr1	5	3	1.8731	0.019566
20	Uba1	6	5	1.55	0.019566
21	Krt19	5	5	1.2569	0.019566

22	Ssrp1	6	3	-0.15156	0.025878
23	Rbm8a	6	5	2.0989	0.026609
24	Gpn1	5	2	-0.87054	0.026609
25	Rbm22	6	6	1.0593	0.040198
26	Cdc20	6	3	-0.20499	0.091054
27	Prkra	6	4	1.5832	0.091054
28	Gm10921	6	5	1.7519	0.094401
29	Sumo2	6	6	1.4153	0.095545
30	Polr2f	6	3	-0.71604	0.10426
31	Snrpd2	6	2	-1.712	0.10426
32	Phb	6	4	0.92018	0.10426
33	Ubl5	4	3	2.8464	0.091054
34	Klhl7	6	5	1.3557	0.124782
35	Tceb2	6	5	1.2447	0.138751
36	Gm5072	6	6	1.1672	0.138751
37	Polr2j	6	4	1.6954	0.151592
38	Narfl	6	5	1.0604	0.170729
39	Mad2l1	5	3	1.4025	0.154377
40	Anapc2	6	4	1.4514	0.220173
41	Il1f5	6	4	1.1125	0.228548
42	Vmn1r194	6	5	0.82062	0.228548
43	Brd4	6	5	1.1158	0.230988
44	Srp68	6	3	-0.77167	0.230988
45	Ncbp2	6	3	-0.78602	0.233684
46	Anapc11	5	4	0.67141	0.230988
47	Rac1	6	4	1.5617	0.233684
48	Gm10058	5	5	0.72008	0.230988
49	Ttpa	5	5	1.0411	0.230988
50	Vmn1r124	6	3	0.70975	0.244954
51	Dhx8	6	4	1.3496	0.244954
52	Polr2g	6	4	1.5521	0.244954
53	Ube2i	6	2	-0.60136	0.251834
54	Rnf113a1	6	4	1.2474	0.251834
55	Las1l	6	5	0.95764	0.283438
56	Rcn2	6	2	-4.3129	0.299593
57	Olfr372	6	5	1.0495	0.312789

58	Anapc5	6	4	0.51609	0.312789
59	Efna1	6	5	1.4216	0.312789
60	Ankle2	6	2	-2.2344	0.312789
61	Fhod1	6	4	0.74743	0.327693
62	Cep95	6	4	0.98307	0.327693
63	Ppil1	6	4	1.2682	0.327693
64	Hspa5	6	4	1.2886	0.327693
65	Ssu72	6	4	1.3089	0.327693
66	Ubl4	6	3	-0.26721	0.332484
67	Spc24	6	4	0.97942	0.344884
68	Skiv2l2	5	3	0.16567	0.356082
69	Gm2913	4	3	1.8502	0.327693
70	Gm20806	4	3	1.433	0.327693
71	Olfr365	6	3	-1.2039	0.384065
72	Ubtf	6	4	1.2429	0.384065
73	Eif3g	6	5	1.0374	0.384065
74	Polr2a	6	4	1.5461	0.388581
75	Rpl13a	6	4	1.018	0.392632
76	Phf5a	6	2	-2.354	0.413493
77	Mtfr1	6	3	-1.593	0.416531
78	Nr2f2	6	3	-1.24	0.425803
79	Chaf1b	6	3	-0.24056	0.425803
80	Cdc5l	5	4	1.2642	0.420111
81	Fthl17	6	4	1.5252	0.443338
82	Rarb	6	3	0.46782	0.515863
83	Ddx19a	5	3	0.43625	0.499352
84	Tagln	6	3	0.45325	0.515863
85	Cdc23	6	4	0.49658	0.515863
86	Npr2	6	3	-0.52187	0.515863
87	Pola1	6	3	0.61449	0.515863
88	4921511M17Rik	6	5	0.6903	0.515863
89	Ercc6l	6	5	0.73047	0.542626
90	Ubap2	6	4	0.81856	0.542626
91	Rhox4a	5	3	1.4628	0.515863
92	D1Ertd622e	6	5	0.96386	0.549811
93	Cd97	6	4	0.85683	0.552788

94	mmu-mir-294	4	2	0.35367	0.515863
95	Mpp1	6	5	0.51831	0.564013
96	Cox6a1	6	2	-0.82412	0.564013
97	Cct3	6	3	0.21689	0.581198
98	Gm16381	5	3	0.3045	0.549811
99	Slmo2	6	4	0.96126	0.587283
100	Gin1	6	5	0.5558	0.590404

Table 8.1: Top 100 positively enriched genes from the "GFP/RiBi down" condition of the genome-wide CRISPR-Cas9 knockout screen in 3T3$^{\text{Fbl-GFP;Rpl18-RFP}}$ cells. The genes represent the top 100 scoring genes from the condition sorted for constant or high tRFP-PEST (RP promoter), but low EGFP-PEST (RiBi promoter) fluorescence intensity. The data were obtained using the bioinformatic tool MAGeCK [Li et al., 2014].

8.2.2 Bottom 100 positively enriched genes from the condition sorted for low expression of *Fbl*-driven EGFP-PEST and median to high expression of *Rpl18*-driven tRFP-PEST ("GFP down")

Rank	Gene	Number of sgRNAs	Good sgRNAs	LogFC	FDR
22411	Ythdf2	6	0	-5.1243	0.999906
22412	Ifna11	6	0	-5.0982	0.999906
22413	Dnm3	6	0	-5.1733	0.999906
22414	Trmt44	5	0	-4.0565	0.999906
22415	Olfr1058	6	0	-4.4388	0.999906
22416	B4galt1	6	0	-4.6496	0.999906
22417	mmu-mir-155	4	0	-4.9825	0.999906
22418	Rabgap1l	6	0	-4.7366	0.999906
22419	Pdc	6	0	-5.3124	0.999906
22420	Isx	6	0	-5.4684	0.999906
22421	NonTargetingControlGuideForMouse_0359	1	0	-6.786	0.999906
22422	Fam19a2	6	0	-4.6648	0.999906
22423	mmu-mir-344c	4	0	-5.0311	0.999906
22424	mmu-mir-344f	4	0	-4.8612	0.999906
22425	Slc35b4	6	0	-4.7655	0.999906
22426	Gcnt3	6	0	-4.958	0.999906
22427	Acads	6	0	-4.8646	0.999906
22428	Nlrp4c	6	0	-5.1246	0.999906

22429	NonTargetingControlGuide ForMouse_0360	1	0	-6.0227	0.999906
22430	Map9	6	0	-5.4881	0.999906
22431	Gng12	6	0	-4.7002	0.999906
22432	Wdr59	6	0	-4.9221	0.999906
22433	NonTargetingControlGuide ForMouse_0744	1	0	-1.9761	0.999906
22434	Syp	6	0	-4.1674	0.999906
22435	H60c	6	0	-4.5111	0.999906
22436	Ube4a	6	0	-5.3031	0.999906
22437	Srek1ip1	6	0	-5.1058	0.999906
22438	Ifi202b	6	0	-4.8396	0.999906
22439	Ltc4s	6	0	-4.1567	0.999906
22440	NonTargetingControlGuide ForMouse_0973	1	0	-5.0666	0.999906
22441	Kdm4b	6	0	-5.2353	0.999906
22442	Kcnmb1	6	0	-4.4878	0.999906
22443	4931409K22Rik	6	0	-4.4962	0.999906
22444	NonTargetingControlGuide ForMouse_0552	1	0	-7.4981	0.999906
22445	Pcdhb13	6	0	-4.7898	0.999906
22446	Zfp61	6	0	-4.6452	0.999906
22447	NonTargetingControlGuide ForMouse_0696	1	0	-6.5687	0.999906
22448	NonTargetingControlGuide ForMouse_0195	1	0	-5.3133	0.999906
22449	NonTargetingControlGuide ForMouse_0918	1	0	-3.9701	0.999906
22450	Vmn2r53	5	0	-5.1505	0.999906
22451	Sprr2e	6	0	-4.9783	0.999906
22452	Tmprss12	6	0	-5.196	0.999906
22453	C2cd2	6	0	-5.7212	0.999906
22454	mmu-mir-3100	4	0	-5.1505	0.999906
22455	Klhl10	6	0	-4.7713	0.999906
22456	Spr	6	0	-4.7637	0.999906
22457	Tas2r130	6	0	-4.5347	0.999906
22458	Tmem200c	6	0	-5.1254	0.999906

22459	mmu-mir-453	3	0	-5.9921	0.999906
22460	NonTargetingControlGuideForMouse_1000	1	0	-5.7792	0.999906
22461	Wdr61	6	0	-4.4555	0.999906
22462	Trpt1	6	0	-5.2879	0.999906
22463	Styxl1	6	0	-5.0645	0.999906
22464	Gsg2	6	0	-4.5772	0.999906
22465	NonTargetingControlGuideForMouse_0056	1	0	-6.0712	0.999906
22466	Metrnl	6	0	-4.2376	0.999906
22467	Tmcc1	6	0	-4.4152	0.999906
22468	Zfhx4	6	0	-5.1942	0.999906
22469	Rps10	6	0	-4.0304	0.999909
22470	Nr4a2	6	0	-3.535	0.999909
22471	NonTargetingControlGuideForMouse_0240	1	0	-4.6266	0.999909
22472	Cldn4	6	0	-5.3932	0.999909
22473	Pddc1	6	0	-5.1379	0.999909
22474	Olfr33	6	0	-4.8219	0.999909
22475	Gm7534	6	0	-3.5611	0.999909
22476	Cap2	6	0	-3.6735	0.999909
22477	Mrpl30	6	0	-5.0562	0.999909
22478	Gm13124	6	0	-5.4314	0.999909
22479	Ttc38	6	0	-4.1005	0.999909
22480	Gadl1	6	0	-5.7827	0.999909
22481	NonTargetingControlGuideForMouse_0897	1	0	-6.4904	0.999909
22482	1110051M20Rik	6	0	-4.9436	0.999909
22483	NonTargetingControlGuideForMouse_0074	1	0	-5.4718	0.999909
22484	Abcg1	6	0	-5.2178	0.999909
22485	Mrpl34	6	0	-5.0849	0.999909
22486	Lrp1b	6	0	-5.0789	0.999909
22487	Slc7a11	6	0	-5.1207	0.999909
22488	Mucl1	5	0	-5.4584	0.999909
22489	Trim7	6	0	-5.1067	0.999909

22490	NonTargetingControlGuide ForMouse_0082	1	0	-5.212	0.999909
22491	Pglyrp3	6	0	-3.9501	0.999909
22492	Pdgfrb	6	0	-5.2773	0.999909
22493	Wipi1	6	0	-5.0801	0.999909
22494	NonTargetingControlGuide ForMouse_0023	1	0	-3.005	0.999909
22495	Hs3st3a1	6	0	-5.0299	0.999909
22496	mmu-let-7f-2	4	0	-4.3354	0.999909
22497	Gfod2	5	0	-5.1986	0.999909
22498	Ambp	6	0	-5.3003	0.999909
22499	Slc17a3	6	0	-4.3235	0.999909
22500	Trim62	6	0	-5.6229	0.999909
22501	NonTargetingControlGuide ForMouse_0515	1	0	-5.9647	0.999909
22502	Vill	6	0	-4.7166	0.999909
22503	Ipo8	6	0	-4.8185	0.999909
22504	Gm11992	6	0	-4.5473	0.999909
22505	Gng2	6	0	-4.3051	0.999909
22506	NonTargetingControlGuide ForMouse_0854	1	0	-4.7797	0.999909
22507	NonTargetingControlGuide ForMouse_0476	1	0	-5.7786	0.999909
22508	Mfsd6l	6	0	-5.4354	0.999909
22509	Abhd4	6	0	-4.1982	0.999909
22510	mmu-mir-196a-2	4	0	-6.0016	0.999909
22511	NonTargetingControlGuide ForMouse_0404	1	0	-5.7544	0.999962

Table 8.2: Bottom 100 positively enriched genes from the "GFP/RiBi down" condition of the genome-wide CRISPR-Cas9 knockout screen in 3T3$^{\text{Fbl-GFP;Rpl18-RFP}}$ cells. The genes represent the bottom 100 scoring genes from the condition sorted for constant or high tRFP-PEST (RP promoter), but low EGFP-PEST (RiBi promoter) fluorescence intensity. The data were obtained using the bioinformatic tool MAGeCK [Li et al., 2014].

8.2.3 Top 100 positively enriched genes from the condition sorted for low expression of *Rpl18*-driven tRFP-PEST and median to high expression of *Fbl*-driven EGFP-PEST ("RFP down")

Rank	Gene	Number of sgRNAs	Good sgRNAs	LogFC	FDR
1	tRFP	4	4	7.014	0.002475
2	Adrm1	6	5	3.2209	0.002475
3	Depdc1a	6	5	1.119	0.222772
4	Vhl	5	5	0.89249	0.491337
5	H60b	5	2	-0.29663	0.757426
6	Olfr799	4	3	1.2109	0.948588
7	Pygb	6	5	0.77045	0.948588
8	E130012A19Rik	6	4	1.0993	0.948588
9	Vmn2r30	4	4	0.83429	0.948588
10	A230065H16Rik	4	2	-0.53777	0.948588
11	Champ1	6	2	-1.7772	0.948588
12	Sult4a1	6	3	0.68461	0.948588
13	Gm5544	6	4	1.0355	0.948588
14	Ppfibp1	6	3	-0.85748	0.948588
15	Syne1	6	3	-1.0322	0.948588
16	Adap1	6	3	0.55248	0.948588
17	Tha1	6	3	-0.83895	0.948588
18	Cwf19l2	6	3	-0.63088	0.948588
19	mmu-mir-3074-1	4	4	0.82883	0.948588
20	Gstm2	6	4	0.89832	0.948588
21	Abcb1a	6	4	1.0043	0.948588
22	Tbrg1	5	4	1.0004	0.948588
23	Lipc	6	4	1.151	0.948588
24	Mettl16	6	2	-4.6332	0.948588
25	Nipa2	6	4	1.0266	0.948588
26	Nedd1	6	3	-1.1985	0.948588
27	Mrpl53	6	4	0.85239	0.948588
28	Lmf1	5	1	-3.2125	0.948588
29	Hoxd9	5	3	1.4486	0.948588
30	Fbxo25	6	2	-2.3488	0.948588

31	Eif4ebp1	6	2	-1.2146	0.948588
32	Itih1	5	2	-3.7901	0.948588
33	Egfl6	5	4	0.84058	0.948588
34	Ltbp1	6	4	0.99053	0.948588
35	Rnf8	6	2	-1.2587	0.948588
36	Cyp2g1	6	4	0.79385	0.948588
37	NonTargetingControlGuideForMouse_0973	1	1	2.4489	0.948588
38	Rbm3	6	4	1.1529	0.948588
39	Trmt10a	6	2	-1.8231	0.948588
40	Wrnip1	6	2	-1.8557	0.948588
41	Fzd7	6	4	1.0052	0.948588
42	mmu-mir-219c	4	3	1.4952	0.948588
43	Gm6484	6	4	0.78966	0.948588
44	Gpsm1	5	1	-3.0541	0.948588
45	Olfr372	6	2	-4.0983	0.948588
46	Mid2	6	3	-1.3226	0.948588
47	Prrc2b	6	3	0.49689	0.948588
48	Cdk5r2	6	1	-3.7739	0.948588
49	Pias4	6	4	0.68036	0.948588
50	Gm10094	6	3	-1.6674	0.948588
51	Grina	6	3	-1.8608	0.948588
52	Gm1647	6	3	0.61477	0.948588
53	Otud6a	6	4	0.69511	0.948588
54	Tbc1d8	6	2	-1.4508	0.948588
55	Hoxa1	6	2	-2.8213	0.948588
56	Crat	6	4	0.96703	0.948588
57	Zfp574	6	3	-0.01928	0.948588
58	Gstm7	6	3	-0.14144	0.948588
59	Rabac1	6	3	-0.44175	0.948588
60	Srp9	5	2	-2.8074	0.948588
61	Tspan12	6	2	-4.2956	0.948588
62	Spata17	6	3	-0.85749	0.948588
63	Supv3l1	6	4	1.1149	0.948588
64	Cdh16	6	1	-3.6577	0.948588
65	Hist1h4f	4	3	1.4081	0.948588

66	Cd38	6	4	0.66886	0.948588
67	Rptor	6	2	-1.9717	0.948588
68	Stk11	6	3	-0.51417	0.948588
69	Fam214a	6	4	0.6064	0.948588
70	2610018G03Rik	6	2	-1.9401	0.948588
71	Olfr690	6	3	-1.7201	0.948588
72	Tipin	6	2	-2.1338	0.948588
73	Nfatc2	5	3	0.95364	0.948588
74	Calm4	5	4	0.92262	0.948588
75	Ubr1	6	1	-4.1845	0.948588
76	Slc34a3	6	3	0.12088	0.948588
77	BC049730	6	2	-3.1144	0.948588
78	Nlrp9b	6	3	-0.97238	0.948588
79	Tex26	6	3	-0.78332	0.948588
80	Cbfa2t2	6	3	-0.4647	0.948588
81	Lrrc20	6	4	0.53527	0.948588
82	Nrxn1	6	3	0.3034	0.948588
83	Calm3	6	3	-1.3108	0.948588
84	Rwdd2b	6	4	0.74128	0.948588
85	Cxxc5	6	2	-2.9154	0.948588
86	Phex	6	3	-0.27708	0.948588
87	Lage3	6	4	0.52258	0.948588
88	Ace2	6	4	0.6511	0.948588
89	Ilvbl	6	1	-4.3571	0.948588
90	Prickle2	6	2	-2.3236	0.948588
91	Pigk	6	3	-1.0504	0.948588
92	Olfr145	5	3	0.82695	0.948588
93	Cd151	6	4	0.71885	0.948588
94	Tmem55a	6	4	0.89227	0.948588
95	Olfr993	6	1	-4.5405	0.948588
96	Gm15080	5	4	0.9781	0.948588
97	1700018B08Rik	6	1	-3.2848	0.948588
98	Ncapg	6	4	0.80771	0.948588
99	Gins1	6	4	0.6535	0.948588

100	Plcxd3	6	4	0.51967	0.948588

Table 8.3: Top 100 positively enriched genes from the "RFP/RP down" condition of the genome-wide CRISPR-Cas9 knock-out screen in 3T3$^{Fbl\text{-}GFP;Rpl18\text{-}RFP}$ cells. The genes represent the top 100 scoring genes from the condition sorted for constant or high EGFP-PEST (RiBi promoter), but low tRFP-PEST (RP promoter) fluorescence intensity. The data were obtained using the bioinformatic tool MAGeCK [Li et al., 2014].

8.2.4 Bottom 100 positively enriched genes from the condition sorted for low expression of *Rpl18*-driven tRFP-PEST and median to high expression of *Fbl*-driven EGFP-PEST ("RFP down")

Rank	Gene	Number of sgRNAs	Good sgRNAs	LogFC	FDR
22411	NonTargetingControlGuideForMouse_0706	1	0	-5.9941	0.999962
22412	Smco1	6	0	-4.9006	0.999962
22413	Epn2	6	0	-5.2318	0.999962
22414	Ogdhl	6	0	-5.0567	0.999962
22415	NonTargetingControlGuideForMouse_0220	1	0	-5.6111	0.999962
22416	1110001J03Rik	6	0	-4.7873	0.999962
22417	Rdh19	6	0	-5.4259	0.999962
22418	NonTargetingControlGuideForMouse_0129	1	0	-7.4636	0.999962
22419	Slc12a2	5	0	-5.3219	0.999962
22420	NonTargetingControlGuideForMouse_0074	1	0	-7.4721	0.999962
22421	NonTargetingControlGuideForMouse_0082	1	0	-4.8772	0.999962
22422	Olfr693	6	0	-4.4473	0.999962
22423	A430105I19Rik	6	0	-5.2032	0.999962
22424	Chst10	6	0	-5.3866	0.999962
22425	Adi1	6	0	-4.9869	0.999962
22426	Acacb	6	0	-5.6172	0.999962
22427	NonTargetingControlGuideForMouse_0463	1	0	-6.5823	0.999962
22428	Rpp25	6	0	-4.9237	0.999962
22429	Prlr	6	0	-4.8116	0.999962

22430	6030458C11Rik	6	0	-4.786	0.999962
22431	Atp6v0d2	5	0	-4.3011	0.999962
22432	Ube2cbp	6	0	-5.6374	0.999962
22433	NonTargetingControlGuideForMouse_0746	1	0	-6.0981	0.999962
22434	Dio1	6	0	-5.0004	0.999962
22435	Uckl1	6	0	-5.4056	0.999962
22436	Apex1	6	0	-5.2485	0.999962
22437	Herpud1	6	0	-5.4893	0.999962
22438	NonTargetingControlGuideForMouse_0410	1	0	-6.6307	0.999962
22439	Gm9573	6	0	-4.5107	0.999962
22440	Smoc1	6	0	-5.5586	0.999962
22441	Slc7a15	6	0	-5.067	0.999962
22442	Fbxo46	5	0	-5.2394	0.999962
22443	Ifnl2	6	0	-5.4898	0.999962
22444	Nudt4	6	0	-5.2459	0.999962
22445	Zfp185	6	0	-4.7627	0.999962
22446	Lrrn3	5	0	-4.4982	0.999962
22447	Csn3	6	0	-5.132	0.999962
22448	Ripk3	6	0	-4.6111	0.999962
22449	NonTargetingControlGuideForMouse_0834	1	0	-4.9577	0.999962
22450	Mfsd7c	6	0	-4.7585	0.999962
22451	Tnfsf10	6	0	-5.3477	0.999962
22452	NonTargetingControlGuideForMouse_0828	1	0	-6.5413	0.999962
22453	Prss36	6	0	-5.6003	0.999962
22454	Ambn	6	0	-5.1403	0.999962
22455	Gm15097	2	0	-5.5288	0.999962
22456	NonTargetingControlGuideForMouse_0267	1	0	-5.4677	0.999962
22457	Las1l	6	0	-5.0968	0.999962
22458	NonTargetingControlGuideForMouse_0693	1	0	-6.7065	0.999962
22459	NonTargetingControlGuideForMouse_0515	1	0	-6.1604	0.999962

22460	Zfp605	6	0	-4.8766	0.999962
22461	Atp13a5	5	0	-5.4866	0.999962
22462	9930104L06Rik	6	0	-5.4858	0.999962
22463	Ppp1r21	6	0	-5.3493	0.999962
22464	Rnase13	6	0	-5.2551	0.999962
22465	Fnta	6	0	-5.0638	0.999962
22466	Rnf126	6	0	-5.0563	0.999962
22467	NonTargetingControlGuide ForMouse_0721	1	0	-6.7384	0.999962
22468	Csf2rb	6	0	-5.3476	0.999962
22469	Acp2	6	0	-5.3532	0.999962
22470	Actr8	6	0	-5.6769	0.999962
22471	NonTargetingControlGuide ForMouse_0097	1	0	-5.8848	0.999962
22472	Ccdc54	6	0	-4.9351	0.999962
22473	Tex15	6	0	-5.026	0.999962
22474	Suox	6	0	-5.2677	0.999962
22475	NonTargetingControlGuide ForMouse_0748	1	0	-6.2846	0.999962
22476	Porcn	6	0	-4.8327	0.999962
22477	Eogt	6	0	-5.7467	0.999962
22478	NonTargetingControlGuide ForMouse_0788	1	0	-6.0763	0.999962
22479	Grpel1	6	0	-5.3494	0.999962
22480	NonTargetingControlGuide ForMouse_0268	1	0	-6.0908	0.999962
22481	Tctn1	6	0	-5.3057	0.999962
22482	Gm7257	6	0	-5.1375	0.999962
22483	NonTargetingControlGuide ForMouse_0476	1	0	-6.7071	0.999962
22484	Olfr1411	6	0	-5.2829	0.999962
22485	mmu-mir-181d	4	0	-5.5033	0.999962
22486	Fam160a1	6	0	-5.5483	0.999962
22487	Ndufs8	6	0	-5.5359	0.999962
22488	Pik3ca	6	0	-5.5633	0.999962
22489	Stra13	6	0	-5.5609	0.999962
22490	Cstl1	6	0	-5.4682	0.999962

22491	Zfp444	6	0	-5.6084	0.999962
22492	NonTargetingControlGuide ForMouse_0409	1	0	-6.0211	0.999962
22493	Efcab14	6	0	-5.2927	0.999962
22494	Rassf4	6	0	-5.55	0.999962
22495	N4bp2l1	6	0	-5.085	0.999962
22496	Krt10	6	0	-5.7029	0.999962
22497	Lce1m	5	0	-5.4961	0.999962
22498	Olfr1258	6	0	-5.4836	0.999962
22499	Rpl10l	6	0	-4.4159	0.999962
22500	Rbak	6	0	-5.3658	0.999962
22501	mmu-mir-1298	4	0	-5.7872	0.999962
22502	Btnl9	5	0	-5.1059	0.999962
22503	NonTargetingControlGuide ForMouse_0108	1	0	-6.134	0.999962
22504	Cldn18	6	0	-5.5825	0.999962
22505	0610009O20Rik	6	0	-5.2927	0.999962
22506	Fah	6	0	-5.8803	0.999962
22507	NonTargetingControlGuide ForMouse_0988	1	0	-6.2241	0.999962
22508	NonTargetingControlGuide ForMouse_0994	1	0	-7.042	0.999962
22509	mmu-mir-7076	4	0	-5.5263	0.999962
22510	NonTargetingControlGuide ForMouse_0611	1	0	-6.2506	0.999962
22511	Pkig	6	0	-5.5039	0.999962

Table 8.4: Bottom 100 positively enriched genes from the "RFP/RP down" condition of the genome-wide CRISPR-Cas9 knockout screen in 3T3$^{\text{Fbl-GFP;Rpl18-RFP}}$ cells. The genes represent the bottom 100 scoring genes from the condition sorted for constant or high EGFP-PEST (RiBi promoter), but low tRFP-PEST (RP promoter) fluorescence intensity. The data were obtained using the bioinformatic tool MAGeCK [Li et al., 2014].

8.2.5 Top 100 positively enriched genes from the condition sorted for high expression of *Rpl18*-driven tRFP-PEST and high expression of *Fbl*-driven EGFP-PEST ("Both up")

Rank	Gene	Number of sgRNAs	Good sgRNAs	LogFC	FDR
1	Psmd6	6	5	2.7237	0.000825
2	Psmc5	6	5	2.8954	0.000825
3	Psmd11	5	3	2.7376	0.000825
4	Psmc4	6	5	2.313	0.000825
5	Pabpn1	5	5	2.1401	0.000825
6	Psmb4	6	5	2.1495	0.000825
7	Psmb1	6	4	1.7014	0.021924
8	Psmb7	6	2	-1.7966	0.025371
9	Psmd3	6	3	0.73305	0.026953
10	Sap18	6	5	1.2639	0.027228
11	Zcchc11	6	4	2.2489	0.033753
12	Psma4	6	5	1.7334	0.034653
13	Ewsr1	5	4	1.3086	0.034653
14	Psmb6	6	3	0.52107	0.04703
15	Psmd14	5	4	1.9102	0.065017
16	Kcnk9	5	3	1.6672	0.08323
17	Snip1	6	4	1.1429	0.138905
18	Cdc73	6	3	0.58369	0.179043
19	Alyref2	6	4	1.1187	0.22698
20	Ankrd28	6	5	1.0975	0.235599
21	Cercam	6	5	1.0908	0.235599
22	Tmem159	6	3	0.17253	0.270125
23	mmu-mir-6376	4	3	1.4368	0.22698
24	Atg4b	6	5	0.84943	0.276657
25	Olfr1424	6	4	1.0803	0.276657
26	Psmc3	6	5	1.4876	0.276657
27	Npm1	6	5	1.178	0.284983
28	Wdr5	6	4	1.0464	0.284983
29	Psmd1	6	4	1.3321	0.284983
30	Ttc19	6	4	1.2261	0.284983

31	Ifna1	6	5	0.95084	0.312318
32	Ppil1	6	3	0.55594	0.312318
33	Psmd12	5	3	1.3753	0.312318
34	Gm10058	5	5	0.7676	0.312318
35	Psmc2	6	3	0.32564	0.363649
36	Wdr38	6	5	0.83332	0.377174
37	Psma2	6	2	0.020425	0.377174
38	Ifna2	6	4	1.2893	0.380797
39	Ccna2	6	3	-1.4688	0.410891
40	Ifitm5	6	4	1.207	0.484545
41	Col1a1	6	5	0.94798	0.490924
42	mmu-mir-31	4	2	0.93683	0.470421
43	Mmp15	6	1	-2.3575	0.538683
44	Psmd8	6	3	0.86735	0.568744
45	Plcb1	6	3	0.39233	0.610525
46	Rtf1	6	4	0.4396	0.610525
47	Psmb5	6	2	0.024449	0.642406
48	Klf16	6	3	-0.2347	0.654356
49	Rbm25	6	3	-0.07741	0.654356
50	Khdc1a	6	5	0.87144	0.735815
51	Nt5e	6	4	1.0248	0.739756
52	Meis3	6	5	0.79514	0.739756
53	Zfp595	6	2	-2.6466	0.739756
54	Prpf31	5	4	0.80728	0.738931
55	Rplp2	6	3	-0.41841	0.739756
56	Sfrs18	6	3	-0.70586	0.739756
57	Nfe2l1	6	3	-0.70078	0.739756
58	Lyrm9	6	3	0.29421	0.739756
59	Tada2b	6	5	0.49974	0.739756
60	Rnasek	6	3	-1.2857	0.739756
61	Srsf1	6	2	-2.1922	0.739756
62	Banf1	6	5	0.43738	0.740249
63	Fap	6	4	0.85299	0.792006
64	Rap1a	5	4	0.82208	0.739756
65	5830403L16Rik	6	4	0.56311	0.792006
66	mmu-mir-539	4	2	0.18213	0.739756

67	Hoxd3	6	3	0.12831	0.801478
68	Sp2	6	5	0.52156	0.804422
69	Cars2	6	3	0.59168	0.804422
70	D830031N03Rik	6	4	1.1015	0.804422
71	Sec14l2	6	3	0.72283	0.804422
72	Plekhj1	6	4	0.98037	0.804422
73	Myl1	6	2	-1.7622	0.804422
74	Rcor3	6	3	0.63784	0.813379
75	Snrnp70	6	4	1.4151	0.831742
76	Olfr1412	6	5	0.36781	0.831742
77	Kcnk4	6	3	0.6016	0.831742
78	Nupl2	6	4	1.0729	0.831742
79	Olfr1167	6	2	-2.0893	0.831742
80	Nudcd2	6	3	0.34785	0.831742
81	Bglap2	6	4	0.92838	0.831742
82	Taf4a	6	2	-2.8255	0.844205
83	1110059E24Rik	6	3	-0.048442	0.844347
84	Tmem59	6	4	0.73944	0.878058
85	mmu-mir-124-1	4	4	0.7182	0.831742
86	Renbp	6	3	0.13416	0.890193
87	Spin2d	2	1	0.074594	0.71025
88	Gpr156	6	5	0.36734	0.890193
89	Npc2	6	3	-0.60222	0.890193
90	Plcz1	6	2	-3.2479	0.890193
91	Olfr1475	6	5	0.46095	0.890193
92	Mapkap1	6	3	-0.40038	0.890193
93	Dzank1	6	3	0.32818	0.890193
94	Itsn1	6	5	0.69652	0.890193
95	Gng7	6	4	0.81488	0.890193
96	Spesp1	6	2	-0.2362	0.890193
97	Olfr736	6	5	0.46696	0.890193
98	Lrrc6	6	3	-0.98133	0.890193
99	Notch4	6	4	0.5817	0.890193

100	Bpifa1	6	2	-1.9557	0.890193

Table 8.5: Top 100 positively enriched genes from the "Both up" condition of the genome-wide CRISPR-Cas9 knockout screen in 3T3$^{\text{Fbl-GFP;Rpl18-RFP}}$ cells. The genes represent the top 100 scoring genes from the condition sorted for high EGFP-PEST (RiBi promoter) and high tRFP-PEST (RP promoter) fluorescence intensity. The data were obtained using the bioinformatic tool MAGeCK [Li et al., 2014].

8.2.6 Bottom 100 positively enriched genes from the condition sorted for high expression of *Rpl18*-driven tRFP-PEST and high expression of *Fbl*-driven EGFP-PEST ("Both up")

Rank	Gene	Number of sgRNAs	Good sgRNAs	LogFC	FDR
22411	NonTargetingControlGuide ForMouse_0748	1	0	-2,2957	1
22412	Slc37a3	6	0	-4,8899	1
22413	Ccdc74a	6	0	-3,6086	1
22414	1700019A02Rik	6	0	-4,1202	1
22415	Rnase10	6	0	-4,8882	1
22416	Brs3	6	0	-4,976	1
22417	NonTargetingControlGuide ForMouse_0693	1	0	-2,5723	1
22418	NonTargetingControlGuide ForMouse_0117	1	0	-7,0469	1
22419	Ang4	6	0	-4,4574	1
22420	Vmn1r175	6	0	-4,5162	1
22421	Klk1b4	6	0	-2,4728	1
22422	Adamts13	6	0	-4,6671	1
22423	Chst13	6	0	-4,5769	1
22424	Sytl2	6	0	-3,9649	1
22425	Olfr643	6	0	-3,5482	1
22426	NonTargetingControlGuide ForMouse_0359	1	0	-5,035	1
22427	4833420G17Rik	6	0	-4,4019	1
22428	Bnip3l	6	0	-4,6811	1
22429	Ptk7	6	0	-4,7098	1
22430	NonTargetingControlGuide ForMouse_0399	1	0	-6,0301	1

22431	Tas2r109	4	0	-4,2555	1
22432	Ccdc8	6	0	-3,9668	1
22433	Nr3c1	6	0	-4,4749	1
22434	NonTargetingControlGuide ForMouse_0503	1	0	-5,4603	1
22435	Rbms3	6	0	-3,3653	1
22436	Fbxo43	6	0	-4,9645	1
22437	Zfp281	5	0	-4,7164	1
22438	NonTargetingControlGuide ForMouse_0644	1	0	-7,0943	1
22439	Ech1	6	0	-5,2078	1
22440	NonTargetingControlGuide ForMouse_0514	1	0	-7,1039	1
22441	Gm3404	1	0	-6,2132	1
22442	F3	6	0	-5,5538	1
22443	NonTargetingControlGuide ForMouse_0982	1	0	-7,127	1
22444	Olfr770	6	0	-4,5917	1
22445	Hyal2	6	0	-4,4443	1
22446	Mtmr6	6	0	-4,4908	1
22447	Vmn1r85	5	0	-5,1952	1
22448	C2cd3	6	0	-3,9238	1
22449	mmu-mir-7094-1	4	0	-5,184	1
22450	Tcea2	6	0	-5,0125	1
22451	mmu-mir-669n	4	0	-5,3203	1
22452	Mcm2	5	0	-4,8233	1
22453	NonTargetingControlGuide ForMouse_0038	1	0	-5,7321	1
22454	C3ar1	6	0	-3,3323	1
22455	Ttc8	6	0	-3,5779	1
22456	Nim1	6	0	-5,3675	1
22457	Clns1a	6	0	-2,6103	1
22458	Cbs	6	0	-4,8828	1
22459	Gm5416	6	0	-4,6937	1
22460	Eif2b3	5	0	-5,4421	1
22461	Crmp1	6	0	-5,1083	1
22462	Adra1d	5	0	-5,1492	1

22463	Xndr-trpc2	6	0	-4,0907	1
22464	Scgb3a1	6	0	-4,8004	1
22465	NonTargetingControlGuideForMouse_0394	1	0	-6,3043	1
22466	Rras2	6	0	-5,6724	1
22467	Sprn	6	0	-4,0795	1
22468	Tbx15	6	0	-4,8028	1
22469	Gng12	6	0	-4,3982	1
22470	Hk1	6	0	-5,2756	1
22471	Myo5b	6	0	-4,8078	1
22472	Ckap2	6	0	-4,7742	1
22473	Styxl1	6	0	-4,9172	1
22474	Cnot3	6	0	-3,655	1
22475	Pcsk2	6	0	-4,6761	1
22476	Bai1	6	0	-4,7678	1
22477	NonTargetingControlGuideForMouse_0090	1	0	-7,2657	1
22478	Dmc1	5	0	-4,9196	1
22479	Ankmy1	6	0	-4,8316	1
22480	Trappc11	6	0	-4,9372	1
22481	Adi1	6	0	-2,7168	1
22482	mmu-mir-6540	4	0	-5,2039	1
22483	NonTargetingControlGuideForMouse_0589	1	0	-3,533	1
22484	EGFP	3	0	-5,4882	1
22485	Exosc10	6	0	-4,9906	1
22486	Gm13124	6	0	-5,3532	1
22487	St6galnac5	6	0	-5,2373	1
22488	Olfr961	6	0	-4,7219	1
22489	Krt4	6	0	-5,241	1
22490	Nono	6	0	-4,3444	1
22491	Vmn2r86	6	0	-5,1194	1
22492	Klhl14	6	0	-4,8015	1
22493	Mid1	6	0	-4,738	1
22494	AW551984	5	0	-5,6221	1
22495	Wipi1	6	0	-4,0394	1
22496	Olfr461	6	0	-5,2129	1

22497	Atp2a2	5	0	-5,1492	1
22498	Tmprss11g	6	0	-4,6521	1
22499	Anks6	6	0	-5,25	1
22500	Vmn2r94	6	0	-4,9861	1
22501	Gtf2a1	6	0	-5,146	1
22502	NonTargetingControlGuideForMouse_0807	1	0	-5,0015	1
22503	NonTargetingControlGuideForMouse_0717	1	0	-6,6148	1
22504	Olfr281	6	0	-5,4971	1
22505	NonTargetingControlGuideForMouse_0773	1	0	-7,76	1
22506	Trim47	6	0	-5,2003	1
22507	Idh3g	6	0	-5,5977	1
22508	Bhlhe40	6	0	-5,3385	1
22509	Olfr317	6	0	-3,9748	1
22510	Olfr118	6	0	-5,2748	1
22511	tRFP	4	0	-6,1336	1

Table 8.6: Bottom 100 positively enriched genes from the "Both up" condition of the genome-wide CRISPR-Cas9 knockout screen in 3T3$^{\text{Fbl-GFP;Rpl18-RFP}}$ cells. The genes represent the bottom 100 scoring genes from the condition sorted for high EGFP-PEST (RiBi promoter) and high tRFP-PEST (RP promoter) fluorescence intensity. The data were obtained using the bioinformatic tool MAGeCK [Li et al., 2014].

8.2.7 Top 100 positively enriched genes from the condition sorted for low expression of *Rpl18*-driven tRFP-PEST and low expression of *Fbl*-driven EGFP-PEST ("Both down")

Rank	Gene	Number of sgRNAs	Good sgRNAs	LogFC	FDR
1	Recql4	6	4	0.70734	0.909674
2	Cdh13	6	3	0.11177	0.909674
3	Lrp5	6	5	0.69146	0.909674
4	Senp1	6	3	0.44218	0.909674
5	4930432M17Rik	6	3	0.1137	0.909674
6	Itga11	6	6	0.45477	0.909674
7	Olfr585	6	5	0.48003	0.909674
8	Uqcrc1	6	3	0.34867	0.909674

9	Olfr186	6	5	1.1352	0.909674
10	Fgf1	6	3	0.55612	0.909674
11	Ttll11	6	3	0.16918	0.909674
12	Slc17a1	6	3	0.22087	0.909674
13	Zbtb24	6	2	-0.041356	0.909674
14	Chst7	6	5	0.76199	0.909674
15	Olfr126	5	4	0.66091	0.909674
16	Commd10	6	3	0.045828	0.909674
17	Sgcg	6	4	0.38126	0.909674
18	Tmem57	6	4	0.34791	0.909674
19	Wdr11	6	3	0.3805	0.909674
20	Prkd1	6	6	0.59261	0.909674
21	Tmem108	6	6	0.32829	0.909674
22	Fmr1	6	1	-0.49756	0.909674
23	Pinlyp	6	6	0.3397	0.909674
24	mmu-mir-669d-2	4	3	0.67509	0.909674
25	Zfp608	5	5	0.75495	0.909674
26	5031439G07Rik	6	5	0.60846	0.909674
27	Tfip11	6	6	0.36569	0.909674
28	Ciita	6	4	0.60545	0.909674
29	Psmb9	6	6	0.40645	0.909674
30	Dazap1	6	2	-0.25523	0.909674
31	Slc35a1	5	3	0.40577	0.909674
32	Gnao1	6	5	0.97102	0.909674
33	Adcyap1	6	4	0.24283	0.909674
34	Frmd4a	5	5	0.41057	0.909674
35	Ufsp2	6	5	0.61477	0.909674
36	Gadd45a	6	5	0.58386	0.909674
37	Nlrc5	6	5	0.76799	0.909674
38	Gemin7	6	3	0.37093	0.909674
39	Art5	6	6	0.56059	0.909674
40	Hspg2	6	5	0.39629	0.909674
41	Use1	6	6	0.22406	0.909674
42	Aprt	6	5	0.65924	0.909674
43	Atp8b5	6	3	-0.041655	0.909674
44	Olfr586	6	6	0.4721	0.909674

45	Olfr632	6	3	0.24955	0.909674
46	Gtf2i	6	2	-0.21185	0.909674
47	Hyal6	6	5	0.61566	0.909674
48	Exo1	6	3	-0.10707	0.909674
49	Olfr656	5	3	0.74538	0.909674
50	Ppih	6	3	0.068643	0.909674
51	Cyp2c69	4	4	0.47593	0.909674
52	Pcdhb7	6	4	0.62089	0.909674
53	Olfr1322	5	3	0.96892	0.909674
54	Samd11	6	5	0.49157	0.909674
55	Amdhd2	6	2	-0.19075	0.909674
56	mmu-mir-145b	4	3	0.68264	0.909674
57	Smpd3	5	5	0.48121	0.909674
58	Tacstd2	6	1	-0.27145	0.940823
59	Kcns3	6	5	0.47008	0.940823
60	Ovol1	6	2	0.079976	0.940823
61	Arhgap21	5	5	0.48383	0.909674
62	1700037C18Rik	6	3	-0.065917	0.940823
63	Crct1	6	3	0.33569	0.952195
64	Ropn1l	6	2	-0.3532	0.952195
65	Robo3	6	4	0.63658	0.952195
66	Akap13	6	3	0.39735	0.952195
67	Xkrx	6	3	0.2347	0.952195
68	mmu-mir-7216	4	4	0.75666	0.909674
69	Ankrd63	6	5	0.68054	0.952195
70	F2	6	3	0.23403	0.952195
71	Tdh	6	2	0.053635	0.952195
72	Maged2	5	3	0.41711	0.952195
73	Anks1b	6	3	0.21755	0.952195
74	Aars2	6	5	0.46935	0.952195
75	Mtfmt	6	4	0.56096	0.952195
76	Mef2c	6	3	-0.28117	0.952195
77	Ccni	6	4	0.63755	0.952195
78	Mcc	6	4	0.53492	0.952195
79	Fam71a	6	3	0.28653	0.952195
80	Edem2	6	2	0.0062623	0.952195

81	Tmed8	6	4	0.64098	0.952195
82	Psmb11	6	4	0.64814	0.952195
83	Igfbp2	6	4	0.49136	0.952195
84	Tfe3	6	3	0.33147	0.952195
85	Lce1m	5	3	0.47675	0.952195
86	Vmn1r52	6	2	-0.59474	0.952195
87	BC005537	6	2	-0.0067918	0.952195
88	Pard6b	6	3	0.10928	0.952195
89	Ptprq	6	3	0.26266	0.952195
90	Hhipl1	6	5	0.64921	0.952195
91	U2af1l4	6	5	0.64964	0.952195
92	Slc15a3	6	4	0.58774	0.952195
93	Rfx7	6	1	-0.48113	0.952195
94	Ibsp	6	2	-0.10062	0.952195
95	Agpat6	6	5	0.53087	0.952195
96	Vkorc1	6	5	0.60307	0.952195
97	Zfp354b	6	3	0.21753	0.952195
98	Slx1b	5	3	0.62477	0.952195
99	Kcnj11	6	4	0.52304	0.952195
100	Bsdc1	6	2	-0.17452	0.952195

Table 8.7: Top 100 positively enriched genes from the "Both down" condition of the genome-wide CRISPR-Cas9 knockout screen in 3T3$^{\text{Fbl-GFP;Rpl18-RFP}}$ cells. The genes represent the top 100 scoring genes from the condition sorted for low EGFP-PEST (RiBi promoter) and low tRFP-PEST (RP promoter) fluorescence intensity. The data were obtained using the bioinformatic tool MAGeCK [Li et al., 2014].

8.2.8 Bottom 100 positively enriched genes from the condition sorted for low expression of *Rpl18*-driven tRFP-PEST and low expression of *Fbl*-driven EGFP-PEST ("Both down")

Rank	Gene	Number of sgRNAs	Good sgRNAs	LogFC	FDR
22411	Olfr1505	6	0	-1.0209	0.99983
22412	Ddb2	6	0	-0.99512	0.99983
22413	Tinf2	6	0	-1.3086	0.99983
22414	E2f3	6	0	-0.96979	0.99983
22415	Cenpe	6	0	-1.327	0.99983
22416	mmu-mir-378a	4	0	-1.7996	0.99983

22417	Fxr1	6	0	-0.88175	0.99983
22418	Wisp2	6	0	-1.8662	0.99983
22419	Gal	6	0	-0.91792	0.99983
22420	Clpx	6	0	-0.59877	0.99983
22421	mmu-mir-496b	4	0	-1.5571	0.99983
22422	mmu-mir-880	4	0	-0.84979	0.99983
22423	Atraid	6	0	-0.67972	0.99983
22424	Kif11	6	0	-0.92094	0.99983
22425	Lhx1	6	0	-1.6046	0.99983
22426	Aadat	6	0	-1.2891	0.99983
22427	mmu-mir-6374	4	0	-1.834	0.99983
22428	Mreg	6	0	-1.2957	0.99983
22429	mmu-mir-7044	4	0	-1.8696	0.99983
22430	Cnot1	6	0	-1.0655	0.99983
22431	Ceacam20	6	0	-0.79475	0.99983
22432	Zcchc8	6	0	-1.3624	0.99983
22433	Trappc2	6	0	-0.96862	0.99983
22434	Mms19	6	0	-0.37726	0.99983
22435	Adam6a	5	0	-0.50041	0.99983
22436	Aamp	5	0	-0.89538	0.99983
22437	Rnf40	6	0	-0.71186	0.99983
22438	mmu-mir-5620	4	0	-1.35	0.99983
22439	Nop10	5	0	-0.88113	0.99983
22440	Dact3	6	0	-0.78431	0.99983
22441	BC051142	6	0	-1.2212	0.99983
22442	Olfr39	5	0	-1.6301	0.99983
22443	Wdr3	5	0	-1.6301	0.99983
22444	Rora	5	0	-1.2094	0.99983
22445	Ift81	6	0	-0.83001	0.99983
22446	Wfdc15b	6	0	-0.90945	0.99983
22447	Tmem176a	6	0	-0.78831	0.99983
22448	Fam219b	6	0	-0.86908	0.99983
22449	Iffo1	6	0	-2.3385	0.99983
22450	1110034G24Rik	6	0	-1.1677	0.99983
22451	Stox1	6	0	-1.2327	0.99983

22452	NonTargetingControlGuide ForMouse_0805	1	0	-1.6037	0.99983
22453	Vmn1r132	1	0	-3.3536	0.99983
22454	Lpar1	6	0	-1.4408	0.99983
22455	Fam98a	5	0	-0.77783	0.99983
22456	Hormad2	6	0	-0.93365	0.99983
22457	Armc9	6	0	-0.92282	0.99983
22458	Mill1	6	0	-0.69736	0.99983
22459	1110032A03Rik	6	0	-0.71492	0.99983
22460	Rps23	5	0	-0.87625	0.99983
22461	Stfa2	4	0	-2.477	0.99983
22462	Zfp433	6	0	-1.1565	0.99983
22463	Npc2	6	0	-1.3009	0.99983
22464	Haus5	6	0	-1.361	0.99983
22465	Tsr3	6	0	-1.1436	0.99983
22466	Olfr1260	6	0	-0.58782	0.99983
22467	Ceacam13	6	0	-1.4615	0.99983
22468	mmu-mir-6344	4	0	-2.0348	0.99983
22469	Coprs	6	0	-0.81102	0.99983
22470	NonTargetingControlGuide ForMouse_0366	1	0	-1.4611	0.99983
22471	Soga3	6	0	-0.84137	0.99983
22472	Ptprj	6	0	-1.0124	0.99983
22473	Echdc2	6	0	-0.78142	0.99983
22474	NonTargetingControlGuide ForMouse_0552	1	0	-1.1058	0.99983
22475	Eef1a1	6	0	-1.0431	0.99983
22476	Gm12886	6	0	-0.44751	0.99983
22477	Rhox1	6	0	-1.0737	0.99983
22478	Tfam	6	0	-1.6223	0.99983
22479	4932418E24Rik	6	0	-0.79547	0.99983
22480	mmu-mir-1906-2	3	0	-1.2381	0.99983
22481	Zfp52	6	0	-0.55944	0.99983
22482	Ttll5	6	0	-1.6524	0.99983
22483	Olfr295	6	0	-1.3245	0.99983
22484	Rac1	6	0	-0.70094	0.99983
22485	Pbld1	6	0	-1.9397	0.99983

22486	Gpr45	6	0	-0.81037	0.99983
22487	Lilra5	6	0	-2.3024	0.99983
22488	Tpx2	6	0	-1.3426	0.99983
22489	Sgtb	6	0	-1.6301	0.99983
22490	mmu-mir-674	4	0	-0.83712	0.99983
22491	Reep6	5	0	-0.95339	0.99983
22492	Ptbp2	6	0	-1.4049	0.99983
22493	Pisd	6	0	-0.90653	0.99983
22494	Dlc1	6	0	-0.96084	0.99983
22495	Spice1	6	0	-1.0827	0.99983
22496	Olfr330	6	0	-1.3314	0.99983
22497	Aipl1	6	0	-0.97645	0.99983
22498	Mms22l	6	0	-0.83212	0.99983
22499	Rps19	6	0	-1.8552	0.99983
22500	NonTargetingControlGuide ForMouse_0575	1	0	-1.1086	0.99983
22501	Pgk1	6	0	-1.6151	0.99983
22502	Pgr	6	0	-2.2274	0.99983
22503	Kif18a	5	0	-2.3128	0.99983
22504	Ikzf3	6	0	-0.78622	0.99983
22505	mmu-mir-703	4	0	-2.2805	0.999859
22506	Zfp709	6	0	-1.343	0.999963
22507	Trmt13	5	0	-1.316	1
22508	Sly	3	0	-2.0052	1
22509	Rab4b	6	0	-1.3327	1
22510	Psd3	6	0	-1.7953	1
22511	Eif3f	6	0	-2.0508	1

Table 8.8: Bottom 100 positively enriched genes from the "Both down" condition of the genome-wide CRISPR-Cas9 knock-out screen in 3T3$^{\text{Fbl-GFP;Rpl18-RFP}}$ cells. The genes represent the bottom 100 scoring genes from the condition sorted for low EGFP-PEST (RiBi promoter) and low tRFP-PEST (RP promoter) fluorescence intensity. The data were obtained using the bioinformatic tool MAGeCK [Li et al., 2014].

8.2.9 Top 102 positively enriched genes from the condition sorted for low expression of *FBL*-driven SCARLET-I-d2 and median to high expression of *SFFV-driven* EGFP-PEST ("Scarlet down")

Rank	Gene	Number of sgRNAs	Good sgRNAs	LogFC	FDR
1	Scarlet	4	4	3.6137	0.00495
2	PAQR9	4	3	1.4892	0.823484
3	KMT2B	4	4	1.1238	0.823484
4	DAZAP2	4	3	1.4306	0.823484
5	ETHE1	4	3	1.5092	0.823484
6	LSR	4	2	0.84191	0.823484
7	ZCWPW2	4	3	1.5141	0.823484
8	IGFBPL1	4	3	1.3619	0.823484
9	CHTF18	4	4	1.0365	0.823484
10	AKR1B1	4	3	1.422	0.823484
11	TRAPPC8	4	2	-2.0282	0.823484
12	DDX6	4	4	1.0801	0.823484
13	PSMC2	4	4	0.97202	0.823484
14	TBC1D19	4	2	0.38292	0.823484
15	IMPA1	4	3	1.3269	0.823484
16	ZCCHC2	4	4	1.5274	0.823484
17	CRB1	4	2	0.24147	0.823484
18	MTF2	4	4	0.95358	0.823484
19	SLC39A2	4	3	1.1236	0.823484
20	EIF3K	4	3	0.72398	0.823484
21	SFTPA2	4	1	-0.56167	0.823484
22	DEFB115	4	3	1.1898	0.823484
23	TRAF4	4	2	0.6555	0.823484
24	FBXO42	4	4	0.92179	0.823484
25	KLF11	4	3	1.1406	0.823484
26	SEPTIN7	4	3	1.0812	0.823484
27	HERC6	4	4	0.95144	0.823484
28	GNGT1	4	3	0.97696	0.823484
29	KIF4A	4	2	-2.0482	0.823484
30	HCST	4	2	-2.0227	0.823484

31	PMF1-BGLAP	4	2	0.92503	0.823484
32	CSNK2A1	4	4	0.67622	0.823484
33	STX6	4	2	0.41723	0.823732
34	LYPD5	4	4	0.67823	0.826005
35	NCEH1	4	2	-0.68385	0.864424
36	TLR9	4	4	0.99115	0.864424
37	CSNK1G2	4	3	1.1549	0.864424
38	TAOK3	4	4	1.0059	0.864424
39	CXorf66	4	1	-1.2167	0.864424
40	OR10H4	4	3	1.0447	0.864424
41	SBDS	4	4	0.75241	0.864424
42	FOXA2	4	2	0.463	0.864424
43	EFCAB5	4	2	0.48339	0.864424
44	NR2C1	4	3	1.2009	0.864424
45	RASGRP2	4	4	0.53037	0.868977
46	FECH	4	4	0.95092	0.869362
47	TOPAZ1	4	1	-2.0059	0.869362
48	HLX	4	3	0.26207	0.869362
49	CYS1	4	4	0.46215	0.869362
50	ATP13A2	4	4	0.57648	0.869362
51	ASAH1	4	3	0.87549	0.869362
52	RBPJL	4	2	0.34684	0.869362
53	KRTAP20-2	4	4	0.90526	0.869362
54	NPIPB6	4	1	-6.3178	0.884518
55	SLC7A2	4	3	0.73151	0.885526
56	SLC35E2	4	2	0.51764	0.885526
57	LGR4	4	4	0.80691	0.885526
58	KRT80	4	4	0.86856	0.885526
59	SUN1	4	2	0.34371	0.885526
60	PRKACB	4	3	1.0811	0.885526
61	TMEM37	4	1	-0.047203	0.885526
62	PLCB4	4	3	1.1442	0.885526
63	LOR	4	4	0.65516	0.885526
64	CCT3	4	4	0.86871	0.885526
65	MYO10	4	4	1.1954	0.885526
66	RGS9BP	4	2	0.19627	0.885526

67	MAPK12	4	2	0.76061	0.885526
68	CDC42EP3	4	2	-1.2264	0.885526
69	SKP2	4	4	0.73362	0.885526
70	CUL9	4	4	0.58543	0.885526
71	TNFRSF25	4	3	0.86296	0.885526
72	ZNF583	4	3	0.71288	0.885526
73	COQ2	4	4	0.83453	0.885526
74	PGBD1	4	3	1.0252	0.885526
75	DPPA4	4	4	0.62515	0.885526
76	GDNF	4	2	0.3618	0.885526
77	SARDH	4	4	0.83296	0.885526
78	MBLAC2	4	3	1.0358	0.885526
79	MOG	4	3	1.0737	0.885526
80	OR2K2	4	2	0.020924	0.885526
81	DACT2	4	4	0.89888	0.885526
82	PGF	4	3	0.77224	0.885526
83	BTG1	4	3	0.79075	0.885526
84	MAGEB3	4	2	0.3714	0.885526
85	NAGK	4	4	0.48265	0.885526
86	ALKBH4	4	4	0.74178	0.885526
87	UBA2	4	1	-0.97201	0.885526
88	MYD88	4	4	0.90135	0.885526
89	COPS8	4	3	1.1733	0.885526
90	ATP6V1C2	4	3	1.0971	0.885526
91	GALM	4	2	0.17346	0.885526
92	PCDHGA10	4	2	-2.0366	0.885526
93	CDC25A	4	3	1.0017	0.885526
94	WDR91	4	3	1.2037	0.885526
95	C5orf63	4	4	0.60599	0.885526
96	MYO16	4	3	0.85856	0.885526
97	NLGN4Y	4	2	-0.16157	0.888639
98	INHA	4	3	1.1117	0.888639
99	FAM222A	4	1	-0.44423	0.892645
100	PARK7	4	4	0.50552	0.892645
101	COL25A1	4	3	1.2186	0.892645

102	MRPL11	4	3	1.1843	0.892645

Table 8.9: Top 102 positively enriched genes from the "Scarlet down" condition of the genome-wide CRISPR-Cas9 knock-out screen in U2OS$^{FBL\text{-}SCARLET;SFFV\text{-}GFP}$ cells. The genes represent the top 102 scoring genes from the condition sorted for constant or high EGFP-PEST (*SFFV* promoter), but low SCARLET-I-d2 (*FBL* promoter) fluorescence intensity. The data were obtained using the bioinformatic tool MAGeCK [Li et al., 2014].

8.2.10 Bottom 100 positively enriched genes from the condition sorted for low expression of *FBL*-driven SCARLET-I-d2 and median to high expression of *SFFV-driven* EGFP-PEST ("Scarlet down")

Rank	Gene	Number of sgRNAs	Good sgRNAs	LogFC	FDR
19016	NABP2	4	0	-6.1548	0.999926
19017	THEGL	4	0	-6.2475	0.999926
19018	HCN3	4	0	-5.5107	0.999926
19019	XG	4	0	-5.4775	0.999926
19020	PGA4	4	0	-5.2104	0.999926
19021	CEP112	3	0	-6.7026	0.999926
19022	ERO1L	4	0	-5.4004	0.999926
19023	MLH3	4	0	-6.0007	0.999926
19024	ADGRA3	4	0	-6.3102	0.999926
19025	ARHGEF37	4	0	-6.1276	0.999926
19026	PPM1N	4	0	-1.7139	0.999926
19027	PAMR1	4	0	-6.6585	0.999926
19028	SIM2	4	0	-4.2967	0.999926
19029	TMA16	4	0	-5.5729	0.999926
19030	PRSS48	4	0	-5.9943	0.999926
19031	MAF	4	0	-6.0478	0.999926
19032	MLLT11	4	0	-6.0692	0.999926
19033	GRM1	4	0	-4.5685	0.999926
19034	RAB44	4	0	-2.5788	0.999926
19035	PHOSPHO1	4	0	-6.4941	0.999926
19036	CYYR1	4	0	-6.0004	0.999926
19037	TRAF2	4	0	-6.1939	0.999926
19038	FAM120C	4	0	-5.9096	0.999926
19039	COL4A4	4	0	-5.6535	0.999926
19040	TLDC1	4	0	-1.8156	0.999926

19041	SERPINB13	4	0	-6.0819	0.999926
19042	BHLHB9	4	0	-5.5622	0.999926
19043	KRT24	4	0	-6.1224	0.999926
19044	UBE2U	4	0	-5.6991	0.999926
19045	R3HDML	4	0	-6.31	0.999926
19046	CRIP2	4	0	-3.676	0.999926
19047	S100A2	4	0	-5.9788	0.999926
19048	FRMD4A	4	0	-5.9541	0.999926
19049	RPL27	4	0	-6.1165	0.999926
19050	ZNF20	4	0	-5.9464	0.999926
19051	SMG1	4	0	-6.5964	0.999926
19052	SH3D19	4	0	-6.2565	0.999926
19053	EIF3D	4	0	-6.2703	0.999926
19054	CCDC170	4	0	-6.0589	0.999926
19055	UPP1	4	0	-2.6822	0.999926
19056	HAS3	4	0	-1.3356	0.999926
19057	FBP1	4	0	-5.6212	0.999926
19058	FBXL19	4	0	-6.1396	0.999926
19059	SNN	4	0	-6.3952	0.999926
19060	OAZ1	4	0	-4.2674	0.999926
19061	OR6T1	4	0	-4.8667	0.999926
19062	PCTP	4	0	-4.05	0.999926
19063	TUBB4B	4	0	-6.013	0.999926
19064	SLC34A2	4	0	-6.6727	0.999926
19065	ABCC11	4	0	-4.9947	0.999926
19066	BOLA2B	4	0	-3.1659	0.999926
19067	ITGAM	4	0	-6.3685	0.999926
19068	ECT2	4	0	-4.182	0.999926
19069	LILRB5	4	0	-5.6333	0.999926
19070	ENPP4	4	0	-1.9443	0.999926
19071	KIAA1211	4	0	-6.6347	0.999926
19072	COL18A1	4	0	-3.7146	0.999926
19073	OR56A3	4	0	-4.0229	0.999926
19074	PHYHD1	4	0	-6.5527	0.999926
19075	MTMR6	4	0	-6.4922	0.999926
19076	PTTG1	4	0	-6.1859	0.999926

19077	LZTR1	4	0	-5.8759	0.999926
19078	TCF21	4	0	-6.1275	0.999926
19079	TBC1D5	4	0	-6.2509	0.999926
19080	ETF1	4	0	-6.2161	0.999926
19081	CHRM5	4	0	-6.0981	0.999926
19082	SH3BGR	4	0	-6.3779	0.999926
19083	RUNDC3B	4	0	-4.767	0.999926
19084	DYX1C1	4	0	-6.2967	0.999926
19085	CELSR1	4	0	-6.7291	0.999926
19086	YIPF6	4	0	-6.5224	0.999926
19087	ANKRD2	4	0	-5.2298	0.999926
19088	BMP5	4	0	-3.6231	0.999926
19089	LSM2	4	0	-1.9544	0.999926
19090	OR6C70	4	0	-3.8689	0.999926
19091	GLRA3	4	0	-6.1616	0.999926
19092	RET	4	0	-2.2264	0.999926
19093	DPH6	4	0	-6.3612	0.999926
19094	VDR	4	0	-6.3452	0.999926
19095	OR4A5	4	0	-5.9685	0.999926
19096	NMNAT2	4	0	-4.7547	0.999926
19097	TIGD6	4	0	-6.3242	0.999926
19098	CDH3	4	0	-5.9199	0.999926
19099	CABLES2	4	0	-6.0956	0.999926
19100	TNFRSF21	4	0	-6.2317	0.999926
19101	LDLR	4	0	-4.0223	0.999926
19102	TSGA10	4	0	-6.3904	0.999926
19103	SOCS3	4	0	-4.7535	0.999926
19104	IAPP	4	0	-5.1219	0.999926
19105	TCEAL7	4	0	-6.2962	0.999926
19106	A3GALT2	4	0	-3.4764	0.999926
19107	C4orf22	4	0	-6.467	0.999926
19108	SNRPE	4	0	-6.401	0.999926
19109	HSPBAP1	4	0	-5.9925	0.999926
19110	ABLIM3	4	0	-1.3635	0.999926
19111	PRDM1	4	0	-6.4849	0.999926
19112	C20orf195	4	0	-6.111	0.999926

19113	TFAP2D	4	0	-6.8724	0.999966
19114	NRBP2	4	0	-6.7301	0.999989
19115	TFAP2B	4	0	-4.1843	0.999989
19116	RPL5	4	0	-6.4938	0.999989

Table 8.10: Bottom 100 positively enriched genes from the "Scarlet down" condition of the genome-wide CRISPR-Cas9 knockout screen in U2OS$^{\text{FBL-SCARLET;SFFV-GFP}}$ cells. The genes represent the bottom 100 scoring genes from the condition sorted for constant or high EGFP-PEST (*SFFV* promoter), but low SCARLET-I-d2 (*FBL* promoter) fluorescence intensity. The data were obtained using the bioinformatic tool MAGeCK [Li et al., 2014].

8.3 Publication record

B. Adhikari, J. Bozilovic, M. Diebold, **J. D. Schwarz**, J. Hofstetter, M. Schröder, M. Wanior, A. Narain, M. Vogt, N. D. Stankovic, A. Baluapuri, L. Schönemann, L. Eing, P. Bhandare, B. Kuster, A. Schlosser, S. Heinzlmeir, C. Sotriffer, S. Knapp, and E. Wolf. PROTAC-mediated degradation reveals a non-catalytic function of AURORA-A kinase. Nature chemical biology, 16(11):1179, nov 2020. doi: 10.1038/S41589-020-00652-Y.

A. Baluapuri, J. Hofstetter, N. D. Stankovic, T. Endres, P. Bhandare, S. M. Vos, B. Adhikari, **J. D. Schwarz**, A. Narain, M. Vogt, S.-Y. Wang, R. Düster, L. A. Jung, J. T. Vanselow, A. Wiegering, M. Geyer, H. M. Maric, P. Gallant, S. Walz, A. Schlosser, P. Cramer, M. Eilers, and E. Wolf. MYC Recruits SPT5 to RNA Polymerase II to Promote Processive Transcription Elongation. Molecular Cell, 74(4):674, may 2019. doi: 10.1016/J.MOLCEL.2019.02.031.

O. Hartmann, M. Reissland, C. R. Maier, T. Fischer, C. Prieto-Garcia, A. Baluapuri, **J. Schwarz**, W. Schmitz, M. Garrido-Rodriguez, N. Pahor, C. C. Davies, F. Bassermann, A. Orian, E. Wolf, A. Schulze, M. A. Calzado, M. T. Rosenfeldt, and M. E. Diefenbacher. Implementation of CRISPR/Cas9 Genome Editing to Generate Murine Lung Cancer Models That Depict the Mutational Landscape of Human Disease. Frontiers in Cell and Developmental Biology, 0:201, mar 2021. ISSN 2296-634X. doi: 10.3389/FCELL.2021.641618.

Parts of this thesis have been submitted for publication as a journal article.

8.4 Acknowledgments

As with every huge project, this work could not have been possible without the support of a plethora of people.

First of all I would like to thank my first supervisor Prof. Dr. Elmar Wolf for having given me the opportunity to pursue my doctoral thesis in his laboratory. I am very grateful for all the scientific discussions and his constant support, especially during the last year.

Moreover, I would like to thank the members of my thesis committee Prof. Dr. Martin Eilers, Dr. Björn von Eyß and Prof. Dr. Andreas Winterpacht for their regular input, as well as the great support, whenever something needed to be done more urgently. I am honestly really grateful for such a great committee.

Special thanks go to our department, with a focus on my working group. In my opinion, one of the most important things during a PhD is a good atmosphere among colleagues. Every single person in this department is incredibly supportive. I also really enjoyed all of the social events in the evenings. It was just a great time. I would especially like to thank André for his wet lab support, Nevenka for constantly offering help, Apoorva and Julia for the regular (scientific) discussions, and Apoorva and Pranjali for their scientific support in terms of analyses and other experiments for my project. Many thanks go to Julia for proof-reading, the comments were very helpful. I would also like to thank Jan and Mahmoud for the experiments they did for the Aldoa project. Also many thanks to all former and present AG Wolf members, especially Ashwin, Lorenz, Benedikt, Isabella, Lara etc., but also Oli and Carina, for the great time outside of the lab!

The main collaborators for the Aldoa project were Marteinn Snaebjornsson and Almut Schulze from the DKFZ in Hedelberg. I would like to thank them very much for the provided materials and the time they invested for all the scientific discussions!

I am grateful, that I could use the electroporator from AG Buchberger, and for the welcoming atmosphere in their laboratory. Special thanks at this point go to Prof. Dr. Alexander Buchberger, Mona Kawan and Susanne Meyer.

Last, but not least, I would like to thank my friends and family for their infinite support during this time. Here, a very special thank you goes to Sören Lukassen. He supported me during my thesis scientifically and privately. Without him, many things would have been much more difficult and tedious or might not even have worked out at all without additional collaborators. So really: many, many thanks!

8.5 Affidavit

Affidavit

I hereby confirm that my thesis entitled *"Genome-wide reporter screens identify transcriptional regulators of ribosome biogenesis"* is the result of my own work. I did not receive any help or support from commercial consultants. All sources and/or materials applied are listed and specified in the thesis.

Furthermore, I confirm that this thesis has not yet been submitted as part of another examination process neither in identical nor in similar form.

.....	.....
Place, Date	Signature

Eidesstattliche Erklärung

Hiermit erkläre ich an Eides statt, die Dissertation *"Genomweite Reporterscreens identifizieren transkriptionelle Regulatoren ribosomaler Biogenese"* eigenständig, d.h. insbesondere selbständig und ohne Hilfe eines kommerziellen Promotionsberaters, angefertigt und keine anderen als die von mir angegebenen Quellen und Hilfsmittel verwendet zu haben.

Ich erkläre außerdem, dass die Dissertation weder in gleicher noch in ähnlicher Form bereits in einem anderen Prüfungsverfahren vorgelegen hat.

.....	.....
Ort, Datum	Unterschrift